CARDIFF UNIVERSITY

DOCTORAL THESIS

Energy minimising multi-crack growth in linear-elastic materials using the extended finite element method with application to Smart-Cut™ silicon wafer splitting

Author:

Danas SUTULA

Supervisors:

Prof. Stéphane P.A. BORDAS

Dr. Pierre KERFRIDEN

Dr. Konstantin K. BOURDELLE

Alexandre BARTHELEMY

A thesis submitted in fulfilment of the requirements

for the degree of Doctor of Philosophy

in

Advanced Materials and Computational Mechanics

School of Engineering

August 19, 2016

To my family and friends,
for their love and support

CARDIFF UNIVERSITY

Abstract

Advanced Materials and Computational Mechanics

School of Engineering

Doctor of Philosophy

Energy minimising multi-crack growth in linear-elastic materials using the extended finite element method with application to Smart-Cut™ silicon wafer splitting

by Danas SUTULA

We investigate multiple crack evolution under quasi-static conditions in an isotropic linear-elastic solid based on the principle of minimum total energy, i.e. the sum of the potential and fracture energies, which stems directly from the Griffith's theory of cracks. The technique, which has been implemented within the extended finite element method, enables minimisation of the total energy of the mechanical system with respect to the crack extension directions. This is achieved by finding the orientations of the discrete crack-tip extensions that yield vanishing rotational energy release rates about their roots. In addition, the proposed energy minimisation technique can be used to resolve competing crack growth problems. Comparisons of the fracture paths obtained by the maximum tension (hoop-stress) criterion and the energy minimisation approach via a multitude of numerical case studies show that both criteria converge to virtually the same fracture solutions albeit from opposite directions. In other words, it is found that the converged fracture path lies in between those obtained by each criterion on coarser numerical discretisations. Upon further investigation of the energy minimisation approach within the discrete framework, a modified crack growth direction criterion is proposed that assumes the average direction of the directions obtained by the maximum hoop stress and the minimum energy criteria. The numerical results show significant improvements in accuracy (especially on coarse discretisations) and convergence rates of the fracture paths. The XFEM implementation is subsequently applied to model an industry relevant problem of silicon wafer cutting based on the physical process of Smart-Cut™ technology where wafer splitting is the result of the coalescence of multiple pressure-driven micro-crack growth within a narrow layer of the prevailing micro-crack distribution. A parametric study is carried out to assess the influence of some of the Smart-Cut™ process parameters on the post-split fracture surface roughness. The parameters that have been investigated, include: mean depth of micro-crack distribution, distribution of micro-cracks about the mean depth, damage (isotropic) in the region of micro-crack distribution, and the influence of the depth of the buried-oxide layer (a layer of reduced stiffness) beneath the micro-crack distribution. Numerical results agree acceptably well with experimental observations.

Acknowledgements

I wish to express my deepest appreciation to my supervisors, Prof. Stéphane Bordas and Dr. Pierre Kerfriden for their mentorship. Thank you for your great many teachings, for your continued patience with me and for the much needed encouragement over the years.

However, I can not thank enough Prof. Bordas for his excellent leadership in this project. You have helped me stay on target and see the big picture of my research, especially at times when I would be consumed by details. You have also shown a lot of confidence in me and encouraged me find my own way around problems and to experience the learning process. For this, I am very grateful. I consider myself very fortunate to have been welcomed to your research group and I hope I have met most of your expectations.

Of course, this project would not have been possible without Soitec and their financial support via the President's Research Scholarship. I particularly wish to thank my industrial supervisors, Dr. Konstantin Bourdelle and Mr. Alexandre Barthelemy for their technical expertise on the Smart-Cut™ process and their mentorship during the course of my PhD.

I wish to express my sincerest appreciation of the whole research group at Cardiff, for their comradery and for the many fruitful scientific discussions and shared perspectives that have contributed directly or indirectly to this thesis. In this respect I want to thank: Daniel Paladim, Ahmad Akbari, Olivier Goury, Changkye Lee, Haojie Lian, Xuan Peng, Claire Heaney, Iulia Mihai, and Vinh Phu Nguyen. A special thanks, however, is reserved to Prof. Anthony Jefferson who had taught me the finite element method in the first place and who initially inspired me to do a research degree in computational mechanics. During my PhD, he showed a keen interest in my research and was open to numerous consultations.

I wish to acknowledge all staff, particularly the wonderful individuals in the Research Office: Chris Lee, Jeanette Whyte, Aderyn Reid for the administrative assistance. I thank the University for the training courses and for supporting me on various conferences.

Finally, I thank my wonderful parents Vesta and Zigmas, and my dear brother Mantas for their unconditional love and support, and for helping me to become the person I am now.

Contents

List of Abbreviations

AFM	**A**tomic **F**orce **M**icroscopy
BEM	**B**oundary **E**lement **M**ethod
BOX	**B**uried silicon **OX**ide layer
CCG	**C**ompeting **C**rack **G**rowth
CDM	**C**ontinuum **D**amage **M**echanics
CMP	**C**hemical **M**echanical **P**polishing
CTOD	**C**rack **T**ip **O**pening **D**isplacement
CZM	**C**ohesive **Z**one **M**odel
DOF	**D**egree **O**f **F**reedom
EFEM	**E**mbedded **F**inite **E**lement **M**ethod
EPFM	**E**lastic-**P**lastic **F**racture **M**echanics
ERR	**E**nergy **R**elease **R**ate
FE	**F**inite **E**lement
FM	**F**racture **M**echanics
FEA	**F**inite **E**lement **A**nalysis
FEM	**F**inite **E**lement **M**ethod
GFEM	**G**eneralised **F**inite **E**lement **M**ethod
LEFM	**L**inear **E**lastic **F**racture **M**echanics
LSM	**L**evel **S**et **M**ethod
MD	**M**olecular **D**ynamics
MERR	**M**aximum **E**nergy **R**elease **R**ate (criterion)
MSED	**M**inimum **S**train **E**nergy **D**ensity (criterion)
MM	**M**eshless **M**ethod
MTS	**M**aximum **T**angential **S**tress (criterion)
ODE	**O**rdinary **D**ifferential **E**quation
PDE	**P**artial **D**ifferential **E**quation
PFM	**P**hase **F**ield **M**ethod
PLS	**P**rinciple of **L**ocal **S**ymmetry (criterion)
PU	**P**artition of **U**nity
SIF	**S**tress **I**ntensity **F**actor
SGFEM	**S**tabilised **G**eneralised **F**inite **E**lement **M**ethod
SOI	**S**ilicon **O**n **I**nsulator
SSY	**S**mall **S**cale **Y**ielding
TLS	**T**hick **L**evel **S**et (model)
VCCT	**V**irtual **C**rack **C**losure **T**echnique
VCEM	**V**irtual **C**rack **E**xtension **M**ethod
XFEM	E**X**tended **F**inite **E**lement **M**ethod
YSM	**Y**ield **S**trip **M**odel

List of Symbols

$\mathcal{I}_\mathrm{c}$	set of all cracks	
$\mathcal{I}_\mathrm{tip}$	set of all crack tips	
$\mathcal{I}^\mathrm{c}_\mathrm{tip}$	set of critical tips	
$\mathcal{W}$	set of trial tip extensions	
n_c	number of cracks	
n_tip	number of crack tips	
n_el	number of finite elements in mesh	
$n^\mathrm{cut}_\mathrm{el}$	number of crack-cut finite elements	
Γ	boundary of solid	m^2
Γ_c	Fracture surface	m^2
Γ^+_c	Upper face of fracture surface	m^2
Γ^-_c	Lower face of fracture surface	m^2
Γ_u	Dirichlet boundary	m^2
Γ_t	Neumann boundary	m^2
Ω	elastic domain	m^3
Ω_el	finite element domain	m^3
$\bar{\Omega}_\mathrm{el}$	finite element domain in natural coordinates	
τ	"time" in the quasi-static sense	
θ	crack extension angle relative to x-axis	rad
ℓ	length of crack tip branch	m
$\dot{\ell}$	growth rate of crack tip branch	m/τ
$\hat{\ell}$	relative growth of crack tip branch	m/m
$\mathcal{A}$	admissible crack tip extensions	m/m
a	crack length	m
$\dot{a}$	rate of crack extension	m/τ
$\hat{a}$	relative crack extension	m/m
a_0	initial crack length	m
a_∞	final crack length	m
A	total fracture area	m^2
λ_t	critical load parameter	
$\mathbf{b}$	body force	N/m^3
$\mathbf{t}$	surface traction	N/m^2
$\mathbf{p}$	fracture surface tractions	N/m^2
$\mathcal{U}$	displacement field trial space	m
$\mathcal{U}_0$	displacement field test space	m
$\mathcal{U}^h$	discrete displacement field trial space	m
$\mathcal{U}^h_0$	discrete displacement field test space	m

$\mathbf{u}$	displacement field	m
$\bar{\mathbf{u}}$	prescribed displacements	m
$\mathbf{u}^h$	discrete displacement field	m
$\mathbf{w}$	displacement test functions	m
ε	small strain tensor	
σ	Cauchy stress tensor	$\mathrm{N/m^2}$
ν	Posson's ratio	
μ	Shear modulus	$\mathrm{N/m^2}$
E	Young's elastic modulus	$\mathrm{N/m^2}$
E_{box}	Young's modulus of silicon dioxide	$\mathrm{N/m^2}$
E_{dmg}	Young's modulus of damaged silicon	$\mathrm{N/m^2}$
E_{Si}	Young's modulus of silicon	$\mathrm{N/m^2}$
$\mathbf{C}$	stress-strain constitutive tensor	$\mathrm{N/m^2}$
γ_s	fracture surface energy	$\mathrm{Nm/m^2}$
γ_p	fracture surface plastic dissipation	$\mathrm{Nm/m^2}$
$\mathcal{D}$	total energy dissipation rate with crack extension	$\mathrm{Nm/m^2}$
$\mathcal{D}_\theta$	total energy dissipation rate with crack rotation	Nm/rad
G_θ	rotational energy release rate	Nm/rad
G_{c}	critical energy release rate	$\mathrm{Nm/m^2}$
G_{s}	fracture energy release rate	$\mathrm{Nm/m^2}$
H_θ	rate of rotational energy release rate	$\mathrm{Nm/rad^2}$
H_{m}	rate of mixed energy release rate	$\mathrm{Nm/m^2/rad}$
H_{s}	rate of fracture energy release rate	$\mathrm{Nm/m^4}$
K_I	mode-I stress intensity factor	$\mathrm{Nm^{1/2}/m^2}$
K_{II}	mode-II stress intensity factor	$\mathrm{Nm^{1/2}/m^2}$
K_{Ic}	fracture toughness (as measured in mode-I)	$\mathrm{Nm^{1/2}/m^2}$
$\mathcal{N}_{\mathrm{S}}$	number of all nodes in the finite element mesh	
$\mathcal{N}_{\mathrm{B}}$	set of all branch-enriched nodes	
$\mathcal{N}_{\mathrm{H}}$	set of all Heaviside-enriched nodes	
$\mathbf{a}_I$	Heaviside enrichment degrees of freedom at node I	m
$\mathbf{b}_I$	branch enrichment degrees of freedom at node I	m
H	Heaviside enrichment function	
$\boldsymbol{B}$	Crack tip branch functions	
$\mathbf{B}$	strain-operator matrix	1/m
$\mathbf{B}_e$	enriched part of strain-operator matrix	1/m
$\mathbf{B}_s$	enriched part of strain-operator matrix	1/m
N_I	finite element shape function at node I	
$\mathbf{N}$	displacement-operator matrix	
$\mathbf{N}_e$	enriched part of displacement-operator matrix	
$\mathbf{N}_s$	enriched part of displacement-operator matrix	
$\mathbf{f}$	generalised global force vector	N
$\mathbf{f}_{\mathrm{el}}$	element force vector	N
$\mathbf{f}_e$	enriched part of the force vector	N
$\mathbf{f}_s$	standard part of the force vector	N
$\mathbf{K}$	generalised global stiffness matrix	N/m
$\mathbf{K}_{\mathrm{el}}$	element stiffness matrix	N/m

$\mathbf{K}_{ee}$	enriched part of stiffness matrix	N/m
$\mathbf{K}_{se}$	standard-enriched part of stiffness matrix	N/m
$\mathbf{K}_{ee}$	enriched parts of stiffness matrix	N/m
Π	potential energy of solid	Nm
$\mathcal{E}$	total energy of system	Nm
$\mathcal{L}$	total Lagrangian of system	Nm
U_{s}	elastic strain energy of solid	Nm
V	potential energy of external load	Nm
W_{ext}	work done by external load	Nm
h_{box}	depth of buried oxide	nm
h_{mean}	mean micro-crack distribution depth	nm
t_{dmg}	micro-crack distribution thickness	nm
R_q	root-mean-square roughness	nm
R_t	peak-valley roughness	nm
R_p	peak roughness	nm
R_v	valley roughness	nm
$\mathbf{s}$	unit tangent vector to surface	
$\mathbf{n}$	unit normal vector to surface	
$\mathbf{T}$	local-to-global coordinate transformation matrix	
$\mathbf{T}'$	global-to-local coordinate transformation matrix	
$\mathbf{T}_{\varepsilon}$	global-to-local strain transformation matrix	
$\mathbf{T}_{\sigma}$	global-to-local stress transformation matrix	

Chapter 1

Background

1.1 Motivation and aims

A technology called Smart-Cut™ is a commercial process of achieving an ultra-thin (a few nanometres thick) silicon layer transfer from one substrate onto another. It is used in the high-volume production of silicon-on-insulator (SOI) wafers that find broad applications in the modern day semiconductor and microelectronics industries, e.g. photovoltaics, integrated circuits, microprocessor, etc. The manufacturing process of an SOI wafer involves cleaving two bonded wafers along a weak plane very close to the bonding interface thereby effectively achieving the transfer of a thin silicon layer. The cleaving (or splitting) is obtained by the coalescence of highly planar and narrowly distributed defects that are induced in the donor wafer via a highly precise hydrogen-ion (H^+) irradiation process prior to bonding of the two wafers. The defects evolve during thermal activation into platelets of a few nanometres in size, then into micro-cracks and, finally, into macro-cracks that propagate catastrophically along the cleavage plane which causes splitting.

The wafer splitting process is an intricate multi-physics phenomenon at several length-scales, with different aspects of physics competing in terms of their relative influence on the defect/platelet/micro-crack evolutions. In the initial stage, thermodynamic forces drive the evolution of atomic-size defects into platelet-like defects of several nanometres. These so-called platelets act as sinks for trapping mobile H^+ ions that subsequently recombine into molecular hydrogen (H_2) and start to exert a significant pressure on the cavity walls. Later in the evolution process, when the platelets have grown into the size range of several tens of micrometres, the hydrogen gas pressure becomes the principle force driving the micro-crack evolution. The final stage of annealing is marked by a highly dynamic coalescence of micro/macro-cracks, which ultimately achieves wafer splitting.

Smart-Cut™ is a relatively novel technology (dating back to under two decades) that is not completely understood to this day, specifically in relation to the platelet/crack growth kinetics as influenced by different driving mechanisms, i.e. competing thermo-dynamic/mechanical actions. More importantly, it is not completely clear how different

Smart-Cut™ process parameters affect the fractured surface topography whose high uniformity is key for the commercial viability of the SOI wafer manufacturing process. Indeed, a great loss of product can be incurred due to the post-split fracture surface defects. Thus, a better understanding of the influence of Smart-Cut™ control parameters is essential.

From the modelling side, the Smart-Cut™ process involves multiple material length-scales, which poses computational challenges in trying to concurrently model the evolution of defects/platelets/micro-cracks/macro-cracks as a means to quantify the effects of different process parameters (e.g. in relation to the initial defect distribution) in terms of the post-split fracture surface topography. We set our focus on one stage of the Smart-Cut™ splitting process that is characterised by the relatively slow evolution and coalescence of micro-cracks. The goal is to determine the relative influence of different process parameters (e.g. in relation to some initial statistically representable micro-crack distribution) on the evolution of micro/macro-cracks and on the resulting post-split surface roughness.

To achieve this goal, the significant part of the current work is devoted to the development of advanced computational techniques for the modelling of fracture. The aim is to develop a robust numerical approach for modelling multi-crack growth problems within the framework of linear-elastic fracture mechanics (LEFM). A particular focus is on employing thermodynamically consistent energy-based principles for the prediction of crack evolution and for resolving competing crack growth, which may naturally arise in multi-crack growth scenarios. The energy-based crack growth formulation is to be implemented within the state-of-the-art numerical discretisation method: the extended finite element method (XFEM), which is especially suited for problems involving arbitrary discontinuities in space evolving over time. As the numerical model is aimed at solving large scale fracture problems, the focus is also on the efficient implementation of the numerical techniques within the *Matlab* programming language with particular attention to robust crack tacking and merging routines.

Finally, the model will be used to simulation wafer splitting as a way to assess the influence of different initial micro-crack distribution parameters on the post-split surface roughness. The parameters include the initial crack distribution depth and thickness, among others.

1.2 Modelling discontinuities in solids

There are different kinds of discontinuities that appear in the solutions of solid mechanics problems. The most obvious example of a discontinuity is a jump in the displacement field across crack surfaces. When the discontinuity occurs in the primary variable, such as the displacement field, the discontinuity is called a *strong* discontinuity. Other discontinuities, such as those appearing at material interfaces (e.g. in composite materials), lead to discontinuous spatial derivatives of the displacement field; in this particular case, the strain normal to the material interface is discontinuous. When the discontinuity occurs in the derivative of the primary variable, the discontinuity is called a *weak* discontinuity. High gradients can also be regarded as a form of a discontinuity, e.g. localisation of plastic strains. In this case, the displacement field is continuous but it varies rapidly over a relatively small length-scale such that the solution closely resembles a strong discontinuity.

Many practical problems that arise in solid mechanics involve some form of a discontinuity. However, modelling discontinuities within the classic solid continuum theory is a difficult task because the partial differential equations that are used to model solid continua are inherently incompatible with discontinuities, e.g. derivatives at discontinuities do not exist. The governing PDE's can be transformed into a set of integro-differential equations thereby allowing less regular solutions with not so well-defined derivatives at every material point; however, it still proves challenging to model the evolution of various discontinuities simply because discontinuities do not naturally arise as part of the solution. Instead, a particular discontinuity in the displacement field can only be captured by having introduced it in the first place via some mechanism (based on an *a priori* knowledge about the solution). For example, a discontinuity can be introduced kinematically by considering a certain solution space where the particular discontinuity can naturally arise, or, in the case of a crack, by considering the crack as an interior boundary of the domain that encloses a zero-volume. In any case, the position of the discontinuity needs to be known in advance and the discontinuity reproducing mechanism needs to be incorporated within the continuum model explicitly. In addition, the model needs to be supplemented with an external criterion for determining when and how the discontinuity evolves over time.

In contrast, the non-continuum modelling of solids (i.e. by considering discrete material particles) allows the displacement discontinuities to emerge naturally as part of the solution. For example, some of the non-continuum methods that have been used to model material failure include: smooth particle hydrodynamics [96, 167, 244], material point method (MPM) [276–278], peridynamics [114, 262, 263], molecular dynamics [4, 123, 125, 304, 306], to name a few. In these approaches, the evolution of discontinuities (e.g. free surfaces) occurs naturally as the bond forces between particles are overcome. In principle, all non-continuum type formulations mimic the molecular dynamics model in the sense that attractive/repulsive forces acting over finite distances govern the particle interactions.

Within the continuum context, there are two ways of modelling failure processes. The problem is approached either from the viewpoint of *continuum damage mechanics* (CDM) [202] or *fracture mechanics* (FM) [12]. CDM considers a smeared crack model: the behaviour of a crack is captured approximately by the localisation of strains along the failure surface. On the other hand, FM considers a discrete crack: a crack is modelled as a strong discontinuity in the displacement field. The two methods are described briefly as follows.

1.2.1 Damage mechanics

The continuum damage mechanics approach to failure modelling comes from the observation that many failure processes are accompanied by progressively diminishing load bearing capacity: decreasing strength and stiffness with increasing strain. This type of material behaviour is known as strain-softening; it can be observed during the failure process of many ductile metals and composites such as concrete. The cause of strain-softening is microscopic damage: nucleation of voids, micro-cracking, debonding, etc. [142, 242, 243]. In CDM, an internal damage variable is used to quantify the level of material damage. Specifically, the damage variable reflects the homogenised effects of the microscopic failure processes on the macroscopic constitutive stress-strain law [213–215]. The relationship between damage and the macroscopic stress-strain law can be obtained either phenomenologically, i.e. by fitting experimental data to a chosen damage-constitutive model, or based on micromechanical solutions, i.e. by resolving the material microstructure in a multi-scale

approach [190, 207]. The simplest damage model is isotropic, i.e. the material stiffness deteriorates isotropically with increasing damage. More advanced formulations take into account anisotropic damage (e.g. due to predominantly uni-directional micro-cracking) and different material responses with respect to compression, tension and shear. Damage evolution is typically governed by a material state law, which needs to be provided as part of the model. Usually, the law is based on the principle of maximal energy dissipation.

The evolution of damage over time naturally leads to the localisation of damage to a surface, which is a characteristic behaviour of a strain-softening material [213]. Theoretically, the high displacement gradients over the failure zone may well resemble the displacement jump due to a discrete crack; however, the classic CDM model becomes ill-posed when damage localises to a surface [23, 236]. This is because energy dissipation within the CDM framework needs to occur over a volume, but instead, due to the localisation of damage to a surface (i.e. a zero volume), no energy can be dissipated with increasing damage, which is physically unacceptable. Numerically, the solution exhibits spurious discretisation dependency such as instability and a failure to converge. In order to pose the CDM model more robustly and, thus, to avoid the numerical difficulties due to damage localisation, one solution is to *regularise* the damage zone over a finite material volume. This leads to the so-called *non-local* continuum damage models [23, 65, 231, 232, 236] where the idea is to replace the local damage parameter at a particular point by a non-local parameter that is computed as the weighted average of the damage over a representative volume centred at that point. The non-local CDM formulation introduces a damage length-scale that is considered as an intrinsic material property. One of the criticisms of the non-local CDM approach is that the damage length-scale may lack a clear physical interpretation.

The main advantage of the CDM approach is that it can be used to model the complete failure process: from the initiation of damage, to damage localisation and, subsequently, to the evolution of the damage zone as a diffusive crack until complete failure is attained. The CDM approach is attractive from the viewpoint that fracture can be modelled completely within the continuum context without having to deal with strong discontinuities. Note that this means that some undamaged material is assumed to always remain in the failure zone that is able to transmit stresses across the failure zone. This is necessary in order

to avoid an ill-conditioned system due to the very small strain energy of the damaged zone. Since damage follows naturally from the continuum solution (in accordance with the damage evolution law), problems analogous to those encountered in the fracture mechanics approach such as: nucleation of cracks, crack bufurcation, determining the crack growth direction and length, as well as managing crack intersections, do not arise.

In the limit of a vanishingly small damage length-scale, the smeared crack model can be expected to converge to the discrete crack solution. In practice, however, the limit is difficult to approach because of the high computational cost of the fine-scale numerical discretisation of the damage zone that is required. For instance, the damage length-scale may be a few orders of magnitude smaller than the size of the structure whereas the numerical discretisation of the material volume needs to be of an even finer resolution so that damage regularisation at the damage length-scale makes sense. Nevertheless, for many practical purposes the diffusive fracture solution can be a satisfactory approximation of the discrete fracture solution, especially when the aim is to model the failure behaviour of the structure without requiring too much detail about the fracture surface topography. The smeared crack model lacks precision in capturing the fine-scale geometrical features of the fracture paths simply because the fracture solution tends to be overly diffusive and a sufficiently fine discretisation tends to be computationally prohibitive. In the end, the interactions between multiple cracks and their intersections are not so well defined.

1.2.2 Fracture mechanics

In the fracture mechanics (FM) approach [12], a crack is modelled as a strong discontinuity in the displacement field. Due to the infinitely sharp crack, the stress solution exhibits a square-root singularity at the crack tip [131, 294, 297], which is numerically a difficult problem to deal with. The accuracy of the tip field is important because various crack growth criteria rely on it to determine how a crack evolves in space and time [40, 247, 310]. Different criteria may be concerned with different aspects of crack growth. In general, the criteria need to determine when a crack grows, by how much, and in which direction. Depending on the physics of the fracture problem, other criteria may be introduced to

determine when a new crack should be nucleated or when an existing crack should bifurcate into multiple branches, e.g. such as in dynamic crack growth [39, 268, 305]. However, with regard to crack nucleation, the classic theory of fracture mechanics predicts that an infinite stress is required to create a new crack inside an elastic solid [105, 106, 176]. Nonetheless, crack nucleation within FM has been attempted by applying non-local criteria such as maximum average stress [211, 257, 258] or maximum energy release [163, 164, 257]. For a comparison of different crack initiation criteria refer to [257, 259, 310]. Alternatively, crack nucleation can be addressed within the CDM framework, whereas FM can be applied to model sufficiently well developed smeared cracks as discrete cracks [14, 36, 241, 288].

The limitation of the fracture mechanics approach to the modelling of the complete failure process can be overcome to some extent. For instance, it is possible to model the various failure processes ahead of a crack tip such as: plastic flow, initiation and coalescence of voids, and micro-cracking by adopting a cohesive zone model (CZM) [19, 20, 73, 120]. A cohesive process zone is considered in a region close to the crack tip whose length is assumed to be an intrinsic material property. The constitutive relationship between the cohesive tractions and the crack tip opening displacements along the process zone is determined phenomenologically so as to reflect the inelastic material behaviour that is observed at the macroscopic scale. A distinction is made between the *physical* crack tip that marks the end of the process zone (where there is zero material cohesion), and the *mathematical* crack tip that marks the beginning of the process zone. The cohesive tractions acting along the process zone are assumed to smoothly close the crack such that the stress singularity at the *mathematical* tip vanishes. In this case, the cohesive law also serves as a crack growth criterion since it implicitly states when a crack should grow; specifically, a given crack tip position is unstable if the cohesive tractions can not close the crack smoothly enough so as to eliminate the stress singularity at the tip, in which case the crack will propagate under the given load. Moreover, the cohesive law is intrinsically related to the rate of energy dissipation during crack growth since the area under the traction-separation curve is equal to the cohesive energy per unit area [248–250].

A method of bridging the gap between continuum damage mechanics and fracture mechanics with seamless consistency is provided by the *variational* approach to brittle fracture,

which is based on the fundamental principles of minimum energy [51, 80, 113, 253, 254], irreversibility of the fracture path [18, 43, 113, 175], and energy conservation [105, 106]. The variational theory was set out in [51, 84, 85] where the basic idea was to consider the fracture surface as an internal variable of the total energy function whose variation induced an energy dissipation. The presented (very general) formulation did not easily lend itself to a numerical framework because the fracture surface was not regularised. The numerical implementations of the variational approach to fracture were presented in [42, 43, 66, 185] where a zero-width crack was replaced by a regularised (diffusive) fracture zone. The regularisation was in a form of a gradient of the internal variable. In principle, the fracture representation was similar to some early non-local gradient-enhanced continuum damage models [86, 174, 206, 232, 237]; however, in the present case, the regularised fracture zone converges to a discrete crack when the regularising parameter tends to zero [66, 95, 177].

Recently, two notable fracture modelling strategies have emerged following the variation principle and non-local continuum damage mechanics, namely: the phase-field model (PFM) [10, 39, 187–189, 264] and the thick level set (TLS) model [36, 194, 239, 271]. In PFM, the fracture zone is described by a global fracture surface functional whose minimum corresponds to an exponentially decaying damage function from where the crack is localised (i.e. location of full damage). As the regularisation length-scale tends to zero, the diffusive fracture surface converges to a sharp crack topology [177, 185]. The main advantage of PFM is that the evolution of the system is entirely governed by a single energy functional whose time-continuous minimisation in terms of the displacement field and internal fracture surface variable yields the solution to the fracture growth problem. In TLS, a level set function [221, 222] is used to separate the undamaged zone from the fully damaged zone by a characteristic width where the damage varies monotonically from zero damage to full damage, i.e. the damage variable is an explicit function of the level set. The propagation of the damage front is driven by the so-called *configurational force* [113, 146, 273] that corresponds to the vector of maximal energy dissipation with respect to the (regularised) extension of the front of the level set. The numerical representation of the fully damaged region can be enhanced by enriching the standard finite element approximation with a ramped Heaviside function to completely decouple the opposite

sides of the fully damaged region [34, 36, 230]. Although the enrichment is not mandatory for TLS, it is beneficial especially for coarser meshes as the enrichment effectively removes any spurious cohesive tractions that may be transferred across the fully damaged zone by those nodes whose support bridges the fully damaged zone. The main advantages of TLS are similar to those of PFM in that the method can naturally initiate cracks, propagate them, and handle crack merging and branching without relying on *ad hoc* criteria. Thus, TLS and PFM are methods that effectively bridge the gap between continuum-damage mechanics and fracture mechanics. A comparison between the methods is given in [162].

The main drawback of PFM and TLS models is the same as of any other CDM based approach, which is the high computational cost of the spatial discretisation that is needed to approximate a discrete crack via strain localisation since a crack is effectively modelled at the constitutive level via the degradation of material stiffness. This cost can be prohibitive if it is required to simulate complex crack patterns such as crack branching and merging with a high resolution. On the other hand, the main difficulty with the FM approach is that a crack needs to be defined within the continuum context at the level of the geometry, i.e. as a moving boundary of the solid, so that the problem governing PDE's make sense within the volume of the solid continuum. Hence, it is necessary to manually track each crack and to manage crack intersections as they occur. In addition, a crack growth criterion needs to be provided to determine when, where and which cracks grow. Finally, the problem of crack nucleation can not be addressed naturally within the FM framework. Nevertheless, FM is the preferred choice when it comes to modelling discrete cracks, despite the practical difficulties. The field of (linear-elastic) fracture mechanics is well-established and the state of the art numerical methods greatly facilitate the integration of arbitrary discontinuities within a continuum discretisation such that accurate fracture solutions are possible.

The field of fracture mechanics was developed thanks to the pioneering work of Griffith [105, 106] who fundamentally changed the understanding of brittle material behaviour. He abandoned the classic notion of material strength, which did not make sense at a sharp crack tip (due to the infinite stress that was predicted by the elastic theory), in favour of a thermodynamically consistent approach which was to consider the energy required to create a unit free surface. Irwin [134, 136] extended the Griffith's relationship between the

thermodynamic driving force for fracture and the material surface energy by including the effects of plasticity and introducing the concept of material toughness which allowed the theory of linear-elastic fracture mechanics to be applied to a wider range of materials. The following section gives an overview of the theory of linear-elastic fracture mechanics.

1.3 Linear-elastic fracture mechanics

Griffith [105, 106] considered that the creation of a fracture surface (i.e. a crack extension) could be represented in an elastic solid by the sudden annihilation of the fracture surface tractions that held the material intact prior to crack growth. At the instance these forces disappear the material state is generally not that of equilibrium. Therefore, as a consequence of the minimum potential energy principle, the system moves to a state of equilibrium resulting in a decrease in potential energy. The potential energy decrease can be shown to be equal the energy that is released from opening a crack (or, equivalently, the work that would be required to close the crack faces). Consider the energy balance involved in a fracture extension ΔA. Under equilibrium conditions, the fracture energy ΔU_{Γ_c} equals the strain energy released ($-\Delta U_s$) plus the external work done ΔW_{ext}:

$$\Delta U_{\Gamma_c} = -\Delta U_s + \Delta W_{\text{ext}}, \tag{1.1}$$

$$\Delta U_{\Gamma_c} = -\Delta U_s + (-\Delta V), \tag{1.2}$$

$$\Delta U_{\Gamma_c} = -\Delta (U_s + V), \tag{1.3}$$

$$\Delta U_{\Gamma_c} = -\Delta \Pi \tag{1.4}$$

Constant external tractions are assumed which is why the external work done is equal to the decrease in the load potential, i.e. $\Delta W_{\text{ext}} = -\Delta V$. Thus, as the solid moves from the equilibrium state before the crack extension to the equilibrium state after the crack extension, the fracture energy equals to the decrease in the potential energy. Griffith supposed that the fracture phenomenon in an ideally brittle material is the macroscopic manifestation of the breaking of the material bonds at the atomic length scale. Accordingly, the average fracture energy per unit fracture area is the energy of inter-atomic cohesion,

which can be given as twice the material's surface energy γ_s (i.e. the energy that is required to create a unit of free surface area). The fracture energy can be expressed in rate form as:

$$\frac{\mathrm{d}U_{\Gamma_c}}{\mathrm{d}A} = 2\gamma_s \tag{1.5}$$

The factor *two* appears in (1.5) because the formation of a crack results in the creation of two identically matching surfaces[1]. It follows from (1.5) that fracture growth takes place as soon as there is sufficient energy available to overcome the resistance of the material:

$$-\frac{\mathrm{d}\Pi}{\mathrm{d}A} \geq 2\gamma_s, \tag{1.6}$$

where equality holds under energy conservation conditions. Although Griffith [105] obtained good agreement between theoretical and experimental result for glass samples, his theory significantly underestimated the fracture strength of metals where the effects of plastic flow are important. Irwin [134, 136] and Orowan [219, 220] independently modified the Griffith's model to account for other possible mechanisms of energy dissipation (that is, other than surface energy alone). Specifically, the application of the Griffith's model was extended to quasi-brittle materials (i.e. materials that can exhibit localised inelastic behaviour in the vicinity of a crack tip) by using a revised form of the fracture energy:

$$\frac{\mathrm{d}U_{\Gamma_c}}{\mathrm{d}A} \equiv 2\gamma_s + \frac{\mathrm{d}W_p}{\mathrm{d}A} \tag{1.7}$$

$$\frac{\mathrm{d}U_{\Gamma_c}}{\mathrm{d}A} \equiv 2(\gamma_s + \gamma_p), \tag{1.8}$$

where it assumed that the rate of plastic work done $\mathrm{d}W_p/\mathrm{d}A$ due to dislocation motion in the vicinity of the crack tip is concentrated in a sufficiently narrow band around the crack such that this phenomenon can be considered an intrinsic material property. In this case, the definition $\frac{\mathrm{d}W_p}{\mathrm{d}A} = 2\gamma_p$ can be used, where $2\gamma_p$ is the material-specific constant of plastic dissipation per unit fracture area. For ductile materials, γ_p is typically several orders of magnitude greater than γ_s. Irwin [135] later generalised the material's resistance to fracture growth be defining G_c as the critical energy release rate of the material. G_c,

[1] Note the difference between *fracture surface area* and *fracture area*; fracture surface area refers to the area of the fracture boundary, whereas fracture area is the area over which material separation takes place, i.e. is synonymous with fracture length in 2D. As such, fracture area is equal to one-half of the fracture surface area.

which is an empirically determined material constant, can include the effects of plasticity, viscoplasticity or viscoelasticity, as well as the effects of micro-scale crack meandering and micro-branching, etc.; however, the basic assumption is that all inelastic phenomena are to be confined within a sufficiently small region near the crack such that the rate of plastic dissipation is constant with respect to fracture growth. Under these assumptions, the size and shape of the plastic zone, which generally depend on the mode of loading at the crack tip, does not significantly influence the value of G_{c}. In other words, G_{c} is considered as the macroscopic material parameter that is effectively the constant of proportionality between the amount of fracture area created (ΔA) and the amount of energy dissipated ($-\Delta\Pi$). In accordance with the energy conservation principle, the energy balance equation for a fracture area extension under equilibrium conditions can be expressed as follows:

$$-\frac{\mathrm{d}U_s}{\mathrm{d}A}+\frac{\mathrm{d}W_{\mathrm{ext}}}{\mathrm{d}A}=G_{\mathrm{c}} \tag{1.9}$$

$$-\frac{\mathrm{d}\Pi}{\mathrm{d}A}=G_{\mathrm{c}} \tag{1.10}$$

Irwin [132–136] defined a fracture driving force G_{s} as the rate of potential energy decrease:

$$G_{\mathrm{s}}=-\frac{\mathrm{d}\Pi}{\mathrm{d}A} \tag{1.11}$$

Consequently, the onset of fracture growth takes place when for a monotonically increasing external load the so-called fracture driving force G_{s} reaches the threshold value of G_{c}.

1.4 Material model

Stress analysis of Smart-Cut™ cracks from the point of view of linear-elastic fracture mechanics (LEFM) has been undertaken by [81, 82, 87, 108–110, 307]. Once the defects have grown to several tens of micro-metres, it is generally accepted that the dominant mechanism driving crack growth is the mechanical action of the hydrogen gas pressure [15, 233]; other mechanism at this length-scale, such as the action of the thermodynamic and chemical forces on the crack evolution are considered to be relatively insignificant. Since the goal is to quantify micro-crack evolution into macro-cracks and to simulate

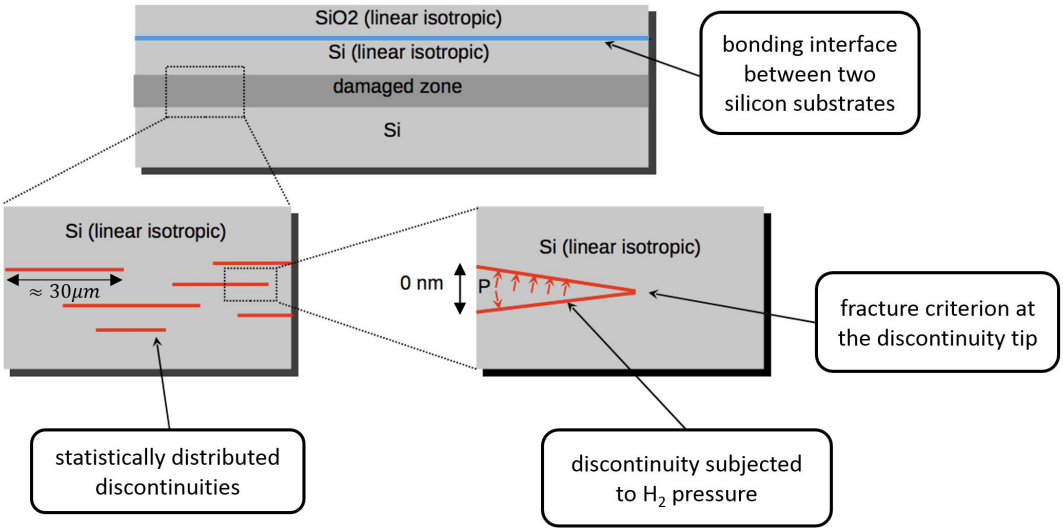

FIGURE 1.1: Linear-elastic fracture mechanics approach to modelling of silicon wafer splitting. The silicon is assumed to be a perfectly brittle homogeneous isotropic continuum with a constant fracture toughness. Cracks is modelled by zero-thickness discontinuities in the displacement field.

wafer splitting, a solid-continuum model of the silicon wafer structure (refer to Figure 1.1) is considered to be an adequate approximation. At the typical Smart-Cut™ annealing temperatures of 500°C, it is fair to assume a brittle and linear-elastic material behaviour and to model micro-cracks as zero-thinness discontinuities in the displacement field. For simplicity, we will assume the different material layers of the wafer structure to be homogeneous and isotropic; with regard to the damaged silicon layer, it will be assumed to have an effectively reduced stiffness relative to the surrounding silicon and to have a uniform and a direction-independent fracture toughness.[2] From the beginning of thermal annealing, the evolution of cavities is observed to be slow up to a critical point when unstable crack growth is set off and an abrupt splitting of the wafers is achieved [233]. Thus, for the majority of the time, it is reasonable to regard the evolution of micro-cracks as essentially a quasi-static process. However, in this final stage when inertial effects become important, the quasi-static assumption limits the ability to describe the material behaviour adequately. Consequently, certain fracture phenomena in the dynamic regime will not

[2] Note that the monocrystalline silicon is naturally an anisotropic material; however, the variations in the mechanical properties are quite small [76, 81]. Furthermore, due to the ion irradiation damage the damaged silicon layer becomes somewhat amorphous such that it is fair to assume homogenised material properties.

be possible to capture using the quasi-static model.[3] Nonetheless, the fracture roughness features that can be attributed to dynamic evolution and coalescence are different from those of quasi-static micro-crack evolution and coalescence. This is because the roughness frequencies of micro and macro crack evolutions are distinct [5]. Thus, in spite of omitting the dynamic aspect, the quasi-static solution is still useful since experimental correlations can be made by focusing on the roughness frequencies that result from micro-crack propagations. Finally, it is important to highlight that quasi-static crack growth normally implies stable crack growth. However, most fracture phenomena are unstable, i.e. the fracture driving force tends to increase with fracture length. The stable (quasi-static) micro-crack growth in silicon can result from hydrogen embrittlement that locally reduces the apparent fracture toughness of silicon [81, 108, 290]. However, as soon as a micro-crack advances, new (virgin) silicon is exposed that has a higher toughness; thus, crack growth halts until either sufficient pressure in the cavity develops and/or the fracture toughness is diminished by the chemical interactions of hydrogen with silicon. Thus, for the majority of the thermal annealing time, crack growth is stable until some critical crack size is reached that triggers the onset of unstable (catastrophic) crack propagation through the wafer.

Figure 1.1 shows a diagram of the bonded wafer structure. Normally, the bonding interface between the two silicon substrates is imperfect [110]. Specifically, when the donor wafer and the handle wafer are bonded together, some bonding flaws exist due to the lack of smoothness of the bonding surfaces and/or due to the contamination of the bonding surfaces with environmental particulates. These bonding flaws reduce the stiffening effect of the handle wafer causing cracks to deviate towards regions of lower relative stiffness. When the wafer structure is subjected to thermal annealing, the interfacial flaws inflate due to some of the mobile hydrogen migrating into the interfacial flaws. The local changes in the stress field influence crack propagations. In our model, we will assume the more ideal case of sufficiently smooth bonding surfaces and environmental control conditions such that the effects of bonding flaws are minimum. In other words, the flaws are assumed to be small relative to the size of micro-cracks and the crack-to-flaw separation distance.

[3] For example, at the onset of dynamic crack growth, sound waves are generated from the fracture tips that propagate and interact with other ongoing cracks. The sound wave reflections and the resulting deflections of macro-cracks are the cause of some particular kinds of defects in the post-split surface [5], e.g. surface pits.

1.5 Numerical method

The finite element method (FEM) [33, 46, 312, 313] is an indispensable numerical tool in modern engineering for finding approximate solutions to partial differential equations (PDE's). Although FEM is best suited to problems involving smoothly varying fields, the method can also be applied to the modelling of *weak* and *strong* discontinuities; however, the discontinuity needs to be taken into account during mesh generation. This can be cumbersome if the discontinuity takes a complex shape or if it evolves over time such that constant remeshing is required. Nonetheless, advances in meshing techniques [94, 166] have enabled FEM to be used effectively to solve elaborate fracture mechanics problems involving multiple crack growth in both 2D and 3D; see for example [40, 41, 224–227].

It is known that the accuracy of the numerical solution close to a crack tip tends to deteriorate because of the singular stress/strains field [131, 294, 297]. The classic FEM approximation is incapable of reproducing the characteristic square-root singular stresses because the classic FEM uses polynomial approximations whose spatial derivatives are bounded; hence, the infinite stresses are impossible to reproduce. One of the earliest methods of numerically coping with the singular stresses/strains at the crack tip was to use local mesh refinement (e.g. a dense concentric mesh at the crack tip) in combination with the so-called *quarter-point* elements [21, 22, 118] that embodied the square-root singular spatial derivatives at the crack tip. These special elements can be derived from standard isoparametric quadratic elements by collapsing one element edge onto the crack tip and then positioning the middle nodes of the element edges emanating from the crack tip to 1/4 the edge length away from the tip. Although this strategy is easy to incorporate within standard FEM implementations and it gives an improvement to the numerical solution it is sub-optimal in terms of the solution convergence rate with mesh refinement.

However, some numerical difficulties can not be easily circumvented within FEM. For instance, accuracy is lost if state variables need to be mapped between different meshes such as in non-linear or history-dependent problems. Also, having to constantly remesh around a propagating crack tip and to adapt the mesh to the fracture surfaces may

eventually lead to practical difficulties especially in multi-crack growth problems where complex crack geometries can naturally arise. Alternative discretisation methods that avoid using a mesh have been applied to the modelling of stationary and growing cracks. These include the boundary element method (BEM) [45, 61, 238] and the meshfree methods (MM) [29, 156]. BEM is not well-developed for non-linear deformations and the resulting system of equations tends to be computationally difficult to solve due to the lack of symmetry and sparsity. Meshless methods are also not as computationally efficient as mesh-based methods; nonetheless, the element-free Galerkin meshless method (EFG) [26, 28, 32] offers some practical advantages in the representation of cracks. Within the meshless framework, a strong discontinuity can be incorporated in either of two ways: (1) by modifying the "visibility" of the weight function, or (2) by enriching the meshless approximation. Firstly, the purpose of the weight function in MM's is to *weight* the importance of the nearby degrees of freedom to the approximation at a particular point. As such, the weight function plays a critical role in the solution accuracy and stability. The idea of the visibility criterion is to sharply terminate the smoothly varying weight function at a crack interface so that the approximation is not influenced by the material points on the opposite side of the crack. This way, the displacement approximation on either side of the crack is naturally decoupled. However, the application of the visibility criterion in the region close to a crack tip tends to be somewhat heuristic; methods such as *diffraction*, *transparency* and *see-through* have been proposed [26, 165, 218]. The second way of incorporating cracks within MM's is by enriching the standard meshless approximation [83, 240, 282] by the addition of special terms that can capture the essential properties of the solution such as discontinuities and singularities. Local enrichments can be realised through the partition of unity method [67, 68, 165], which will be described later in this section. A review of meshless methods for fracture modelling is given by [29, 209].

The major weak points of MM's in comparison to the mesh-based methods is the high computational cost of the meshless basis functions since they need to be constructed at every point anew. Furthermore, these shape functions are non-polynomial (rational) functions which means that a high order integration scheme is required to compute the weak form of Galerkin-type meshless methods, such as EFG. Also, the essential boundary

conditions are not as simple to enforce as in FEM since the meshless shape functions lack the so-called Kronecker delta property; however, a few techniques are available such as the Lagrangian multiplier method, penalty method and the Nitche's method [209, 245].

In fracture mechanics problems that involve cohesive cracks (where the stress singularity is no longer an issue), remeshing within the FEM framework may be circumvented entirely as well as the need for crack growth criteria. This is achieved by incorporating zero-thickness *interface* elements along inter-element boundaries that can intrinsically exhibit a cohesive traction-separation law pertinent to the material at hand [99, 256, 305]. Consequently, crack initiation, branching and bifurcation can be captured naturally as part of the solution, which is especially useful in solving dynamic crack propagation problems where such phenomena tend to arise. On the downside, because interface elements are placed along inter-element boundaries prior to the simulation, the fracture path suffers to some extent from mesh bias; specifically, the crack path tends to zigzag in an unstructured mesh, which leads to an overestimated fracture energy. In addition, a cohesive law introduces a non-linearity into the system, which means that the discrete equilibrium equations needs to be solved iteratively. Nonetheless, interface elements are desirable in applications where the crack path is known in advance, such as in modelling delamination of composites [9, 186, 280] or inter-granular failure of polycrystalline materials [78, 79].

To enable a more natural appearance of cracks within elements and to circumvent the need for adaptive remeshing during crack propagation, a viable alternative within the cohesive crack context is the embedded finite element method (EFEM) [169, 171, 215, 216, 301]. The idea is to enrich the continuous displacement approximation of the standard finite elements that are cut by a crack with the addition of discontinuous displacement modes so that the features of the cohesive crack can be reproduced naturally. Subsequently, the degrees of freedom associated with the discontinuous enrichments can be condensed out at the element level (i.e. prior to the assembly of equations) by imposing equilibrium conditions between the stresses in the bulk of the element and the tractions corresponding to the cohesive laws acting on the crack surfaces. The main criticism of EFEM is that the displacement jumps are not continuous across element boundaries and that this inconsistency can lead to unexpected approximation errors. Nevertheless, the method is

convergent with mesh refinement and the enriched elements can capture the behaviour of a crack well in general. In contrast to using cohesive interface elements, EFEM requires a crack growth criterion to determine when and which elements need to be enriched with discontinuous modes. To this end, the maximal tension criterion is typically used, in which case the crack growth direction is normal to the plane of maximum tension and the onset of crack growth occurs once this stress exceeds the yield strength of the material.

EFEM can be categorised as an element-enrichment approach since the enrichment is introduced at the element level. An alternative enrichment strategy is to enrich the finite element basis at the nodes. This is done via the partition of unity method (PUM) [179, 180].

First of all, the partition of unity (PU) is a property of a set of function $\{N_I\}$ defined in a domain Ω whose sum at any point is equal to unity, i.e. $\forall \mathbf{x} \in \Omega$, $\sum_{\forall I} N_I(\mathbf{x}) = 1$. The finite element basis functions form a PU, which enables the finite elements to reproduce rigid body translations and to satisfy the patch-test (i.e. the ability of an element patch to undergo constant strains). These are essential properties of finite elements for the convergence of solutions [313]. Within nodally-enriched formulations, the enrichment functions are introduced via the partition of unity method. As a result, any enrichment function $\Psi(\mathbf{x})$ introduced via PUM can be reproduced exactly, e.g. $\sum_{\forall I} N_I(\mathbf{x})\Psi(\mathbf{x}) = \Psi(\mathbf{x})$.

One of the first nodal enrichment methods was the cloud-based *hp* finite element method (*hp*-FEM) [67, 68, 92, 212]. The idea of *hp*-FEM is to locally enhance the approximation properties of the standard finite element basis by introducing hierarchical polynomial functions via PUM. The resulting functions, called *hp*-clouds, have local support where the cloud basis functions are defined (e.g. over a patch of size h), and the basis functions can recover the enrichment polynomial (of degree p) exactly via their linear combination. The particular advantage of the cloud-based *hp*-FEM is that adaptive *hp*-refinement can be carried out locally without changes to the underlying mesh. This is in contrast to the classic *hp*-FEM [17] where finite elements of variable size (h) and polynomial degree (p) are used to adaptively refine the discretisation. However, p-refinement usually breaks the continuity between inter-element boundaries; hence, special blending (or transitional) elements are needed in order to smoothly *blend* different orders of approximations.

Nodal-enrichment is also the idea of the extended finite element method (XFEM) [27, 30, 192], which was developed around the same time as the cloud-based *hp*-FEM. In XFEM, the kinematics of the classic (continuous) finite element space is *extended* by the addition of discontinuous functions associated with the non-smooth features of a crack: discontinuous displacements, the high strain gradients and the strain singularity at the crack tip. In contrast to EFEM, nodal enrichment allows the displacement jumps to be continuous across element boundaries. Moreover, XFEM is naturally suited to modelling cohesionless cracks, which means that the linearity of the system of equations is preserved.

In the context of linear-elastic fracture mechanics (LEFM), the idea of XFEM is to use two kinds of enrichment functions for the representation of cracks. These enrichment functions are, namely: the branch functions – a set of singular functions that span the leading order solution of plane-elasticity crack tip asymptotic fields [294, 297], and a Heaviside enrichment function – a discontinuous function that causes a jump in the field across the crack interface [27, 57, 292]. In XFEM, a PU for the nodal enrichment is typically formed using Lagrangian polynomials of compact support (oftentimes by reusing the finite element shape functions). This allows an enrichment function to be defined locally where it is needed, e.g. at a discontinuity in the displacement field or close to a crack tip where the stresses are singular. The local enrichment property of XFEM is different from some of the alternative enrichment strategies that enrich globally, such as in the generalised finite element method (GFEM) [179, 180, 272].[4] Concerning the computer solution to the discrete elasticity problem, local support of an enrichment function has the benefit of preserving the sparsity of the system of equations. Hence, the equations are computationally more efficient to solve. The computational benefits of sparsity would be lost if an enrichment function were to be added directly to the finite element approximation without using the PU method. In addition, the degrees of freedom of the enriched basis functions allow for some local readjustment of the enrichment function so that the finite element solution is more optimal (in the minimum energy sense). A comparison of EFEM with XFEM involving cohesive cracks and the Heaviside enrichment function is presented by [216]. The solution accuracy and convergence rates were found to be similar although

[4] Although recently, methods under the GFEM name have assumed local PU enrichment [31, 69, 153].

EFEM was found to be more efficient on coarser meshes and with an increasing number of cracks. Comprehensive reviews of XFEM/GFEM can be found in [3, 31, 89, 91, 150, 309].

An efficient way to describe static or moving surfaces within XFEM/GFEM is by using the level set method (LSM) [221, 222]. In LMS, an interface is represented implicitly by the zero value of its level set function, where the level set function is a signed-distance function to the interface. In a discrete framework, the level set can be conveniently stored at the element nodes. Subsequently, the finite element shape functions can be used to interpolate the level set within an element (e.g. for evaluating enrichment functions). As an interface evolves over time, the level set can be updated by solving the level set equation (an advection-type partial differential equation) [221, 222] or, in the case of cracks, by simply recomputing the level set where it is required (since most of the crack surface remains fixed) [50, 281, 282]. XFEM, coupled with LSM, has been used to solve problems involving weak discontinuities, such as: the elastic field due to a matrix inclusion [27, 275], material solidification and phase transformation [58, 141, 183], biofilm growth [70], convection-dominated high-gradient [2] and multi-phase fluid flow [255] problems. Also, XFEM and LSM go hand-in-hand in modelling strong discontinuities, such as: evolution of multiple cracks [50, 62, 72, 104, 270, 281], cohesive crack growth [139, 140, 153, 184, 193, 311], hydraulic fracturing [100–102], fatigue [60, 93, 229, 269, 274] and dynamic [182, 201, 293] crack growths. However, in the case of cracks, which from the viewpoint of the level set are open surfaces, at least two level set function are needed per crack [72, 270]: one to localise the fracture front and another for the fracture surface. The fracture front is then defined as the intersection of the zero level sets of the two functions.

Even though LSM and XFEM couple quite naturally, LSM is not mandatory for XFEM. Besides, the fully implicit description of cracks by level sets is not the most convenient method of tracking multiple cracks because detecting crack intersections between non-planar crack surfaces tends to be computationally cumbersome and prone to inaccuracies [72, 90, 93, 124]. A more pragmatic approach is to adopt a hybrid (explicit-implicit) crack representation [90, 93] whereby the crack geometry is represented explicitly (e.g. as a poly-line in 2D or a polygonal surface in 3D) and the level set functions for the fracture surface and fracture front are computed based on the explicit crack geometry only for the

purposes of evaluating the enrichment functions. Within this framework, crack geometry is tracked and updated explicitly during crack growth and the intersections between cracks are determined exactly. The hybrid approach offers increased robustness and accuracy in comparison to the fully implicit description of cracks [72, 104, 270, 282].

The present numerical model combines XFEM with the hybrid crack representation technique, i.e. the crack geometry is described explicitly and the enrichment functions are evaluated based on the level sets constructed with respect to the explicit crack geometry. The main limitations of the proposed numerical method is that crack nucleation and bifurcation are not possible to capture naturally.[5] Specifically, the XFEM discretisation of the solid is mainly concerned with resolving the elastic field with (potentially) multiple intersecting cracks. Since the fracture path is not part of the elastic solution, an appropriate crack growth criterion needs to be introduced in order to model crack growth within XFEM. The following section reviews some basic criteria that are commonly used in LEFM.

1.6 Crack growth criteria

This section gives a reviews of some of the classic crack propagation criteria that are used in solving linear-elastic fracture mechanics (LEFM) problems. The discussion of the different criteria is separated into two parts. The first subsection focuses more on the crack growth direction, wheres the following subsection address the onset of crack growth.

1.6.1 Crack growth direction

According to the theory of linear-elastic fracture mechanics (LEFM), the stress field close to a crack tip is square-root singular [294, 297]; specifically, the stress can be expressed as:

$$\sigma_{ij} \approx \frac{K}{\sqrt{2\pi r}} f_{ij}(\theta), \tag{1.12}$$

[5] Such phenomena may be captured using appropriate criteria; however, this is beyond the present research scope. Moreover, there is no evidence that crack bifurcations are possible during quasi-static crack growth.

where (r, θ) are the polar coordinates centred at the crack tip, $f_{ij}(\theta)$ are functions of the polar angle θ that depend on the geometry and loading conditions, and where K is the so-called stress intensity factor [136, 137] that scales linearly with the external load magnitude. Due to the infinite stresses at the crack tip (even for an infinitesimally small load) it is not possible to directly apply the classic material yield criteria as fracture criteria. In the framework of LEFM, material failure (i.e. crack growth) is assessed by considering the *intensity* of the stresses at the crack tip, i.e. the stress intensity factors (SIF's). The SIF's are the coefficients of the leading order (singular) terms of the linear-elastic near-tip asymptotic stress solution [294, 297]. These coefficients are denoted by: K_I, K_{II} and K_{III}, and they are respectively called: the mode-I (symmetric opening mode), mode-II (antisymmetric sliding mode) and mode-III (out-of-plane antisymmetric tearing mode) stress intensity factors [136, 137]. The SIF's are sufficient to completely characterise the near-tip field of any structural geometry or loading conditions. The fracture toughness K_{Ic} (Pa$\sqrt{\text{m}}$) is usually measured under pure mode-I loading conditions (although fracture toughnesses with respect to other modes of loading can also be measured). The typical fracture mechanics problem is to assess the SIF's for a given fracture geometry and loading conditions and to determine the direction of crack growth and if crack growth is possible.

In the framework LEFM, there are various criteria that have been proposed for solving mixed-mode crack propagation problems. Most commonly used criteria can determine both: the instance of crack growth and the direction of crack growth; however, some criteria can only determine one but not the other. The most well known criteria in LEFM are: the maximum tangential stress (MTS) criterion [44, 75, 178, 195, 196] (also referred to as the maximum hoop stress criterion), the maximum energy release rate (MERR) criterion [116, 128, 149, 205, 223, 298–300] and the minimum strain energy density (MSED) criterion [260, 261]. The aforementioned criteria can be used to determine both the direction and the onset of crack growth. On the other hand, the criterion based on the principle of local symmetry (PLS) [97, 122, 148] can only be used to determine the direction of crack growth. A comparison of different crack propagation criteria can be found in [40, 74, 247, 257, 259].

A brief review of the different criteria is given as follows. The MTS criterion is based on the consideration of the stress close to a crack tip, i.e. $r \to 0$. According to the MTS

criterion, a crack propagates in the direction perpendicular to the plane of maximum stress and when the stress intensity reaches a critical material value. This can be expressed as:

$$\frac{\partial \sigma_{\theta\theta}}{\partial \theta} = 0 \tag{1.13}$$

$$\frac{\partial^2 \sigma_{\theta\theta}}{\partial \theta^2} < 0 \text{ at } \theta = \theta_{\mathrm{c}} \tag{1.14}$$

$$\sigma_{\theta\theta \mathrm{c}} = \frac{K_{I\mathrm{c}}}{\sqrt{2\pi r_0}} \tag{1.15}$$

The critical crack growth angle θ_{c} is determined on the basis that the plane of maximum (principle) stress $\sigma_{\theta\theta \mathrm{c}}$ needs to coincide with the plane of vanishing shear stress $\tau_{r\theta}$. Within the LEFM theory, θ_{c} is obtained as the solution to the following equation [74, 75, 195]:

$$K_I \sin\theta_{\mathrm{c}} + K_{II}(3\cos\theta_{\mathrm{c}} - 1) = 0, \tag{1.16}$$

$$\therefore \theta_{\mathrm{c}} = 2\arctan\left(\frac{1 - \sqrt{1 + 8(K_{II}/K_I)^2}}{4K_{II}/K_I}\right) \tag{1.17}$$

From (1.17), the bounds on the tip deflection angle are: $\lim_{K_{II}/K_I \to \pm\infty} \theta_{\mathrm{c}} = \mp \arccos(1/3)$. The maximum energy release rate criterion (MERR) is an extension of Griffith's theory of fracture. The criterion is generally stated as:

$$\frac{\partial G_{\mathrm{s}}}{\partial \theta} = 0 \tag{1.18}$$

$$\frac{\partial^2 G_{\mathrm{s}}}{\partial \theta^2} < 0 \text{ at } \theta = \theta_{\mathrm{c}} \tag{1.19}$$

$$G_{\mathrm{c}} = \frac{K_{Ic}^2}{E} \tag{1.20}$$

The Irwin's formula for the energy release rate G_{s} at any crack branch angle θ is given in terms of the SIF's k_I and k_{II} existing at the tip of the infinitesimally small crack branch [116, 134, 253]: $G_{\mathrm{s}} = (k_I^2 + k_{II}^2)/E$. However, the closed form solutions to $k_I = k_I(K_I, K_{II}, \theta)$ and $k_{II} = k_{II}(K_I, K_{II}, \theta)$ are not available at present. Nevertheless, expansions of the SIF's k_I and k_{II} have been proposed by several authors [11, 116, 149, 161, 253, 254, 298–300]. The minimum strain energy density (MSED) criterion postulates that crack growth takes place in the direction of minimum strain energy density and when the strain energy

density factor S reaches the critical material value S_c. The MSED criterion can be given as:

$$\frac{\partial S}{\partial \theta} = 0 \tag{1.21}$$

$$\frac{\partial^2 S}{\partial \theta^2} > 0 \text{ at } \theta = \theta_c \tag{1.22}$$

$$S_c = \frac{K_{Ic}^2}{8\pi\mu}(\kappa - 1) \tag{1.23}$$

where μ is the shear modulus, $\kappa = 3 - 4v$ for plane strain and $\kappa = (3 - v)/(1 + v)$ for plane stress problems. The strain energy density factor is defined in closed form as [260, 261]:

$$S = a_{11}K_I^2 + 2a_{12}K_I K_{II} + a_{22}K_{II}^2 \tag{1.24}$$

where

$$a_{11} = \frac{1}{16\pi\mu}(1 + \cos\theta)(\kappa - \cos\theta), \tag{1.25}$$

$$a_{12} = \frac{1}{16\pi\mu}\sin\theta(2\cos\theta - \kappa + 1), \tag{1.26}$$

$$a_{22} = \frac{1}{16\pi\mu}\left((\kappa + 1)(1 - \cos\theta) + (1 + \cos\theta)(3\cos\theta - 1)\right) \tag{1.27}$$

The criterion of local symmetry (PLS) states that a crack shall grow in the direction where the local stress field at the tip of an infinitesimal crack branch is of mode-I type, i.e. the mode-II stress field vanishes ($k_{II} = 0$). Note that the PLS criterion can only be used for isotropic materials and only for determining the direction of crack growth; it can not be used to determine the onset of crack growth. Consequently, the PLS criterion needs to be augmented by another criterion that can determine the onset of crack growth [195, 196].

1.6.2 Onset of crack growth

Most of the fracture criteria in LEFM make use of the crack tip SIF's to determine the onset of crack propagation. Essentially, a given criterion evaluates a particular combination of the SIF's under general mixed-mode loading conditions to determine if the combination is critical for the onset of crack growth [157, 197, 254]. The exclusive reliance on the crack tip SIF's K_I and K_{II} (for plane-strain or plane-stress, and K_{III} for 3D applications) is

reasonable because the SIF's characterise the near-tip field uniquely and because fracture is a local phenomenon from the viewpoint of LEFM, i.e. crack growth is governed by the material state at the crack tip. For example, the previous criteria: MTS, MSED, and (theoretically) MERR can be expressed in terms of the SIF's K_I and K_{II} (assuming 2D). Thus, it is generally possible to define a *fracture locus* that determines when a particular combination of the SIF's is critical and, hence, when crack growth is likely to take place.

The fracture locus, is either the byproduct of a crack growth criterion (e.g. MTS, MERR, MSED) or it can be derived empirically for a specific material. As an example, it is possible to consider a fracture locus model of the following form [157, 197]: $\left(\frac{K_I}{K_{Ic}}\right)^a + \left(\frac{K_{II}}{K_{IIc}}\right)^b = 1$, where a and b are some real coefficients that are determined theoretically or experimentally. Some generic criteria include: linear ($a = b = 1$), elliptic ($a = b = 2$), quadratic models. Of course, the criterion model can be tuned to more precisely fit a particular application, e.g. Advani/Lee [6], Awaji/Sato [16] and Palanisawamy/Knauss [223] fracture loci models. If the material experiences small scale yielding (SSY) at the crack tip [127, 249], it can be practical to use a material specific fracture locus for determining the onset of crack growth. On the other hand, the direction criterion can be chosen so as to best reflect experiments.

When a significant region around the crack tip has undergone plastic deformation, other criteria may be more suitable for determining the possibility of crack growth. Within the framework of elastic-plastic fracture mechanics (EPFM), Dugdale [73] proposed a yield-strip model of the plastic zone in front of the crack tip. From experimental observations of mode-I crack growth in thin metal sheets [73, 115], the yielded zone was observed to localise in a narrow strip just ahead of the crack. The vertical thickness of this strip was observed to approach that of the thin metal sheet. Dugdale, proposed a superposition analysis to solve for the critical length of the yield strip by considering two elastic solutions: before and after the strip was introduced. Constant tractions equal to the yield strength of the material were assumed along the length of the strip. The strip length was calculated on the basis that the stress singularity should vanish at the tip of the fictitious crack extension. Later, Wells [291] proposed a crack propagation criterion based on the crack tip opening displacement (CTOD) for materials exhibiting considerable plasticity at the crack tip. The equivalence between Dugdale's yield-strip criterion (in terms of the critical length of

yield strip) and the CTOD criterion (in terms of the critical crack mouth opening) was demonstrated by Wells to be in close agreement with respect to the crack extension force. The equivalence between Dugdale's and Wells' criteria was verified by Rice [248] via the J-integral. At around the time Dugdale proposed the yield-strip model, Barenblatt [19, 20] introduced the cohesive zone model (CZM). The model was a more general approach to the approximation of the yielded zone because it allowed for non-constant tractions along the length of the cohesive zone that depended on the material traction-separation law. The main difference between Barenblatt's model and Griffith's approach [105, 106] was that Griffith supposed that the interatomic attraction caused no deformation of the material on the macroscopic scale since the interactions were assumed to act over a zero distance.

One of the most powerful computational methods of assessing the fracture driving force in non-linearly elastic solids is the J-integral. It was first introduced by Eshelby [77] and then popularised by Rice [248–250] and Cherepanov [56]. The expression for the J-integral is derived based on the conservation principles of energy and momentum; hence, the integral is path-independent. When the J-integral is evaluated around a notch, it gives a measure of the strain energy concentration; when it is evaluated around a crack tip, it gives the rate of potential energy decrease with respect to the crack extension, i.e. the J value is equal to the fracture energy release rate ($G_{\mathrm{s}} = J$). Furthermore, as a generalisation of non-linearly elastic material behaviour, the J-integral can be applied to elastoplastic fracture problems as a criterion for the onset of crack growth [1, 25, 248], e.g. when J reaches a critical material value of $J_{I\mathrm{c}}$. Although the original form of the J-integral does not allow for the unloading of the material that has undergone plastic deformation, it is possible to include these effects in terms of residual strains/stresses [12, 157, 197]. Despite the versatility of the J-integral in assessing the fracture driving force in non-linearly elastic or plastic materials, The J-integral does not provide the crack growth direction under general mixed-mode loading conditions. In other words, the crack is always assumed to be growing along a straight path. Nonetheless, the concept of the J-integral can be extended to evaluate the crack tip SIF's [308], which can then be used in other crack growth criteria. The following section describes some of the methods used in the extraction of SIF's.

1.7 Evaluation of SIF's and ERR's

Crack tip stress intensity factors (SIF's): K_I (opening mode), K_{II} (sliding mode), and K_{III} (out-of-plane tearing mode) are important quantities LFEM as they uniquely quantify the stress intensity and the deformation at the crack tip due to some remote loading. Since the SIF's are able to characterise the crack tip field uniquely, regardless of the loading conditions or structural geometry [294, 297], they are often used in LEFM to determine crack growth; specifically, for determining the onset and the direction of crack propagation. Consequently, it is important to determine the crack tip SIF's accurately in order to be able to predict when and where cracks grow. Several methods have been proposed in the literature for the extraction of SIF's. These methods can be grouped as either *direct* or *indirect*. Direct techniques tend to be the simplest to apply, but also tend to be the least accurate. The SIF are determined by directly correlating the crack tip field quantities of the solution to the problem at hand with a known (auxiliary) solution (e.g. near-tip asymptotic pure mode-I, II, or III field). Most often, correlations of the crack tip opening displacements are used [157, 197]. Indirect methods, on the other hand, are usually based on domain integral quantities. As a general rule, indirect methods are more accurate due to the averaging effect of integration, which filters out small numerical oscillations. One of the most well-known indirect method is the so-called J-integral (a type of a path independent energy conservation integral) [248–250] and its domain variant [98, 198, 265] for determining the crack tip energy release rate (ERR). However, the J-integral only provides the net ERR under self-similar crack growth conditions. As such, the crack tip needs to be subjected to a single (and a known) mode of loading (e.g. pure mode-I, II or III) in order to obtain the corresponding SIF form the ERR. Nonetheless, the J-integral serves as the foundation for many other energy/momentum conservation integrals for the evaluation of crack tip quantities under general mixed-mode loading conditions. One such closely related integral is the so-called *interaction* integral (also referred to as the M-integral) [308]. As the name suggests, the integral extracts one of the SIF's by means of superposing two solutions: the current solution and a suitable auxiliary solution (e.g. near-tip asymptotic pure mode-I, II, or III field), and then commuting the

interactive part of the J-integral (ERR); the interactive part can then be related to the particular SIF being sought. The method essentially exploits the property that the total ERR is the superposition of ERR's with respect to each different mode. To determine all SIF's of the current solution, the M-integral needs to be evaluated with respect to each mode separately. A more pragmatic approach [172, 302, 303] is to embed SIF's as unknown degrees of freedom (DOF's) in the enriched displacement field approximation of XFEM/GFEM by employing the DOF's gathering enrichment strategy [7, 8, 158, 279]. In this case, the crack tip SIF's are determined as part of the solution to the linear system of discrete equilibrium equations. For the good accuracy of the SIF's using the DOF's gathering approach, the enriched displacement field approximation needs to contain not only the leading order but also higher order terms of the linear-elastic crack tip asymptotic field [7, 172, 302, 303]. A similar technique for obtaining the SIF's or even the ERR's is to evaluate the Irwin's crack closure integral [132–134, 136] in closed form using the enriched DOF's that correspond to the coefficients of the crack tip asymptotic field functions [159, 203]. A simpler alternative to the explicit evaluation of the Irwin's crack closure integral is the virtual crack closure technique (VCCT) [117, 155, 203]. The principle is essentially the same as Irwin's in that the the work required to close the crack over a certain length must be equal to the energy required to propagate the crack over that same length; however, the main difference is that the VCCT was originally applied within the classic finite element framework considering nodal forces on opposite crack surface nodes and then computing the work required by these forces to bring the crack surface nodes together. Subsequently, the crack opening and sliding energies (works of crack closure) could be related to the crack tip SIF's using the Irwin-Griffith relationship [134]. A very versatile method for computing the crack tip energy release rate is the virtual crack extension method (VCEM) [117, 129, 130, 168] and the closely related stiffness derivative approach [63, 168, 228, 286]. Essentially, both methods compute the energy release rate (and, if required, its derivatives) by differentiating the potential energy of the system with respect to the crack tip extension length. In discrete form, this leads to perform differentiation of the stiffness matrix with respect to the local changes in the mesh geometry surrounding the crack tip. Crack tip SIF's can also be obtained by applying the superposition principle [308]; specifically, a particular SIF can be extracted by superposing the solution at hand with an auxiliary

solution and then computing the interactive part of the energy release rate from which the SIF can be determined. The main advantage of the stiffness derivative method is that it provides a very general framework for computing energy release rates (and their rates) with respect to arbitrary changes in the fracture geometry. This property will be exploited in Chapter 3 in determining the crack extension ERR with respect to different directions.

1.8 On crack kinking

The three most often used criteria are: the maximum tension criterion [74, 75, 195], the local symmetry criterion [122, 147], and the maximum energy release rate criterion [105, 128, 219]. The maximum tension criterion states that a crack will branch in the direction that is perpendicular to maximum tension. As the near-tip stress field of a straight crack is completely characterised by the stress intensity factors (SIF) K_I and K_{II} [297], the crack extension direction can be determined analytically as a function of mode-mixity $\gamma = \frac{K_{II}}{K_I}$, i.e. $\Delta\theta_{\mathrm{c}}(\gamma) = 2\arctan\frac{1-\sqrt{1+8\gamma^2}}{4\gamma}$ [195, 261]. With regard to the maximum energy release rate criterion, the Irwin-Griffith relationship $G_{\mathrm{s}} = \frac{k_I^2+k_{II}^2}{E}$ [134] between the crack tip energy release rate G_{s} and the SIF k_I and k_{II} at the tip of an infinitesimally small crack branch is valid for any angle of kink [116, 147]. It is assumed that the critical kink angle corresponds to a stationary G_{s}, i.e. $\frac{\partial G_{\mathrm{s}}}{\partial\theta} = 0$. Finally, the criterion of local symmetry [97, 122] states that a crack will follow a path where the local stress field is of mode-I type. Hence, the condition for the critical kink angle is a vanishing local mode-II SIF, i.e. $k_{II} = 0$.

Within a discrete framework, the aforementioned criteria may be implemented either explicitly or implicitly in the *time* dimension. An explicit crack growth criterion relies on post-processing the local crack tip stress/strain fields, following the solution to the material equilibrium problem, in order to determine the subsequent crack propagations. In this case, the problems of material equilibrium and crack growth are decoupled. As such, they can be solved separately for a particular solution time. An implicit-in-time implementation of a crack growth criterion involves solving the problems of material equilibrium and crack growth simultaneously. Since the solutions are non-linearly coupled, an iterative solution scheme is usually required. For example, consider the local symmetry

criterion. The criterion is explicit in time if the crack extension direction is required to satisfy a vanishing mode-II stress field at the tip of an infinitesimally small crack branch; conversely, the criterion is implicit in time if the vanishing mode-II stress field is sought at the end of the (finite) crack extension. A possible solution approach is to use the small crack kink angle approximation (1.29) to iteratively update the fracture extension direction until the mode-II SIF becomes sufficiently small at the new crack tip. Similarly, the energy minimisation approach is an implicit formulation whose explicit counterpart is the maximum incipient crack tip energy release rate criterion. The proposed solution approach for the energy minimisation problem, is to update the fracture extension directions using Newton's algorithm in order to find the orientations of the crack extensions that yield vanishing energy release rate with respect to their rotations about their extension vertices.

It has been shown in [116, 147] that the local SIF k_I and k_{II} at the tip of an infinitesimally small branch of an initially straight crack can be determined as linear combination of the SIF K_I and K_{II} existing at the tip of the main crack prior to kinking: $k_i = f_{ij}(\Delta\theta)K_j$, where the functions f_{ij} are independent of geometry or loading conditions and only depend on the kink angle. Although a closed form expression for f_{ij} is not available, the small kink angle approximation $\tilde{f}_{ij}(\Delta\theta)$ to within $\mathcal{O}(\Delta\theta^2)$ can be given as follows [147]:

$$\tilde{f}_{11} = 1 - \frac{3}{8}\Delta\theta^2, \quad \tilde{f}_{12} = -\frac{3}{4}\Delta\theta, \quad \tilde{f}_{21} = \frac{1}{2}\Delta\theta, \quad \tilde{f}_{22} = 1 - \frac{7}{8}\Delta\theta^2. \tag{1.28}$$

For predominately mode-I loading conditions, the solution for $\Delta\theta_c$ can be shown to be the same for all criteria provided the terms of order $\mathcal{O}(\Delta\theta^3, K_{II}^2, K_{II}\Delta\theta^2)$ are ignored [147]:

$$\Delta\theta_c = -2\frac{K_{II}}{K_I} \tag{1.29}$$

This means that for predominantly mode-I loading conditions the crack kink direction simultaneously corresponds to maximum k_I and $\sigma_{\theta\theta}$ (for maximum hoop-stress), maximum G_s, and a vanishing k_{II}. The small kink angle approximation (1.29) for a straight crack segment is valid for up to fairly large angles of kink [149], e.g. $\Delta\theta_c < 30°$. Figure 1.2 gives a comparison of the solutions for $\Delta\theta_c$ based on different criteria for arbitrary mixed-mode

loading conditions. The relationship $k_i = f_{ij}(\Delta\theta)K_j$ is assumed in the criteria where the values of the coefficients f_{ij} for various kink angles can be found tabulated in [116].

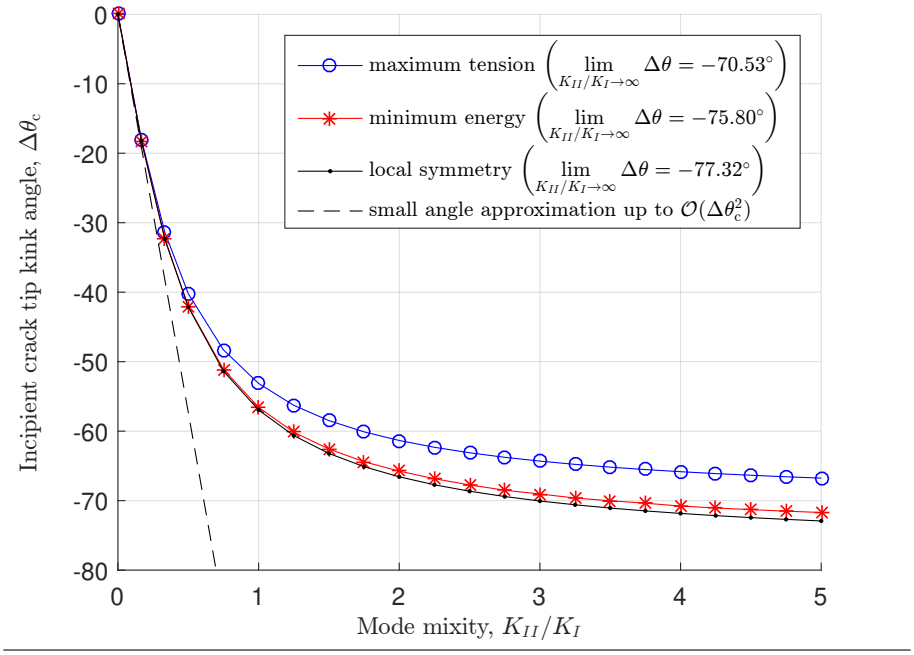

FIGURE 1.2: Crack tip kink angles for a straight crack and arbitrary mixed-mode loading conditions. The criteria are: maximum tension (hoop stress) [75], maximum energy release rate [116], and the criterion of local symmetry [122] (i.e. vanishing mode-II SIF at the tip of the crack branch). Note that the results of the last two criteria are obtained numerically in [116].

According to the aforementioned criteria, a straight crack will kink if $K_{II} \neq 0$. Otherwise, if $K_{II} = 0$ but $\partial K_{II}/\partial \ell \neq 0$ then an initially straight crack will curve smoothly [147, 148]. Concerning the fracture evolution immediately following an initial kink, any criterion should subsequently predict a smoothly curving fracture path under constant remote loading conditions. In other words, in the limit of a vanishingly small crack extension, no subsequent kinking should take place of the crack branch as this would imply the possibility of double kinking of the main crack in the limit the length of the branch tends to zero. The prospect of double kinking (or infinite curvature of the fracture path) at the tip of the main crack is difficult to justify on a physical basis. That being said, the explicit maximum tension and the maximum energy release rate criteria indicate subsequent crack tip kinking since the mode-II stress field does not generally vanish at the tip of an infinitesimal branch [11, 53, 147]. The practical consequences of crack kinking whenever

$K_{II} \neq 0$ is that the fracture path solution will converge to the one obtained by the local symmetry criterion in the limit of vanishingly small (straight) crack extensions. This, however, assumes that (1) the classic leading-order crack tip solution by Williams [297] for a flat crack is also valid close to the tip of a non-flat crack (so long as the crack is composed of piece-wise straight crack segments), and (2) the different criteria used in the prediction of the onset of fracture growth effectively identify the same crack tip(s) to be critical. Note that the second assumption may not apply in cases of multiple cracks due to a potential discrepancy in what is deemed to be the most critical fracture extension solution by different criteria. In other words, different criteria can lead to different fracture paths simply because of the different incipient crack kink directions and the correspondingly different fracture driving forces that are associated with those kink directions.

Concerning the fracture solution by the global energy minimisation approach, the incipient fracture growth direction is generally not one of vanishing mode-II stress field [11, 53, 254]. The mode-II SIF can only gradually decay with respect to the evolution of the fracture length due to the (presumed non-negotiable) requirement of a smooth fracture path [53]. The decay rate of the mode-II stress field is usually rapid. Under predominately mode-I loading conditions, the decay rate is exponential according to [122]. For this reason, no significant difference in the fracture solutions by different criteria can be observed on the material length scale since all the criteria approximately lead to the mode-I fracture path.

Nonetheless, there appears to be an inconsistency between the explicit-in-time and implicit-in-time formulations of the the crack growth criteria. The explicit-in-time formulation of either the stress or the energy based criterion indicates that crack tip kinking occurs if $K_{II} \neq 0$; since the mode-II SIF does not generally vanish at the tip of an infinitesimal crack extension (refer to Figure 1.2), both criteria imply subsequent crack kinking and, hence, an infinite curvature of the crack. In other words, the crack curves about its tip until it aligns with the vanishing mode-II stress field. This infinite curvature of the crack, which directly follows from the time-explicit criteria, is not a physically reasonable manifestation. Furthermore, it has a significant implication on the evolution of external load parameter – the load parameter is discontinuous in time. The following example explains this. During the initial loading stage of a pre-cracked structure, the load parameter gradually increases

with no change in the fracture length. The time-explicit maximum energy release rate criterion predicts that the crack will kink in a particular direction such that $G = G_{\max}$. At the inception of kinking, the load parameter is such that crack growth satisfies energy conservation, i.e. $G = G_{\mathrm{c}}$. However, as soon as the crack advances by an infinitesimal amount, the maximum energy release rate direction abruptly changes since the local mode-II SIF is generally non-vanishing. This means that the current crack growth direction is no longer favourable and that the crack needs to kink again so that $G = G_{\max}$. However, with respect to the current crack growth, the load parameter is such that $G = G_{\mathrm{c}}$. Thus, if the crack kinks in the new direction then it must mean that $G_{\max} > G_{\mathrm{c}}$. The subsequent material state is physically not possible; hence, the load parameter needs to abruptly decrease so that energy conservation can be satisfied, i.e. $G_{\max} = G_{\mathrm{c}}$. This peculiarity of the time-explicit crack growth criteria is also remarked upon in the works of [53, 80, 195]. In general, the time-implicit formulation of a crack growth criterion can be reasonably expected to produce a smooth fracture path and a continuously evolving load parameter in the limit of vanishingly small crack extensions, even if the mode-II SIF does not vanish.

It is not clear how the inconsistency between the explicit and implicit criteria arises as the respective solutions should theoretically coincide in the limit of a vanishingly small crack branch (assuming the limit exists). One plausible explanation is that the presence of a sharp kink influences stress field at the crack tip such that the William's solution for a flat crack is no longer valid for a kinked crack configuration (even if the crack branch is straight). In other words, once the crack has kinked, the relationship between the critical growth direction and the SIF at the tip of the crack branch may not be the same as the relationship for a flat crack. Moreover, the SIF may be inaccurate as well since they are determined based on the auxiliary fields from the William's solution in the first place. However, the SIF K_I and K_{II} fundamentally quantify the symmetric and anti-symmetric crack tip deformation modes and not the precise displacement field at the crack tip. If the SIF are computed using a non-local SIF correlation method rather than by locally matching the crack tip field quantities with those of known auxiliary fields (such as those from William's solution), the SIF may reasonably well quantify the symmetric and anti-symmetric crack tip deformation components even in the case of a kinked crack.

Consider the fact that the local symmetry criterion does not directly rely on the exact crack tip displacement field but that instead the crack growth direction is governed by the fundamental principle: the vanishing of the anti-symmetric crack tip deformation mode. From this viewpoint, even if the SIF are computed using a non-local approach based on the auxiliary fields from William's solution for a flat crack, the implicit-in-time formulation of the local symmetry criterion will be more robust than the explicit formulation because the former requires only of the anti-symmetric deformation mode to vanish whereas the latter relies not only on the accuracy of the SIF's but also on the accuracy of the crack tip field for the general case of a non-flat crack. By the same reasoning, the implicit-in-time formulation of the maximum hoop stress criterion that, according to William's solution, only requires of the mode-I deformation to be maximum, will be a more robust formulation than its explicit counterpart that directly invokes William's solution for the local stress field in order to express the critical crack growth direction in terms of the ratio of the SIF. Likewise, the implicit-in-time formulation of the maximum energy release rate criterion is more robust than the time-explicit formulation; however, its equivalent form that is the global energy minimisation approach poses the maximum energy release rate criterion even more robustly since it neither involves the crack tip field nor the crack tip SIF's.

Fundamentally, fracture is a local phenomenon; hence, the onset of fracture growth should correspond to the solution given by the time-explicit formulation of the crack growth criterion. On the other hand, from a pragmatic point of view, the time-implicit formulation of the fracture criterion yields a more conservative solution for the onset of fracture growth and for the prediction of the fracture path. Consequently, one may be more inclined to adopt the time-implicit approach for solving practical engineering problems.

1.9 Outline of thesis

In Chapter 2, the problem of quasi-static crack growth in a linear-elastic isotropic homogeneous solid is considered. The static equilibrium equations are formulated in a variational form and the problem of fracture evolution is posed as a total energy minimisation by following Griffith's theory of brittle fracture. Subsequently, the problem of competing

crack growth is addressed, which is characterised by the existence of multiple fracture growth solutions of equivalent energy dissipation rate such that the critical solution is not immediately obvious. This leads to solve to a quadratic constrained optimisation problem that governs competing crack growth. Several solution methods are proposed. Finally, the problem of the crack growth direction (crack kinking) is addressed. The minimum energy principle is formulated as the principle of vanishing rotational energy release rate of an infinitesimal fracture extension. The main advantage of this approach is that it is readily extendable to the discrete framework where the crack extensions have finite lengths.

In Chapter 3, the discrete fracture growth problem is considered. Depending on the behaviour of the total energy function, different solution methods for the fracture evolution problem are put forth. These techniques are based on: crack length control, load control, and on the energy gradient. For the most general case of fracture growth it is proposed to use the gradient based solution approach because it is more robust than the other solution strategies which are extremum-based and, consequently, limited to fracture problems where the total energy function is convex. Finally, the problem of competing crack growth is tackled. A criterion for detecting crack tip competition and when the competition needs to be resolved explicitly is discussed. An effective method for resolving crack tip competition is proposed, which is suitable even for fixed-length crack tip extensions.

In Chapter 4, the focus is on an efficient XFEM implementation within the *Matlab* programming language in order facilitate fast solution times of moderate size fracture growth problems, e.g. several million degrees of freedom and hundreds of interacting cracks. Methods are described for the efficient updating of system of equations, keeping track of topological and enrichment data, and managing multiple crack intersections. The proposed implementation enables multiple overlapping enrichments, their addition and subtraction (where needed) on the fly and an efficient integration of domain quantities by tailoring quadrature routines according to the hierarchy of enrichment functions over an element. The proposed implementation offers a significant speed-up of several times over the more "naive" approach that a novice to XFEM might initially choose to adopt for multi-crack growth problems as an extension of XFEM to modelling of stationary cracks.

In Chapter 5, the XFEM implementation considering different crack growth criteria is verified via multiple benchmarks. It is demonstrated that the crack growth directions determined by different criteria lead to virtually the same fracture paths since every criterion predicts a crack growth direction towards diminishing mode-II stress field. The criteria predominantly stand apart as concerns initial crack kinking and the onset of crack growth; however, the consequences that this has on the overall fracture path seem minor. Based on multiple numerical benchmark studies concerning the fracture paths by the stress and energy based criteria, a modified crack growth direction criterion is proposed. The criterion assumes the average direction of those obtained by the stress and energy criteria. Although the proposed alternative has little physical significance and is purely a heuristic criterion, it is found to be effective in solving practical fracture growth problems, especially on coarse discretisations, as it significantly improves the accuracy of the fracture paths as well as the fracture path convergence rate with respect to mesh refinement.

In Chapter 6, the problem of silicon wafer splitting is simulated using the proposed 2D fracture model. The effects of two types of boundary conditions on the final post-split fracture surface roughness are studied. The two kinds of boundary conditions correspond to the so-called mechanical splitting and pressure-driven splitting of the wafer specimen. In the blade splitting case, the wafer is modelled as a double cantilever beam with a built-in end and prescribed opening displacements at the other end. For the pressure splitting case, a rectangular domain with horizontally fixed left and right ends is assumed such that the micro-crack cavity pressure provides the only driving force for micro-crack growth to achieve splitting of the wafer specimen. The pressure and blade boundary conditions are considered in a set of parametric studies aimed at assessing the influence of different Smart-Cut™ process parameters on the post-split fracture roughness. The parameters of interest include: micro-crack mean distribution depth, thickness of micro-crack distribution, thickness of the buried oxide layer, and the relative stiffness of the damaged zone (the micro-crack inhabited zone) relative to the surrounding silicon.

Chapter 2

Problem Statement

2.1 Introduction

A two-dimensional (2D) problem of multiple crack growth in a brittle linear-elastic solid in plane-strain (or plane-stress) is considered. All cracks are assumed to already exist in the solid and that no new cracks can be nucleated. Each pre-existing crack is idealised as a zero-thickness void that is initially perfectly closed such that its top and bottom surfaces meet sharply at the crack tips (i.e. the radius of curvature at the crack tip is approaches zero). The growth of these cracks is assumed to be possible only at the crack tips. Furthermore, crack growth is assumed to be sufficiently slow (or quasi-static) such that the solid is effectively in static equilibrium with the external loads. No crack closure or healing is assumed. Firstly, the elasto-static equilibrium problem of the 2D solid is stated. This part describes the geometrical aspects of the solid and defines the partial differential equations (PDE) and boundary conditions (BC) that need to be satisfied. Next, a variational form of the equilibrium problem is derived. In this step, the point-wise form of the equilibrium equations is converted to an integral form. The integral statement defines a type of an energy functional whose minimum corresponds to the equilibrium state of the solid. In describing the transient behaviour of a cracked elastic solid, it is supposed that the evolution of the mechanical system is sufficiently slow (quasi-static) such that the effects of inertial forces and kinetic energy can be disregarded. As such, the evolution process can be described as a sequence of states of static-equilibrium. The principle of energy conservation is applied within the framework of linear-elastic fracture mechanics to define the crack growth law in accordance with Griffith's theory. Based on this law, a total energy function is derived whose minimisation governs crack growth. The equations describing the equilibrium state of the solid and the fracture growth law are treated in a unified framework. It is shown that the evolution of the mechanical system corresponds to the minimisation of the total energy function. Thus, the problems of static-equilibrium and fracture growth are described by a single energy function whose time-continuous minimisation yields the solution to the evolution of the system. The solution to the problem of multiple crack growth is addressed by first considering the evolution of the crack lengths and then the law governing the crack growth direction.

2.2 The problem of static equilibrium

Consider a two-dimensional (2D) brittle linear-elastic body $\Omega \subset \mathbb{R}^2$ in the (x, y)-plane (Figure 2.1). The body has a boundary $\Gamma = \Gamma_u \cup \Gamma_t \cup \Gamma_c$, where Γ_u is a prescribed-displacement boundary and where Γ_t and Γ_c are the prescribed-traction boundaries. Γ_c is assumed to constitute n_c fracture surfaces such that $\Gamma_c = \Gamma_c^1 \cup \Gamma_c^2 \cup \cdots \cup \Gamma_c^{n_c}$. The static-equilibrium equations (2.1) and boundary conditions (2.2)-(2.5) are given as follows:

$$\sigma_{ij,j} + b_i = 0 \qquad \text{in } \Omega \tag{2.1}$$

$$u_i = \bar{u}_i \qquad \text{on } \Gamma_u \tag{2.2}$$

$$\sigma_{ij}\, n_j = t_i \qquad \text{on } \Gamma_t \tag{2.3}$$

$$-n_i\, \sigma_{ij} n_j = p_{nn} \qquad \text{on } \Gamma_c \tag{2.4}$$

$$-s_i\, \sigma_{ij} n_j = p_{sn} \qquad \text{on } \Gamma_c \tag{2.5}$$

where $\boldsymbol{\sigma} = \left[\begin{smallmatrix} \sigma_{xx} & \sigma_{xy} \\ \sigma_{yx} & \sigma_{yy} \end{smallmatrix}\right]$ is the Cauchy stress tensor; $\mathbf{u} = [u_x, u_y]$ is the displacement field; $\mathbf{n} = [n_x, n_y]^{\mathrm{T}}$ denotes the unit (outward) normal to the boundary Γ; $\mathbf{s}$ is a unit tangent vector such that $\mathbf{s} = [n_y, -n_x]^{\mathrm{T}}$; $\bar{\mathbf{u}}$ is the prescribed displacement on Γ_u; $\mathbf{b} = [b_x, b_y]^{\mathrm{T}}$ is the body force acting in Ω; $\mathbf{t} = [t_x, t_y]^{\mathrm{T}}$ is the prescribed traction on Γ_t; p_{sn} and p_{nn} are the local fracture surface tractions: tangential shear and normal pressure that act on Γ_c.

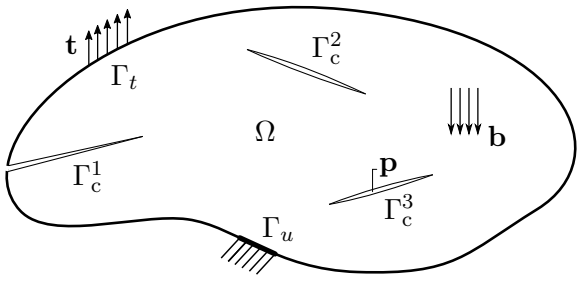

FIGURE 2.1: Diagram of a 2D model problem of a multiply cracked linear-elastic solid in static-equilibrium with the external loading action.

The stress-strain relationship for a linear-elastic solid can be given by Hooke's law:

$$\sigma_{ij} = C_{ijkl}\,\varepsilon_{kl} \quad i,j,k,l \in \{1,2\} \tag{2.6}$$

$$\sigma_{ij} = \sigma_{ji} \tag{2.7}$$

where $\mathbf{C}$ is a symmetric 4^{th}-order constitutive tensor for an isotropic homogeneous material, and where $\boldsymbol{\varepsilon} = \left[\begin{smallmatrix} \varepsilon_{xx} & \varepsilon_{xy} \\ \varepsilon_{yx} & \varepsilon_{yy} \end{smallmatrix}\right]$ is a small-deformation strain tensor that is defined as:

$$\varepsilon_{ij} = \frac{1}{2}(u_{i,j} + u_{j,i}) \quad i,j \in \{1,2\} \tag{2.8}$$

Note that $\boldsymbol{\varepsilon}$ is symmetric by definition, i.e. $\varepsilon_{ij} \equiv \varepsilon_{ji}$. The constitutive tensor $\mathbf{C}$ can be defined in a simplified (matrix) form according to the type of a 2D problem at hand:

$$\mathbf{C} \equiv \begin{bmatrix} C_{xxxx} & C_{xxyy} & C_{xxxy} \\ C_{yyxx} & C_{yyyy} & C_{yyxy} \\ C_{xyxx} & C_{xyyy} & C_{xyxy} \end{bmatrix} = \begin{cases} \frac{E}{1-\nu^2} \left[\begin{smallmatrix} 1 & \nu & 0 \\ \nu & 1 & 0 \\ 0 & 0 & \frac{1-\nu}{2} \end{smallmatrix}\right] & \text{Plane-stress} \\ \frac{E}{(1+\nu)(1-2\nu)} \left[\begin{smallmatrix} 1-\nu & v & 0 \\ \nu & 1-\nu & 0 \\ 0 & 0 & \frac{1-2\nu}{2} \end{smallmatrix}\right] & \text{Plane-strain} \end{cases} \tag{2.9}$$

The two independent material constants E and ν are, respectively, the Young's modulus of elasticity and the Poisson's ratio (i.e. ν is the ratio of the contraction strain transverse to the applied tension to the extension strain in the direction of the applied tension).

2.3 Derivation of the variational form

The weak-form [313] of static equilibrium is derived by multiplying the equilibrium equations in (2.1) by a set of arbitrary weight functions w_i, where $i \in \{1,2\}$ denotes each spatial dimension, integrating over the domain Ω and requiring the integral to vanish in a weighted-average sense for any suitable choice of w_i (i.e. so that the integral makes sense):

$$\int_{\Omega} w_i \left(\sigma_{ij,j} + b_i\right) \mathrm{d}V = 0 \tag{2.10}$$

If $\mathbf{w}$ are sufficiently regular functions [46], i.e. possess generalised (or weak) derivatives of at least first order, the continuity requirements of $\boldsymbol{\sigma}$ can be relaxed by using the product rule of integration to transfer the partial derivatives from $\boldsymbol{\sigma}$ to $\mathbf{w}$. Hence, (2.10) becomes:

$$\int_\Omega w_{i,j}\sigma_{ij}\,\mathrm{d}V = \int_\Omega (w_i\sigma_{ij})_{,j}\,\mathrm{d}V + \int_\Omega w_i b_i\,\mathrm{d}V \tag{2.11}$$

Next, the divergence theorem can be used to convert the domain integral $\int_\Omega (w_i\sigma_{ij})_{,j}\,\mathrm{d}V$ to a boundary integral of the form $\int_\Gamma w_i\sigma_{ij}n_j\,\mathrm{d}A$; however, it is practical to set $\mathbf{w}$ to vanish on the Dirichlet boundary Γ_u (or for $\mathbf{w}$ to have finite support) since the displacement solution is already known there. In this case, the boundary integral only needs to be evaluated over the Neumann boundary $\Gamma_t \cup \Gamma_\mathrm{c}$ (and not on Γ_u where the tractions are not known *a priori*):

$$\begin{aligned}\int_\Omega w_{i,j}\sigma_{ij}\,\mathrm{d}V = \int_\Omega w_i b_i\,\mathrm{d}V + \int_{\Gamma_t} w_i t_i\,\mathrm{d}A \\ + \sum_{k=1}^{n_c} \oint_{\Gamma_\mathrm{c}^k} w_i\left\{n_i(-p_{nn}) + s_i(-p_{sn})\right\}\mathrm{d}A\end{aligned} \tag{2.12}$$

It is possible to simplify the integral over the fracture boundary Γ_c by supposing that there is a mirror relationship between the surface normals on the directly opposing sides, i.e. $\mathbf{n}^+ = -\mathbf{n}^-$. In this case, the fracture boundary $\Gamma_\mathrm{c} = \Gamma_\mathrm{c}^- \cup \Gamma_\mathrm{c}^+$ is composed of identical top (+) and bottom (-) surfaces, namely Γ_c^- and Γ_c^+. Subsequently, equation (2.12) reads:

$$\begin{aligned}\int_\Omega w_{i,j}\sigma_{ij}\,\mathrm{d}V = \int_\Omega w_i b_i\,\mathrm{d}V + \int_{\Gamma_t} w_i t_i\,\mathrm{d}A \\ + \sum_{k=1}^{n_c} \int_{\Gamma_\mathrm{c}^{k-}} [\![w_i]\!]\left\{n_i^- p_{nn} + s_i^- p_{sn}\right\}\mathrm{d}A,\end{aligned} \tag{2.13}$$

where $[\![\cdot]\!] = (\cdot)^+ - (\cdot)^-$ denotes a jump in quantity $(\cdot)$ from Γ_c^- to Γ_c^+. Moreover, the sum of the products $w_{i,j}\sigma_{ij}$ can be replaced by $\varepsilon_{ij}(\mathbf{w})\sigma_{ij}$ (because $\boldsymbol{\sigma}$ is symmetric, i.e. $\sigma_{ij} = \sigma_{ji}$) and $\boldsymbol{\sigma}$ can be substituted with the relevant constitutive law (2.6)-(2.9) such that we have:

$$\begin{aligned}\int_\Omega \varepsilon_{ij}(\mathbf{w})C_{ijkl}\varepsilon_{kl}(\mathbf{u})\,\mathrm{d}V = \int_\Omega w_i b_i\,\mathrm{d}V + \int_{\Gamma_t} w_i t_i\,\mathrm{d}A \\ + \sum_{k=1}^{n_c} \int_{\Gamma_\mathrm{c}^{k-}} [\![w_i]\!]\left\{n_i^- p_{nn} + s_i^- p_{sn}\right\}\mathrm{d}A\end{aligned} \tag{2.14}$$

In order for the integral in (2.14) to be well-posed, the trial and test functions (i.e. $\mathbf{w}$ and $\mathbf{u}$, respectively) need to satisfy the essential properties of smoothness and integrability [46]. In this case, both $\mathbf{w}$ and $\mathbf{u}$ need to be continuous functions with weak differentiability and square-integrability (in the Lebesque sense). As such, $\mathbf{w}$ and $\mathbf{u}$ should generally belong to the special class of Sobolev functions denoted by $S^{2,1}$; for example, if $q \in S^{2,1}(\Omega)$ then:

$$\int_{\Omega} (q^2 + q_{,i}^2)\, \mathrm{d}V < \infty \tag{2.15}$$

states that q and its first derivatives are square integrable over Ω, i.e. the integrals are finite (or bounded). Provided $\mathbf{w}$ and $\mathbf{u}$ satisfy (2.15) (when substituted in place of q), the terms in the variational form (2.14) will be bounded as well. Since Sobolev functions are considered equivalent if they only differ on a Lebesque measure zero [46] (e.g. at a point or along a boundary where the functions are defined), it is necessary of $\mathbf{u}$ to explicitly satisfy the prescribed displacement boundary conditions on Γ_u and of $\mathbf{w}$ to vanish on Γ_u. For this purpose, the admissible test and trial function spaces can be defined as follows:

$$\mathcal{U} = \{\mathbf{u} \in H^1(\Omega) : \mathbf{u}|_{\Gamma_u} = \bar{\mathbf{u}}\} \tag{2.16}$$

$$\mathcal{U}_0 = \{\mathbf{w} \in H^1(\Omega) : \mathbf{w}|_{\Gamma_u} = \mathbf{0}\} \tag{2.17}$$

where $H^1 = S^{2,1}$ is the Hilbert space of real vector-valued continuous functions possessing square-integrable generalised (weak) derivatives at least up to order 1. For some $\mathbf{u} \in \mathcal{U}$ to satisfy the weak form, equation (2.14) is required to hold true for all test functions $\mathbf{w} \in \mathcal{U}_0$. Hence, the weak-form of elasto-static equilibrium is stated as follows. Find $\mathbf{u} \in \mathcal{U}$ so that:

$$\forall \mathbf{w} \in \mathcal{U}_0 \quad \int_{\Omega} \varepsilon_{ij}(\mathbf{w}) C_{ijkl} \varepsilon_{kl}(\mathbf{u})\, \mathrm{d}V = \int_{\Omega} w_i b_i\, \mathrm{d}V + \int_{\Gamma_t} w_i t_i\, \mathrm{d}A + \sum_{k=1}^{n_c} \int_{\Gamma_c^{k-}} [\![w_i]\!] T_{ij} p_j\, \mathrm{d}A \tag{2.18}$$

In (2.18), $\mathbf{T} = [\mathbf{s}^-, \mathbf{n}^-] \equiv \left[\begin{smallmatrix} \cos\theta & -\sin\theta \\ \sin\theta & \cos\theta \end{smallmatrix}\right]$ is the local-to-global rotation matrix that transforms the local crack surface tractions $\mathbf{p} = [p_{\mathrm{sn}}, p_{\mathrm{nn}}]$ to their global equivalent; here, θ is the anticlock-wise angle between the global y-axis and the unit normal vector $\mathbf{n}^-$ to the

fracture surface Γ_c^-. It can be shown that the weak-form (2.18) is in fact a variational statement where the test space $\mathcal{U}_0$ spans the admissible variations of the field $\mathbf{u}$, i.e. $\delta\mathbf{u} \in \mathcal{U}_0$ such that $\delta\mathbf{u} = \mathbf{0}$ on Γ_u. Thus, equation (2.18) can be equivalently stated as:

$$\forall \delta\mathbf{u} \in \mathcal{U}_0 \quad \int_\Omega \varepsilon_{ij}(\delta\mathbf{u}) C_{ijkl} \varepsilon_{kl}(\mathbf{u}) \, \mathrm{d}V = \int_{\Gamma_t} \delta u_i t_i \, \mathrm{d}A + \sum_{i=1}^{n_c} \int_{\Gamma_c^{i-}} [\![\delta u_i]\!] T_{ij} p_j \, \mathrm{d}A + \int_\Omega \delta u_i b_i \, \mathrm{d}V, \tag{2.19}$$

The variational statement (2.19) can be rearranged to describe a vanishing variation of a particular functional. The variation of this yet-unknown functional can be defined as:

$$\delta\Pi = \int_\Omega \varepsilon_{ij}(\delta\mathbf{u}) C_{ijkl} \varepsilon_{kl}(\mathbf{u}) \, \mathrm{d}V - \int_{\Gamma_t} \delta u_i t_i \, \mathrm{d}A - \sum_{i=1}^{n_c} \int_{\Gamma_c^{i-}} [\![\delta u_i]\!] T_{ij} p_j \, \mathrm{d}A - \int_\Omega \delta u_i b_i \, \mathrm{d}V \tag{2.20}$$

Since the strains $\varepsilon_{ij}(\mathbf{u})$ are linear in $\mathbf{u}$ such that $\delta\varepsilon_{ij}(\mathbf{u}) = \varepsilon_{ij}(\delta\mathbf{u})$, and the constitutive matrix $\mathbf{C}$ is symmetric, the variational symbol δ can be placed outside the integrals:

$$\delta\Pi = \delta \int_\Omega \frac{1}{2} \varepsilon_{ij}(\mathbf{u}) C_{ijkl} \varepsilon_{kl}(\mathbf{u}) \, \mathrm{d}V - \delta \left(\int_{\Gamma_t} u_i t_i \, \mathrm{d}A + \sum_{i=1}^{n_c} \int_{\Gamma_c^{i-}} [\![u_i]\!] T_{ij} p_j \, \mathrm{d}A + \int_\Omega u_i b_i \, \mathrm{d}V \right) \tag{2.21}$$

In turn, the sought functional $\Pi(\mathbf{u})$ can be determined to take the following form:

$$\Pi(\mathbf{u}) = \frac{1}{2} \int_\Omega \varepsilon_{ij}(\mathbf{u}) C_{ijkl} \varepsilon_{kl}(\mathbf{u}) \, \mathrm{d}V - \left(\int_{\Gamma_t} u_i t_i \, \mathrm{d}A + \sum_{i=1}^{n_c} \int_{\Gamma_c^{i-}} [\![u_i]\!] T_{ij} p_j \, \mathrm{d}A + \int_\Omega u_i b_i \, \mathrm{d}V \right) \tag{2.22}$$

Since $\Pi(\mathbf{u})$ appears as a positive-definite quadratic form of the displacement field $\mathbf{u}$, the solution $\mathbf{u} \in \mathcal{U}$ that satisfies the variation-form (2.19) also happens to be a global minimizer of $\Pi(\mathbf{u})$; conversely, $\mathbf{u} \in \mathcal{U}$ that minimises $\Pi(\mathbf{u})$ also satisfies (2.19). Thus, the problem of static equilibrium, whose strong-form is given by equations (2.1)-(2.5), can be weakly posed as a minimisation problem where $\Pi(\mathbf{u})$ is to be minimised in terms of $\mathbf{u} \in \mathcal{U}$.

Consequence, were we to seek an approximate solution $\mathbf{u}^h \in \mathcal{U}^h$ that exists in a finite-dimensional space of all possible solutions $\mathcal{U}^h$, such that $\mathcal{U}^h \subset \mathcal{U}$ and $\mathcal{U}_0^h = \mathcal{U}^h - \bar{\mathbf{u}}$, the solution to the variational-form (2.19) would ensure that $\mathbf{u}^h \in \mathcal{U}^h$ is the optimal solution from that particular space $\mathcal{U}^h$. This is because, solving the variational-form (2.19) means that $\mathbf{u}^h \in \mathcal{U}^h$ is a minimizer of $\Pi(\mathbf{u}^h)$; in turn, the approximation $\mathbf{u}^h$ is the nearest-possible solution to the true solution $\mathbf{u} \in \mathcal{U}$ with respect to the minimum of the potential energy. The functional $\Pi(\mathbf{u})$ is formally known as the potential energy of the mechanical system [313]. It is composed of two principal parts, namely: the elastic strain energy $U_{\mathrm{s}}(\mathbf{u})$ and the potential energy of the external load $V(\mathbf{u})$; the definitions are given in line with (2.22):

$$\Pi(\mathbf{u}) = U_{\mathrm{s}}(\mathbf{u}) + V(\mathbf{u}) \tag{2.23}$$

$$U_{\mathrm{s}}(\mathbf{u}) = \int_{\Omega} \frac{1}{2} \varepsilon_{ij}(\mathbf{u}) C_{ijkl} \varepsilon_{kl}(\mathbf{u}) \, \mathrm{d}\Omega \tag{2.24}$$

$$V(\mathbf{u}) = -\left(\int_{\Gamma_t} u_i t_i \, \mathrm{d}\Gamma + \sum_{i=1}^{n_c} \int_{\Gamma_{\mathrm{c}}^{i-}} [\![u_i]\!] T_{ij} p_j \, \mathrm{d}\Gamma + \int_{\Omega} u_i b_i \, \mathrm{d}\Omega \right) \tag{2.25}$$

Note that the minus sign in $V(\mathbf{u})$ implies that the load potential decreases as the external force does work, i.e. as the force displaces in its direction. Since the reference value of the load potential is inconsequential in practice it can be assumed as zero, i.e. $V_0 \equiv V(\mathbf{0}) = 0$.

Finally, it should be remarked that the *weak* solution $\mathbf{u} \in \mathcal{U}$ to the variational formulation (2.19) is generally not the *strong* solution to the original problem defined by (2.1)-(2.5). This is because the PDE (2.1) requires the existence of continuous second derivatives of the solution $\mathbf{u}$ in order for the PDE to be satisfied at every point in the domain. However, the weak formulation "weakens" this requirement by admitting a solution that only needs to be continuous and weakly differentiable. The weak and strong solutions coincide only if the problem coefficients in (2.1)-(2.5) are continuous functions. Nonetheless, the weak formulation essentially embodies the original problem of elasto-static equilibrium.

The displacement solution will be presumed to automatically satisfy the condition of no fracture surface interpenetration, i.e. $[\![u_i]\!] n_i \geq 0$ on Γ_{c}^{-}. Hence, the contact constraint on the displacement solution will not be enforced. The fracture problems of practical interest (such as wafer splitting in Chapter 6) will involve predominantly mode-I loaded cracks.

2.4 Evolution of crack lengths

The problem of crack growth is analysed (in 2D) in two parts: (1) the evolution of the crack lengths, and (2) the problem of determining the crack growth direction.[1] The first part is addressed in this section (Section 2.4) whereas the second part will be tackled in Section 2.6. In this section, the 1D evolution of cracks in a 2D multiply cracked solid is considered. Firstly, the crack representation is described to allow for a simpler association between the possible fracture propagations and the resulting energy release rates. Within this framework, the Griffith's fracture growth criterion is applied to multiple cracks. Based on the Griffith's crack growth law, the principle governing multiple crack behaviour is defined. The principle states that the quasi-static fracture evolution maximises energy dissipation. Subsequently, the problem of fracture growth is posed as a total energy minimisation problem. For competing crack growth (i.e. when the local energy dissipation rates at multiple crack tips are equivalent), the fracture advance solution based on the maximum energy dissipation rate is no longer unique in terms of the crack tip growth rates.Three solution methods are proposed to solve the competing crack growth problem. The different solution strategies are applied based on the local behaviour of the total energy function (in terms of its curvature) in order to solve the problem efficiently.

2.4.1 Description of cracks

In describing the evolution of multiple cracks it is practical to consider unique crack branches that stem from the tips of the pre-exciting cracks. The reason for this approach is that it simplifies the association of the crack tip energy release rate $G_{\mathrm{s}i}$ with a particular crack tip branch $i \in \{1, 2, \ldots, n_{\mathrm{tip}}\}$. For this purpose, let us denote the set of pre-existing cracks by $\mathcal{I}_{\mathrm{c}} = \{1, 2, \ldots, n_{\mathrm{c}}\}$ and the set of crack tip branches by $\mathcal{I}_{\mathrm{tip}} = \{1, 2, \ldots, n_{\mathrm{tip}}\}$ such that the number of crack tips is related to the number of cracks via $n_{\mathrm{tip}} = 2n_{\mathrm{c}}$. In this reference frame (see Figure 2.2 for details), a crack $i \in \mathcal{I}_{\mathrm{c}}$ is considered to have a pre-existing (constant) length a_{0i}, whereas a crack-tip branch $i \in \mathcal{I}_{\mathrm{tip}}$ is supposed to have

[1] The problem of fracture growth can be split this way because the crack growth directions are independent of the crack growth rates (Section 2.7). The two problems are addressed separately for the sake of simplicity.

a *time*-dependent length $\ell_i(\tau)$. Here $\tau \in [0, \tau_\infty]$ is a pseudo time variable that characterises the time-line of the quasi-static process from beginning to end. Therefore, at the initial time $\tau = 0$ the length of any fracture branch is zero, i.e. $\ell_i(0) = 0$, and for $\tau > 0$ it is generally $\ell_i(\tau) \geq 0$. It is emphasised that, at any point in time, the crack growth rate is assumed to be non-negative, i.e. $\forall \tau \in [0, \tau_\infty] : \dot{\ell}_i(\tau) \geq 0$ where $i \in \mathcal{I}_{\text{tip}}$ and $\dot{\ell}_i = \mathrm{d}\ell_i/\mathrm{d}\tau$.

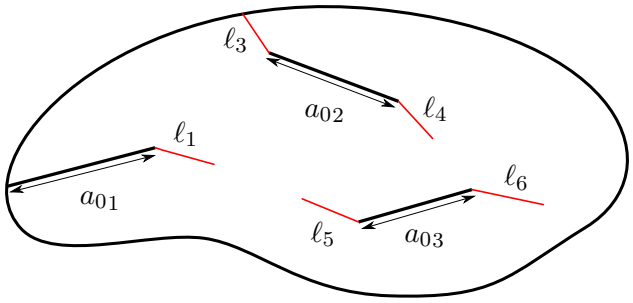

FIGURE 2.2: The proposed crack representation scheme. A pre-existing crack is assumed to have a fixed length a_{0i} where $i \in \mathcal{I}_{\text{c}}$. The length of a crack tip branch, which is assumed to evolve over time, is ℓ_j where $j \in \mathcal{I}_{\text{tip}}$.

Within this framework of crack representation, the length a_i of a crack $i \in \mathcal{I}_{\text{c}}$ is determined as the sum of its pre-existing length a_{0i} and the lengths of its tip branches, ℓ_{2i-1} and ℓ_{2i}:

$$i \in \mathcal{I}_{\text{c}} \quad a_i = a_{0i} + \ell_{2i-1} + \ell_{2i} \tag{2.26}$$

Then the rate of crack growth $\dot{a}_i = \mathrm{d}a_i/\mathrm{d}\tau$ with respect to time τ may be expressed as:

$$\begin{aligned} i \in \mathcal{I}_{\text{c}} \quad & \dot{a}_i = \dot{\ell}_{2i-1} + \dot{\ell}_{2i} \\ \text{assuming} \quad & \dot{\ell}_{2i-1} \geq 0 \text{ and } \dot{\ell}_{2i} \geq 0 \end{aligned} \tag{2.27}$$

However, *time* τ is not an ideal variable for parametrising the evolution of a quasi-static process. The main reason is that it has no physical relation to the problem. A more suitable alternative is to use the total fracture length (because it is assumed to be irreversible):

$$a = \textstyle\sum_{i=1}^{n_{\text{c}}} a_i \tag{2.28}$$

$$a = \textstyle\sum_{i=1}^{n_{\text{c}}} a_{0i} + \sum_{i=1}^{n_{\text{tip}}} \ell_i \tag{2.29}$$

The total fracture length $a \in [a_0, a_\infty]$ is considered to span the interval from the initial fracture length of a_0 to the final value of a_∞, which marks the end of the fracture process; the interval bounds can be said to correspond to times $\tau = 0$ and τ_∞ respectively. The rate of crack and crack-tip growth, relative to the the total fracture length, can be defined as:

$$i \in \mathcal{I}_\mathrm{c} \qquad \hat{a}_i = \frac{\mathrm{d}a_i}{\mathrm{d}a} \tag{2.30}$$

$$i \in \mathcal{I}_\mathrm{tip} \quad \hat{\ell}_i = \frac{\mathrm{d}\ell_i}{\mathrm{d}a} \tag{2.31}$$

The second form (2.31) is more useful in describing multiple crack-tip propagations because it refers specifically to the growth of tips. The relative crack-tip growth rates (2.31) can be defined in terms of a vector $\hat{\boldsymbol{\ell}} \in \mathcal{A}$, where $\mathcal{A}$ is the space of admissible growth rates:

$$\mathcal{A} = \left\{ \hat{\boldsymbol{\ell}} : \forall i \in \mathcal{I}_\mathrm{tip},\ \hat{\ell}_i \in [0,1] \text{ subject to } \textstyle\sum_{i \in \mathcal{I}_\mathrm{tip}} \hat{\ell}_i = 1 \right\} \tag{2.32}$$

A typical instance in the fracture process is marked by the total fracture length $a^\star \in [a_0, a_\infty]$. The corresponding crack-tip branch lengths $\boldsymbol{\ell} = \boldsymbol{\ell}(a^\star)$ can then be obtained by integrating the relative crack tip growth rates with respect to the total fracture length variable a:

$$\ell_i = \int_{a_0}^{a^\star} \hat{\ell}_i(a)\, \mathrm{d}a, \quad \text{where } i \in \mathcal{I}_\mathrm{tip} \tag{2.33}$$

2.4.2 Crack growth principle

Irwin [132–135] restated the Griffith's [105, 106] model in a way that is better suited to solving practical engineering problems by generalising the energy release rate of a crack tip extension to arbitrary loading and structural configurations. The energy release rate $G_{\mathrm{s}i}$ of a crack tip $i \in \mathcal{I}_\mathrm{tip}$ is defined as the rate of strain energy liberation $(-\mathrm{d}U_\mathrm{s}/\mathrm{d}\ell_i)$ plus

the rate of external work done $\mathrm{d}W_{\mathrm{ext}}/\mathrm{d}\ell_i$ with respect to a crack-tip branch length ℓ_i:

$$G_{\mathrm{s}i} = -\frac{\mathrm{d}U_s}{\mathrm{d}\ell_i} + \frac{\mathrm{d}W_{\mathrm{ext}}}{\mathrm{d}\ell_i} \tag{2.34}$$

$$G_{\mathrm{s}i} = -\frac{\mathrm{d}U}{\mathrm{d}\ell_i} - \frac{\mathrm{d}V}{\mathrm{d}\ell_i} \tag{2.35}$$

$$G_{\mathrm{s}i} = -\frac{\mathrm{d}\Pi}{\mathrm{d}\ell_i}, \tag{2.36}$$

where $\mathrm{d}W_{\mathrm{ext}}/\mathrm{d}\ell_i$ has been expressed in terms of the decrease rate of the load potential $(-\mathrm{d}V/\mathrm{d}\ell_i)$ by supposing that the external load stays constant during an infinitesimal crack tip increment $\mathrm{d}\ell_i$. As a result, $G_{\mathrm{s}i}$ is equal to the negative rate of change (or the decrease rate) of the potential energy Π with respect to the crack-tip branch length ℓ_i. Considering the general case of simultaneous multiple crack tip growth, the effective energy release rate G_{s} with respect to the crack tip extension rate $\hat{\boldsymbol{\ell}} \in \mathcal{A}$ can be computed as follows:

$$G_{\mathrm{s}} = -\frac{\mathrm{d}\Pi}{\mathrm{d}a} \tag{2.37}$$

$$G_{\mathrm{s}} = G_{\mathrm{s}i}\frac{\mathrm{d}\ell_i}{\mathrm{d}a} \tag{2.38}$$

$$G_{\mathrm{s}} = G_{\mathrm{s}i}\hat{\ell}_i \tag{2.39}$$

If the crack tips happen to exist in distinct materials that are characterised by different critical energy release rates $G_{\mathrm{c}i}$ where $i \in \mathcal{I}_{\mathrm{tip}}$, the equivalent G_{c} (or, the equivalent resistance of the material to fracture growth) can be determined analogously to (2.39):

$$G_{\mathrm{c}} = G_{\mathrm{c}i}\hat{\ell}_i \tag{2.40}$$

Since the onset of crack growth occurs at the instance the fracture driving force (G_{s}) overcomes the material resistance (G_{c}), the crack growth criterion can be stated as follows:

$$\forall \hat{\boldsymbol{\ell}} \in \mathcal{A} \quad \begin{cases} (G_{\mathrm{s}i} - G_{\mathrm{c}i})\,\hat{\ell}_i < 0 & \text{(no growth)} \\ (G_{\mathrm{s}i} - G_{\mathrm{c}i})\,\hat{\ell}_i = 0 & \text{(growth)} \end{cases} \tag{2.41}$$

Note that the driving energy release rate $G_{\mathrm{s}} = G_{\mathrm{s}i}\hat{\ell}_i$ is always bounded (from above) by the critical energy release rate $G_{\mathrm{c}} = G_{\mathrm{c}i}\hat{\ell}_i$. This is because a material can not physically exist in a state where its capacity to resist fracture growth is exceeded by the applied fracture driving force. Consequently, the necessary condition for the physical consistency between the crack-tip and the critical energy release rates can be generally expressed as:

$$\forall i \in \mathcal{I}_{\mathrm{tip}} \quad G_{\mathrm{s}i} \leq G_{\mathrm{c}i} \tag{2.42}$$

If a particular crack tip growth rate $\hat{\boldsymbol{\ell}} \in \mathcal{A}$ satisfies the growth condition in (2.41) then that growth rate is (naturally) the most energetically favourable (i.e. critical) growth rate. The critical growth rate $\hat{\boldsymbol{\ell}}_{\mathrm{c}} \in \mathcal{A}$ must in turn satisfy the following equation:

$$\hat{\boldsymbol{\ell}}_{\mathrm{c}} = \underset{\hat{\boldsymbol{\ell}} \in \mathcal{A}}{\arg\max} \left(\left(G_{\mathrm{s}i} - G_{\mathrm{c}i} \right) \hat{\ell}_i \right), \tag{2.43}$$

to ensure that the physical consistency condition (2.42) of the crack-tip energy release rates is not violated at the instance crack growth takes place. Based on (2.43), the critical fracture path $\boldsymbol{\ell}_{\mathrm{c}} = \int_{a_0}^{a_\infty} \hat{\boldsymbol{\ell}}_{\mathrm{c}} \, \mathrm{d}a$ must continuously maximise the so-called dissipation rate:

$$\mathcal{D}(\hat{\boldsymbol{\ell}}) = \left(G_{\mathrm{s}i} - G_{\mathrm{c}i} \right) \hat{\ell}_i \tag{2.44}$$

such that, at any point in time in the evolution process, the following equation holds true:

$$\mathcal{D}(\hat{\boldsymbol{\ell}}_{\mathrm{c}}) = \max_{\forall \hat{\boldsymbol{\ell}} \in \mathcal{A}} \mathcal{D}(\hat{\boldsymbol{\ell}}) \tag{2.45}$$

2.4.3 The total energy function

Following from the result that the critical fracture path produces maximum dissipation (2.45), it is possible to formulate a total energy function $\mathcal{E} = \mathcal{E}(\boldsymbol{\ell})$ whose time-continuous minimisation, in terms of the fracture length variable $\boldsymbol{\ell}$, would yield the solution to the

fracture path. The first step towards obtaining $\mathcal{E}$ is to define the following relationship:

$$-\frac{\mathrm{d}\mathcal{E}}{\mathrm{d}a} = \mathcal{D}(\hat{\boldsymbol{\ell}}), \tag{2.46}$$

which states that the decrease rate of $\mathcal{E}$ with respect to the total fracture length a is equal to the energy per unit fracture length that is available for dissipation. The total energy function $\mathcal{E}(\boldsymbol{\ell})$ can then be obtained by integrating equation (2.46) with respect to a:

$$\mathcal{E}(\boldsymbol{\ell}) = \int \left(-G_{\mathrm{s}i} + G_{\mathrm{c}i}\right) \hat{\ell}_i \, \mathrm{d}a \tag{2.47}$$

$$\mathcal{E}(\boldsymbol{\ell}) = \int \left(\frac{\mathrm{d}\Pi}{\mathrm{d}\ell_i} + G_{\mathrm{c}i}\right) \mathrm{d}\ell_i \tag{2.48}$$

$$\mathcal{E}(\boldsymbol{\ell}) = \Pi(\mathbf{u}(\boldsymbol{\ell}), \boldsymbol{\ell}) + \int G_{\mathrm{c}i}(\boldsymbol{\ell}) \, \mathrm{d}\ell_i \tag{2.49}$$

It has been emphasised in equation (2.49) that the displacement field $\mathbf{u}$ is considered to be a function of the fracture length variable $\boldsymbol{\ell}$. At this point, it is not so important to define the relationship between $\mathbf{u}$ and $\boldsymbol{\ell}$ but only to assume that such a relationship exists.[2] However, it is important to recognise that $\mathcal{E}(\boldsymbol{\ell})$ can be used as a self-contained function to completely describe the evolution of the crack-tip lengths $\boldsymbol{\ell}$; specifically, (1) to determine if crack growth is favourable and (2) to determine the critical fracture path. These two objectives are accomplished seamlessly by the following means: (1) fracture growth is determined as favourable if $\mathcal{E}(\boldsymbol{\ell})$ can decrease or remain constant with increasing fracture length $\boldsymbol{\ell}$ and (2) the critical fracture path is obtained by the time-continuous minimisation of $\mathcal{E}(\boldsymbol{\ell})$ with respect to $\boldsymbol{\ell}$. With regard to point (2), the term *time-continuous* refers to a minimisation process whereby $\mathcal{E}(\boldsymbol{\ell})$ follows the path of steepest descent rate with respect to $\boldsymbol{\ell}$.

Finally, the term *available energy* in the current crack growth formulation implies positive dissipation, i.e. $\mathcal{D}(\hat{\boldsymbol{\ell}}) > 0$. This may appear as a direct contradiction with the physical consistency requirement between the critical and the crack tip energy release rates that is specified in (2.42). To clarify, the idea of *available energy* serves purely as a mathematical tool to determine if crack growth is favourable, i.e. $-\mathrm{d}\mathcal{E}/\mathrm{d}a \geq 0$. The fracture path will be

[2] A relationship between $\mathbf{u}$ and $\boldsymbol{\ell}$ exists because $\mathbf{u}$ is uniquely determined by solving the static equilibrium problem for a given fracture boundary Γ_{c}, which depends on $\boldsymbol{\ell}$. This is explained in Section 2.4.4.

physically consistent (or critical) if dissipation (2.46) is maximised as required by (2.43). Hence, the fracture growth criterion that embodies the growth principle can be stated as:

$$\max_{\forall \hat{\boldsymbol{\ell}} \in \mathcal{A}} \left(-\frac{\mathrm{d}\mathcal{E}}{\mathrm{d}a}\bigg|_{\hat{\boldsymbol{\ell}}} \right) \begin{cases} < 0 & \text{(no growth)} \\ \geq 0 & \text{(growth)} \end{cases} \tag{2.50}$$

where equality holds for crack growth under energy conservation conditions. In order to uphold energy conservation, the magnitude of the external load is required to be scaled such that fracture growth is just favourable. This is explained in detail in Section 2.4.5.

2.4.4 Total energy minimisation

It has been determined so far that the evolution of the crack-tip branch lengths $\boldsymbol{\ell}$ is governed by the time-continuous minimisation of the total energy function $\mathcal{E}(\boldsymbol{\ell})$. However, up to this point, the problem of fracture growth has been considered independently of the equilibrium state of the solid. The purpose of this section is to resolve the problem of crack evolution in a manner that is consistent with the static-equilibrium equations.

In the definition of $\mathcal{E}(\boldsymbol{\ell})$ in equation (2.49), the potential energy $\Pi = \Pi(\mathbf{u}(\boldsymbol{\ell}), \boldsymbol{\ell})$ was expressed in terms of the fracture length variable $\boldsymbol{\ell}$. It is worth clarifying how this relationship arises because in the initial definition of Π in equation (2.22), which was given in the context of static-equilibrium alone, the functional was expressed singly in terms of the displacement field $\mathbf{u}$; all other problem parameters, including the fracture boundary Γ_{c}, were assumed to be invariant. However, in the context of fracture growth, Γ_{c} is indeed a variable. As such, Π will depend not only on the displacement field $\mathbf{u}$ but also on the fracture boundary Γ_{c}, both of which are parameterizable in terms of the variable $\boldsymbol{\ell}$.

In practice, however, the relationship between $\mathbf{u}$ and $\boldsymbol{\ell}$ is an implicit one because it needs to be imposed via the condition of static-equilibrium; specifically, the potential energy $\Pi = \Pi(\mathbf{u}, \boldsymbol{\ell})$ is required to be minimised (or rendered stationary) in terms of $\mathbf{u}$ for a given

$\boldsymbol{\ell}$.[3] As such, the relationship $\mathbf{u} = \mathbf{u}(\boldsymbol{\ell})$ is embedded in the solution of the variational form (2.19) of static-equilibrium. The set of governing equations can be basically expressed as:

$$\left.\frac{\partial \Pi}{\partial \tilde{\mathbf{u}}}\right|_{\tilde{\mathbf{u}}=\mathbf{u},\Gamma_{\mathrm{c}}(\boldsymbol{\ell})} = \mathbf{0}, \tag{2.51}$$

where $\tilde{\mathbf{u}}$ denotes a dummy displacement field variable. Although an explicit functional relationship between $\mathbf{u}$ and $\boldsymbol{\ell}$ is not readily available, we will nevertheless apply the functional notation $\mathbf{u}(\boldsymbol{\ell})$ to highlight that $\mathbf{u}$ is assumed to be parametrized in terms of $\boldsymbol{\ell}$ such that $\mathbf{u}(\boldsymbol{\ell})$ is consistent with the state of static-equilibriums of solid. At any rate, it is possible to explicitly resolve the differential relationship $\mathrm{d}\mathbf{u}/\mathrm{d}\boldsymbol{\ell}$ that will prove to be useful later. To this end, it is only necessary to suppose that the condition of static-equilibrium is maintained during the infinitesimal crack extension $\delta\boldsymbol{\ell} = \hat{\boldsymbol{\ell}}\,\delta a$. Consequently, we have:

$$\begin{aligned} \forall i \in \mathcal{I}_{\mathrm{tip}} \quad & \frac{\mathrm{d}}{\mathrm{d}\ell_i}\left(\frac{\partial \Pi}{\partial \mathbf{u}}\right) = \mathbf{0} \\ & \frac{\partial}{\partial \ell_i}\left(\frac{\partial \Pi}{\partial \mathbf{u}}\right) + \frac{\partial^2 \Pi}{\partial \mathbf{u}^2}\frac{\mathrm{d}\mathbf{u}}{\mathrm{d}\ell_i}^{\mathrm{T}} = \mathbf{0} \\ & \frac{\mathrm{d}\mathbf{u}}{\mathrm{d}\ell_i} = -\frac{\partial}{\partial \ell_i}\left(\frac{\partial \Pi}{\partial \mathbf{u}}\right)^{\mathrm{T}}\left(\frac{\partial^2 \Pi}{\partial \mathbf{u}^2}\right)^{-1} \end{aligned} \tag{2.52}$$

where $\mathbf{u} = [u_x, u_y]$, $\frac{\partial}{\partial \mathbf{u}} = \left[\frac{\partial}{\partial u_x}, \frac{\partial}{\partial u_y}\right]^{\mathrm{T}}$ and $\frac{\partial^2}{\partial \mathbf{u}^2} = \frac{\partial}{\partial \mathbf{u}}\frac{\partial}{\partial \mathbf{u}}^{\mathrm{T}}$. In assuming that the solid is in a state of static-equilibrium, the computation of the rate of change of the total energy function $\left(-\frac{\mathrm{d}\mathcal{E}}{\mathrm{d}a}\big|_{\hat{\boldsymbol{\ell}}}\right)$ can be made simpler; this specifically affects to the determination of the fracture driving force G_{s}. Continuing from equation (2.36), the fundamental relationship between $G_{\mathrm{s}i}$ and the rate of change of $\Pi(\mathbf{u}(\boldsymbol{\ell}), \boldsymbol{\ell})$ in terms of the length ℓ_i of a specific crack-tip branch $i \in \mathcal{I}_{\mathrm{tip}}$, can be revised as follows:

$$\begin{aligned} G_{\mathrm{s}i} &= -\frac{\mathrm{d}\Pi}{\mathrm{d}\ell_i} \\ G_{\mathrm{s}i} &= -\frac{\partial \Pi}{\partial \ell_i} - \frac{\mathrm{d}\mathbf{u}}{\mathrm{d}\ell_i}\frac{\partial \Pi}{\partial \mathbf{u}} \\ G_{\mathrm{s}i} &= -\frac{\partial \Pi}{\partial \ell_i} \end{aligned} \tag{2.53}$$

[3] This is to say that, in general, $\Pi = \Pi(\mathbf{u}, \boldsymbol{\ell})$ is considered as a function of two independent variables: $\mathbf{u}$ and $\boldsymbol{\ell}$, but that the relationship $\mathbf{u} = \mathbf{u}(\boldsymbol{\ell})$ is established when static equilibrium of the solid is supposed.

Thus, the result of (2.53) is that the total derivative that appears in the standard definition of $G_{\mathrm{s}i}$ in equation (2.36) is now reduced to a partial derivative instead. Accordingly, G_{s} can be determined based solely on the geometrical variations of the fracture surface $\Gamma_{\mathrm{c}}(\boldsymbol{\ell})$ and the material domain $\Omega(\boldsymbol{\ell})$, as affected by $\delta\boldsymbol{\ell}$. The simplified form of G_s (2.53) combined with the principles that govern fracture growth (2.43) and the static-equilibrium of the solid (2.18), collectively describe the system's tendency to minimise its total energy $\mathcal{E}(\mathbf{u}, \boldsymbol{\ell})$ in terms of the variables $\mathbf{u}$ and $\boldsymbol{\ell}$, which can now be considered as a pair of independent variables. Thus, it is useful to express the total energy function in a more general form as:

$$\mathcal{E}(\mathbf{u}, \boldsymbol{\ell}) = \Pi(\mathbf{u}, \boldsymbol{\ell}) + \int G_{\mathrm{c}i}(\boldsymbol{\ell})\, \mathrm{d}\ell_i, \tag{2.54}$$

where the subtle change from the previous definition of $\mathcal{E}$ in equation (2.49) is in considering the displacement field $\mathbf{u}$ as independent of the fracture length variable $\boldsymbol{\ell}$. To recapitulate: (i) at any point in time in the fracture evolution process, the total energy of the solid $\mathcal{E}(\mathbf{u}, \boldsymbol{\ell})$ is minimised in terms of the displacement field $\mathbf{u}$ for static-equilibrium to hold true, and (ii) in the state of static-equilibrium, the evolution of the fracture lengths $\boldsymbol{\ell}$ is such that the total energy $\mathcal{E}(\mathbf{u}, \boldsymbol{\ell})$ follows the path of steepest rate of descent. Altogether, the evolution of the mechanical system can be described by the time-continuous minimisation of $\mathcal{E}(\mathbf{u}, \boldsymbol{\ell})$ with respect to the variable pair $\{\mathbf{u}, \boldsymbol{\ell}\}$. If the evolution process is assumed to be parameterized in terms of the combined fracture length variable a, such that $\{\mathbf{u}, \boldsymbol{\ell}\} = \{\mathbf{u}, \boldsymbol{\ell}\}(a)$, then at a typical instance during fracture growth $a = a^\star$, where $a^\star \in [a_0, a_\infty]$, the state of the solution is determined by the following set of equations:

$$\begin{cases} \boldsymbol{\ell} = \int_{a_0}^{a^\star} \hat{\boldsymbol{\ell}}(a)\mathrm{d}a \\ \mathbf{u} = \underset{\mathbf{u}_* \in \mathcal{U}(\Gamma_{\mathrm{c}})}{\arg\min}\, \mathcal{E}(\mathbf{u}_*, \boldsymbol{\ell}) \\ \hat{\boldsymbol{\ell}}_{\mathrm{c}} = \underset{\hat{\boldsymbol{\ell}}_* \in \mathcal{A}(\Gamma_{\mathrm{c}})}{\arg\min} \left(\frac{\partial \mathcal{E}}{\partial \boldsymbol{\ell}}\Big|_{\mathbf{u}} \cdot \hat{\boldsymbol{\ell}}_* \right) \\ \hat{\boldsymbol{\ell}} = \begin{cases} \hat{\boldsymbol{\ell}}_{\mathrm{c}} & \text{if } \ \frac{\partial \mathcal{E}}{\partial \boldsymbol{\ell}}\Big|_{\mathbf{u}} \cdot \hat{\boldsymbol{\ell}}_{\mathrm{c}} \leq 0 \\ 0 & \text{otherwise} \end{cases} \end{cases} \tag{2.55}$$

A more practical form of (2.55) can be put forth as:

$$\begin{cases} \boldsymbol{\ell} = \int_{a_0}^{a^\star} \hat{\boldsymbol{\ell}}(a)\mathrm{d}a \\ \mathbf{u} = \underset{\mathbf{u}_* \in \mathcal{U}(\Gamma_\mathrm{c})}{\arg\min}\, \Pi(\mathbf{u}_*, \boldsymbol{\ell}) \\ \hat{\boldsymbol{\ell}}_\mathrm{c} = \underset{\hat{\boldsymbol{\ell}}_* \in \mathcal{A}(\Gamma_\mathrm{c})}{\arg\max}\, \mathcal{D}(\mathbf{u}, \boldsymbol{\ell}, \hat{\boldsymbol{\ell}}_*) \\ \hat{\boldsymbol{\ell}} = \begin{cases} \hat{\boldsymbol{\ell}}_\mathrm{c} & \text{if } \mathcal{D}(\mathbf{u}, \boldsymbol{\ell}, \hat{\boldsymbol{\ell}}_\mathrm{c}) \geq 0 \\ 0 & \text{otherwise} \end{cases} \end{cases} \tag{2.56}$$

where the dissipation-like term $\mathcal{D}$ is considered as:[4]

$$\mathcal{D}(\mathbf{u}, \boldsymbol{\ell}, \hat{\boldsymbol{\ell}}) = \big(G_{\mathrm{s}i}(\mathbf{u}, \boldsymbol{\ell}) - G_{\mathrm{c}i}(\boldsymbol{\ell})\big)\hat{\ell}_i, \quad \text{where } i \in \mathcal{I}_\mathrm{tip} \tag{2.57}$$

The system of equations (2.55) serves four key purposes, which can be summarised as follows: to determine (1) the current crack tip branch lengths (given the history of crack evolution), (2) the current equilibrium displacement field, (3) the critical (or the most energetically favourable) crack-tip growth rate, and (4) to determine if this growth rate is indeed possible, i.e. does the total energy of the system decrease or at least stay the same.

In conclusion, the evolution of the mechanical system is determined by the time-continuous minimisation of $\mathcal{E}(\mathbf{u}, \boldsymbol{\ell})$ in terms of the variable pair $\{\mathbf{u}, \boldsymbol{\ell}\}$. Based on this formulation, the fractures and the equilibrium material state can evolve naturally insofar as $\mathcal{E}(\mathbf{u}, \boldsymbol{\ell})$ can be minimised in terms of $\{\mathbf{u}, \boldsymbol{\ell}\}$ for the given external load application.

2.4.5 Energy conservation

The crack growth formulation based on the total energy minimisation considers fixed boundary conditions at every point in time in the evolution process. At a given instance, crack growth is favourable provided that the total energy function can decrease or stay constant. The former condition is not energy conserving because it implies that there is

[4] This is a more inclusive form of $\mathcal{D}$ than initially defined in (2.44) as it highlights the relevant variables.

more energy being liberated than is converted to fracture surface energy. On the other contrary, crack growth that is characterised by a constant total energy function upholds the energy conservation principle such that the rate of energy liberation exactly matches the rate of energy dissipation via fracture surface creation. Although energy conservation does not affect the fracture path *per se*, in order to respect the energy conservation principle, the external load is required to adapt appropriately over time such that the total energy stays constant during the entire evolution of the mechanical system.[5] Under these conditions, fracture growth can be considered as *just possible*. For simplicity, it will be supposed that the external load, say $\mathbf{t}_0$, can be scaled by a factor λ_t, such that the effective applied load is: $\mathbf{t} = \lambda_t \mathbf{t}_0$. For a linear-elastic solid, its potential energy is proportional to the square of the magnitude of the applied load; hence, the same relationship also needs to hold for the crack tip energy release rate by virtue of the relationship in (2.34). Assuming $G_{\mathrm{s}i} = G_{\mathrm{s}i}(\mathbf{t}_0)$, the load-factor λ_t for a particular crack growth configuration $\hat{\boldsymbol{\ell}} \in \mathcal{A}$ under energy conservation conditions is obtained as:

$$\lambda_t = \sqrt{\frac{G_{\mathrm{c}i}\hat{\ell}_i}{G_{\mathrm{s}i}\hat{\ell}_i}}, \quad \text{where } i \in \mathcal{I}_{\mathrm{tip}} \tag{2.58}$$

2.5 Competing crack growth

Concerning the problem of multi-crack growth, it is possible that under certain geometrical and loading conditions the maximum dissipation rate is attained at several crack tips simultaneously. For the so-called problem of *competing crack growth* (CCG), a unique crack growth solution based on the maximum dissipation rate can not be determined because any admissible combination of the critical crack tip extension rates gives an equivalent energy dissipation rate (2.44). For this reason, it is necessary to consider the rate at which the dissipation rate changes with respect to the growth rates of the critical crack tips. Say If $\hat{\boldsymbol{\ell}} = \{\hat{\ell}_i\}$, where $i \in \mathcal{I}^{\mathrm{c}}_{\mathrm{tip}}$, is a set of critical crack tip growth rates, then the rate of change

[5] The total energy is required to stay constant because the system is considered as an isolated system.

of energy dissipation is computed as follows:

$$\left.\frac{\mathrm{d}\mathcal{D}}{\mathrm{d}a}\right|_{\hat{\boldsymbol{\ell}}} = \left.\frac{\mathrm{d}\mathcal{D}}{\mathrm{d}\boldsymbol{\ell}}\right|_{\hat{\boldsymbol{\ell}}} \tag{2.59}$$

$$\left.\frac{\mathrm{d}\mathcal{D}}{\mathrm{d}a}\right|_{\hat{\boldsymbol{\ell}}} = -\frac{\partial^2\mathcal{E}(\boldsymbol{\ell})}{\partial\ell_i\partial\ell_j}\hat{\ell}_i\hat{\ell}_j \tag{2.60}$$

$$\left.\frac{\mathrm{d}\mathcal{D}}{\mathrm{d}a}\right|_{\hat{\boldsymbol{\ell}}} = \left(-\frac{\partial^2\Pi(\boldsymbol{\ell})}{\partial\ell_i\partial\ell_j} + \frac{\mathrm{d}G_{\mathrm{c}i}}{\mathrm{d}\ell_j}\right)\hat{\ell}_i\hat{\ell}_j \tag{2.61}$$

The solution to the CCG problem in terms of the favourable crack tip growth rate $\hat{\boldsymbol{\ell}}_{\mathrm{c}} \in \mathcal{A}_{\mathrm{c}}$, is determined as the one that maximises the rate at which the dissipation rate changes:

$$\hat{\boldsymbol{\ell}}_{\mathrm{c}} = \underset{\hat{\boldsymbol{\ell}}\in\mathcal{A}_{\mathrm{c}}}{\arg\max}\left.\frac{\mathrm{d}\mathcal{D}}{\mathrm{d}a}\right|_{\hat{\boldsymbol{\ell}}} \tag{2.62}$$

Here, $\mathcal{A}_{\mathrm{c}} \subseteq \mathcal{A}$ denotes the admissible crack tip growth rates of the set of crack tips that are critical $\mathcal{I}^{\mathrm{c}}_{\mathrm{tip}} \subseteq \mathcal{I}_{\mathrm{tip}}$; $\mathcal{A}_{\mathrm{c}}$ is, therefore, analogous to the definition of $\mathcal{A}$ in equation (2.32):

$$\mathcal{A}_{\mathrm{c}} = \left\{\hat{\boldsymbol{\ell}} : \forall i \in \mathcal{I}^{\mathrm{c}}_{\mathrm{tip}},\ \hat{\ell}_i \in [0,1] \text{ subject to } \textstyle\sum_{i\in\mathcal{I}^{\mathrm{c}}_{\mathrm{tip}}}\hat{\ell}_i = 1\right\} \tag{2.63}$$

The crack tips in the set $\mathcal{I}^{\mathrm{c}}_{\mathrm{tip}}$ are assumed to satisfy the condition of critical dissipation:

$$\forall j \in \mathcal{I}^{\mathrm{c}}_{\mathrm{tip}}, \quad \mathcal{D}_j = \max_{\forall i\in\mathcal{I}_{\mathrm{tip}}}\mathcal{D}_i \tag{2.64}$$

Before the CCG problem is tackled, it is useful to address the concept of *fracture stability*, which is characterised by the sign of $\left.\frac{\mathrm{d}\mathcal{D}}{\mathrm{d}a}\right|_{\hat{\boldsymbol{\ell}}}$, as it play an important part in the solution.

2.5.1 Stability of cracks

The rate of change of dissipation (2.61) describes the property of stability of a fracture extension. The concept of fracture growth stability refers two possible fracture growth regimes, namely: one that is *stable* and one that is *unstable*. The terms are respectively used

to describe a decreasing and an increasing (or an otherwise constant) rate of dissipation:

$$\text{stable growth}: \quad \left.\frac{\mathrm{d}\mathcal{D}}{\mathrm{d}a}\right|_{\hat{\boldsymbol{\ell}}} < 0 \tag{2.65}$$

$$\text{unstable growth}: \quad \left.\frac{\mathrm{d}\mathcal{D}}{\mathrm{d}a}\right|_{\hat{\boldsymbol{\ell}}} \geq 0 \tag{2.66}$$

The significance of fracture stability, for a crack tip near the threshold of satisfying the fracture growth criterion (2.50), is as follows. If fracture growth is stable (2.65) then given a small load increment there exists an equilibrium fracture front position that the crack tip will advance to and subsequently arrest. Conversely, if fracture growth is unstable (2.66), an equilibrium fracture front position does not exist upon the application of a load increment. Thus, in the unstable case (2.66), crack growth may persist indefinitely.[6] The classification of fracture growth stability can also serve as a means to interpret the local curvature of the total energy function $\mathcal{E}(\boldsymbol{\ell}) = \mathcal{E}\big(\mathbf{u}(\boldsymbol{\ell}), \boldsymbol{\ell}\big)$ with respect to the evolution of the fracture lengths $\boldsymbol{\ell}$. Figure 2.3 illustrates two different behaviours of $\mathcal{E}(\boldsymbol{\ell})$ corresponding to a stable and an unstable evolutions of cracks. However, in order to characterise the shape of $\mathcal{E}(\boldsymbol{\ell})$ with respect to all tip perturbations that preserve the current fracture area, the following three cases can be defined in reference to the stability of the fracture front:

$$\text{stable fracture front}: \quad \frac{\partial^2 \mathcal{E}}{\partial \ell_i \partial \ell_j}\delta\ell_i\delta\ell_j > 0, \quad \forall \delta\boldsymbol{\ell} \in \mathbb{R}^{n_{\text{tip}}} \text{ s.t.} \sum_{i=1}^{n_{\text{tip}}} \delta\ell_i = 0 \tag{2.68}$$

$$\text{unstable fracture front}: \quad \frac{\partial^2 \mathcal{E}}{\partial \ell_i \partial \ell_j}\delta\ell_i\delta\ell_j \leq 0, \quad \forall \delta\boldsymbol{\ell} \in \mathbb{R}^{n_{\text{tip}}} \text{ s.t.} \sum_{i=1}^{n_{\text{tip}}} \delta\ell_i = 0 \tag{2.69}$$

$$\text{partially stable front}: \quad \frac{\partial^2 \mathcal{E}}{\partial \ell_i \partial \ell_j}\delta\ell_i\delta\ell_j \geq 0, \quad \exists \delta\boldsymbol{\ell} \in \mathbb{R}^{n_{\text{tip}}} \text{ s.t.} \sum_{i=1}^{n_{\text{tip}}} \delta\ell_i = 0 \tag{2.70}$$

[6] The nature of unstable crack growth can conflict with the the quasi-static assumption of the evolution of the mechanical system because a quasi-static model typically relies on the load to increase for the system to progress in time. This naturally implies stable crack growth. However, for the quasi-static assumption to make physical sense in the unstable case, the magnitude of the applied load, say $\lambda_{\mathbf{t}}$, is required to decrease at such a rate that the dissipation term has a net tendency to decrease as well. In general, to ensure that a quasi-static process is physically possible, the following inequality needs to be satisfied at the time of growth:

$$\begin{aligned} \frac{\partial \mathcal{D}}{\partial \boldsymbol{\ell}} + \frac{\partial \mathcal{D}}{\partial \lambda_{\mathbf{t}}}\frac{\mathrm{d}\lambda_{\mathbf{t}}}{\mathrm{d}\boldsymbol{\ell}} &< 0 \\ \frac{\mathrm{d}\lambda_{\mathbf{t}}}{\mathrm{d}\boldsymbol{\ell}} &< -\left(\frac{\partial \mathcal{D}}{\partial \lambda_{\mathbf{t}}}\right)^{-1}\frac{\partial \mathcal{D}}{\partial \boldsymbol{\ell}} \end{aligned} \tag{2.67}$$

The reason is as follows. If the strain energy release rate $G_{\text{s}}(\boldsymbol{\ell})$ at the instance of crack growth increases faster than the critical energy release rate of the material $G_{\text{c}}(\boldsymbol{\ell})$, i.e. $\mathrm{d}\mathcal{D}/\mathrm{d}\boldsymbol{\ell} > 0$, then, by virtue of energy conservation, the solid will start-to-begin to gain kinetic energy $U_k(\boldsymbol{\ell})$ such that $\mathrm{d}^2 U_k/\mathrm{d}\boldsymbol{\ell}^2 = \mathrm{d}\mathcal{D}/\mathrm{d}\boldsymbol{\ell}$. This can in turn undermine the quasi-static assumption regarding the slow evolution of the mechanical system.

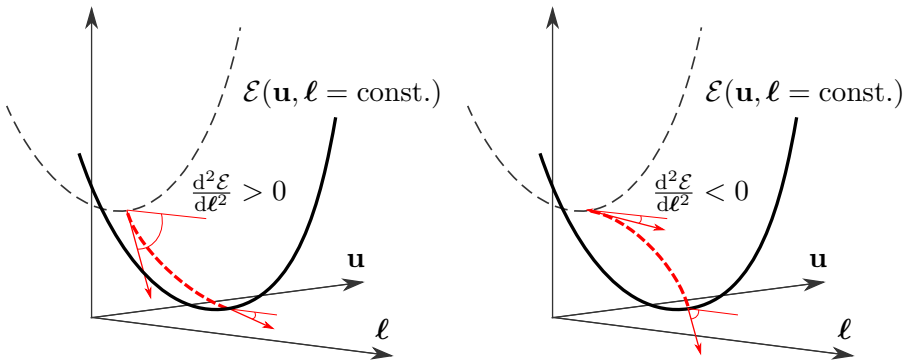

(a) Stable crack growth: $\frac{\mathrm{d}\mathcal{D}}{\mathrm{d}\ell} < 0$ (b) Unstable crack growth: $\frac{\mathrm{d}\mathcal{D}}{\mathrm{d}\ell} > 0$

FIGURE 2.3: Stable (a) and unstable (b) crack growth with the corresponding behaviours of the energy function $\mathcal{E}(\mathbf{u}(\ell), \ell)$. Note that a constant external load is supposed and that a decreasing total energy function simply means that there is available energy for crack growth (given the assumed load).

Therefore, a stable fracture front corresponds to a (locally) convex $\mathcal{E}(\ell)$, an unstable front is associated with a concave $\mathcal{E}(\ell)$, whereas a partially stable front results when $\mathcal{E}(\ell)$ is a saddle function. Note that the total (combined) fracture length of the fracture configuration is unchanged. In other words, the admissible perturbations include both positive and negative variations in the crack lengths such that the total fracture length is preserved.

The behaviour of $\mathcal{E}(\ell)$ plays an important part in the solution to the competing crack growth (CCG) problem whereby several crack tips attain the maximum dissipation rate. Since a unique solution to the crack tip growth rates is not possible based on the maximum dissipation rate alone, it becomes necessary to consider the rate at which the dissipation rate changes. This ultimately leads to solve an optimisation problem for which a closed-form analytical solution is difficult. Therefore, an efficient numerical technique will typically exploit the properties of the curvature of the total energy function, i.e. the stability property of the critical part of the fracture front (2.68) -(2.70). Several effective solution methods to solve the CCG problem are proposed in the subsequent section.

2.5.2 Crack growth solution

The solution to the competing crack growth (CCG) problem, as stated in equation (2.62), are the crack tip extension rates $\hat{\boldsymbol{\ell}} \in \mathcal{A}_{\mathrm{c}}$ that maximise the rate at which the dissipation rate changes. From a mathematical viewpoint, the CCG problem can be considered as a constrained quadratic optimisation problem. This is because the crack tip extension rates appear in a quadratic form in the expression of $\frac{\mathrm{d}\mathcal{D}}{\mathrm{d}a}\big|_{\hat{\boldsymbol{\ell}}}$ in equation (2.61), and the constraints on the solution arise by having to consider the admissible space of the critical crack tip extension rates $\mathcal{A}_{\mathrm{c}}$, as defined in (2.63). The constraints are, namely: (1) the crack tip growth rates must add-up to a unit growth rate (i.e. $\sum_{i\in\mathcal{I}^{\mathrm{c}}_{\mathrm{tip}}} \hat{\ell}_i = 1$), and (2) the growth rates must be non-negative (i.e. $\hat{\ell}_i \geq 0 \;\forall i \in \mathcal{I}^{\mathrm{c}}_{\mathrm{tip}}$). Consequently, the CCG problem can be postulated in a way that better lends itself to the mathematical treatment; that is, by explicitly stating the objective function to be maximised and the constraints to be satisfied:

$$\begin{aligned} \text{objective}: \quad & \max \Psi(\boldsymbol{v}) = \frac{1}{2} H_{sij} v_i v_j \\ \text{subject to}: \quad & C(\boldsymbol{v}) \equiv v_i \mathbf{e}_i - 1 = 0, \\ & v_i \geq 0 \quad \forall i \in \mathcal{I}^{\mathrm{c}}_{\mathrm{tip}} \end{aligned} \tag{2.71}$$

In (2.71), the objective function to be maximised is $\Psi(\boldsymbol{v})$. $C(\boldsymbol{v})$ defines the equality constraint to be satisfied by any trial fracture growth rate $\boldsymbol{v} = \{v_i\}$, where $i \in \mathcal{I}^{\mathrm{c}}_{\mathrm{tip}}$. Additionally, the condition of fracture growth irreversibility is enforced by requiring that $v_i \geq 0$ $\forall i \in \mathcal{I}^{\mathrm{c}}_{\mathrm{tip}}$. The constant term $H_{\mathrm{s}ij}$, where $i, j \in \mathcal{I}^{\mathrm{c}}_{\mathrm{tip}}$, corresponds to the negative element of the Hessian matrix of the total energy function $\mathcal{E}(\boldsymbol{\ell})$ that is evaluated for the particular fracture front configuration at hand; specifically:

$$H_{\mathrm{s}ij} = -\frac{\partial^2 \mathcal{E}(\boldsymbol{\ell})}{\partial \ell_i \partial \ell_j} \tag{2.72}$$

$$H_{\mathrm{s}ij} = -\frac{\partial^2 \Pi(\boldsymbol{\ell})}{\partial \ell_i \partial \ell_j} + \frac{\partial G_{\mathrm{c}i}}{\partial \ell_j} \tag{2.73}$$

The constraint of a unit combined fracture growth rate that any solution $\boldsymbol{v}$ needs to satisfy is enforced via the equality constraint equation $C(\boldsymbol{v}) = 0$. In addition, the constraint of a

non-negative fracture growth rate is imposed via the inequality constraint $v_i \geq 0$, where $i \in \mathcal{I}^{\mathrm{c}}_{\mathrm{tip}}$. Finally note that the fraction "$1/2$" in equation (2.71) is introduced purely for the convenience in applying a suitable solution methodology. Since the analytical solution to the CCG problem (2.71) is difficult, a numerical approach will need to be applied instead. In order to solve the CCG problem efficiently, a numerical scheme will have to be based around the particular shape (or curvature) of $\Psi(\boldsymbol{v})$ within the confines of the feasible solution space, as defined by the constraint conditions in (2.71). Within this solution space, the function $\Psi(\boldsymbol{v})$ can be downward-convex (concave), upward-convex (convex) or a generalised saddle function. These three behaviours of $\Psi(\boldsymbol{v})$ can be generalised as stable (2.68), unstable (2.69), and partially (un)stable (2.70) fracture front configurations, respectively. In the vicinity of a feasible solution $\boldsymbol{v} \geq \mathbf{0}$ the curvature of $\Psi(\boldsymbol{v})$ can be examined by assessing its second variation subject to satisfying $C(\boldsymbol{v}) = 0$:

$$\delta^2\Psi = H_{sij}\delta v_i \delta v_j \quad \forall \delta \boldsymbol{v} \,:\, \delta v_i \nabla C_i = 0, \tag{2.74}$$

where the gradient of $C(\boldsymbol{v})$ is simply a vector of ones, i.e. $\nabla C \equiv \mathbf{e}$. In (2.74), the equality-constraint reduces the available space of the variation $\delta\boldsymbol{v}$ by requiring that it be orthogonal to the gradient of $C(\boldsymbol{v})$, i.e. $\delta v_i \nabla C_i = 0$. Therefore, the type of curvature that $\Psi(\boldsymbol{v})$ can exhibit along any feasible perturbation $\delta\boldsymbol{v}$ is determined by the definitiveness of the second order term $\delta^2\Psi(\mathbf{V}^*) = H_{\mathrm{s}ij}V_i^*V_j^*$ for all real-valued vectors $\mathbf{V}^*$ that satisfy $V_i^*\nabla C_i = 0$. To this end, $\mathbf{V}^*$ can be constructed from any same-dimension real-valued vector $\mathbf{V}$ by subtracting $\mathbf{V}$'s component in the direction of ∇C; therefore, $\mathbf{V}^*$ can be given as shown:

$$\mathbf{V}^* = \left(\mathbf{I} - \frac{\nabla C \nabla C^{\mathrm{T}}}{\nabla C^{\mathrm{T}} \nabla C}\right)\mathbf{V} \tag{2.75}$$

The definitiveness of $\delta^2\Psi(\mathbf{V}^*) = H_{sij}V_i^*V_j^*$, where $\mathbf{V}^*$ is constrained, can be effectively described in terms of that of $\delta^2\Psi^*(\mathbf{V}) = H^*_{\mathrm{s}\,ij}V_iV_j$, where $\mathbf{V}$ is unconstrained and where the matrix H^*_{s} is the projection of H_{s} on the feasible solution plane; hence, H^*_{s} is given as:

$$H^*_{\mathrm{s}} = \left(\mathbf{I} - \frac{\nabla C \nabla C^{\mathrm{T}}}{\nabla C^{\mathrm{T}} \nabla C}\right)^{\mathrm{T}} H_{\mathrm{s}} \left(\mathbf{I} - \frac{\nabla C \nabla C^{\mathrm{T}}}{\nabla C^{\mathrm{T}} \nabla C}\right) \tag{2.76}$$

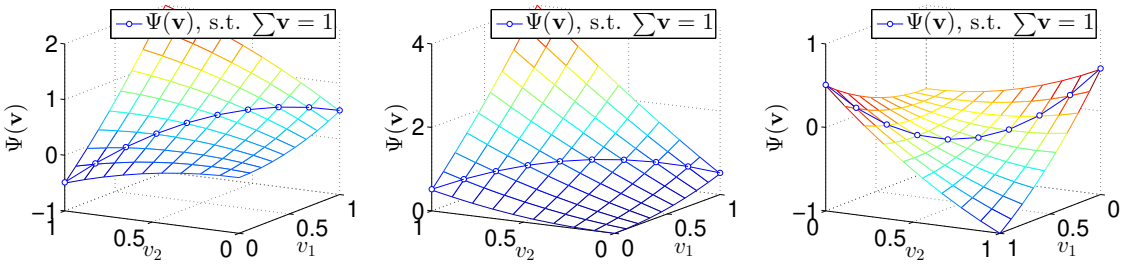

(a) H_{s} - indefinite; H_{s}^* - negative semidefinite

(b) H_{s} - positive definite; H_{s}^* - negative semidefinite

(c) H_{s} - indefinite; H_{s}^* - positive semidefinite

FIGURE 2.4: Three instances of a pair of competing cracks, each showing a different shape of the objective function $\Psi(\boldsymbol{v})$ with its behaviour highlighted within the feasible solution space. The surface of $\Psi(\boldsymbol{v})$ is governed by H_{s}, whereas its behaviour within the feasible solution space is governed by H_{s}^*.

It is remarked that the resulting symmetric matrix H_{s}^* is semidefinite because at least one eigenvalue is zero, e.g. $\nabla C_i H_{s\,ij}^* \nabla C_j = 0$. Nonetheless, the signs of the remaining eigenvalues of H_{s}^* can be used to characterise the relevant behaviour of $\Psi(\boldsymbol{v})$ within the feasible solution space. Therefore, $\Psi(\boldsymbol{v})$ is convex with respect to $\boldsymbol{v}$, subject to $C(\boldsymbol{v}) = 0$, if H_{s}^* is positive semidefinite (i.e. all the remaining eigenvalues of H_{s}^* are positive); $\Psi(\boldsymbol{v})$ is concave if H_{s}^* is negative semidefinite (i.e. the eigenvalues are negative); $\Psi(\boldsymbol{v})$ is a saddle function if H_{s}^* is indefinite (i.e. the eigenvalues are of mixed signs).

The stability property of the fracture front can be characterised using H_{s}^* in the same way. Thus, the fracture front is stable if H_{s}^* is negative semidefinite; the fracture front is unstable if H_{s}^* is positive semidefinite; the fracture front is partially (un)stable if H_{s}^* is indefinite. Figure 2.4 illustrates the usefulness of H_{s}^* in describing the relevant behaviour of $\Psi(\boldsymbol{v})$ for a few different instances involving a pair of competing crack tips.

The following subsections delineate numerical solution methods for solving the competing crack growth problem (2.71) for arbitrary numbers of competing crack tips. The numerical solution methodologies are tailored based on the stability property of the critical crack tips. Consequently, solution are provided for the three cases of: stable (2.68), unstable (2.69), and partially (un)stable (2.70) fracture front configurations.

Fracture front is unstable

The simplest case arises when the critical fracture front is unstable (2.69). In this case, H_{s}^{*} is positive semidefinite by reason that it has no negative eigenvalues. The solution $\boldsymbol{v}$ that maximises $\Psi(\boldsymbol{v})$ can be determined by inspection of H_{s} alone; specifically, the solution is obtained as $v_{i^\star} = 1$ where $i^\star \in \mathcal{I}_{\mathrm{tip}}^{\mathrm{c}}$ is the tip that corresponds to the largest entry on the main diagonal of H_{s}, i.e. $i^\star = \arg\max_{i \in \mathcal{I}_{\mathrm{tip}}^{\mathrm{c}}} H_{\mathrm{s}ii}$. Figure 2.4c illustrates the particular case.

Under these conditions, only a single crack tip can advance since only then does the growth maximise the objective function $\Psi(\boldsymbol{v})$ subject to satisfying the constraints. This has an important implication concerning symmetric problems where there are at least a few critical crack tips; specifically, it reveals that the symmetric fracture advance is unstable since an asymmetric solution (growth at one crack tip) is energetically favoured better. Case in point is a 2D problem with a center crack subjected symmetric boundary conditions such that $H_{\mathrm{s}11} > H_{\mathrm{s}12}$, and where $H_{\mathrm{s}11} = H_{\mathrm{s}22}$ and $H_{\mathrm{s}12} = H_{\mathrm{s}21}$. An analogous case is depicted in Figure 2.4c. Firstly, by assuming a symmetric solution, i.e. $v_1 = v_2 = \frac{1}{2}$, the objective function acquires the value $\Psi_{\mathrm{sym}} = \frac{1}{8}(H_{\mathrm{s}11} + H_{\mathrm{s}22} + 2H_{\mathrm{s}12})$. On the other hand, assuming an asymmetric solution, i.e. growth of only one crack tip, gives $\Psi_{\mathrm{asym}} = \frac{1}{2}H_{\mathrm{s}11} = \frac{1}{2}H_{\mathrm{s}22}$. The difference in Ψ is therefore $\Psi_{\mathrm{asym}} - \Psi_{\mathrm{sym}} \equiv \frac{1}{4}(H_{\mathrm{s}11} - H_{\mathrm{s}12}) > 0$. This proves that the 2D problem favours an asymmetric solution, i.e. growth of only one crack tip, rather than a symmetric solution, i.e. simultaneous growth of both crack tips.

Fracture front is stable

When the fracture front is stable (2.68), the matrix H_{s}^{*} is negative semidefinite, i.e. H_{s}^{*} has no positive eigenvalues. As a result, the function $\Psi(\boldsymbol{v})$ is concave (convex-down) within the feasible solution space. To find $\boldsymbol{v}$ that maximise $\Psi(\boldsymbol{v})$ (or that causes $\Psi(\boldsymbol{v})$ to decrease least) requires to solve the constrained quadratic optimisation problem (2.71). Since a closed-form solution is difficult by virtue of the inequality constraint, a more practical approach is to apply an iterative solution scheme. One such technique that is well suited for handling inequality constrains is the active-set method for convex quadratic

programming problems [210]. The method consists of first making a feasible guess for the initial solution (such that it satisfies all constraint conditions), then seeking to improve it in a series of equality-constrained optimizations. In more detail, the algorithm at iteration step k projects the current solution $\boldsymbol{v}^k$ for a set of crack tips $\mathcal{W}^k \subseteq \mathcal{I}^{\mathrm{c}}_{\mathrm{tip}}$ (called the working-set) along a feasible direction $\boldsymbol{d}^k$ that maximises the objective function, subject to all equality constraints being met. The extent to which the solution is advanced along $\boldsymbol{d}^k$ is determined by a weight factor w^k such the objective function $\Psi(\boldsymbol{v}^k + w^k\boldsymbol{d}^k)$ is either maximised locally (i.e. reaches an extremum) or it is maximised up to the point the solution hits an inequality constrain. When it is the latter cause, the subsequent iteration $k+1$ treats the about-to-fail inequality constraint as an equality constraint. This effectively leads to a reduced working set $\mathcal{W}^{k+1} = \mathcal{W}^k \backslash i$ of tips in the incremental solution process.

It is remarked that the inequality constraints only provide the bounds to the extent the solution can be projected towards the maximum value of Ψ^{k+1} for a working-set $\mathcal{W}^k$ at step k. Therefore, insofar as it concerns the problem of determining the optimum marching direction, the method of Lagrangian multipliers can be applied directly since the problem at hand is an equality-constrained optimisation. As such, the Lagrangian at step k reads:

$$\mathcal{L}(\boldsymbol{v}^{k+1}, \lambda^{k+1}) = \frac{1}{2} H_{sij}\, v_i^{k+1} v_j^{k+1} + \lambda^{k+1}(\mathbf{e}_i v_i^{k+1} - 1), \quad \text{for } i, j \in \mathcal{W}^k \tag{2.77}$$

The solution to $\{\boldsymbol{v}^{k+1}, \lambda^{k+1}\}$ corresponds to the stationary point of the Lagrangian. Taking the variation of $\mathcal{L}(\boldsymbol{v}^{k+1}, \lambda^{k+1})$ with respect to each variable in turn produces two equations:

$$H_{sij} v_j^{k+1} + \mathbf{e}_i \lambda^{k+1} = 0 \tag{2.78}$$

$$\mathbf{e}_i v_i^{k+1} - 1 = 0 \tag{2.79}$$

Solving (2.78) and (2.79) will yield the solution to the *idealised* rate of fracture advance, $\boldsymbol{v}^{k+1}$. The solution $\boldsymbol{v}^{k+1}$ is termed *idealised* because the requirement for a strictly non-negative solution is unenforced. Nonetheless, the solution advance direction $\boldsymbol{d}^k = \boldsymbol{v}^{k+1} - \boldsymbol{v}^k$ at

iteration step k can be used. In this case, $\boldsymbol{d}^k$ can be shown to take the following form:

$$d_i^k = \frac{{H_s^{-1}}_{ij}\,\mathbf{e}_j}{{H_s^{-1}}_{ij}\,\mathbf{e}_i\,\mathbf{e}_j} - v_i^k \quad \text{for } i \in \mathcal{W}^k \tag{2.80}$$

The amount the current solution $\boldsymbol{v}^k$ is advanced along the direction $\boldsymbol{d}^k$ is determined by the weight-factor $w^k \in [0,1]$ such that the new solution is $\boldsymbol{v}^{k+1} = \boldsymbol{v}^k + w^k\boldsymbol{d}^k$. The weight factor w^k is computed based on the distance from the current solution $\boldsymbol{v}^k$ to the most imminent boundary of any inequality constraint such that $v_i^{k+1} \geq 0$ for $i \in \mathcal{W}^k$. This leads to the following expression for the maximum (positive) value of the weight:

$$w^k = \min\left(\left\{\frac{v_i^k}{-d_i^k}, 1\right\}\right), \quad \text{where } i \in \mathcal{W}^k \tag{2.81}$$

Fracture front is partially stable

For the general case of a partially stable fracture front (2.70), the matrix H_{s}^* is indefinite, i.e. H_{s}^* has eigenvalues of mixed signs. As a result, the function $\Psi(\boldsymbol{v})$ behaves as a generalised saddle function within the feasible solution space. This, in turn, prevents the two previously delineated techniques from being used effectively since they are limited to convex problems only. The non-convexity of $\Psi(\boldsymbol{v})$ gives rise to a solution space that can contain many extrema, among which it can prove difficult to determine the solution that globally maximises $\Psi(\boldsymbol{v})$. For this reason it may be necessary to examine all stationary solutions as well as the solutions that lie on the vertices of the feasible domain. In order to solve the present variant of the CCG problem (2.71), we adopt a gradient-based solution methodology. Specifically, the solution advance direction is determined as the projection of the gradient of $\Psi(\boldsymbol{v})$ on the plane that is orthogonal to ∇C. The solution $\boldsymbol{v}^k$ at iteration step k is advanced following the active-set framework, as described in Section 2.5.2; however, any chance of downward convexity of Ψ along a particular solution advance directions is exploited. In this formulation, the solution advance vector $\boldsymbol{d}^k$ can be obtained as:

$$d_i^k = \left(\delta_{ij} - \frac{\nabla C_i\,\nabla C_j}{\nabla C_q \nabla C_q}\right)\nabla\Psi_j^k, \quad \text{where } i,j,q \in \mathcal{W}^k \tag{2.82}$$

where the gradient of the objective function is $\nabla\Psi_i^k = H_{sij}\, v_j^k$. Since the gradient of the equality constraint is a vector of ones, i.e. $\nabla C_i = \mathbf{e}_i$, equation (2.82) can be simplified to:

$$d_i^k = \nabla\Psi_i^k - \text{mean}(\nabla\Psi^k) \tag{2.83}$$

The solution is projected along $\boldsymbol{d}^k$ using the weight factor $w^k \in [0, \infty)$ to the extent that no inequality constraint is violated, i.e. $v_i^{k+1} = v_i^k + w^k d_i^k \geq 0$ for $i \in \mathcal{W}^k$. Thus, w^k is similar to that in (2.81), though the upper-bound $w^k \leq 1$ can be omitted so long as $\Psi(\boldsymbol{v}^k + w^k\boldsymbol{d}^k)$ is upward-convex with respect to w^k, i.e. $H_{sij}d_i^k d_j^k > 0$; hence, the solution for w^k reads:

$$w^k = \min\left(\left\{\frac{v_i^k}{-d_i^k}\right\}\right), \quad \text{where } i \in \mathcal{W}^k \tag{2.84}$$

In case $\Psi(\boldsymbol{v}^k + w^k\boldsymbol{d}^k)$ is downward-convex with respect to w^k, i.e. $H_{sij}d_i^k d_j^k < 0$, an optimum weight factor w^k can be determined via a line-search technique. The locally optimal value of the weight factor w^k is obtained by solving for stationarity value of $\Psi(\boldsymbol{v}^k + w^k\boldsymbol{d}^k)$ with respect to w^k while minding the inequality constrains via (2.84):

$$w^k = -\frac{H_{sij}d_i^k v_j^k}{H_{sij}d_i^k d_j^k}, \text{ provided } H_{sij}d_i^k d_j^k < 0 \text{ and} \tag{2.85}$$
$$\text{subject to } w^k < \min\left(\left\{\frac{v_i^k}{-d_i^k}\right\}\right), \text{ where } i, j \in \mathcal{W}^k$$

It is reminded that the converged solution $\boldsymbol{v}^n$, when $n \to \infty$, can depend on the initial (trial) solution $\boldsymbol{v}^0$. For this reason, it is generally required to assess different starting points, e.g. the vertices of the feasible solution space, in order to safe-guard against a converged solution that may only be locally optimal. A pseudo-code of the algorithm for solving the competing crack growth problem (2.71) for the general case of a partially (un)stable fracture front is provided in Appendix A.2.

The subsequent section is concerned with the problem of the crack kink direction. Crack kinking based on the maximum dissipation rate is considered first. The governing principle is then extended to finite crack extensions whereby the crack tip branch direction is determined as the direction that minimises (on average) the total energy of the system.

2.6 Direction of crack growth

In a 2D framework, the incipient growth direction of any crack tip $i \in \mathcal{I}_{\text{tip}}$ can be specified in terms of the crack tip growth angle θ_i (or, alternatively, in terms of the crack tip angle of kink $\Delta\theta_i$). If $\delta\boldsymbol{\ell} \in \mathbb{R}^n_{>0}$ consists of n small crack tip extensions, i.e. $\delta\ell_i \to 0^+ \; \forall i \in \mathcal{W}$, where $\mathcal{W} \subseteq \mathcal{I}_{\text{tip}}$, then minimising the total energy $\mathcal{E}(\delta\boldsymbol{\ell}, \Delta\boldsymbol{\theta})$ with respect to $\Delta\boldsymbol{\theta}$ is equivalent to finding $\Delta\boldsymbol{\theta}$ that maximises the incipient energy dissipation rate $\mathcal{D}(\boldsymbol{\ell}, \Delta\boldsymbol{\theta}) \equiv \mathcal{D}_i(\boldsymbol{\ell}, \Delta\theta_i)\hat{\ell}_i$:

$$\min_{\Delta\boldsymbol{\theta}\in\mathbb{R}^n} \mathcal{E}(\boldsymbol{\ell} + \delta\boldsymbol{\ell}, \Delta\boldsymbol{\theta}) \equiv \frac{\left[\min\limits_{\Delta\boldsymbol{\theta}\in\mathbb{R}^n} \mathcal{E}(\boldsymbol{\ell} + \delta\boldsymbol{\ell}, \Delta\boldsymbol{\theta})\right] - \mathcal{E}(\boldsymbol{\ell})}{\sum_{i\in\mathcal{W}} \delta\ell_i} \tag{2.86}$$

$$\min_{\Delta\boldsymbol{\theta}\in\mathbb{R}^n} \mathcal{E}(\boldsymbol{\ell} + \delta\boldsymbol{\ell}, \Delta\boldsymbol{\theta}) \equiv \min_{\Delta\boldsymbol{\theta}\in\mathbb{R}^n} \frac{\mathcal{E}(\boldsymbol{\ell} + \delta\boldsymbol{\ell}, \Delta\boldsymbol{\theta}) - \mathcal{E}(\boldsymbol{\ell})}{\delta a} \tag{2.87}$$

$$\min_{\Delta\boldsymbol{\theta}\in\mathbb{R}^n} \mathcal{E}(\boldsymbol{\ell} + \delta\boldsymbol{\ell}, \Delta\boldsymbol{\theta}) \equiv \min_{\Delta\boldsymbol{\theta}\in\mathbb{R}^n} \frac{\partial\mathcal{E}(\boldsymbol{\ell}, \Delta\boldsymbol{\theta})}{\partial\ell_i}\frac{\mathrm{d}\ell_i}{\mathrm{d}a} \tag{2.88}$$

$$\min_{\Delta\boldsymbol{\theta}\in\mathbb{R}^n} \mathcal{E}(\boldsymbol{\ell} + \delta\boldsymbol{\ell}, \Delta\boldsymbol{\theta}) \equiv \max_{\Delta\boldsymbol{\theta}\in\mathbb{R}^n} \mathcal{D}_i(\boldsymbol{\ell}, \Delta\theta_i)\frac{\mathrm{d}\ell_i}{\mathrm{d}a} \tag{2.89}$$

$$\min_{\Delta\boldsymbol{\theta}\in\mathbb{R}^n} \mathcal{E}(\boldsymbol{\ell} + \delta\boldsymbol{\ell}, \Delta\boldsymbol{\theta}) \equiv \max_{\Delta\boldsymbol{\theta}\in\mathbb{R}^n} \mathcal{D}(\boldsymbol{\ell}, \Delta\boldsymbol{\theta}) \tag{2.90}$$

For $\mathcal{D}(\boldsymbol{\ell}, \Delta\boldsymbol{\theta})$ to be maximum, the individual crack tip energy dissipation rates $\mathcal{D}_i(\boldsymbol{\ell}, \Delta\theta_i)$ must be maximum regardless of the relative crack tip growth rates $\hat{\ell}_i = \mathrm{d}\ell_i/\mathrm{d}a$ for $i \in \mathcal{W}$:

$$\min_{\Delta\boldsymbol{\theta}\in\mathbb{R}^n} \mathcal{E}(\delta\boldsymbol{\ell}, \Delta\boldsymbol{\theta}) \equiv \max_{\Delta\boldsymbol{\theta}\in\mathbb{R}^n} \mathcal{D}_i(\boldsymbol{\ell}, \Delta\theta_i)\frac{\mathrm{d}\ell_i}{\mathrm{d}a} \tag{2.91}$$

$$\min_{\Delta\boldsymbol{\theta}\in\mathbb{R}^n} \mathcal{E}(\delta\boldsymbol{\ell}, \Delta\theta_i) \equiv \max_{\Delta\theta_i\in\mathbb{R}} \mathcal{D}_i(\boldsymbol{\ell}, \Delta\theta_i) \quad \forall i \in \mathcal{W} \tag{2.92}$$

Consequently, the solution to the crack tip extension directions is the solution that maximises the individual crack tip energy dissipation rates (2.92). In other words, based on the principle of maximum dissipation (2.45), any crack tip $i \in \mathcal{I}_{\text{tip}}$ has a preferred growth direction that locally maximises $\mathcal{D}_i(\theta_i) = G_{\text{s}i}(\theta_i) - G_{\text{c}i}(\theta_i)$. The optimality condition for θ_i, in the sense of a maximum $\mathcal{D}_i(\theta_i)$, can be formulated as the following stationary condition:

$$\frac{\mathrm{d}\mathcal{D}_i}{\mathrm{d}\theta_i} = 0, \text{ subject to } \frac{\mathrm{d}^2\mathcal{D}_i}{\mathrm{d}^2\theta_i} < 0 \tag{2.93}$$

where it is assumed that $\mathcal{D}_i(\theta_i)$ is a concave function of θ_i. Alternatively, (2.93) can be formulated as a principle of stationary (minimum) total energy $\mathcal{E}(\Delta\ell_i, \theta_i)$ with respect to the sweeping crack tip extension $\Delta\ell_i > 0$ through the angle θ_i in the limit the extension tends to zero, i.e. $\Delta\ell_i \to 0^+$. This alternative form can be obtained directly from (2.93) by integrating $\mathcal{D}_i = -\mathrm{d}\mathcal{E}/\mathrm{d}\ell_i$ with respect to ℓ_i over the infinitesimal crack tip extension $\Delta\ell_i$:

$$\lim_{\Delta\ell_i \to 0^+} \left(-\frac{\mathrm{d}\mathcal{E}}{\mathrm{d}\theta_i}\bigg|_{\Delta\ell_i} \right) = 0, \text{ subject to } \lim_{\Delta\ell_i \to 0^+} \left(-\frac{\mathrm{d}^2\mathcal{E}}{\mathrm{d}\theta_i^2}\bigg|_{\Delta\ell_i} \right) < 0 \tag{2.94}$$

For the purpose of notational convenience, let us define a variable $\mathcal{D}_{\theta i}$ to represent the average rotational dissipation of the fracture extension $\Delta\ell_i$ with respect to its angle θ_i:

$$\mathcal{D}_{\theta i} = -\frac{\mathrm{d}\mathcal{E}}{\mathrm{d}\theta_i}\bigg|_{\Delta\ell_i} \tag{2.95}$$

The rotational dissipation term $\mathcal{D}_{\theta i}$ describes how the total energy $\mathcal{E}$ of the mechanical system changes with respect to the rotation of the crack tip extension $\Delta\ell_i$ in terms of its angle of kink θ_i. Substituting (2.95) in (2.94) gives the criterion for the incipient crack growth angle θ_i in terms of the fracture state of zero rotational dissipation:[7]

$$\lim_{\Delta\ell_i \to 0^+} \mathcal{D}_{\theta i} = 0, \text{ subject to } \lim_{\Delta\ell_i \to 0^+} \left(\frac{\mathrm{d}\mathcal{D}_{\theta i}}{\mathrm{d}\theta_i} \right) < 0, \tag{2.96}$$

To sum up, the fundamental crack-growth direction criterion in (2.93), which is based on the principle of maximum dissipation, has been reformulated in (2.94) as a minimum total energy principle that considers the angle of a virtual crack tip extension. The state of minimum total energy has been equivalently represented in (2.96) as the state of a vanishing rotational dissipation $\mathcal{D}_{\theta i}$ with respect to the crack tip extension angle θ_i. The main advantage of the minimum energy formulation (2.96) over the maximum dissipation principle (2.93) is that is readily extensible to finite crack increments (i.e. a discrete framework) by disregarding the limit of a vanishing $\Delta\ell$ in the computations.

[7] As the fracture increments are assumed to be vanishingly small, their mutual interactions are irrelevant; hence, to assert $\forall i \in \mathcal{I}_{\text{tip}}$ that θ_i is optimal in terms of $\mathcal{D}_{\theta i} = 0$, it suffices to determine that $\mathrm{d}\mathcal{D}_{\theta i}/\mathrm{d}\theta_i < 0$.

2.7 The case of a constant G_{c}

In Chapter 3, the evolution problem of the mechanical system will be solved within a discrete framework. The special case of a material with a constant critical energy release rate will be considered for simplicity. Although some generality of the problem is lost as a result of the simplification, the fundamental principles governing the discrete problem and its solution are unchanged. The following subsections provide the simplified forms of the equations governing the evolution of crack lengths (2.56) and crack tip kinking (2.96).

Evolution of crack lengths

Assuming a constant material G_{c}, the total energy function $\mathcal{E}(\mathbf{u}, \boldsymbol{\ell})$ (2.54) can be written as:

$$\mathcal{E}(\mathbf{u}, \boldsymbol{\ell}) = \Pi(\mathbf{u}, \boldsymbol{\ell}) + G_{\mathrm{c}} \sum_{i=1}^{n_{\mathrm{tip}}} \ell_i \tag{2.97}$$

Then the solution $\{\mathbf{u}, \boldsymbol{\ell}\}(a)$ at a particular instance in the fracture evolution process $a = a^\star$, where $a^\star \in [a_0, a_\infty]$, is governed by the following set of equations:

$$\begin{cases} \boldsymbol{\ell} = \int_{a_0}^{a^\star} \hat{\boldsymbol{\ell}}(a) \mathrm{d}a \\ \mathbf{u} = \underset{\mathbf{u}_* \in \mathcal{U}(\Gamma_{\mathrm{c}})}{\arg\min}\, \Pi(\mathbf{u}_*, \boldsymbol{\ell}) \\ \hat{\boldsymbol{\ell}}_{\mathrm{c}} = \underset{\hat{\boldsymbol{\ell}}_* \in \mathcal{A}(\Gamma_{\mathrm{c}})}{\arg\max} \left(G_{\mathrm{s}i} \hat{\ell}_{*i} \right) \\ \hat{\boldsymbol{\ell}} = \begin{cases} \hat{\boldsymbol{\ell}}_{\mathrm{c}} & \text{if } G_{\mathrm{s}i} \hat{\ell}_{\mathrm{c}i} \geq G_{\mathrm{c}} \\ 0 & \text{otherwise} \end{cases} \end{cases} \tag{2.98}$$

In (2.98), the critical fracture path $\boldsymbol{\ell}_{\mathrm{c}} = \int_{a_0}^{a_\infty} \hat{\boldsymbol{\ell}}_{\mathrm{c}} \, \mathrm{d}a$ is determined by the time-continuous maximisation of the energy release rate $G_{\mathrm{s}} = G_{\mathrm{s}i} \hat{\ell}_i$, subject to satisfying static equilibrium. Crack growth takes place if there is sufficient fracture driving force G_{s} to overcome the material resistance G_{c} (however, the principle of energy conservation requires $G_{\mathrm{s}} \leq G_{\mathrm{c}}$).

Direction of crack growth

For a material with a constant G_c the equations governing crack kinking can be simplified. Firstly, the criterion for the incipient crack tip kink angle θ_i can be written as follows:

$$\frac{\mathrm{d}G_{si}}{\mathrm{d}\theta_i} = 0, \text{ subject to } \frac{\mathrm{d}^2 G_{si}}{\mathrm{d}^2\theta_i} < 0 \tag{2.99}$$

The alternative form of (2.99) in terms of the minimum potential energy $\Pi(\Delta\ell_i, \theta_i)$ is obtained by integrating $G_{si} = -\mathrm{d}\Pi/\mathrm{d}\ell_i$ with respect to ℓ_i over the extension $\Delta\ell_i \to 0^+$:

$$\lim_{\Delta\ell_i \to 0^+} \left(-\frac{\mathrm{d}\Pi}{\mathrm{d}\theta_i}\bigg|_{\Delta\ell_i} \right) = 0, \text{ subject to } \lim_{\Delta\ell_i \to 0^+} \left(-\frac{\mathrm{d}^2\Pi}{\mathrm{d}\theta_i^2}\bigg|_{\Delta\ell_i} \right) < 0 \tag{2.100}$$

Next, it is useful to define a new variable $G_{\theta i}$ as the rotational energy release rate of the fracture extension $\Delta\ell_i$ with respect to its kink angle θ_i:

$$G_{\theta i} = -\frac{\mathrm{d}\Pi}{\mathrm{d}\theta_i}\bigg|_{\Delta\ell_i} \tag{2.101}$$

Finally, the crack tip kinking criterion in terms of a vanishing rotational energy release rate is obtained by substituting (2.101) into (2.100):

$$\lim_{\Delta\ell_i \to 0^+} G_{\theta i} = 0, \text{ subject to } \lim_{\Delta\ell_i \to 0^+} \left(\frac{\mathrm{d}G_{\theta i}}{\mathrm{d}\theta_i} \right) < 0 \tag{2.102}$$

2.8 Summary

This chapter has mainly focused on three issues: the problem of static equilibrium of an elastic solid, the principle governing fracture behaviour (according to Griffith's theory), the problem of competing crack growth, and the alternative formulation of the crack growth direction criterion (which was still based on Griffith's theory).

Firstly, the problem of static equilibrium of a pre-cracked linear-elastic solid was formulated in what is called the *weak-form* (2.18). The solution to the weak-form satisfies the equilibrium equations in an integral sense rather than point-wise; this has the great advantage of reducing the smoothness requirement of the trial displacement field $\mathbf{u}$, which allows for the first derivatives of $\mathbf{u}$ to be discontinuous. The practical consequence is that the weak solution can naturally capture solutions with discontinuous strains, such as those appearing across material interfaces. Otherwise, if the elastic coefficients (2.9) are spatially continuous functions, then the weak from implies the strong form (2.1), i.e. the weak solution coincides with the strong. It was shown that the weak form could be interpreted as a variational statement (2.20) that described when a particular functional $\Pi(\mathbf{u})$, called the potential energy of the mechanical system, was stationary (2.19) in terms of $\mathbf{u}$. Since $\Pi(\mathbf{u})$ is generally convex, the static-equilibrium solution $\mathbf{u}$ is one that minimises $\Pi(\mathbf{u})$.

The problem of fracture growth within the framework of linear-elastic fracture mechanics (LEFM) was considered next. In this context, a crack is represented by a zero thickness discontinuity in the displacement field and the solid is assumed to be perfectly brittle, i.e. internal (elastic) energy dissipation is through fracture surface energy alone (Section 1.3). It was assumed that the fracture behaviour was governed by Griffith's law (2.41), which states that a crack grows when the fracture driving force (i.e. the fracture energy release rate) (2.39) overcomes the resistance of the material (i.e. the critical energy release rate) (2.40). Within the LEFM framework, Griffith's law (2.41) was shown to naturally lead to the principle of maximal energy dissipation (2.43) with respect to the increase in the total fracture length (2.29). Subsequently, the problem of fracture evolution was posed as a *time-continuous* minimisation (2.55) of the so-called *total-energy* functional (2.54) whereby the total energy is minimised with respect to the increase in the total fracture length.

In case of competing crack growth, which is defined as the instance when multiple crack tips have equivalent energy dissipation rates (2.44), the condition of maximum energy dissipation rate (2.43) is no longer sufficient to determine the critical competing crack growth solution because any admissible solution (2.63) yields an equivalent energy dissipation rate. In order to effectively apply the principle of maximal energy dissipation to determine the critical competing crack growth solution, it is required to consider higher

order terms in the total energy function (2.61). This means that the critical solution needs to maximise the rate of energy dissipation (2.62) with respect to the increase in the total fracture length. This leads to a quadratic constrained optimisation problem (2.71) for the solution of the competing crack tip growth rates (2.31). Three solution methods were proposed to tackle the three different cases of competing crack growth. The choice of a particular solution approach was tailored to the curvature of the total energy function; specifically, whether the energy function was convex, concave or a generalised saddle function. These three behaviours of the energy function were described in terms of a physically more meaningful classification of the fracture configuration; specifically, weather the fracture front was stable (2.68), unstable (2.69), or partially stable (2.70).

Finally, the direction of crack growth was considered in line with the maximum total energy dissipation principle. Since the global maximality condition (2.90) automatically implies local maximality (2.92), the incipient direction of crack growth can be determined separately for each crack tip, regardless of crack tip extension rates (2.31). The principle of maximum local dissipation (2.93) with respect to the incipient crack growth direction was reformulated in a more convenient form stating that the total energy function had to be minimised with respect to the extension direction of an infinitesimal crack branch (2.94). At this point, it was convenient to introduce the concept of *rotational dissipation* (2.95) to define the rate at which the total energy of the system decreased with respect to the rotation of a fracture extension (2.94). Subsequently, the minimum total energy principle could be posed as the principle of vanishing rotational dissipation (2.96).

The main advantage of determining multiple crack evolutions based on the energy minimisation approach (2.55) is that the method can be applied to the discrete framework (i.e. for finite crack extensions) more robustly and yet more easily than the principle of maximal dissipation (2.43). This is because both the static-equilibrium and the fracture evolution problems can be solved just by minimising the total energy of the system.

Chapter 3

Discrete Solution

3.1 Introduction

As described in Section 2.4.4, the evolution of fracture lengths is governed by the time-continuous minimisation of the total energy function $\mathcal{E}(\mathbf{u}(a), \boldsymbol{\ell}(a))$ with respect to a, where $a \in [a_0, a_\infty]$ is the combined fracture length variable, which also parametrises the time-line of the fracture evolution process. Let us first consider the evolution of the mechanical system in terms of the variable triplet $\{\mathbf{u}, \boldsymbol{\ell}, \boldsymbol{\theta}\}(a)$ as a rate problem. In this case, the solution to $\{\mathbf{u}, \hat{\boldsymbol{\ell}}, \Delta\boldsymbol{\theta}\}(a)$, where $\hat{\boldsymbol{\ell}}$ are the relative crack tip extensions rates (2.31), is theoretically obtained as follows: (1) determine the equilibrium displacement field $\mathbf{u}(a)$ for the current fracture configuration $\Gamma_c(a)$ (2.19), (2) determine the optimal crack tip extension directions in terms of the crack tip growth angles $\Delta\boldsymbol{\theta}(a)$ (2.96), and (3) determine the relative crack tip growth rates $\hat{\boldsymbol{\ell}}(a)$ such that energy dissipation is maximised (2.45).

In the discrete framework that supposes straight finite-length crack tip extensions at sharp kink angles, the evolution of the variable triplet $\{\mathbf{u}, \boldsymbol{\ell}, \boldsymbol{\theta}\}(a)$ is considered as a sequence of solutions $\{\mathbf{u}, \boldsymbol{\ell}, \boldsymbol{\theta}\}(a^k)$ where $a^k = a_0 + k\Delta a$ is the total fracture length (2.29) at some discrete time instance $k \in \{1, 2, \dots\}$ and where Δa is the discrete fracture length increment per time-step k. The discrete solution process consists of a sequence of minimisations of the functional $\mathcal{E}^k = \mathcal{E}(\mathbf{u}^k, \boldsymbol{\ell}^k + \Delta\boldsymbol{\ell}^k, \boldsymbol{\theta} + \Delta\boldsymbol{\theta}^k)$ in terms of the variable triplet $\{\mathbf{u}, \Delta\boldsymbol{\ell}, \Delta\boldsymbol{\theta}\}^k$, where $\Delta\boldsymbol{\ell}^k$ are the crack tip extension lengths (such that $\sum_{i \in \mathcal{I}^k_{\text{inc}}} \Delta\ell^k_i = \Delta a$) and where $\Delta\boldsymbol{\theta}^k$ are the crack tip kink angles. Consequently, at a particular time-step, there is the non-linear interdependence between: (1) the set of crack tips to extend, (2) their extension lengths, and (3) their extension directions. Thus, the discrete solution increment needs to be solved iteratively, starting from some initial guess. In general, the trial set of crack tips is selected quite conservatively so that the most energetically favourable crack extension solution can be found by iteratively updating the trial solution (and possibly excluding the energetically unfavourable crack tips) based on some solution strategy.

Three solution strategies will be outlined for the discrete fracture growth problem that are respectively based on: (1) load-control, (2) fracture area-control, and on the (3) energy-gradient. The application of each technique is tailored to the stability property of the

fracture configuration, as defined by (2.68)-(2.70), which is used to characterise the important behaviour of the total energy function at a given time-step. The three solution methods have pros and cons in terms of the kind of fracture problems that can be solved. For instance, the technique based on load-control is limited to problems where the fracture front is unconditionally stable for all crack tip extensions (2.68). On the other hand, the scheme based on the fracture length-control relaxes the requirement for a strictly convex $\mathcal{E}^k$ insofar that $\mathcal{E}^k$ only needs to be convex within the feasible solution space, as constrained by a fixed amount of fracture length increment, i.e. $\sum_{i\in\mathcal{I}^k_{\text{inc}}} \Delta\ell^k_i = \Delta a$. Finally, the formulation based on the energy gradient is aimed at solving general fracture problems.

3.2 Preliminaries

Henceforth, we will concern ourselves with the special case of a constant crack tip G_{c}. This allows focusing on the key principles of the solution methodology instead of having to deal with an arbitrary G_{c}, e.g. as a function of crack tip position. With this in mind, the expressions for the rates of the crack tip energy release rates can be simplified. For convenience sake, let us recall the definitions of the relevant crack tip quantities. Firstly, the discrete fracture extension force and the rotational energy release rate can be given as:

$$G_{\text{s}i} = -\frac{\partial\Pi(\mathbf{u},\Delta\boldsymbol{\ell},\Delta\boldsymbol{\theta})}{\partial\Delta\ell_i} \tag{3.1}$$

$$G_{\theta i} = -\frac{\partial\Pi(\mathbf{u},\Delta\boldsymbol{\ell},\Delta\boldsymbol{\theta})}{\partial\Delta\theta_i} \tag{3.2}$$

where $i \in \mathcal{I}_{\text{inc}}$. Similarly, the rates of the crack tip energy release rates are given as:

$$H_{\text{s}ij} = -\frac{\partial^2\mathcal{E}(\Delta\boldsymbol{\ell},\Delta\boldsymbol{\theta})}{\partial\Delta\ell_i\Delta\partial\ell_j} = -\frac{\partial^2\Pi(\Delta\boldsymbol{\ell},\Delta\boldsymbol{\theta})}{\partial\Delta\ell_i\partial\Delta\ell_j} \tag{3.3}$$

$$H_{\theta ij} = -\frac{\partial^2\mathcal{E}(\Delta\boldsymbol{\ell},\Delta\boldsymbol{\theta})}{\partial\Delta\theta_i\partial\Delta\theta_j} = -\frac{\partial^2\Pi(\Delta\boldsymbol{\ell},\Delta\boldsymbol{\theta})}{\partial\Delta\theta_i\partial\Delta\theta_j} \tag{3.4}$$

$$H_{\text{m}ij} = -\frac{\partial^2\mathcal{E}(\Delta\boldsymbol{\ell},\Delta\boldsymbol{\theta})}{\partial\Delta\ell_i\partial\Delta\theta_j} = -\frac{\partial^2\Pi(\Delta\boldsymbol{\ell},\Delta\boldsymbol{\theta})}{\partial\Delta\ell_i\partial\Delta\theta_j} \tag{3.5}$$

where $i,j \in \mathcal{I}_{\text{inc}}$. A practical way of computing the higher order rate terms (3.3)-(3.5) can be provided by considering the displacement field explicitly in the potential energy

function. Thus, the rate of the energy release rate $H_{\mathrm{s}ij} \equiv \frac{\mathrm{d}G_{\mathrm{s}i}}{\mathrm{d}\Delta\ell_j}$ can be computed as shown:

$$H_{\mathrm{s}ij} = \frac{\mathrm{d}}{\mathrm{d}\Delta\ell_j}\left(-\frac{\partial\Pi(\mathbf{u}(\Delta\boldsymbol{\ell},\Delta\boldsymbol{\theta}),\Delta\boldsymbol{\ell},\Delta\boldsymbol{\theta})}{\partial\Delta\ell_i}\right) \tag{3.6}$$

$$H_{\mathrm{s}ij} = \frac{\partial}{\partial\Delta\ell_j}\left(-\frac{\partial\Pi}{\partial\Delta\ell_i}\right) + \frac{\mathrm{d}\mathbf{u}}{\mathrm{d}\Delta\ell_j}\frac{\partial}{\partial\mathbf{u}}\left(-\frac{\partial\Pi}{\partial\Delta\ell_i}\right) \tag{3.7}$$

$$H_{\mathrm{s}ij} = -\frac{\partial^2\Pi}{\partial\Delta\ell_i\partial\Delta\ell_j}\bigg|_{\mathbf{u}} + \frac{\partial}{\partial\Delta\ell_i}\left(\frac{\partial\Pi}{\partial\mathbf{u}}\right)^{\mathrm{T}}\left(\frac{\partial^2\Pi}{\partial\mathbf{u}^2}\right)^{-1}\frac{\partial}{\partial\Delta\ell_j}\left(\frac{\partial\Pi}{\partial\mathbf{u}}\right) \tag{3.8}$$

where in (3.7) the substitution for $\mathrm{d}\mathbf{u}/\mathrm{d}\Delta\ell_i$ is in accordance with the result in equation (2.52). Analogous expressions hold for $H_{\mathrm{s}ij} \equiv \frac{\mathrm{d}G_{\mathrm{s}i}}{\mathrm{d}\Delta\ell_j}$ and $H_{\mathrm{m}ij} \equiv \frac{\mathrm{d}G_{\mathrm{s}i}}{\mathrm{d}\Delta\theta_j} \equiv \frac{\mathrm{d}G_{\theta j}}{\mathrm{d}\Delta\ell_i}$ as well:

$$H_{\theta ij} = -\frac{\partial^2\Pi}{\partial\Delta\theta_i\partial\Delta\theta_j}\bigg|_{\mathbf{u}} + \frac{\partial}{\partial\Delta\theta_i}\left(\frac{\partial\Pi}{\partial\mathbf{u}}\right)^{\mathrm{T}}\left(\frac{\partial^2\Pi}{\partial\mathbf{u}^2}\right)^{-1}\frac{\partial}{\partial\Delta\theta_j}\left(\frac{\partial\Pi}{\partial\mathbf{u}}\right) \tag{3.9}$$

$$H_{\mathrm{m}ij} = -\frac{\partial^2\Pi}{\partial\Delta\ell_i\partial\Delta\theta_j}\bigg|_{\mathbf{u}} + \frac{\partial}{\partial\Delta\ell_i}\left(\frac{\partial\Pi}{\partial\mathbf{u}}\right)^{\mathrm{T}}\left(\frac{\partial^2\Pi}{\partial\mathbf{u}^2}\right)^{-1}\frac{\partial}{\partial\Delta\theta_j}\left(\frac{\partial\Pi}{\partial\mathbf{u}}\right) \tag{3.10}$$

Note that a constant external load has been supposed in the computations of H_{s}, H_θ and H_{m} even though the load is expected to change with crack growth to satisfy energy conservation. This assumption, however, is not detrimental because the load is assumed to be uniformly variable by means of a load scaling factor (2.58), which ensures that the crack tip energy release rates are physical, i.e. $G_{\mathrm{s}i} \leq G_{\mathrm{c}}\ \forall i \in \mathcal{I}_{\mathrm{tip}}$. Therefore, as the external load scales uniformly, the energy release rates (and their rates) scale uniformly (quadratically) at every crack tip in the domain. Consequently, the relative magnitudes of the crack tip energy release rates (and their rates), which are the quantities that actually govern the fracture paths, can be assessed even if a nominal external load is supposed for simplicity.

3.3 Methods for the discrete solution

We will consider 3 different solution strategies for solving the problem of multi-crack evolution following the principle of total energy minimisation (2.55). The first strategy assumes energy minimisation subject to the constraint of fracture length-control (or, area-control, to be more precise) whereby the energy is minimised for a given (fixed) total fracture length increment. This approach is suitable for both stable (2.65) and unstable

(2.66) crack growth regimes; however, the fracture front is required to be stable (2.68) as the method counts on the energy function to be convex (2.68) such that its stationary point is its global minimum. In the second method, load-control is assumed. This strategy is limited to stable fracture growth (2.65) and a stable fracture front (2.68). The solution for the fracture extensions at each time-step is obtained automatically by incrementing the external load parameter. Finally, the third strategy uses the gradient of the total energy function to minimise the energy with respect to the fracture extensions subject to a fixed total crack increment length. The method is suitable for solving general crack growth problems involving both stable (2.65) and unstable (2.66) crack growth regimes as well as stable (2.68), unstable (2.69) or partially stable (2.70) fracture front configurations.

3.3.1 Crack growth by crack length control

In the present formulation, it will be supposed that the displacement field is automatically determined by the prevailing values of the variable tuple $\{\Delta\boldsymbol{\ell}^k, \Delta\boldsymbol{\theta}^k\}$, as determined by the solution to the discrete equilibrium problem. Consequently, the evolution of fracture can be considered as the sequential minimisation of the energy function $\mathcal{E}^k = \mathcal{E}(\Delta\boldsymbol{\ell}^k, \Delta\boldsymbol{\theta}^k)$ in terms of $\{\Delta\boldsymbol{\ell}^k, \Delta\boldsymbol{\theta}^k\}$ over the discrete time $k \in \{1, 2, \dots\}$. At a typical time-step k, the constraints imposed on the working-set of crack tips $\mathcal{W}^k \subseteq \mathcal{I}^k_{\text{tip}}$ are: (1) a prescribed unit of fracture growth, i.e. $\sum_{i\in\mathcal{W}^k} \Delta\ell_i = \Delta a$, and (2) the condition of fracture growth irreversibility, i.e. $\Delta\ell_i \geq 0\ \forall i \in \mathcal{W}^k$. The minimisation problem can be formally written as:

$$\text{for} : \quad k \in \{1, 2, \dots\},\ i \in \mathcal{W}^k \subseteq \mathcal{I}^k_{\text{tip}} \tag{3.11}$$

$$\text{minimise} : \quad \mathcal{E}^k = \mathcal{E}(\Delta\boldsymbol{\ell}^k, \Delta\boldsymbol{\theta}^k) \tag{3.12}$$

$$\text{subject to} : \quad \sum \Delta\ell^k_i = \Delta a, \tag{3.13}$$

$$\Delta\ell^k_i \geq 0 \tag{3.14}$$

where the displacement field $\mathbf{u}^k = \mathbf{u}(\Delta\boldsymbol{\ell}^k, \Delta\boldsymbol{\theta}^k)$ is implicitly accounted for in the minimisation of $\mathcal{E}(\Delta\boldsymbol{\ell}^k, \Delta\boldsymbol{\theta}^k)$ by requiring $\mathbf{u}^k$ to satisfy static equilibrium at all times. As such,

the Lagrangian of the constrained minimisation problem (3.11)-(3.14) can be defined as:

$$\forall i \in \mathcal{W}^k \quad \mathcal{L}(\Delta\ell_i^k, \Delta\theta_i^k, \lambda_s^k, \mu_i^k) = \mathcal{E}(\Delta\ell_i^k, \Delta\theta_i^k) + \lambda_s^k \left(\mathbf{e}_i \Delta\ell_i^k - \Delta a\right) + \mu_i^k \left(-\Delta\ell_i^k\right), \quad (3.15)$$

where $\lambda_s^k > 0$, $\mu_i^k \geq 0$ are the Karush-Kuhn-Tucker (KKT) multipliers. The necessary (but generally insufficient) set of conditions for a stationary point of $\mathcal{L}^k$ to correspond to a global minimizer of $\mathcal{E}^k$ (subject to satisfying all constraints) is summarised below:

- The stationarity condition:

$$\forall i \in \mathcal{W}^k \quad \frac{\partial \mathcal{L}^k}{\partial \Delta\ell_i} \equiv \frac{\partial \mathcal{E}^k}{\partial \Delta\ell_i} + \lambda_s^k \mathbf{e}_i + \mu_i^k(-1) = 0 \quad (3.16)$$

$$\frac{\partial \mathcal{L}^k}{\partial \Delta\theta_i} \equiv \frac{\partial \mathcal{E}^k}{\partial \Delta\theta_i} = 0 \quad (3.17)$$

$$\frac{\partial \mathcal{L}}{\partial \lambda_s} \equiv \mathbf{e}_i \Delta\ell_i - \Delta a = 0 \quad (3.18)$$

- Primal feasibility condition:

$$\forall i \in \mathcal{W}^k \quad \Delta\ell_i^k \geq 0 \quad (3.19)$$

- Dual feasibility condition:

$$\forall i \in \mathcal{W}^k \quad \mu_i^k \geq 0 \quad (3.20)$$

An example solution to the equation system (3.16)-(3.20) concerning the problem of two crack tips is shown graphically in Figure 3.1. Subsequently, however, it is convenient to disregard the dual feasibility condition (3.20) and the associated μ-multipliers from the standard Lagrangian form in (3.15) as this adds no practical advantage over the primal feasibility condition $\Delta\ell_i \geq 0$ by virtue of the simplicity of the inequality constraint. In other words, it is chosen to enforce the inequality constraint $\Delta\ell_i^k \geq 0$ directly instead of having to do it implicitly via the enforcement of the dual feasibility constraint $\mu_i \geq 0$. The system of non-linear equations (3.16)-(3.18) that arises from the stationary principle of the Lagrangian can be linearised and put in an iterative from using Newton's formula:

$$\begin{bmatrix} \frac{\partial \mathcal{E}(\Delta\boldsymbol{\ell},\Delta\boldsymbol{\theta})}{\partial\Delta\ell_i\partial\Delta\ell_j} & \frac{\partial \mathcal{E}(\Delta\boldsymbol{\ell},\Delta\boldsymbol{\theta})}{\partial\Delta\ell_i\partial\Delta\theta_j} & \mathbf{e}_i \\ \frac{\partial \mathcal{E}(\Delta\boldsymbol{\ell},\Delta\boldsymbol{\theta})}{\partial\Delta\theta_i\partial\Delta\ell_j} & \frac{\partial \mathcal{E}(\Delta\boldsymbol{\ell},\Delta\boldsymbol{\theta})}{\partial\Delta\theta_i\partial\Delta\theta_j} & 0 \\ \mathbf{e}_j & 0 & 0 \end{bmatrix}_{k,m} \begin{bmatrix} \delta\Delta\ell_j \\ \delta\Delta\theta_j \\ \delta\lambda_s \end{bmatrix}_{k,m} = - \begin{bmatrix} \frac{\partial \mathcal{E}(\Delta\boldsymbol{\ell},\Delta\boldsymbol{\theta})}{\partial\Delta\ell_i} + \mathbf{e}_i\lambda_s \\ \frac{\partial \mathcal{E}(\Delta\boldsymbol{\ell},\Delta\boldsymbol{\theta})}{\partial\Delta\theta_i} \\ \mathbf{e}_i\Delta\ell_i - \Delta a \end{bmatrix}_{k,m} \quad (3.21)$$

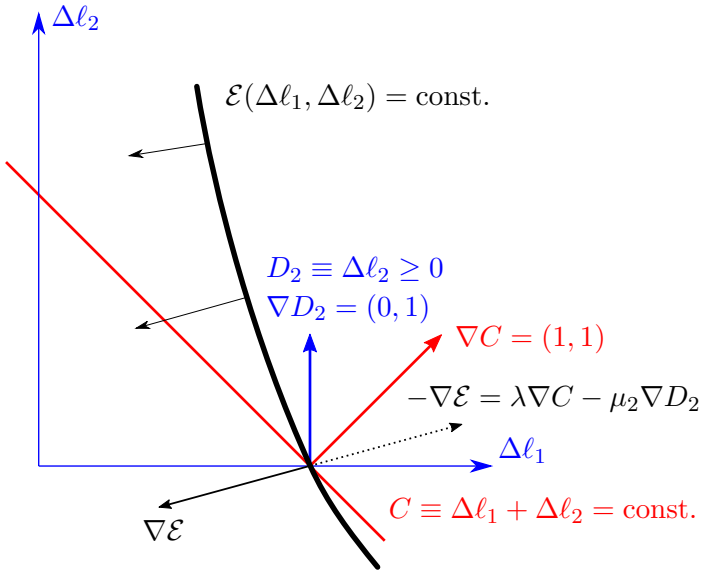

FIGURE 3.1: Graphical representation of the critical point of the Lagrangian with one active inequality-constraint. Note that $\lambda > 0$ and $\mu_2 > 0$.

The now linearised system of equations can be solved to determine the change in the solution $\{\delta\Delta\boldsymbol{\ell}, \delta\Delta\boldsymbol{\theta}, \delta\lambda_s\}^{k,m}$ at time-step $k \in \{1, 2, \dots\}$ and iteration number $m \in \{1, 2, \dots\}$; however, it is practical to make a few simplifications beforehand. Firstly, the system of equations (3.21) can be rearranged in order to solve for the multiplier λ_s directly. Secondly, it is convenient to suppose that the initial (trial) solution $\Delta\boldsymbol{\ell}^{k,m=1}$ satisfies the equality constraint (3.18) from the beginning; this way, the residual of the constraint equation will vanish for all iterations, making it somewhat easier to maintain the feasibility of the iterated solution with regard to the inequality constraints (3.19). Finally, the derivatives of the total energy function can be substituted with the corresponding energy release rates, as defined by equations (3.1)-(3.10). Altogether, the change in the solution is given as:

$$\begin{bmatrix} \delta\Delta\boldsymbol{\ell} \\ \delta\Delta\boldsymbol{\theta} \\ \lambda_s \end{bmatrix}_{k,m} = - \begin{bmatrix} H_{\mathrm{s}} & H_{\mathrm{m}} & -\mathbf{e} \\ {H_{\mathrm{m}}}^{\mathrm{T}} & H_\theta & 0 \\ -\mathbf{e}^{\mathrm{T}} & 0 & 0 \end{bmatrix}^{-1}_{k,m} \begin{bmatrix} G_{\mathrm{s}} - G_{\mathrm{c}} \\ G_\theta \\ 0 \end{bmatrix}_{k,m} \tag{3.22}$$

where it can be asserted (by inspection of the third equation) that the net change in the total crack extension will be zero, i.e. $\sum_{i \in \mathcal{W}^{k,m}} \delta\Delta\ell_i^{k,m} = 0$. Consequently, the equality constraint (3.18) that was satisfied by the trial solution would likewise be satisfied by the

incremented solution: $\Delta\boldsymbol{\ell}^{k,m+1} = \Delta\boldsymbol{\ell}^{k,m} + \delta\Delta\boldsymbol{\ell}^{k,m}$. Nonetheless, $\Delta\boldsymbol{\ell}^{k,m+1}$ is also required to uphold the inequality constraints (3.19), i.e. $\Delta\ell_i^{k,m+1} \geq 0 \; \forall i \in \mathcal{W}^{k,m}$. To this end, the solution increment $\{\delta\Delta\boldsymbol{\ell}, \delta\Delta\boldsymbol{\theta}\}^{k,m}$ generally needs to be scaled by a factor w^m (as ruled by the most imminent inequality constraint) in order to maintain feasibility of $\Delta\boldsymbol{\ell}^{k,m+1}$:

$$w^m = \min\left(\left\{\frac{\Delta\ell_i^m}{-\delta\Delta\ell_i^m}, 1\right\}\right), \text{ where } i \in \mathcal{W}^m \tag{3.23}$$

Equation (3.23) states that the maximum change in the crack extensions solution $\Delta\boldsymbol{\ell}^{k,m}$ at iteration m is $w^m\delta\Delta\boldsymbol{\ell}^{k,m}$ that still maintains feasibility of $\Delta\boldsymbol{\ell}^{k,m+1}$, i.e. $\Delta\ell_i^{k,m+1} \geq 0$ $\forall i \in \mathcal{W}^{k,m}$. Hence, the solution after the m'th iteration is finally obtained as:

$$\begin{bmatrix}\Delta\boldsymbol{\ell}\\ \Delta\boldsymbol{\theta}\end{bmatrix}^{k,m+1} = \begin{bmatrix}\Delta\boldsymbol{\ell}\\ \Delta\boldsymbol{\theta}\end{bmatrix}^{k,m} + w^m \begin{bmatrix}\delta\Delta\boldsymbol{\ell}\\ \delta\Delta\boldsymbol{\theta}\end{bmatrix}^{k,m} \tag{3.24}$$

The same scaling factor is applied to the change in crack tip kink angles $\delta\Delta\boldsymbol{\theta}^{k,m}$ since they are linearly related to $\delta\Delta\boldsymbol{\ell}^{k,m}$. Also note, if $w^m = 1$ no inequality constraint limits the ideal change in the solution as a means to enforce the feasibility condition (3.19). For the subsequent iteration m+1, and assuming the same working-set of crack tips $\mathcal{W}^{k,m+1} \leftarrow \mathcal{W}^{k,m}$, if it is found that a change in the solution is prevented by some inequality constraint, say at crack tip $i \in \mathcal{W}^{k,m+1}$ by virtue of having $w^{m+1} = 0$, then this limiting crack tip is discarded from the working-set and the solution at m+1 is recomputed considering the updated working-set $\mathcal{W}^{k,m+1} \leftarrow \mathcal{W}^{k,m+1}\backslash i$. The m-iterations are continued in this way (updating the working-set as required) until the solution converges for time-step k. Upon convergence, the solution is advanced to the subsequent time-step k+1 and the iterative solution process repeated for a new set of candidate crack tip extensions $\mathcal{W}^{k+1,m=1} \subseteq \mathcal{I}_{\text{tip}}^k$. For the current algorithm to converge to the globally minimising solution of the energy function $\mathcal{E}(\Delta\boldsymbol{\ell}^k, \Delta\boldsymbol{\theta}^k)$ in a single trial attempt, the function needs to be convex within the feasible solution space, as defined by the constraint equations (3.13) and (3.14). Consider the set of active crack tips $\mathcal{W}^{k,m\to\infty}$ at convergence, whose size is $n = |\mathcal{W}^{k,m\to\infty}|$, the

second order sufficiency condition for $\mathcal{E}^k$ to be minimised (at least locally) can be given as:

$$\forall \delta\Delta\boldsymbol{\ell} \in \{\boldsymbol{v} \in \mathbb{R}^n : \textstyle\sum_{i=1}^n v_i = 0\},\ \forall \delta\Delta\boldsymbol{\theta} \in \mathbb{R}^n$$
$$\begin{bmatrix} \delta\Delta\ell_i & \delta\Delta\theta_i \end{bmatrix} \begin{bmatrix} H_{\mathrm{s}ij} & H_{\mathrm{m}ij} \\ H_{\mathrm{m}ji} & H_{\mathrm{s}ij} \end{bmatrix}_{k,m} \begin{bmatrix} \delta\Delta\ell_j \\ \delta\Delta\theta_j \end{bmatrix} \leq 0 \tag{3.25}$$

The feasible variation $\delta\Delta\boldsymbol{\ell}$ can be expressed in terms of an arbitrary variation $\delta\Delta\boldsymbol{\ell}^* \in \mathbb{R}^n$ by computing the projection of $\delta\Delta\boldsymbol{\ell}^*$ onto the feasible $(n-1)$-dimensional hyperplane that is defined by the zero-variation of the equality constraint equation (i.e. $\sum_{i=1}^n \delta\Delta\ell_i = 0$):

$$\delta\Delta\ell_i = \left(I_{ij} - \frac{\mathbf{e}_i \mathbf{e}_j}{\mathbf{e}_i \mathbf{e}_i} \right) \delta\Delta\ell_j^* \tag{3.26}$$
$$\delta\Delta\ell_i = \delta\Delta\ell_i^* - \mathrm{mean}(\delta\Delta\boldsymbol{\ell}^*) \tag{3.27}$$

Hence, the second order sufficiency condition (3.25) can be expressed more usefully as:

$$\forall \delta\Delta\boldsymbol{\ell}, \delta\Delta\boldsymbol{\theta} \in \mathbb{R}^n$$
$$\begin{bmatrix} \delta\Delta\ell_i & \delta\Delta\theta_i \end{bmatrix} \begin{bmatrix} H^*_{\mathrm{s}\,ij} & H^*_{\mathrm{m}ij} \\ H^*_{\mathrm{m}ji} & H_{\theta ij} \end{bmatrix}_{k,m} \begin{bmatrix} \delta\Delta\ell_j \\ \delta\Delta\theta_j \end{bmatrix} \leq 0 \tag{3.28}$$

where H^*_{s} and H^*_{m} are defined as follows:

$$H^*_{\mathrm{s}\,ij} = \left(I_{iq} - \frac{\mathbf{e}_i \mathbf{e}_q}{\mathbf{e}_i \mathbf{e}_i} \right) H_{\mathrm{s}qr} \left(I_{rj} - \frac{\mathbf{e}_r \mathbf{e}_j}{\mathbf{e}_i \mathbf{e}_i} \right) \tag{3.29}$$
$$H^*_{\mathrm{m}ij} \equiv \left(H^{*\,\mathrm{T}}_{\mathrm{m}} \right)_{ji} = \left(I_{iq} - \frac{\mathbf{e}_i \mathbf{e}_q}{\mathbf{e}_i \mathbf{e}_i} \right) H_{\mathrm{m}qj} \tag{3.30}$$

In summary, the algorithm described in this section is suitable for stable/unstable, competing/non-competing crack growth problems; however, the fundamental requirement is that at each solution time-step $k \in \{1, 2, \dots\}$ the total energy function $\mathcal{E}(\Delta\boldsymbol{\ell}^k, \Delta\boldsymbol{\theta}^k)$ needs to be convex within the confines of the feasible solution space. If this condition is met, the solution that minimises $\mathcal{E}(\Delta\boldsymbol{\ell}^k, \Delta\boldsymbol{\theta}^k)$ can be determined in a single trial; otherwise, if the energy function is not convex the minimisation algorithm is not robust even if multiple trials are attempted. In the non-convex case, the converged result (even though it

may be a critical point of the energy function) does not necessarily correspond to the point of minimum energy if the energy function is concave or a generalised saddle function.

In solving a non-convex minimisation problem it is usually more reliable to use a gradient-based solution approach whereby the iterated solution is improved upon by advancing it along the feasible direction that leads to the greatest decrease in the objective function. In case the objective function happens to be convex along a particular advance direction, a line-search technique can be employed in order to estimate the optimal solution change. Before we set about to describe in detail a type of a gradient-based solution approach, it is worth outlining one more solution method that is exclusively suited for solving stable crack growth problems. For this specific case, the fracture front is required to be stable, i.e. the total energy function needs to be convex for all admissible fracture front configurations (see equation (2.68)). In this approach, an external load control scheme is used (as opposed to fracture-length control) in order to cause incremental crack growth with each load-step.

3.3.2 Crack growth by external load control

Crack growth stability depends on a number of factors. At the most basic level, stable crack growth in a solid is attained for certain geometrical and loading configurations; some examples include: the double cantilever problem or the wedge-splitting problem (2D/3D) [296], a small embedded crack (2D/3D) with counter-balancing point loads applied on the top and bottom crack surfaces [266], a pull-out test (3D) whereby a conical shape crack surface develops with an expanding circular fracture front [14, 241]. Another aspect that tends to promote stable crack growth by virtue of an increasing G_c (at least in the short-term of growth and especially in metals) is small scale yielding and the expansion of the plastic region at the crack tip. Finally, environmental conditions can also play a part in crack growth stability in a phenomena called static fatigue [220, 295]. The chemically active environment can locally reduce the material's resistance to fracture well below the critical value observed in an otherwise inert environment such that as the crack propagates and exposes virgin material the effective G_c increases. A common example of environmentally assisted crack growth is the slow fracture of glass in the presence of moisture [54, 55, 295].

Let us assume the type of solid geometry and boundary conditions that can be associated with a convex total energy function $\mathcal{E}(\Delta\boldsymbol{\ell}, \Delta\boldsymbol{\theta})$ in terms of all possible crack tip extensions $\Delta\boldsymbol{\ell} \in \mathbb{R}^{n_{\text{tip}}}$ and their angular orientations $\Delta\boldsymbol{\theta} \in \mathbb{R}^{n_{\text{tip}}}$, where n_{tip} is the number of crack tips. In this case, it is assumed that the (unconstrained) Hessian of $\mathcal{E}(\Delta\boldsymbol{\ell}, \Delta\boldsymbol{\theta})$ is positive definite (or, equivalently, that the matrix of the rates of the crack tip energy release rates is negative definite) with respect to all perturbations of the crack tip positions in space:

$$\forall \delta\Delta\boldsymbol{\ell}, \delta\Delta\boldsymbol{\theta} \in \mathbb{R}^{n_{\text{tip}}}$$
$$\begin{bmatrix} \delta\Delta\ell_i & \delta\Delta\theta_i \end{bmatrix} \begin{bmatrix} H_{\text{s}ij} & H_{\text{m}ij} \\ H_{\text{m}ji} & H_{\text{s}ij} \end{bmatrix}_{k,m} \begin{bmatrix} \delta\Delta\ell_j \\ \delta\Delta\theta_j \end{bmatrix} \leq 0 \tag{3.31}$$

At time $k \in \{1, 2, \dots\}$, the external load is increased by $\Delta\mathbf{t}^k = \mathbf{t}_0 \Delta\lambda_t^k$, where $\mathbf{t}_0$ is a nominal load and $\Delta\lambda_t^k$ is a change in the load scaling factor. Upon the application of the load increment, the system is generally not in a state of equilibrium; consequently, the new equilibrium state is obtained by minimising $\mathcal{E}(\Delta\boldsymbol{\ell}^k, \Delta\boldsymbol{\theta}^k)$ in terms of $\{\Delta\boldsymbol{\ell}, \Delta\boldsymbol{\theta}\}^k$ subject to $\Delta\ell_i^k \geq 0 \; \forall i \in \mathcal{I}_{\text{tip}}^k$. Since the energy function is convex, it suffices to consider a single trial solution for it to converge to the point that globally minimises $\mathcal{E}(\Delta\boldsymbol{\ell}^k, \Delta\boldsymbol{\theta}^k)$. For instance, the maximum hoop stress criterion can be used to uniformly extend all crack tips in the working-set $\mathcal{W}^{k,m=1} \subseteq \mathcal{I}_{\text{tip}}^k$ as an initial solution. At any rate, the linearised system of equations to be solved at a typical iteration step $m \in \{1, 2, \dots\}$ is similar to that of the previous formulation that was based on crack-length control; however, no equality-constraints are active this time such that the resulting set of equations reads:

$$\begin{bmatrix} \frac{\partial\mathcal{E}(\Delta\boldsymbol{\ell},\Delta\boldsymbol{\theta})}{\partial\Delta\ell_i\partial\Delta\ell_j} & \frac{\partial\mathcal{E}(\Delta\boldsymbol{\ell},\Delta\boldsymbol{\theta})}{\partial\Delta\ell_i\partial\Delta\theta_j} \\ \frac{\partial\mathcal{E}(\Delta\boldsymbol{\ell},\Delta\boldsymbol{\theta})}{\partial\Delta\theta_i\partial\Delta\ell_j} & \frac{\partial\mathcal{E}(\Delta\boldsymbol{\ell},\Delta\boldsymbol{\theta})}{\partial\Delta\theta_i\partial\Delta\theta_j} \end{bmatrix}_{k,m} \begin{bmatrix} \delta\Delta\ell_j \\ \delta\Delta\theta_j \end{bmatrix}_{k,m} = - \begin{bmatrix} \frac{\partial\mathcal{E}(\Delta\boldsymbol{\ell},\Delta\boldsymbol{\theta})}{\partial\Delta\ell_i} \\ \frac{\partial\mathcal{E}(\Delta\boldsymbol{\ell},\Delta\boldsymbol{\theta})}{\partial\Delta\theta_i} \end{bmatrix}_{k,m} \tag{3.32}$$

The inequality-unbounded solution change $\{\delta\Delta\boldsymbol{\ell}, \delta\Delta\boldsymbol{\theta}\}^{k,m}$ can be determined straightforwardly from (3.32). For notational convenience, let us substitute the appropriate definitions of the energy release rates (3.1)-(3.10) in place of the derivatives of the energy

function that appear in (3.32) so that the solution to $\{\delta\Delta\boldsymbol{\ell}, \delta\Delta\boldsymbol{\theta}\}^{k,m}$ can be given as:

$$\begin{bmatrix} \delta\Delta\boldsymbol{\ell} \\ \delta\Delta\boldsymbol{\theta} \end{bmatrix}_{k,m} = - \begin{bmatrix} H_s & H_m \\ H_m^{\mathrm{T}} & H_\theta \end{bmatrix}^{-1}_{k,m} \begin{bmatrix} G_{\mathrm{s}} - G_c \\ G_\theta \end{bmatrix}_{k,m} \tag{3.33}$$

Since the total energy function is presumed to be convex, the tangent matrix in (3.33) will be negative definite. Consequently, the problem of determining the new equilibrium crack tip positions for a given external load increase $\Delta\mathbf{t}^k$ is, effectively, a problem of growing cracks to the point that no crack tip exceeds the critical value of the energy release rate G_{c}. The complete solution process for time-step k is analogous to the one described in the previous Section 3.3.1, which was concerned with the solution algorithm based on crack-length control. In short, the solution $\{\Delta\boldsymbol{\ell}, \Delta\boldsymbol{\theta}\}^k$ at a typical time-step k is determined iteratively, by solving (3.33) for $\{\delta\Delta\boldsymbol{\ell}, \delta\Delta\boldsymbol{\theta}\}^{k,m}$ and updating the crack tip positions to $\{\Delta\boldsymbol{\ell}, \Delta\boldsymbol{\theta}\}^{k,m+1}$ in accordance with equations (3.23) and (3.24) as a means to uphold the constraint of fracture irreversibility, i.e. $\Delta\ell_i^{k,m} \geq 0 \; \forall i \in \mathcal{W}^{k,m}$. In case the solution progression at iteration step m is stopped by an active inequality constraint at a particular crack tip $i \in \mathcal{W}^{k,m}$, then this crack tip is discarded from the working-set $\mathcal{W}^{k,m}$ and the ideal solution change $\{\delta\Delta\boldsymbol{\ell}, \delta\Delta\boldsymbol{\theta}\}^{k,m}$ is recomputed for iteration m by considering the reduced set of crack tips $\mathcal{W}^{k,m} \leftarrow \mathcal{W}^{k,m} \backslash i$. The m-iterations are continued in this way (updating the working-set as required) until the solution converges for time-step k. At this point, the solution time-step is advanced to k+1, the external load is incremented by $\Delta\mathbf{t}^{k+1}$ and the iterative solution process is repeated for a new set of crack tips $\mathcal{W}^{k+1,m=1} \subseteq \mathcal{I}^k_{\mathrm{tip}}$.

The reader can consult the work of David *et al.* [63, 64] for details on a 3D implementation regarding planar crack growth that follows an analogous formulation. The main shortcoming of the load-control formulation is that its application is limited to a convex total energy function $\mathcal{E}(\Delta\boldsymbol{\ell}, \Delta\boldsymbol{\theta})$. A convex energy function rarely arises in typical fracture problems, unless the material undergoes toughening during fracture growth such that the effective value of the material parameter G_{c} increases at a sufficiently high rate.

3.3.3 Energy-gradient based crack growth

The crack growth solution algorithms based on crack length-control and external load-control schemes (Sections 3.3.1 and 3.3.2, respectively) are limited to the kinds of fracture problems that can be described in terms of a convex total energy function of the system. Concerning the crack length-control scheme, for example, it is required that the energy function $\mathcal{E}(\Delta\boldsymbol{\ell}, \Delta\boldsymbol{\theta})$ be convex within the feasible solution space (as constrained by the fixed total fracture extension). To this end, the second order sufficiency condition, given by equation (3.28), must hold true for all possible fracture configurations. On the other hand, the application of the load-control scheme necessitates that the (unconstrained) energy function $\mathcal{E}(\Delta\boldsymbol{\ell}, \Delta\boldsymbol{\theta})$ be simply a convex function. This condition is satisfied if the tangent matrix in equation (3.33) is negative definite for all possible fracture configurations.

Assuming the convexity property of the energy function is satisfactory for the particular scheme adopted, it is sufficient to use a single trial solution for the solution iterations to convergence to the globally minimising solution of $\mathcal{E}(\Delta\boldsymbol{\ell}, \Delta\boldsymbol{\theta})$. Although this property is computationally advantageous, neither method is well-suited for solving the general case of crack growth that may be associated with a non-convex energy function.

In order to overcome this limitation, an alternative solution method is pursued whereby a mixture of an extremum-based and a gradient-based energy minimisation techniques is used. The two techniques are employed alternately to determine the directions and the lengths of the crack tip extensions in turn. The two sets of variables, namely: the crack tip extension angles ($\Delta\boldsymbol{\theta} = \{\Delta\theta_i\}$ for $i \in \mathcal{I}_{\text{tip}}$) and the crack tip extension lengths ($\Delta\boldsymbol{\ell} = \{\Delta\ell_i\}$ for $i \in \mathcal{I}_{\text{tip}}$) are considered as decoupled sets of variables in each iteration, i.e. the *inter*-dependence (3.5) (but, not the *intra*-dependence) is omitted; however, with each iteration, the crack tip extension angles are updated to match any changes in the lengths. The act of first computing the crack tip extension directions (assuming constant extension lengths) and subsequently updating the extension lengths is allowed by reason that all interactions between the members of $\Delta\boldsymbol{\ell}$ and those of $\Delta\boldsymbol{\theta}$ vanish in the limit each crack tip extension tends to zero, regardless of the relative crack tip extension lengths.

At a typical time-step $k \in \{1, 2, \dots\}$ in the fracture evolution process, the first part of an iteration $m \in \{1, 2, \dots\}$ is concerned with finding the crack growth directions for the working-set of crack tips $\mathcal{W}^{k,m} \subseteq \mathcal{I}_{\text{tip}}$ by using a convex minimisation scheme to minimise the system's total energy $\mathcal{E}^{k,m} = \mathcal{E}(\Delta\boldsymbol{\theta}^{k,m}, \Delta\boldsymbol{\ell}^{k,m})$ (or potential energy $\Pi^{k,m}$ if G_{c} is assumed to be constant) with respect to the crack tip extension angles $\Delta\boldsymbol{\theta}^{k,m}$ while keeping $\Delta\boldsymbol{\ell}^{k,m}$ fixed. In this case, the energy minimum is supposed to correspond to its stationary value; hence, the stationary principle for the crack tip kinking can be stated as:

$$\text{find } \Delta\theta_i \in \mathbb{R}_{(-\pi,\pi)} \text{ s.t. : } G_{\theta_j}^{k,m} = 0 \quad \forall i, j \in \mathcal{W}^{k,m} \tag{3.34}$$

$$\text{assuming : } H_{\theta_{ij}}^{k,m} \delta\Delta\theta_i \delta\Delta\theta_j \leq 0 \quad \forall \delta\Delta\theta_i \in \mathbb{R} \tag{3.35}$$

The solution to the non-linear problem (3.34) in terms of the crack tip kink angles $\Delta\boldsymbol{\theta}^{k,m}$ is determined by using Newton's method. The solution at the n'th iteration step reads:

$$\Delta\theta_i^{k,m,n+1} = \Delta\theta_i^{k,m,n} - (H_\theta{}^{-1})_{ij}^{k,m,n} G_{\theta_j}^{k,m,n} \quad \text{where } i, j \in \mathcal{W}^{k,m} \tag{3.36}$$

The n-iterations are repeated until the change in the solution between iterations becomes sufficiently small, e.g. $\|\Delta\theta^{k,m,n+1} - \Delta\theta^{k,m,n}\|_\infty < \epsilon$ where ϵ is a small positive number. In the second part of the m'th iteration, the crack tip extension lengths are updated by applying a gradient-based solution scheme to minimise the energy of the system with respect to crack tip extension lengths $\Delta\boldsymbol{\ell}^{k,m}$ whilst keeping constant $\Delta\boldsymbol{\theta}^{k,m} \leftarrow \Delta\boldsymbol{\theta}^{k,m,n\to\infty}$, as determined by (3.36). In this case, the change in the crack tip extension lengths should theoretically take place in the direction of the vector $d_i^{k,m} = G_{\text{s}_i}{}^{k,m} - \text{mean}(G_{\text{s}}{}^{k,m})$ where $i \in \mathcal{W}^{k,m}$ such that the constraint of a unit total fracture increment is preserved, i.e. $\sum_{i\in\mathcal{W}^{k,m}} d_i^{k,m} = 0$. However, the numerical discretisation (XFEM) used within the current framework imposes a constraint on the allowable crack tip extension lengths such that, in practice, it is only possible to consider fixed-length crack tip extensions, i.e. crack tip growth is switched either *on* or *off*.[1] For this reason, the gradient-descent method needs

[1] The aspect of the discretisation (XFEM) that sets a restriction on the minimum crack extension length, is the requirement of finite size enrichment radius of the crack tip field that, crucially, needs to be small enough so that the displacement discontinuity introduced via enrichment does not extend past the crack tip increment (where the discontinuity should not exist). Although it is possible to map the discontinuous

to be adapted to deal with this constraint explicitly; henceforth, the crack tip extension lengths are updated in accordance with the following boolian-like criterion:

$$\forall i \in \mathcal{W}^{k,m}, \quad \Delta\ell_i^{k,m+1} = \begin{cases} \Delta\ell_{\text{inc}} & \text{if } {G_{\text{s}}}_i^{k,m} \geq \text{mean}\left({G_{\text{s}}}^{k,m}\right) \\ 0 & \text{otherwise.} \end{cases} \tag{3.37}$$

This step effectively results in the annihilation of the crack tip extensions that are energetically favoured to undergo some amount of closure and the retention of the crack tip extensions that are energetically favoured to undergo further opening. The new working-set of crack tips $\mathcal{W}^{k,m+1} \subseteq \mathcal{W}^{k,m}$ for the subsequent iteration $m+1$ consists only of the remaining crack tip extensions, i.e. $\mathcal{W}^{k,m+1} = \{i \in \mathcal{W}^{k,m} : \Delta\ell_i^{k,m+1} > 0\}$.

Although the gradient-descent approximation in (3.37) is quite rough, the proposed method will nonetheless converge (with respect to finer crack growth discretisations) to energetically optimal fracture paths provided at least one of the following two conditions is met: (1) crack tip competition is absent or (2) the total energy function is convex. This means that under condition (1) the energy function can be convex or non-convex (e.g. concave or a saddle), and that under condition (2) crack tip competition can be resolved naturally. In all such cases that satisfy (1) or (2), a single trial solution suffices, e.g. uniformly incrementing all promising crack tips in the set $\mathcal{W}^{k,m=1} \subseteq \mathcal{I}_{\text{tip}}^k$. On the contrary, the current method can not be applied robustly to solve the case of competing crack growth at the instance the energy function becomes non-convex. This is due to the possibility of multiple locally optimal solutions that the algorithm can converge to, depending on the starting solution; see for example Figure 3.2. Furthermore, if the energy function is non-convex, it is possible from this point onward to completely diverge from the critical fracture path by virtue of following only a locally optimal solution. A few examples of such cases that involve multiple competing crack tips are given in Figure 3.7.

crack tip enrichment functions along a curving crack increment [83] or even along a crack with a sharp kink [72] and thus introduce the benefits of enrichment quite flexibly, the current formulation of discrete crack representation is fundamentally based on piece-wise straight crack segments and a simpler crack tip enrichment scheme. In this frame, the enrichment radius at the crack tip is large enough (typically covering at least a few rings of elements around the crack tip domain) to reproduce crack tip stress field with better accuracy [303], yet small enough so as to be entirely contained within the crack tip segment such that no

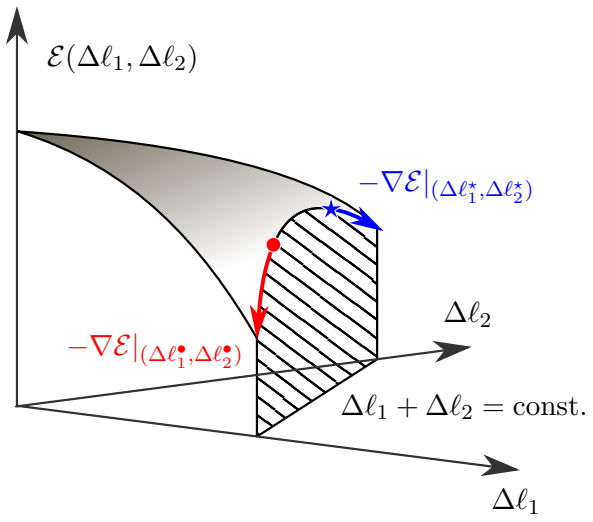

FIGURE 3.2: Converged solution dependence on the starting point. The idealised fracture problem is governed by a concave energy function within the feasible solution space. Using a gradient-descent method can lead to a sub-optimal solution, depending on the starting point. Hence, a gradient approach is generally not robust, unless multiple trial solutions are assessed.

Overall, the proposed approach is more versatile than the extremum-based convex minimisation methods, as described in Sections 3.3.1 and 3.3.2, because it can be applied even if the total energy function is non-convex (provided, of course, crack competition does not arise). On the other hand, the main shortcoming (in comparison to the previous formulations) is reduced order of precision due to: (1) the decoupling of the crack tip extension lengths $\Delta\boldsymbol{\ell}^{k,m}$ from the extension directions $\Delta\boldsymbol{\theta}^{k,m}$ (which means that the interactive terms between $\Delta\boldsymbol{\ell}^{k,m}$ and $\Delta\boldsymbol{\theta}^{k,m}$ are disregarded during m-iterations), and (2) the assumption of a fixed-length crack tip increment (which is a constraint imposed entirely by the numerical discretisation that is used to solve the problem of static-equilibrium).

The satisfactory performance of the proposed solution approach is verified by a number of fabricated test case that are designed to reflect the possible conditions that may arise in solving competing/non-competing crack growth problems for convex/non-convex behaviours of the energy function. The numerical results are presented as part of Section 3.4.

special mapping of the enrichment functions along the crack is required. The current form of discretisation is thought to be adequate for the purposes of describing the key aspects of the gradient-based solution approach.

3.4 Resolving competing crack growth

Several formulations have been described for solving multi-crack growth problems within a discrete framework. The different solution strategies lend themselves to certain types of fracture growth problems rather than to others, as governed by the shape of the energy function; however, non of the strategies are completely robust in the case of competing crack growth and unstable (2.69) or partially stable (2.70) fracture front configurations. To this end, the energy-gradient based method (Section 3.3.3) holds most promise in solving general competing crack growth problems; however, the constraint of fixed length crack tip extensions, which is imposed by the current XFEM discretisation (refer to Section 4.3 for details), adds some complexity. Nonetheless, an effective solution method is proposed. The following sub-sections focus on the method for the detection of crack tip competition, determination when crack tip competition needs to be resolved explicitly, and the description of the proposed solution method.[2] The proposed strategy for resolving crack tip competition, particularly in the case of an unstable (2.69) or a partially stable (2.70) fracture front configuration, is verified by solving several fabricated benchmark problems. Finally, the energy-gradient solution algorithm is described with the help of a flow chart.

3.4.1 Detection of crack tip competition

As the gradient-based energy minimisation technique (3.37) is not robust in the non-convex competing crack growth case, it is recommended to use a brute-force alternative to minimise the energy function once crack tip competition is encountered. In this context a brute-force approach refers to a solution method whereby multiple trial solutions are evaluated in an attempt to find the critical solution that minimises the energy function. A brute-force energy minimisation routine is necessary when two conditions are met: (1) all crack tips in the set $\mathcal{W}^{k,m}$ are competing (or quasi-competing), which is to say that the crack tips in question have sufficiently similar energy release rates such that

[2] Note that the proposed method is necessary due to the assumption of fixed-length crack tip extensions. If the discretisation were to allow for arbitrary crack tip extension lengths, the energy-gradient method could be used directly to solve the general case of competing crack growth. However, multiple initial (trial) solutions would still need to be assessed to ensure that the converged solution is the globally optimal solution.

the affects of the higher order energy release rates, namely those of: H_{s}, H_{m} and H_{θ}, can become significant (given the finite-length extensions), and (2) the energy function $\Pi(\Delta\boldsymbol{\ell}^{k,m}, \Delta\boldsymbol{\theta}^{k,m})$ is determined to be non-convex following the solution to equation (3.36), i.e. as assessed in the fracture state of minimum potential energy with respect to $\Delta\boldsymbol{\theta}^{k,m}$.

Although the second order KKT sufficiency condition (3.28) can be used to evaluate if $\Pi(\Delta\boldsymbol{\ell}^{k,m}, \Delta\boldsymbol{\theta}^{k,m})$ is convex in both of its variables, it is possible to reduce the complexity of this criterion (3.28) by assuming small crack tip extension lengths such that the second order interactive effects between different crack tips in terms of the quantities of $H_{\mathrm{m}ij}$ and $H_{\theta ij}$ where $i \neq j$ vanish relative to the self-interactions for $i = j$, where $i, j \in \mathcal{W}^{k,m}$. On the other hand, the same reasoning can not be applied to the terms of $H_{\mathrm{s}ij}$ for $i \neq j$ because non-vanishing interactions exist for vanishing crack tip lengths. To state it another way, the interactions between different crack tip extensions in terms of the second order derivatives of the energy function can be ignored if some of the derivatives are taken with respect to the crack tip extension angles and the crack tip extension lengths themselves happen to be small. In general, for small crack tip extensions the self-interactions will dominate over the cross-interactions, meaning that the matrices H_{m} and H_{θ} will be diagonally dominant.

By considering the fact that the fracture state at time $\{k, m\}$ corresponds to the minimum energy state with respect to the crack tip extension angles $\Delta\boldsymbol{\theta}^{k,m}$, it can be inferred that the self-interaction of the terms in $H_{\mathrm{m}ii} \equiv \frac{\partial}{\partial\theta_i}\left(-\frac{\partial\Pi}{\partial\ell_i}\right) \equiv \frac{\partial G_{\mathrm{s}i}}{\partial\theta_i}$ for $i \in \mathcal{W}^{k,m}$ must vanish for small crack tip extensions because for the minimum energy state to hold true, the crack tip energy release rates $G_{\mathrm{s}i}$ at the individual crack tips $i \in \mathcal{W}^{k,m}$ need to be maximised (or stationary) with respect to the crack tip extension angles; hence, $\forall i \in \mathcal{W}^{k,m} \lim\limits_{\Delta\ell_i \to 0^+} \frac{\partial G_{\mathrm{s}i}}{\partial\theta_i}\Big|_{\Delta\boldsymbol{\ell}} = 0$. All in all, if the crack tip extensions are sufficiently small, the following condition can be used to assess if the energy function is non-convex:

$$\exists \delta\Delta\boldsymbol{\ell}, \delta\Delta\boldsymbol{\theta} \in \mathbb{R}^{|\mathcal{W}^{k,m}|}$$
$$\begin{bmatrix} \delta\Delta\ell_i & \delta\Delta\theta_i \end{bmatrix} \begin{bmatrix} H^{*}_{\mathrm{s}\,ij} & \mathbf{0} \\ \mathbf{0} & H_{\theta ii} \end{bmatrix}_{k,m} \begin{bmatrix} \delta\Delta\ell_j \\ \delta\Delta\theta_i \end{bmatrix} > 0, \tag{3.38}$$

where the matrix H_{s}^{*} is a projection of H_{s} onto the feasible solution plane that is defined by the constraint equation of a fixed unit of total crack growth (3.13); the definition of H_{s}^{*} is given in (3.29). With regarding to the detection of competing crack growth, although it can be somewhat arbitrary to define a criterion within a discrete framework, a sensible choice is proposed as follows. A competing crack growth regime is highlighted during the discrete solution process when the differences in the crack tip energy release rates are on the order of the changes in the energy release rates that result from the extensions of the crack tips. One possibility of a criterion for detecting crack tip competition may be:

$$\forall i \in \mathcal{W}^{k,m} \quad |{G_{\mathrm{s}}}_{i}^{k,m} - \mathrm{mean}({G_{\mathrm{s}}}^{k,m})| < \Delta\ell_{\mathrm{inc}} \|{H_{\mathrm{s}}}^{k,m}\|_{\infty} \tag{3.39}$$

If equations (3.38) and (3.39) are satisfied after the optimal crack tip extension directions have been determined (3.36) for a set of active tips $\mathcal{W}^{k,m}$, then a brute-force energy minimisation routine will be required. To this end, multiple trial solutions need to be assessed in an attempt to converge to the solution that most minimises the energy function per fixed unit of total fracture advance. The total amount of crack growth in each converged solution needs to be the same because the optimal solution must be sought within the same solution space, which is defined (in part) by the constraint equation: $\sum_{i \in \mathcal{W}^{k}} \Delta\ell_{i}^{k} = \Delta a$.

However, the current numerical framework is ill-suited to solving the non-convex competing crack growth case because the space of possible crack growth solutions is significantly reduced by having to consider only fixed length crack tip increments. For example, a competing crack growth solution that consists of several crack tips advancing at different rates can not be reproduced within the current numerical framework. Although the inability to account for arbitrary crack tip growth rates does not necessarily preclude capturing the critical fracture path, the reduced solution search space does raise the possibility to misidentify the critical crack tips. The consequence of extending the wrong crack tips can be detrimental to resolving the competing crack growth problem effectively; in particular, if the sub-optimal extension solution happens to be locally optimal, the fracture path will begin to diverge from the critical path, which ultimately leads to the loss of solution. On the other hand, if the critical set of tips is identified exactly, the relative fracture extension

rates have a lesser impact on the solution accuracy and on the ability to capture the critical fracture path. This is because the simultaneous growth of multiple crack tips indicates that the energy function is convex in the vicinity of the critical solution; a convex energy function has the property of smoothing-out a sub-optimal fracture front such that the fracture path tends to adhere to the optimal path. In practice, advancing a sub-set of critical crack tips at time k leads to a relatively greater increase in the energy release rates of the remaining critical crack tips at time $k+1$, which prompts their growth subsequently. In other words, so long as none other than the critical crack tips (or at least some of them) are advanced at time k, the critical fracture path solution will not be lost even if constant length crack tip extensions are supposed. Therefore, the main challenge pertaining to fixed length crack tip incrementation is identifying the most critical crack tips exactly.

3.4.2 Description of solution method

To get around the problem of not being able to minimise the energy function for arbitrary crack tip extension lengths and, thus, to determine the set of critical crack tips reliably (even to the point of vanishingly small crack tip extensions) it is proposed to (1) construct an explicit approximation of the discrete energy function such that it is free from the discretisation related constraints and (2) to minimise this energy function so as to better predict the set of critical crack tips that are favoured to grow. Although the solution to the crack tip extension lengths (herein referred to as the *off-line* solution) will be sub-optimal by virtue of the underlying approximation, it should suffice to identify the set of critical crack tips exactly. Once the set of critical crack tips has been determined, the transition from the off-line solution to the discrete solution can be made by a simple operation of scaling-and-rounding of the off-line solution to fit the particular numerical discretisation.

For small crack tip extensions and small changes in the fracture front configuration relative to some reference state, the energy function can be considered as essentially a quadratic function. Information about its local behaviour, as governed by G_{s}, G_{θ}, H_{s}, H_{m} and H_{θ}, can be used to extrapolate it about a reference solution point. As such, the approximation is written as a second order Taylor's series expansion of $\Pi(\Delta\boldsymbol{\ell}^k, \delta\Delta\boldsymbol{\theta}^k)$ about a

reference fracture configuration $\{\Delta\boldsymbol{\ell}_0^k, \Delta\boldsymbol{\ell}_0^k\}$ with respect to the crack tip extension lengths $\Delta\boldsymbol{\ell}^k = \Delta\boldsymbol{\ell}_0^k + \delta\Delta\boldsymbol{\ell}^k$ and the relative changes in their kink angles $\delta\Delta\boldsymbol{\theta}^k = \Delta\boldsymbol{\theta}^k - \Delta\boldsymbol{\theta}_0^k$:

$$\begin{aligned}\tilde{\Pi}(\Delta\boldsymbol{\ell}^k, \delta\Delta\boldsymbol{\theta}^k) = \Pi^{k-1} - \Big[&\left(G^0_{\mathrm{s}\,i} - H^0_{\mathrm{s}\,ij}\Delta\ell^k_{0\,j}\right)\Delta\ell^k_i + G^0_{\theta i}\delta\Delta\theta^k_i + \dots \\ &+ \frac{1}{2}H^0_{\mathrm{s}\,ij}\Delta\ell^k_i\Delta\ell^k_j + H^0_{\mathrm{m}ij}\Delta\ell^k_i\delta\Delta\theta^k_j + \frac{1}{2}H^0_{\theta\,ij}\delta\Delta\theta^k_i\delta\Delta\theta^k_j\Big]\end{aligned} \tag{3.40}$$

The reference fracture configuration $\{\Delta\boldsymbol{\ell}_0^k, \Delta\boldsymbol{\theta}_0^k\}$ is the fracture increment solution at the instance crack tip competition is detected; all terms in (3.40) that are superscripted with a nought are computed in the reference configuration, i.e. $(\cdot)^0 = (\cdot)(\Delta\boldsymbol{\ell}_0^k, \Delta\boldsymbol{\theta}_0^k)$. Since the energy function $\Pi(\Delta\boldsymbol{\ell}_0^k, \Delta\boldsymbol{\theta}_0^k)$ is minimised (stationary) with respect to $\Delta\boldsymbol{\theta}_0^k$ following the solution to (3.36), the rotational energy release rates can be assumed to vanish in (3.40), i.e. $\forall i \in \mathcal{W}^{k,m}\ G^0_{\theta i} = 0$. Subsequently, the changes in the crack tip kink angles $\delta\Delta\boldsymbol{\theta}^k$ can be expressed in terms of the crack tip extension lengths $\Delta\boldsymbol{\ell}^k$ by supposing that the energy function $\Pi(\Delta\boldsymbol{\ell}^k, \Delta\boldsymbol{\theta}^k - \Delta\boldsymbol{\theta}_0^k)$ remains stationary with respect to $\Delta\boldsymbol{\theta}^k$ for a given $\Delta\boldsymbol{\ell}^k$:

$$\delta\Delta\theta^k_i \frac{\partial}{\partial\theta_i}\left(\frac{\partial\Pi}{\partial\theta_j}\right)\bigg|_{\Delta\boldsymbol{\ell}_0^k, \Delta\boldsymbol{\theta}_0^k} + \delta\Delta\ell^k_i \frac{\partial}{\partial\ell_i}\left(\frac{\partial\Pi}{\partial\theta_j}\right)\bigg|_{\Delta\boldsymbol{\ell}_0^k, \Delta\boldsymbol{\theta}_0^k} = 0 \tag{3.41}$$

$$\delta\Delta\theta^k_i = -(\Delta\ell^k_j - \Delta\ell^k_{0\,j})H^0_{\mathrm{m}jI}\left(H^{0\,-1}_\theta\right)_{Ii}, \quad \text{where } i, j, I \in \mathcal{W}^{k,m} \tag{3.42}$$

At this point it is possible to make the claim that the variation $\delta\Delta\boldsymbol{\theta}^k$ is negligible due to the following three reasons: (1) the long-distance interactions between different crack tips are negligible if the crack tip extensions are small relative to the problem geometry, i.e. $H_{\mathrm{m}ij} \equiv \frac{\partial G_{\mathrm{s}i}}{\partial\theta_j} \to 0$ and $H_{\theta ij} \equiv \frac{\partial G_{\theta i}}{\partial\theta_j} \to 0$ for $i \neq j$, (2) the self-interaction $H_{\mathrm{m}ii}$ will tend to vanish for small crack tip extensions likewise as the state of minimum energy with respect to the crack tip kink angles implies that the energy release rates at the individual crack tips are maximum, i.e. $G_{\mathrm{s}i}$ is stationary such that $H_{\mathrm{m}ii} \equiv \frac{\partial G_{\mathrm{s}i}}{\partial\theta_i} \to 0$, finally (3) the effect of the self-interaction $(H_\theta{}^{-1})_{ii} = \mathcal{O}(1/\Delta\ell^k_0)$ will cancel out with $(\Delta\ell^k_j - \Delta\ell^k_{0\,j}) = \mathcal{O}(\Delta\ell^k_0)$ such that the products have no significant influence on $\delta\Delta\boldsymbol{\theta}^k$. For the same reasons, the last two terms in the expression for $\tilde{\Pi}(\Delta\boldsymbol{\ell}^k, \delta\Delta\boldsymbol{\theta}^k)$ in equation (3.40) can be disregarded since their influence will be small relative to that of the remaining terms. As a result, $\tilde{\Pi}(\Delta\boldsymbol{\ell}^k, \delta\Delta\boldsymbol{\theta}^k)$

is predominately governed by $\Delta\boldsymbol{\ell}^k$ such that its expression in (3.40) can be reduced to:

$$\tilde{\Pi}(\Delta\boldsymbol{\ell}^k) = \Pi^{k-1} - \left[\left(G^0_{\mathrm{s}\,i} - H^0_{\mathrm{s}\,ij}\Delta\ell^k_{0\,j}\right)\Delta\ell^k_i + \frac{1}{2}H^0_{\mathrm{s}\,ij}\Delta\ell^k_i\Delta\ell^k_j\right] \tag{3.43}$$

The approximation above contains sufficient information to be able to resolve the general case competing crack growth for small crack tip extensions such that by minimising $\tilde{\Pi}(\Delta\boldsymbol{\ell}^k)$ the critical extension lengths can be determined. The explicit energy minimisation can be equivalently posed as a maximization of the energy decrease so that the constant Π^{k-1} can omitted. The competing crack growth problem is finally stated as follows:

$$\text{objective}: \quad \Delta\tilde{\boldsymbol{\ell}}^k = \underset{\Delta\boldsymbol{\ell}^k\in\mathbb{R}^{n_{\mathrm{tip}}}_{\geq 0}:\,\sum\Delta\ell^k_i=\Delta a}{\arg\max}\left(-\Delta\tilde{\Pi}(\Delta\boldsymbol{\ell}^k)\right) \tag{3.44}$$

$$\text{assuming}: \quad -\Delta\tilde{\Pi}(\Delta\boldsymbol{\ell}^k) = \left(G^0_{\mathrm{s}\,i} - H^0_{\mathrm{s}\,ij}\Delta\ell^k_{0\,j}\right)\Delta\ell^k_i + \frac{1}{2}H^0_{\mathrm{s}\,ij}\Delta\ell^k_i\Delta\ell^k_j \tag{3.45}$$

$$\text{where}: \quad \forall i \in \mathcal{W}^{k,m}\ \Delta\theta^k_{0\,i} = \arg(G^0_{\theta i} = 0), \tag{3.46}$$

$$\forall i \in \mathcal{W}^{k,m}\ \Delta\ell^k_{0\,i} = \Delta\ell_{\mathrm{inc}} \tag{3.47}$$

Although the term in the parenthesis in (3.45) will almost never have all equal elements, which is to say that competing crack growth at any discrete time instance will almost never arise in the numerical solution to the discrete problem (unless the fracture problem has symmetry), the purpose of (3.44) is to capture the competing crack growth solution as crack tip competition occurs between two discrete times. With regard to the constant Δa in (3.44), ideally it should be chosen such that the off-line solution $\Delta\tilde{\boldsymbol{\ell}}^k$ can be reproduced by the discrete solution $\Delta\boldsymbol{\ell}^k$ exactly. However, this is not generally possible if the off-line solution consists of multiple crack tips advancing at different rates (as opposed to the extension of single crack tip). Nonetheless, a good compromise for the value of Δa is the characteristic length of a crack tip extension that is specific to the discrete problem, e.g. $\Delta a = \Delta\ell_{\mathrm{inc}}$. Now, if the off-line solution indicates multiple crack tip growth then this leads to infer that the energy function is convex in the vicinity of the critical solution; thus, reproducing the crack tip extensions exactly is not as critical as growing the right crack tips. For this reason, the off-line crack tip extension lengths can be adjusted to fit the discrete solution, e.g. by scaling and rounding the off-line solution, regardless of Δa.

The solution to the off-line competing crack growth problem (3.44) can be carried out using standard iterative solution methods for solving constrained quadratic programming problems. In the present implementation, an active-set solution approach is used where the solution is updated along the feasible gradient of the objective function such that all solution constrains are respected, i.e. $\sum \Delta\ell_i^k = \Delta a$ and $\Delta\ell_i^k \geq 0$ where $i \in \mathcal{W}^{k,m}$. In addition, a line search routine is introduced within the gradient-based solution framework so as to find locally optimal solutions along a particular solution advance direction.

If the energy is non-convex within the constrained solution space, multiple trial solutions need to be attempted to find the global optimum. Since competing crack growth of more than a few crack tips is a relatively rare occurrence in typical fracture problems, it is reasonable to consider the extension of each crack tip as a viable initial solution to the off-line problem. In doing so, the solution to the competing crack growth problem can be solved (always) if the energy function is concave as only one crack tip can advance in this case. Otherwise, a locally optimal solution found on a convex part of the energy function can be captured using the aforementioned line search routine. Although the success of finding the globally optimal solution based on any trial attempt can not be guaranteed *a priori* if the energy function (3.43) is non-convex, the likelihood of leaving out the optimal solution is small if there are very few (quasi-)competing (3.39) crack tips at a given time.

As the off-line solution is usually of a much finer resolution than that which can be reproduced by discretely, the off-line solution will generally need to be coarsened so as to fit into the discrete framework, i.e. to satisfy the constraint of fixed-length crack tip extensions. One way to do this is to (1) scale the off-line crack tip extensions such that the maximum extension equals the discrete increment length and (2) round-off the remaining crack tip extensions relative to the discrete increment length. For example, the off-line solution $\Delta\tilde{\boldsymbol{\ell}}^k$ can be coarsened to obtain the discrete solution $\Delta\boldsymbol{\ell}^k$ as shown:

$$\Delta\ell_i^k = \text{round}\left(\frac{\Delta\tilde{\ell}_i^k}{\max(\Delta\tilde{\boldsymbol{\ell}}^k)}\right)\Delta\ell_{\text{inc}}, \quad \text{where } i \in \mathcal{W}^{k,m} \tag{3.48}$$

Following the discrete solution to the crack tip extension lengths $\Delta\boldsymbol{\ell}^k$, it is desirable to make an adjustment to the crack tip kink angles since the existing solution, which is the

reference solution $\Delta\boldsymbol{\theta}_0^k$, is sub-optimal due to the finite changes in the crack tip extension lengths that have take place relative to the reference solution $\Delta\boldsymbol{\ell}_0^k$. As the changes in the crack tip kink angles are expected to be small (by virtue of small crack tip extensions and, thus, diminishingly small interactions between the extension lengths and angles), a few iterations of equation (3.36) should suffice to obtain the optimal solution for $\Delta\boldsymbol{\theta}^k$. Further changes in the crack tip extension lengths $\Delta\boldsymbol{\ell}^k$ can be disregarded since for small crack tip extensions the competing crack growth solution has been shown (3.43) to be predominately governed by the crack tip extension lengths rather than the kink angles.

In summary, at the instance competing crack growth is discovered (3.39) at the m'th iteration of the gradient-based solution approach (Section 3.3.3), the solution method switches to brute-force energy minimisation where a simplified energy minimisation problem (3.44) is solved off-line, i.e. irrespective of the discretisation. Generally, multiple trial solutions are required when the energy function is non-convex (3.38). Since the off-line solution can not generally be reproduced within a discrete framework, a coarsening of the off-line solution is carried out (3.48) to determine the final discrete solution for time k.

The subsequent section verifies the proposed formulation for solving competing crack growth problems within the discrete framework. Several representative case studies are considered that are designed to test the method's robustness against competing/non-competing crack growth for convex/non-convex behaviours of the energy function.

3.4.3 Verification of solution algorithm

The gradient-based and the brute-force energy minimisation methods assuming fixed-length crack tip extensions are verified in a number of test cases involving multiple crack tips. The underlying assumption about each test case is that at any time $k \in \{1, 2, \dots\}$ the energy function $\Pi(\Delta\boldsymbol{\ell}^k, \Delta\boldsymbol{\theta}^k)$ is convex in $\Delta\boldsymbol{\theta}^k \in \mathbb{R}^{n_{\text{tip}}}_{(-\pi,\pi)}$ but not necessarily convex in $\Delta\boldsymbol{\ell}^k \in \mathbb{R}^{n_{\text{tip}}}_{\geq 0}$. In other words, it is assumed that for a given $\Delta\boldsymbol{\ell}^k$ a unique stationary point of $\Pi(\Delta\boldsymbol{\ell}^k, \Delta\boldsymbol{\theta}^k)$ can always be found in terms of $\Delta\boldsymbol{\theta}^k$ such that the energy is minimised. Consequently, the test cases can be simplified to only consider $\Delta\boldsymbol{\ell}^k$ as the solution for $\Delta\boldsymbol{\theta}^k$ will be implicit. Moreover, it is sufficient to suppose a quadratic energy function as this is

consistent with small crack tip extensions. Thus, the energy function can be defined as:

$$\Pi(\boldsymbol{\ell}) = \Pi_0 - G_{\mathrm{s}i}\ell_i - \frac{1}{2}H_{\mathrm{s}ij}\ell_i\ell_j \tag{3.49}$$

The aim of the verification studies is to show that the critical fracture path can be captured using fixed-length crack tip extensions, even at the instance of competing crack growth. Four representative benchmark problems are studied: (non-)competing crack growth and a (non-)convex energy function. Each case (out of four) assesses the solution convergence (or non-convergence) for 3, 6 and 12 crack tips. The forthcoming numerical results are the "worst" results that could be obtained from a sizeable batch of randomly generated cases. The intention is to demonstrate the potential capabilities/limitations of different discrete solution approaches. For the sake of brevity we will use the key-word *proposed* in the context of a gradient-based solution approach to indicate that the gradient-based method assumes the constraint of fixed-length crack tip extensions and that a single trial solution is used in an attempt to solve for the optimal crack tip extensions (as described in Section 3.3.3). The key-word *standard* will be used within the context of a gradient-based solution approach to indicate that the method is not restricted to fixed-length crack tip extensions but, instead, constrained by a fixed-unit of total crack growth per time-step. Additionally, a line search routine will be used to find locally optimal solutions along a particular solution advance direction on convex parts of the energy function. Furthermore, multiple trial solutions will be attempted (e.g. extending each crack tip as an individual initial solution) as a way to raise the odds of converging to the globally optimal solution.[3]

The solution obtained by the *standard* gradient-based method is used as a reference against which the solutions by the *proposed* and the *brute-force* methods are compared. In each test case, the fracture evolution is allowed to persist until the total amount of crack growth reaches $\Delta a_{\mathrm{tot}} = 1$. At this point, the Euclidean norm of the difference between the final crack tip positions, as obtained by different methods, is plotted against the crack growth rate $\Delta\ell_{\mathrm{inc}}/\Delta a_{\mathrm{tot}}$. This is repeated for several different crack growth rates. The results and the relevant commentary pertaining to each test case are given with Figures 3.3-3.8.

[3] The main differences between the standard gradient-based method and the brute-force approach is that the latter method assumes a simplified (quadratic) energy function to solve for the optimal solution; also, the solution is subsequently coarsened to fit the discrete framework of fixed-length crack tip extensions in XFEM.

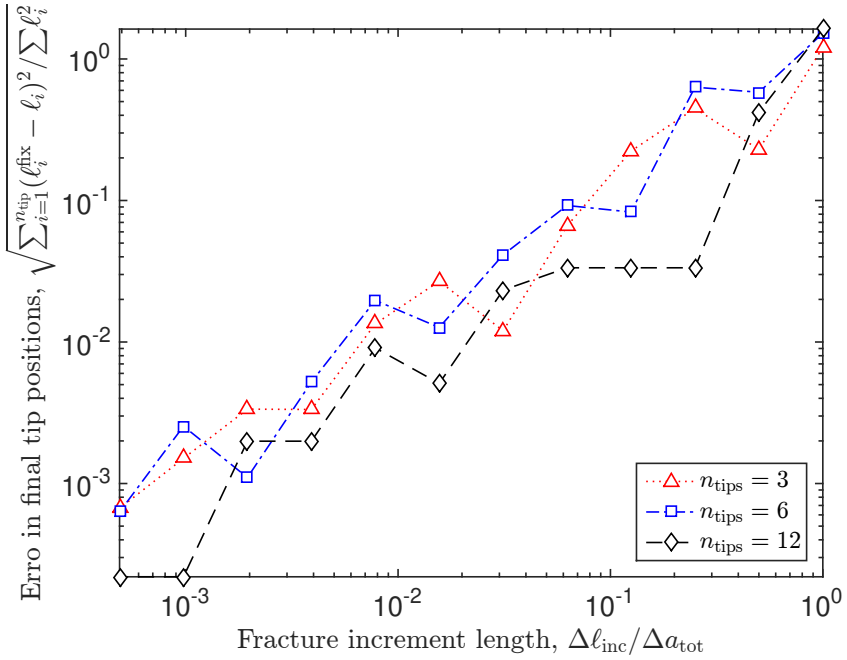

FIGURE 3.3: Non-competing crack growth and a convex energy function. Convergence of the crack tip paths towards the same solution. The proposed gradient-based solution approach is robust.

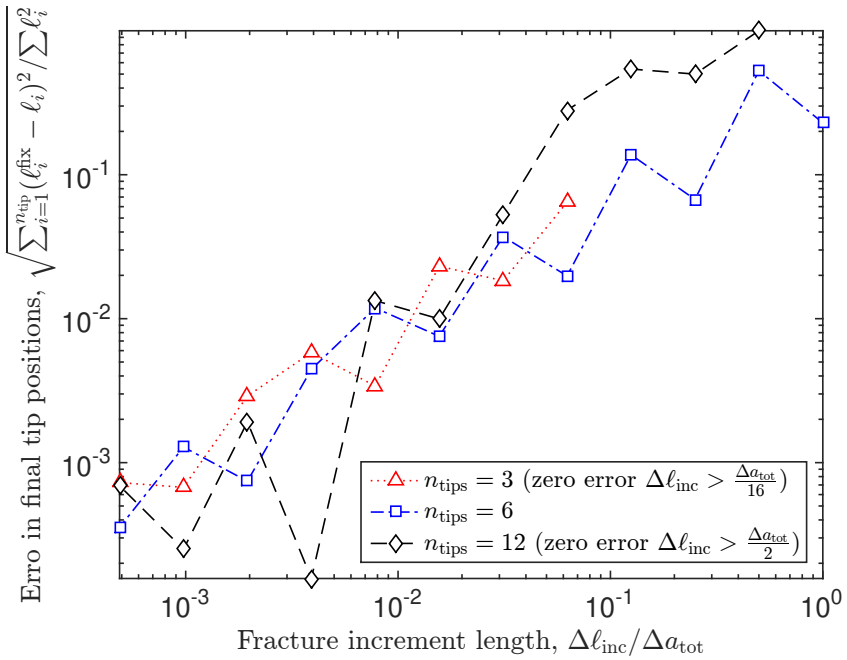

FIGURE 3.4: Non-competing crack growth and a non-convex energy function. Convergence of the crack tip paths towards the same solution. The proposed gradient-based solution approach is robust.

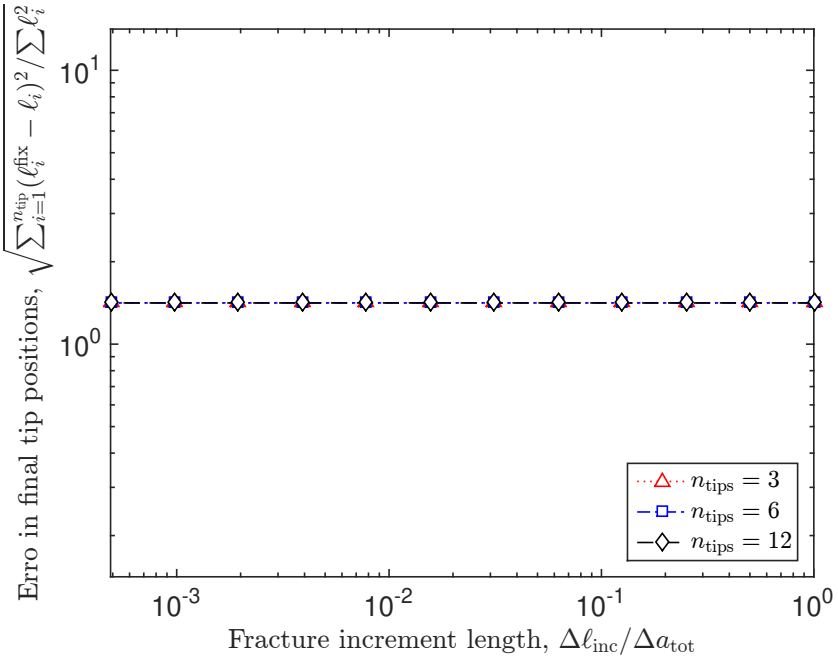

FIGURE 3.5: Competing crack growth and a concave energy function. The proposed gradient-based solution approach is not robust because the initial (trial) solution does not converge to the optimal solution.

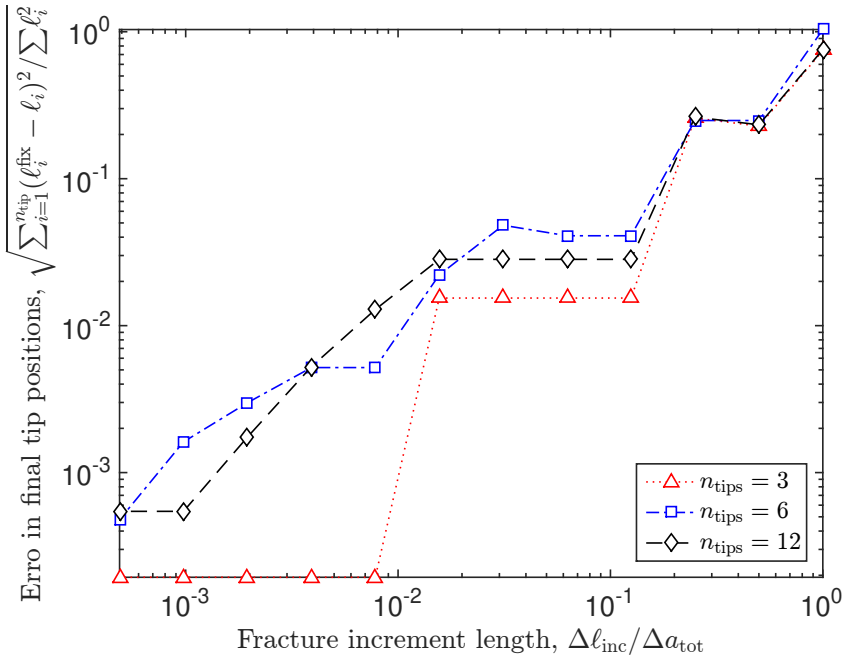

FIGURE 3.6: Competing crack growth and a convex energy function. Convergence of the crack tip paths towards the same solution. The proposed gradient-based solution approach is robust.

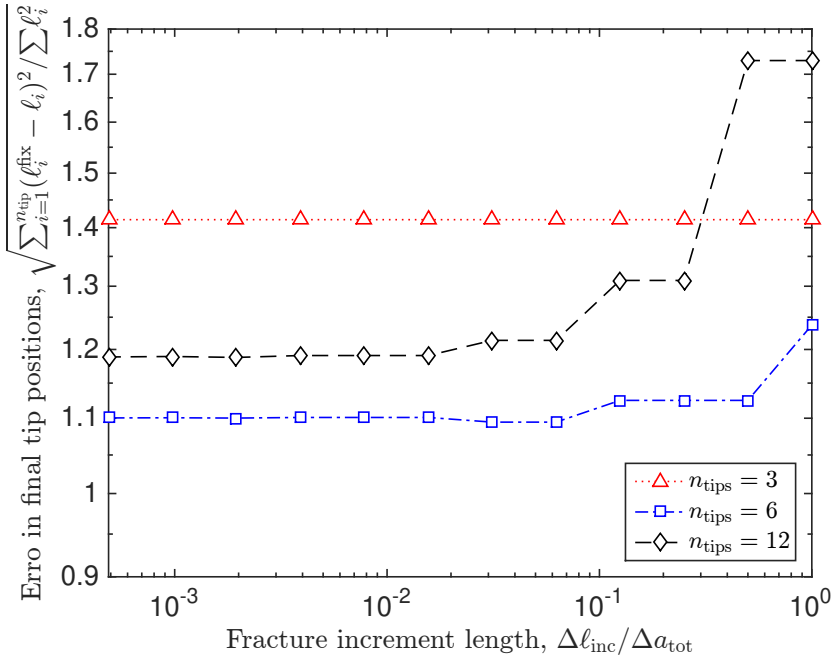

FIGURE 3.7: Competing crack growth and a non-convex energy function. Fracture paths converge to different solutions. The proposed gradient-based solution approach fails. This is due to a single trial solution and a reduced solution search space, i.e. fixed-length crack tip extensions, which leads to misidentify the critical crack tips. Figure 3.8 shows the results for the same test cases but where the critical crack tips are identified in an *off-line* stage.

In conclusion, the gradient-descent solution approach is adequate for most fracture problems but the conditions that may lead to the loss of the solution is when two things occur simultaneously: (1) competing crack growth in the presence of (2) a non-convex energy function. These conditions gives rise to multiple locally optimal solutions meaning that the converged solution will depend on the starting point. Consequently, the gradient-based method is not robust in general. Therefore, it is recommended to switch from the gradient-based solution method to a more reliable means of resolving the non-convex competing crack growth problem by adopting a brute-force energy minimisation routine.

On a final note, it is possible to resolve the competing crack growth problem for two competing crack tips without having to compute higher order energy release rates by simply exploiting the symmetry property of H_{s}. The crack growth solution can be captured by incrementing both crack tips by the same amount. The reason that the critical fracture path can always be captured is that the matrix of the rates of the energy release rates H_{s}

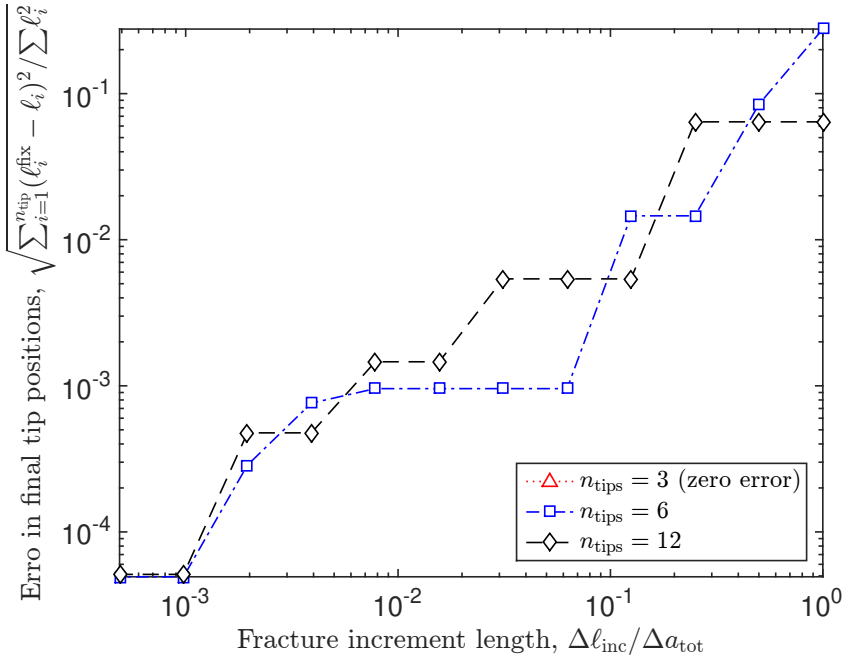

FIGURE 3.8: Competing crack growth and a non-convex energy function. Fracture paths converge to towards the same solutions if a brute-force approach is used rather then the proposed gradient-based method. This is due to the methods capacity to assess multiple trial solutions and to search for a solution within an enhanced solution space, which allows for an accurate identification of the critical set of crack tips, which is vital.

is symmetric and when its size is two-by-two, the energy function's behaviour within the constraint of a fixed total fracture extension can either be convex or concave (not a saddle). In the former (convex) case, extending both crack tips by the same amount is a satisfactory solution as the fracture path will tend to automatically adhere to the optimal path even though the most optimal crack tip growth rates are not reproduced. With regard to the latter (concave) case, extending both cracks by the same amount leads to the more critical crack tip accumulating a higher energy release rate in the post incremented fracture configuration, such that the more energetically favourable crack tip is predisposed to grow in the subsequent time-step. Thus, the critical fracture path solution will not be lost.

3.4.4 Crack growth solution flowchart

The solution steps for solving the discrete fracture growth problem based on the energy-gradient/brute-force energy minimisation methods and assuming fixed-length crack tip extensions can be broken down as follows:

1. Estimate which tips may grow at time k, i.e. get the initial working set $\mathcal{W}^{k,m=0} \subseteq \mathcal{I}_{\text{tip}}$,
2. Grow each tip $i \in \mathcal{W}^{k,m=0}$ by $\Delta\ell_{\text{inc}}$ in direction $\Delta\theta_i^{k,m}$ as obtained by a local criterion,
3. For $m \geq 0$, determine the optimal fracture kinks $\Delta\boldsymbol{\theta}^{k,m}$ by iteratively solving (3.36),
4. Check if crack tips are competing by applying (3.39); do (a) if true, do (b) otherwise:
   (a) Switch to a brute-force method: solve (3.48) and (3.48) for the critical crack tip extension lengths; then do step-(3) and, subsequently, continue from step-(6),
   (b) Update the working-set $\mathcal{W}^{k,m}$ to $m \leftarrow (m+1)$ by using the criterion in (3.37),
5. Repeat steps (3) and (4) for $m = \{1, 2, \dots\}$ until a single crack tip extension remains,
6. The equilibrium load for time k is obtained by scaling the magnitude of a nominal load by $\lambda_t = \sqrt{G_{\text{c}}/\max G_{\text{s}}}$, where G_{c} is the critical energy release rate of the material.
7. Solution is complete for time-step k; advance to $k \leftarrow k+1$ and repeat from step (1).

It is emphasised that the fracture growth criterion is evaluated in the post-incremented fracture configuration by assessing the crack tip energy release rates using the *J*-integral [248, 249]. The need to resolve the correct load magnitude is the result of quasi-statics and the fact that a physically admissible material state must satisfy $G_{\text{s}i} \leq G_{\text{c}}\ \forall i \in \mathcal{I}_{\text{tip}}$, as implied by the growth criterion in (2.41). Therefore, as indicated in step-6 of the foregoing solution outline, the fracture growth criterion is satisfied by scaling the external load magnitude by a factor λ_t. Since for a linear-elastic material G_{s} is proportional to the square of the applied load, which can either be in a form of a surface traction or a displacement boundary condition, the load scaler is determined as $\lambda_t = \sqrt{G_c/\max G_{\text{s}}}$, where generally $\lambda_t \in [0, 1]$. For example, in case of a prescribed external traction on Γ_t, the critical load for the onset of fracture growth is $\mathbf{t} = \lambda_t \mathbf{t}_0$, where $\mathbf{t}_0$ is a reference (maximum) load.

3.5 Discretisation of mechanical system

This section describes the extended finite element method (XFEM) for the 2D discretisation of the cracked solid body. The extended finite element approximation is used to obtained the discrete static-equilibrium equations (2.19), compute the discrete potential energy (2.23) of the solid, and to evaluate the fracture energy release rates (3.1)-(3.5), which are to be used in the prediction of the fracture evolution. The fracture energy release rates are computed by considering algebraic derivatives of the discrete potential energy, which is more accurate than using numerical differencing of the potential energy (to be examined in Section 5.2). The procedure primarily entails the evaluation the derivatives of the generalised stiffness matrix and the force vector. An efficient way to compute the derivatives within the XFEM framework is proposed. Details are provided of how the algebraic derivatives of different terms appearing in the equations are computed.

3.5.1 Discrete equilibrium equation

As the variational formulation (2.18) is based on the Galerkin method, the test and trial spaces are identical except that the test functions are required to vanish wherever displacements are prescribed. Both function spaces are supposed to consist of continuous functions with square-integrable generalised derivatives of up to order 1, i.e. they belong to $\mathcal{H}^1(\Omega)$ Hilbert space. The finite-dimensional test and trial spaces are defined as follows:

$$\mathcal{U}^h = \{\, \mathbf{v}^h \in \mathcal{H}^1(\Omega) : \mathbf{v}^h = \bar{\mathbf{u}} \text{ on } \Gamma_u \text{ , } \mathbf{v}^h \text{ is discontinuous on } \Gamma_c \,\} \tag{3.50}$$

$$\delta\mathcal{U}^h = \{\, \mathbf{v}^h \in \mathcal{H}^1(\Omega) : \mathbf{v}^h = \mathbf{0} \text{ on } \Gamma_u \text{ , } \mathbf{v}^h \text{ is discontinuous on } \Gamma_c \,\} \tag{3.51}$$

Subsequently, the discrete problem of static equilibrium (2.19) is to find $\mathbf{u}^h \in \mathcal{U}^h$ such that:

$$\forall \delta\mathbf{u}^h \in \delta\mathcal{U}^h \quad \int_\Omega \varepsilon_{ij}(\delta\mathbf{u}^h) C_{ijkl} \varepsilon_{kl}(\mathbf{u}^h)\, \mathrm{d}V = \int_{\Gamma_t} \delta u_i^h t_i \, \mathrm{d}s + \sum_{k=1}^{n_c} \int_{\Gamma_c^k} [\![\delta u_i^h]\!] T_{ij} p_j \, \mathrm{d}s \tag{3.52}$$

The local-to-global cordinate transformation matrix reads: $\mathbf{T} = [\mathbf{s}^-, \mathbf{n}^-] \equiv \left[\begin{smallmatrix} \cos\theta & -\sin\theta \\ \sin\theta & \cos\theta \end{smallmatrix}\right]$ and $\mathbf{p} = [p_{sn}, p_{nn}]$. The following section describes the process of constructing the interpolants for $\mathbf{u}^h \in \mathcal{U}^h$ based on the framework of the extended finite element method (XFEM).

3.5.2 Extended finite element method

The extrinsically enriched XFEM approximation takes the following shifted form [89, 91]:

$$\begin{aligned}\mathbf{u}^h(\mathbf{x}) = \sum_{I\in\mathcal{N}_S} N_I(\mathbf{x})\mathbf{u}_I + \sum_{i=1}^{n_{\text{crk}}} \sum_{I\in\mathcal{N}_H^i} N_I(\mathbf{x}) \Big(H^i(\mathbf{x}) - H^i(\mathbf{x}_I)\Big)\mathbf{a}_I^i \\ + \sum_{i=1}^{n_{\text{tip}}} \sum_{\alpha=1}^{4} \sum_{I\in\mathcal{N}_B^i} N_I(\mathbf{x}) \left(B^{i,\alpha}(\mathbf{x}) - B^{i,\alpha}(\mathbf{x}_I)\right)\mathbf{b}_I^{i,\alpha},\end{aligned} \tag{3.53}$$

where $N_I(\mathbf{x})$ are the piece-wise continuous interpolation functions and where $\mathcal{N}_S$, $\mathcal{N}_H^i$ and $\mathcal{N}_B^i$ denote the nodal sets corresponding, respectively, to the standard degrees of freedom (DOF) $\mathbf{u}_I$, the Heaviside enrichment DOF $\mathbf{a}_I^i$ for cracks $i \in \{1, 2, \ldots, n_{\text{crk}}\}$, and the branch enrichment DOF $\mathbf{b}_I^{i,\alpha}$ for crack tips $i \in \{1, 2, \ldots, n_{\text{tip}}\}$ and branch functions $\alpha \in \{1, 2, 3, 4\}$. The enriched nodal degrees of freedom serve to adjust the enrichment so that it can better approximate the solution at hand. Thus, the enrichment functions need not be precisely the local solution to the problem. This is a useful property of a PU based enrichment because the enrichment functions are sometimes approximations themselves. For example, the singular enrichment functions, or branch functions, are the asymptotic near crack tip displacement field functions characterizing the local deformation at the crack tip in terms of polar coordinates[297]. The basis of these functions is given below:

$$\{B_\alpha(r,\theta)\}_{\alpha=1}^4 = \left\{\sqrt{r}\sin\frac{\theta}{2}, \sqrt{r}\cos\frac{\theta}{2}, \sqrt{r}\sin\frac{\theta}{2}\sin\theta, \sqrt{r}\cos\frac{\theta}{2}\sin\theta\right\}, \tag{3.54}$$

where (r, θ) is a polar coordinate system with its origin centered at the crack tip. In addition to the branch enrichment, which makes sense only close to the crack tip, a Heaviside (or discontinuous) enrichment is used to introduce a jump in the displacement field at a general location along a crack [27]. The Heaviside function $H(\mathbf{x})$ is $+1$ if $\mathbf{x} \in \Omega$ lies on one side of the fracture surface and -1 otherwise. As such, the Heaviside can be defined as

the sign of the signed-distance function:

$$H(\mathbf{x}) = \begin{cases} +1 & \text{if } (\mathbf{x} - \mathbf{x}_c) \cdot \mathbf{n}_c \geq 0, \\ -1 & \text{otherwise} \end{cases} \tag{3.55}$$

where $\mathbf{n}_c$ is a unit normal to Γ_c and $\mathbf{x}_c \in \Gamma_c$ is the most proximate point to $\mathbf{x}$. The equilibrium equations (2.19) for a discrete system can be generally written as:

$$\mathbf{K}\mathbf{u} = \mathbf{f}, \tag{3.56}$$

where $\mathbf{K}$ is called the stiffness matrix, $\mathbf{u}$ is the generalised vector of degrees of freedom (comprising both standard and enriched DOF), and where $\mathbf{f}$ is the nodal force vector. The potential energy (2.22) of the linear-elastic solid is given as:

$$\Pi = \frac{1}{2}\mathbf{u}^{\mathrm{T}}\mathbf{K}\mathbf{u} - \mathbf{u}^{\mathrm{T}}\mathbf{f} \tag{3.57}$$

The discrete equilibrium system can be written more explicitly so as to distinguish between the standard and enriched parts:

$$\begin{bmatrix} \mathbf{K}_{ss} & \mathbf{K}_{se_1} & \cdots & \mathbf{K}_{se_n} \\ \mathbf{K}_{se_1}^{\mathrm{T}} & \mathbf{K}_{e_1e_1} & \cdots & \mathbf{K}_{e_1e_n} \\ \vdots & \vdots & \ddots & \vdots \\ \mathbf{K}_{se_n}^{\mathrm{T}} & \mathbf{K}_{e_1e_n}^{\mathrm{T}} & \cdots & \mathbf{K}_{e_ne_n} \end{bmatrix} \begin{bmatrix} \mathbf{u}_s \\ \mathbf{u}_{e_1} \\ \vdots \\ \mathbf{u}_{e_n} \end{bmatrix} = \begin{bmatrix} \mathbf{f}_s \\ \mathbf{f}_{e_1} \\ \vdots \\ \mathbf{f}_{e_n} \end{bmatrix} \tag{3.58}$$

where $\mathbf{u}_s$ and $\mathbf{u}_e$ denote (respectively) the standard (displacement) DOF and the generalised enrichment DOF for the specific enrichment used, e.g. Heaviside or branch. The individual members of the stiffness matrix and the force vector are computed as follows:

$$\mathbf{K}_{ss} = \int_\Omega \mathbf{B}_s(\mathbf{x})^{\mathrm{T}}\mathbf{C}\mathbf{B}_s(\mathbf{x})\,\mathrm{d}V \tag{3.59}$$

$$\mathbf{K}_{se_i} = \int_\Omega \mathbf{B}_s(\mathbf{x})^{\mathrm{T}}\mathbf{C}\mathbf{B}_e^i(\mathbf{x})\,\mathrm{d}V \tag{3.60}$$

$$\mathbf{K}_{e_ie_j} = \int_\Omega \mathbf{B}_e^i(\mathbf{x})^{\mathrm{T}}\mathbf{C}\mathbf{B}_e^j(\mathbf{x})\,\mathrm{d}V \tag{3.61}$$

$$\mathbf{f}_s = \int_\Omega \mathbf{N}_s(\mathbf{x})^{\mathrm{T}}\mathbf{b}\,\mathrm{d}V + \int_{\Gamma_t} \mathbf{N}_s(\mathbf{x})^{\mathrm{T}}\mathbf{t}\,\mathrm{d}s \tag{3.62}$$

$$\mathbf{f}_{e_i} = \int_\Omega \mathbf{N}_e^i(\mathbf{x})^{\mathrm{T}}\mathbf{b}\,\mathrm{d}V + \int_{\Gamma_t} \mathbf{N}_e^i(\mathbf{x})^{\mathrm{T}}\mathbf{t}\,\mathrm{d}s + \int_{\Gamma_c} [\![\mathbf{N}_e^i]\!](\mathbf{x})^{\mathrm{T}}\mathbf{T}\mathbf{p}\,\mathrm{d}s \tag{3.63}$$

The standard strain operator matrix (B-matrix) reads:

$$\mathbf{B}_{sI} = \begin{bmatrix} N_{I,x} & 0 \\ 0 & N_{I,y} \\ N_{I,y} & N_{I,x} \end{bmatrix}, \qquad \forall I \in \mathcal{N}_S \tag{3.64}$$

The B-matrix for the discontinuous enrichment for crack i is:

$$\mathbf{B}_{eI}^i = \begin{bmatrix} N_{I,x}\,(H^i - H_I^i) & 0 \\ 0 & N_{I,y}\,(H^i - H_I^i) \\ N_{I,y}\,(H^i - H_I^i) & N_{I,x}\,(H^i - H_I^i) \end{bmatrix}, \qquad \forall I \in \mathcal{N}_H^i \tag{3.65}$$

whereas for the singular enrichment in the vicinity of crack tip j it is:

$$\mathbf{B}_{eI}^j = \begin{bmatrix} \left(N_I(\boldsymbol{B}^j - \boldsymbol{B}_I^j)\right)_{,x} & 0 \\ 0 & \left(N_I(\boldsymbol{B}^j - \boldsymbol{B}_I^j)\right)_{,y} \\ \left(N_I(\boldsymbol{B}^j - \boldsymbol{B}_I^j)\right)_{,y} & \left(N_I(\boldsymbol{B}^j - \boldsymbol{B}_I^j)\right)_{,x} \end{bmatrix}, \qquad \forall I \in \mathcal{N}_B^j \tag{3.66}$$

where $\boldsymbol{B}^j$ is a vector of the singular crack tip j enrichment functions, as defined by (3.54).

The so-called displacement operator matrices (N-matrices) are given as follows:

$$\mathbf{N}_{sI} = \begin{bmatrix} N_I & 0 \\ 0 & N_I \end{bmatrix}, \qquad \forall I \in \mathcal{N}_S \tag{3.67}$$

$$\mathbf{N}_{eI}^i = \begin{bmatrix} N_I(H^i - H_I^i) & 0 \\ 0 & N_I(H^i - H_I^i) \end{bmatrix}, \qquad \forall I \in \mathcal{N}_H^i \tag{3.68}$$

$$\mathbf{N}_{eI}^j = \begin{bmatrix} N_I(\boldsymbol{B}^j - \boldsymbol{B}_I^j) & 0 \\ 0 & N_I(\boldsymbol{B}^j - \boldsymbol{B}_I^j) \end{bmatrix}, \qquad \forall I \in \mathcal{N}_B^j \tag{3.69}$$

The jump in the enriched N-matrices is defines as:

$$[\![\mathbf{N}_{eI}]\!] = \mathbf{N}_{eI}^{+} - \mathbf{N}_{eI}^{-} \tag{3.70}$$

For Heaviside enrichment, the jump is:

$$[\![\mathbf{N}_{eI}^{i}]\!] = \mathbf{N}_{sI}[\![H^{i}]\!], \qquad \forall I \in \mathcal{N}_{H}^{i} \tag{3.71}$$

whereas for branch enrichment, it is:

$$[\![\mathbf{N}_{eI}^{j}]\!] = \mathbf{N}_{sI}[\![\boldsymbol{B}^{j}]\!], \qquad \forall I \in \mathcal{N}_{B}^{j} \tag{3.72}$$

Note that only the first branch function exhibits a jump across the fracture interface (the other three are continuous); hence,

$$\{[\![B_{\alpha}]\!](r,\theta)\}_{\alpha=1}^{4} = \left\{2\sqrt{r}, 0, 0, 0\right\} \tag{3.73}$$

The jump in the Heaviside enrichment across the fracture interface, according to (3.55), is:

$$[\![H]\!] = 2 \tag{3.74}$$

This completes the summary of how the constituents of the stiffness matrix and force vector are defined. The following section describes how the discrete energy release rates are computed using algebraic differentiation.

3.6 Discrete energy release rates

The potential energy of a discrete mechanical system is written in matrix notation as:

$$\Pi = \frac{1}{2}\mathbf{u}^{\mathrm{T}}\mathbf{K}\mathbf{u} - \mathbf{u}^{\mathrm{T}}\mathbf{f} \tag{3.75}$$

where $\mathbf{u}$, $\mathbf{K}$, and $\mathbf{f}$ are, respectively, the generalised displacement vector, the stiffness matrix, and the nodal force vector. The rotational energy release rate of a crack extension $\Delta\ell_i$ is computed analogously to the works of [130, 168]:

$$G_{\theta i} = -\frac{1}{2}\mathbf{u}^{\mathrm{T}}\delta_i\mathbf{K}\mathbf{u} + \mathbf{u}^{\mathrm{T}}\delta_i\mathbf{f} - \delta_i\mathbf{u}^{\mathrm{T}}(\mathbf{K}\mathbf{u} - \mathbf{f}) \tag{3.76}$$

$$G_{\theta i} = -\frac{1}{2}\mathbf{u}^{\mathrm{T}}\delta_i\mathbf{K}\mathbf{u} + \mathbf{u}^{\mathrm{T}}\delta_i\mathbf{f} \tag{3.77}$$

where, for brevity's sake, δ_i is used to denote a derivative with respect to the free variable, in this case θ_i. Note that the last term in (3.76) vanishes due to the assumed equilibrium of the discrete system, i.e. $\mathbf{K}\mathbf{u} = \mathbf{f}$. The rates of the rotational energy release rates for a multiply cracked solid are computed as follows:

$$H_{\theta ij} = -\left(\frac{1}{2}\mathbf{u}^{\mathrm{T}}\delta_{ij}^2\mathbf{K}\mathbf{u} - \mathbf{u}^{\mathrm{T}}\delta_{ij}^2\mathbf{f}\right) - \delta_j\mathbf{u}^{\mathrm{T}}\left(\delta_i\mathbf{K}\mathbf{u} - \delta_i\mathbf{f}\right) \tag{3.78}$$

$$H_{\theta ij} = -\left(\frac{1}{2}\mathbf{u}^{\mathrm{T}}\delta_{ij}^2\mathbf{K}\mathbf{u} - \mathbf{u}^{\mathrm{T}}\delta_{ij}^2\mathbf{f}\right) + (\delta_j\mathbf{K}\mathbf{u} - \delta_j\mathbf{f})^{\mathrm{T}}\mathbf{K}^{-1}(\delta_i\mathbf{K}\mathbf{u} - \delta_i\mathbf{f}) \tag{3.79}$$

where in (3.78), $\delta_j\mathbf{u}$ is determined from the condition that the variations of the equilibrium equations are vanishing, i.e. $\delta_i(\mathbf{K}\mathbf{u} + \mathbf{f}) = \mathbf{0}$. The force variations $\delta_i\mathbf{f}$ and $\delta_{ij}^2\mathbf{f}$ need only be accounted for if the applied loads act on the virtual crack rotation, e.g. crack face tractions and body-type loads. In (3.79), the first term containing the second order derivatives captures the local interaction between the rotations of different crack increments; on the other hand, the second term encompassing the products of first order variations represents the remote interaction. Concerning the second order cross-differentials $\delta_{ij}(\cdot)$ where $i \neq j$, unless there is a strong geometrical coupling between the different virtual crack rotations, the cross derivatives are null; hence only the "self-interaction" $\delta_{ii}^2(\cdot)$ needs to be accounted for. The local cross-interactions tend to arise only when crack tips are sufficiently close.

3.6.1 Stiffness and force derivatives

Concerning the second order variations $\delta_{ij}^2(\cdot)$ it will be considered for simplicity's sake that the fracture configuration at hand is one where the crack extensions are sufficiently far

apart such that the cross-variations do not arise, i.e. $\delta^2_{ij}(\cdot) = 0$ for $i \neq j$. However, when the local-interactions do arise (eventually), say for a pair of nearby crack tips, the tips tend to already be too close for practical handling and so a crack intersection is forced instead. Note that the remote coupling between the different rates of rotational energy release rates $H_{\theta ij}$ when $i \neq j$ is retained by the products of the first order variations that appear as the second term in (3.79). For convenience, the equations for the discrete potential energy, the energy release rates and the rates of the energy release rates are recalled:

$$\Pi = \frac{1}{2}\mathbf{u}^{\mathrm{T}}\mathbf{K}\mathbf{u} - \mathbf{u}^{\mathrm{T}}\mathbf{f}, \tag{3.80}$$

$$G_i = -\frac{1}{2}\mathbf{u}^{\mathrm{T}}\delta_i\mathbf{K}\mathbf{u} + \mathbf{u}^{\mathrm{T}}\delta_i\mathbf{f}, \tag{3.81}$$

$$H_{ij} = -\left(\frac{1}{2}\mathbf{u}^{\mathrm{T}}\delta^2_{ii}\mathbf{K}\mathbf{u} - \mathbf{u}^{\mathrm{T}}\delta^2_{ii}\mathbf{f}\right) + (\delta_j\mathbf{K}\mathbf{u} - \delta_j\mathbf{f})^{\mathrm{T}}\mathbf{K}^{-1}(\delta_i\mathbf{K}\mathbf{u} - \delta_i\mathbf{f}) \tag{3.82}$$

where in (3.82) only the self interaction $\delta^2_{ii}(\cdot)$ needs to be resolved. Henceforth, the subscript(s) in δ_i and δ^2_{ii} will be omitted. The global stiffness matrix $\mathbf{K}$ is obtained by summing the element-level stiffness matrices:

$$\mathbf{K} = \sum_{i=1}^{n_{\mathrm{el}}} \mathbf{K}_{\mathrm{el}} \tag{3.83}$$

$$\mathbf{K} = \sum_{i=1}^{n_{\mathrm{el}}} \int_{\bar{\Omega}_{\mathrm{el}}} \mathbf{B}^{\mathrm{T}}\mathbf{C}\mathbf{B}\det(\mathbf{J})\,\mathrm{d}\xi\mathrm{d}\eta \tag{3.84}$$

where $\bar{\Omega}_{\mathrm{el}}$ describes an element in the parametrized coordinate space (ξ, η), $\mathbf{B}$ is a strain operator matrix, $\mathbf{C}$ is the constitutive matrix and $\mathbf{J}$ is the Jacobian of the mapping between the parametric and Cartesian (x, y) coordinate spaces. The first and second order variations of the element stiffness matrix $\mathbf{K}_{\mathrm{el}}$ for any element can be generally computed as:

$$\delta\mathbf{K}_{\mathrm{el}} = \int_{\Omega_{\mathrm{el}}} (\delta\mathbf{B}^{\mathrm{T}}\mathbf{C}\mathbf{B} + \mathbf{B}^{\mathrm{T}}\mathbf{C}\delta\mathbf{B})\det(\mathbf{J})\,\mathrm{d}\xi\mathrm{d}\eta + \int_{\Omega_{\mathrm{el}}} \mathbf{B}^{\mathrm{T}}\mathbf{C}\mathbf{B}\,\delta\det(\mathbf{J})\,\mathrm{d}\xi\mathrm{d}\eta \tag{3.85}$$

$$\begin{aligned}\delta^2\mathbf{K}_{\mathrm{el}} &= \int_{\Omega_{\mathrm{el}}} (\delta^2\mathbf{B}^{\mathrm{T}}\mathbf{C}\mathbf{B} + 2\delta\mathbf{B}^{\mathrm{T}}\mathbf{C}\delta\mathbf{B} + \mathbf{B}^{\mathrm{T}}\mathbf{C}\delta^2\mathbf{B})\det(\mathbf{J})\,\mathrm{d}\xi\mathrm{d}\eta \\ &+ \int_{\Omega_{\mathrm{el}}} 2(\delta\mathbf{B}^{\mathrm{T}}\mathbf{C}\mathbf{B} + \mathbf{B}^{\mathrm{T}}\mathbf{C}\delta\mathbf{B})\,\delta\det(\mathbf{J})\,\mathrm{d}\xi\mathrm{d}\eta + \int_{\Omega_{\mathrm{el}}} \mathbf{B}^{\mathrm{T}}\mathbf{C}\mathbf{B}\,\delta^2\det(\mathbf{J})\,\mathrm{d}\xi\mathrm{d}\eta\end{aligned} \tag{3.86}$$

where $\mathbf{C}$ is assumed to be constant for a homogeneous isotropic material. The global force vector due to local fracture surface tractions is obtained by summing the element level

contributions of those elements cut by the cracks:

$$\mathbf{f} = \sum_{i=1}^{n_{\mathrm{el}}^{\mathrm{cut}}} \mathbf{f}_{\mathrm{el}} \tag{3.87}$$

$$\mathbf{f} = \sum_{i=1}^{n_{\mathrm{el}}^{\mathrm{cut}}} \int_{\Gamma_{\mathrm{c}}^{i}} [\![\mathbf{N}]\!]^{\mathrm{T}} \mathbf{T}\mathbf{p} \, \frac{\mathrm{d}l}{\mathrm{d}\zeta} \, \mathrm{d}\zeta \tag{3.88}$$

where $[\![\mathbf{N}]\!]$ denotes a jump in the displacement-like matrix $\mathbf{N}$ across the fracture interface, $\frac{\mathrm{d}l}{\mathrm{d}\zeta}$ is the Jacobian of the mapping between the parametric (ζ) and the physical coordinate (l) that is on the part of the fracture surface that cuts a particular element. The first and second differentials of the element force vector can be generally computed as follows:

$$\delta\mathbf{f}_{\mathrm{el}} = \int_{\Gamma_{\mathrm{c}}} \left(\delta[\![\mathbf{N}]\!]^{\mathrm{T}}\mathbf{T} + [\![\mathbf{N}]\!]^{\mathrm{T}}\delta\mathbf{T}\right) \mathbf{p} \, \frac{\mathrm{d}l}{\mathrm{d}\zeta} \, \mathrm{d}\zeta \; + \; \int_{\Gamma_{\mathrm{c}}} [\![\mathbf{N}]\!]^{\mathrm{T}}\mathbf{T}\mathbf{p} \, \frac{\mathrm{d}}{\mathrm{d}\zeta}(\delta l) \, \mathrm{d}\zeta \tag{3.89}$$

$$\begin{aligned}\delta^2\mathbf{f}_{\mathrm{el}} = &\int_{\Gamma_{\mathrm{c}}} \left(\delta^2[\![\mathbf{N}]\!]^{\mathrm{T}}\mathbf{T} + 2\,\delta[\![\mathbf{N}]\!]^{\mathrm{T}}\delta\mathbf{T} + [\![\mathbf{N}]\!]^{\mathrm{T}}\delta^2\mathbf{T}\right) \mathbf{p} \, \frac{\mathrm{d}l}{\mathrm{d}\zeta} \, \mathrm{d}\zeta \\ &+ \int_{\Gamma_{\mathrm{c}}} \left(\delta[\![\mathbf{N}]\!]^{\mathrm{T}}\mathbf{T} + [\![\mathbf{N}]\!]^{\mathrm{T}}\delta\mathbf{T}\right) \mathbf{p} \, \frac{\mathrm{d}}{\mathrm{d}\zeta}(\delta l) \, \mathrm{d}\zeta + \int_{\Gamma_{\mathrm{c}}} [\![\mathbf{N}]\!]^{\mathrm{T}}\mathbf{T}\mathbf{p} \, \frac{\mathrm{d}}{\mathrm{d}\zeta}(\delta^2 l) \, \mathrm{d}\zeta\end{aligned} \tag{3.90}$$

where the local tractions $\mathbf{p}$ were assumed to be independent of rotation. The matrix $\mathbf{T}(\theta) = \left[\begin{smallmatrix} \cos\theta & -\sin\theta \\ \sin\theta & \cos\theta \end{smallmatrix}\right]$ is the local-to-global transformation matrix that operates on $\mathbf{p}$.

3.6.2 Element-level derivatives

For the elements in partial rotation that are cut by a crack, the variations of the strain and displacement operator matrices are more intricate to compute due to the involvement of integration over the element's sub-cells. In order to compute these variations, it is necessary to determine the variations of the element shapes functions and their cartesian derivatives. To this end, there is a constraint equation that needs to be satisfied:

$$N_I^{\mathrm{e}}(\mathbf{X}^{\mathrm{e}} + \delta\mathbf{X}^{\mathrm{e}}) \, (\mathbf{x}_I^{\mathrm{e}} + \delta\mathbf{x}_I^{\mathrm{e}}) - N_I^{\mathrm{e}}(\mathbf{X}^{\mathrm{e}})\mathbf{x}_I^{\mathrm{e}} = N_J^{\mathrm{c}}(\mathbf{X}^{\mathrm{c}}) \, \delta\mathbf{x}_J^{\mathrm{c}} \tag{3.91}$$

The equation states that the displacements of two coincident material points due to the distortion of the element, as interpolated by the shape functions of the element and the

shape functions of a particular sub-cell, need to be the same. The constraint equation yields a relationship for the variation of the element's parametric coordinates $\delta\mathbf{X}^{\mathrm{e}}$:

$$N_I^{\mathrm{e}}\,\delta\mathbf{x}_I^{\mathrm{e}} + \delta\mathbf{X}^{\mathrm{e}}\frac{\mathrm{d}N_I^{\mathrm{e}}}{\mathrm{d}\mathbf{X}^{\mathrm{e}}}\,\mathbf{x}_I^{\mathrm{e}} = N_J^{\mathrm{c}}\,\delta\mathbf{x}_J^{\mathrm{c}} \tag{3.92}$$

$$\delta\mathbf{X}^{\mathrm{e}} = (N_J^{\mathrm{c}}\,\delta\mathbf{x}_J^{\mathrm{c}} - N_I^{\mathrm{e}}\,\delta\mathbf{x}_I^{\mathrm{e}})\left(\frac{\mathrm{d}N_I^{\mathrm{e}}}{\mathrm{d}\mathbf{X}^{\mathrm{e}}}\,\mathbf{x}_I^{\mathrm{e}}\right)^{-1} \tag{3.93}$$

The displacement of an interior point due to the displacement of the elements nodes is $\delta\mathbf{x}^{\mathrm{e}} = N_I^{\mathrm{e}}\delta\mathbf{x}_I^{\mathrm{e}}$ whereas the displacement of the same point, as interpolated by the shapes of the element's sub-cell, is $\delta\mathbf{x}^{\mathrm{c}} = N_I^{\mathrm{c}}\delta\mathbf{x}_I^{\mathrm{c}}$. Generally, these two displacements do not coincide, i.e. $\delta\mathbf{x}^{\mathrm{e}} \neq \delta\mathbf{x}^{\mathrm{c}}$, and so consistency is enforced by $\delta\mathbf{X}^{\mathrm{e}}$, as determined by (3.93). The variations $\delta\mathbf{X}^{\mathrm{e}}$ and likewise $\delta^2\mathbf{X}^{\mathrm{e}}$ will not be zero if the displacement mismatch variations $\delta\bar{\mathbf{x}}$ and $\delta^2\bar{\mathbf{x}}$ are not zero. The latter variations can be defined as follows:

$$\delta\bar{\mathbf{x}} = N_J^{\mathrm{c}}\,\delta\mathbf{x}_J^{\mathrm{c}} - N_I^{\mathrm{e}}\,\delta\mathbf{x}_I^{\mathrm{e}} \tag{3.94}$$

$$\delta^2\bar{\mathbf{x}} = \left(N_J^{\mathrm{c}}\,\delta^2\mathbf{x}_J^{\mathrm{c}} + \delta N_J^{\mathrm{c}}\,\delta\mathbf{x}_J^{\mathrm{c}}\right) - \left(N_I^{\mathrm{e}}\,\delta^2\mathbf{x}_I^{\mathrm{e}} + \delta N_I^{\mathrm{e}}\,\delta\mathbf{x}_I^{\mathrm{e}}\right) \tag{3.95}$$

$\delta\bar{\mathbf{x}}$ and $\delta^2\bar{\mathbf{x}}$ can then be used to determine $\delta\mathbf{X}^{\mathrm{e}}$ and $\delta^2\mathbf{X}^{\mathrm{e}}$:

$$\delta\mathbf{X}^{\mathrm{e}} = \delta\bar{\mathbf{x}}\,\mathbf{J}^{-1} \tag{3.96}$$

$$\delta^2\mathbf{X}^{\mathrm{e}} = \delta^2\bar{\mathbf{x}}\,\mathbf{J}^{-1} + \delta\bar{\mathbf{x}}\,\delta(\mathbf{J}^{-1}) \tag{3.97}$$

The variations of the element shape functions δN_I^{e} and $\delta^2 N_I^{\mathrm{e}}$ can be determined straighforwardly since $\delta\mathbf{X}^{\mathrm{e}}$ and $\delta^2\mathbf{X}^{\mathrm{e}}$ are known. The enriched shape function jump variations $\delta[\![N_I]\!]$ and $\delta^2[\![N_I]\!]$ along a crack are only due to the variations of the PU shape functions N_I^{e} that multiply the enrichment function jumps $[\![\psi]\!]$. The enrichment function jumps are constant with respect to the rotation of a crack branch. The variations of the enriched shape functions are not zero if an element undergoes a distortion and zero if the element undergoes a uniform translation or a rotation. In the former case, the variations are generally not zero because the translation of some of the elements nodes causes a change in PU shape function values N_I^{e} at a quadrature point $\mathbf{x}$. Thus, for an element in partial rotation, e.g. the element that contains the crack-kink, the variations of the enriched shape

functions $\delta[\![N_I]\!]$ and $\delta^2[\![N_I]\!]$ are computed as follows:

$$\delta[\![N_I]\!] = \delta N_I[\![\psi]\!], \tag{3.98}$$

$$\delta^2[\![N_I]\!] = \delta^2 N_I[\![\psi]\!], \tag{3.99}$$

where $\boldsymbol{N}$ make up the PU basis, i.e. the standard shape functions of an element, and where $[\![\psi]\!]$ denotes a generic enrichment function jump across a crack, i.e. ψ can be either the Heaviside function (3.55) or one of the branch functions (3.54). The variations of the components of equations (3.85), (3.86), (3.89) and (3.90) are detailed below: (note that the vector derivative are defined as: $\partial/\partial\mathbf{X} = [\partial/\partial\xi\ \partial/\partial\eta]^{\mathrm{T}}$, and $\partial/\partial\mathbf{x} = [\partial/\partial x\ \partial/\partial y]^{\mathrm{T}}$)

$$\delta\mathbf{J} = \frac{\partial N_I}{\partial\mathbf{X}}\delta\mathbf{x}_I + \delta\left(\frac{\partial N_I}{\partial\mathbf{X}}\right)\mathbf{x}_I \tag{3.100}$$

$$\delta^2\mathbf{J} = \frac{\partial N_I}{\partial\mathbf{X}}\delta^2\mathbf{x}_I + 2\,\delta\left(\frac{\partial N_I}{\partial\mathbf{X}}\right)\delta\mathbf{x}_I + \delta^2\left(\frac{\partial N_I}{\partial\mathbf{X}}\right)\mathbf{x}_I \tag{3.101}$$

The determinant of the Jacobian and its variations are given below:

$$\det(\mathbf{J}) = \left(\frac{\partial N_I}{\partial\xi}\frac{\partial N_J}{\partial\eta} - \frac{\partial N_I}{\partial\eta}\frac{\partial N_J}{\partial\xi}\right)x_I\,y_J \tag{3.102}$$

$$\begin{aligned}\delta\det(\mathbf{J}) = &\left(\frac{\partial N_I}{\partial\xi}\frac{\partial N_J}{\partial\eta} - \frac{\partial N_I}{\partial\eta}\frac{\partial N_J}{\partial\xi}\right)\delta x_I\,y_J + \delta\xi\frac{\partial}{\partial\xi}\left(\frac{\partial N_I}{\partial\xi}\frac{\partial N_J}{\partial\eta} - \frac{\partial N_I}{\partial\eta}\frac{\partial N_J}{\partial\xi}\right)x_I\,y_J\\ &+\left(\frac{\partial N_I}{\partial\xi}\frac{\partial N_J}{\partial\eta} - \frac{\partial N_I}{\partial\eta}\frac{\partial N_J}{\partial\xi}\right)x_I\,\delta y_J + \delta\eta\frac{\partial}{\partial\eta}\left(\frac{\partial N_I}{\partial\eta}\frac{\partial N_J}{\partial\xi} - \frac{\partial N_I}{\partial\eta}\frac{\partial N_J}{\partial\xi}\right)x_I\,y_J\end{aligned} \tag{3.103}$$

$$\begin{aligned}\delta^2\det(\mathbf{J}) = &\left(\frac{\partial N_I}{\partial\xi}\frac{\partial N_J}{\partial\eta} - \frac{\partial N_I}{\partial\eta}\frac{\partial N_J}{\partial\xi}\right)\delta^2 x_I\,y_J + \delta\xi^2\frac{\partial^2}{\partial\xi^2}\left(\frac{\partial N_I}{\partial\xi}\frac{\partial N_J}{\partial\eta} - \frac{\partial N_I}{\partial\eta}\frac{\partial N_J}{\partial\xi}\right)x_I\,y_J\\ &+\left(\frac{\partial N_I}{\partial\xi}\frac{\partial N_J}{\partial\eta} - \frac{\partial N_I}{\partial\eta}\frac{\partial N_J}{\partial\xi}\right)2\delta x_I\,\delta y_J + 2\delta\xi\delta\eta\frac{\partial^2}{\partial\xi\partial\eta}\left(\frac{\partial N_I}{\partial\eta}\frac{\partial N_J}{\partial\xi} - \frac{\partial N_I}{\partial\eta}\frac{\partial N_J}{\partial\xi}\right)x_I\,y_J\\ &+\left(\frac{\partial N_I}{\partial\xi}\frac{\partial N_J}{\partial\eta} - \frac{\partial N_I}{\partial\eta}\frac{\partial N_J}{\partial\xi}\right)x_I\,\delta^2 y_J + \delta\eta^2\frac{\partial^2}{\partial\eta^2}\left(\frac{\partial N_I}{\partial\eta}\frac{\partial N_J}{\partial\xi} - \frac{\partial N_I}{\partial\eta}\frac{\partial N_J}{\partial\xi}\right)x_I\,y_J\end{aligned} \tag{3.104}$$

The variations of the inverse of the Jacobian are (note the use of the identity $\mathbf{J}^{-1}\mathbf{J} = \mathbf{I}$):

$$\delta\mathbf{J}^{-1} = -\,\mathbf{J}^{-1}\,\delta\mathbf{J}\,\mathbf{J}^{-1} \tag{3.105}$$

$$\delta^2\mathbf{J}^{-1} = -\,\mathbf{J}^{-1}\,\delta^2\mathbf{J}\,\mathbf{J}^{-1} + 2\,\mathbf{J}^{-1}\,\delta\mathbf{J}\,\mathbf{J}^{-1}\,\delta\mathbf{J}\,\mathbf{J}^{-1} \tag{3.106}$$

The variations of the shape function Cartesian derivatives for elements that require integration over sub-cells (note, this only pertains to elements that have the crack kink):

$$\delta\frac{\partial N_I}{\partial \mathbf{x}} = \delta\mathbf{J}^{-1}\,\frac{\partial N_I}{\partial \mathbf{X}} + \mathbf{J}^{-1}\,\delta\frac{\partial N_I}{\partial \mathbf{X}} \tag{3.107}$$

$$\delta^2\frac{\partial N_I}{\partial \mathbf{x}} = \delta^2\mathbf{J}^{-1}\,\frac{\partial N_I}{\partial \mathbf{X}} + \mathbf{J}^{-1}\,\delta^2\frac{\partial N_I}{\partial \mathbf{X}} \tag{3.108}$$

where the first and second order variations of the shape functions are given as:

$$\delta\begin{bmatrix}\frac{\partial N_I}{\partial x}\\ \frac{\partial N_I}{\partial y}\end{bmatrix} = \delta\mathbf{J}^{-1}\begin{bmatrix}\frac{\partial N_I}{\partial \xi}\\ \frac{\partial N_I}{\partial \eta}\end{bmatrix} + \mathbf{J}^{-1}\delta\begin{bmatrix}\frac{\partial N_I}{\partial \xi}\\ \frac{\partial N_I}{\partial \eta}\end{bmatrix} \tag{3.109}$$

$$\delta^2\begin{bmatrix}\frac{\partial N_I}{\partial x}\\ \frac{\partial N_I}{\partial y}\end{bmatrix} = \delta^2\mathbf{J}^{-1}\begin{bmatrix}\frac{\partial N_I}{\partial \xi}\\ \frac{\partial N_I}{\partial \eta}\end{bmatrix} + 2\,\delta\mathbf{J}^{-1}\delta\begin{bmatrix}\frac{\partial N_I}{\partial \xi}\\ \frac{\partial N_I}{\partial \eta}\end{bmatrix} + \mathbf{J}^{-1}\delta^2\begin{bmatrix}\frac{\partial N_I}{\partial \xi}\\ \frac{\partial N_I}{\partial \eta}\end{bmatrix} \tag{3.110}$$

The shape function variations of the elements that are not cut by a crack simplify to:

$$\delta\begin{bmatrix}\frac{\partial N_I}{\partial x}\\ \frac{\partial N_I}{\partial y}\end{bmatrix} = \delta\mathbf{J}^{-1}\begin{bmatrix}\frac{\partial N_I}{\partial \xi}\\ \frac{\partial N_I}{\partial \eta}\end{bmatrix} \tag{3.111}$$

$$\delta^2\begin{bmatrix}\frac{\partial N_I}{\partial x}\\ \frac{\partial N_I}{\partial y}\end{bmatrix} = \delta^2\mathbf{J}^{-1}\begin{bmatrix}\frac{\partial N_I}{\partial \xi}\\ \frac{\partial N_I}{\partial \eta}\end{bmatrix} \tag{3.112}$$

The variations of the strain matrix read:

$$\delta\mathbf{B}_I = \begin{bmatrix}\delta\frac{\partial N_I}{\partial x} & 0 & \delta\frac{\partial N_I}{\partial y}\\ 0 & \delta\frac{\partial N_I}{\partial y} & \delta\frac{\partial N_I}{\partial x}\end{bmatrix} \tag{3.113}$$

$$\delta^2\mathbf{B}_I = \begin{bmatrix}\delta^2\frac{\partial N_I}{\partial x} & 0 & \delta^2\frac{\partial N_I}{\partial y}\\ 0 & \delta^2\frac{\partial N_I}{\partial y} & \delta^2\frac{\partial N_I}{\partial x}\end{bmatrix} \tag{3.114}$$

The jump-like matrix is defined as:

$$[\![\mathbf{N}]\!]_I^\alpha = \begin{bmatrix} N_I[\![\psi]\!]^\alpha & 0 \\ 0 & N_I[\![\psi]\!]^\alpha \end{bmatrix} \tag{3.115}$$

where α denotes any of the enrichment functions. The spatial (x, y) variations can be expressed solely in terms of the variations in the polar angle θ since the radius r is constant:

$$\delta_i x = -y\,\delta\theta_i, \qquad \delta_i y = \quad x\,\delta\theta_i \tag{3.116}$$

$$\delta_i^2 x = -x\,\delta\theta_i, \qquad \delta_i^2 y = -y\,\delta\theta_i \tag{3.117}$$

3.7 Determination of the crack growth direction

Equations (3.77) and (3.79) can be used to determine the energy release rates and the rates of the energy release rates associated with the rotations of different crack tip extensions. The most energetically favourable crack growth directions of a set of fracture increments $\mathcal{I}_{\text{inc}} \subseteq \mathcal{I}_{\text{tip}}$ are those that yield zero rotational energy release rates, i.e. $G_{\theta i} = 0$ for $i \in \mathcal{I}_{\text{inc}}$. This is a non-linear problem; thus, the solution to the crack extension angle θ_i^k, where $i \in \mathcal{I}_{\text{inc}}^k$, is written in the form of Newton's iterations at time-step k and iteration step m:

$$\theta_i^{k,m+1} = \theta_i^{k,m} - \left(H_\theta{}^{-1}\right)_{ij}^{k,m} G_{\theta j}^{k,m} \tag{3.118}$$

The solution for $\boldsymbol{\theta}^k$ is considered to have numerically converged when the difference between two consecutive iterations satisfies the criterion $\max_{i\in\mathcal{I}_{\text{inc}}}(|\theta_i^{k,m+1} - \theta_i^{k,m}|) < \epsilon$, where ϵ is a small positive number, e.g. $\epsilon = 10^{-3}$. Note that within the discrete framework that supposes straight crack tip extensions (such as the current one), two consecutive extensions at the same crack tip $i \in \mathcal{I}_{\text{inc}}^{k+1} \cap \mathcal{I}_{\text{inc}}^k$ will always result in a crack kink under mixed mode loading conditions, i.e. $\theta_i^{k+1} - \theta_i^k \neq 0$. This phenomenon is purely due to discretisation and does not reflect the actual physics of crack growth. In other words, the fracture path should be smooth under normal conditions. The discrete fracture solution approaches the smooth solution in the limit of vanishingly small crack tip extensions.

3.8 Summary

Three methods have been described for the solution of the discrete fracture growth problem. These solution methods were based on: crack length-control, load-control, and on the energy-gradient. The first method was considered to be best suited to problems where the fracture front was stable. This meant that the energy function was required to be convex in the feasible solution space that was defined by a fixed total length fracture extension. The method could be used to solve both stable and unstable crack propagation problems. The second strategy was based on load-control. It was considered to be the simplest method albeit limited to fracture problems that were characterised by a convex energy function, i.e. for stable crack growth and stable fracture front configurations. In this case, the fracture solution was automatically captured by incrementing the load parameter at each time-step and minimising the energy function with respect to the crack tip extensions (subject to irreversibility). Finally, the third solution strategy utilised the gradient of the energy function to determine the instantaneous fracture advance vector that would yield the greatest rate of energy minimisation (or maximum energy dissipation).

The energy-gradient based solution approach had to be adapted to the constraint of fixed-length crack tip extensions that is intrinsic to the current XFEM implementation (Section 4.3). The solution algorithm was modified such that at a given iteration step the energetically less favourable crack tip extensions were annihilated completely whereas the more favourable extensions were retained and carried over to the next iteration step. In this proposed adaptation, the favourability of a crack tip extension was decided based on the energy release rate at the tip relative to the mean energy release rate of all other tips in the trial set of crack extensions. Note that by resorting to this solution approach, the vital constraint of a fixed unit of total fracture advance per time step was violated in the search for the optimal crack extension solution. Nonetheless, this violation was shown not to have a detrimental effect on the fracture solution for most case, e.g. non-competing crack growth. The proposed simplification lacked robustness only in the case of competing crack growth and a non-convex energy function; hence, the method could still be used successfully to resolve competing crack growth provided the energy function was convex.

To tackle the aforementioned limitation of the discretisation-adapted energy-gradient based solution approach to resolving competing crack growth for fixed-length crack tip extensions, it was proposed to minimise a quadratic approximation of the energy function with respect to the crack tip extension lengths. The so-called *off-line* solution stage would be invoked upon reaching convergence of the solution for the crack tip extensions directions and determining that these crack tips were competing. In carrying out this off-line energy minimisation, which is not subject to the discretisation related constraints, the most critical crack tips and their relative growth rates could be determined sufficiently accurately such that by coarsening the off-line solution to fit the discrete framework the crack tip competition could be effectively resolved. The off-line solution approach was verified by solving several fabricated benchmark problems involving competing cracks.

The second part of this chapter focused on the extended finite element method and the resulting system of equations that needed to be solved for the discrete static equilibrium. Details were provided on the computations of the fracture energy release rates within the XFEM framework based on the stiffness derivative approach. The steps of performing the algebraic differentiation of the XFEM stiffness matrix and the force vector were described. Overall, this chapter has focused on the solution procedure for the problem of fracture evolution as governed by the minimum energy principle. The necessary equations for the numerical solution have been defined. The computer implementation of the proposed solution method within the *Matlab* environment is delineated in the following chapter.

Chapter 4

Implementation

4.1 Introduction

This chapter addresses the computer implementation of the extended finite element method (XFEM) within the *Matlab* programming language for modelling multi-crack growth with intersections. It is important for the numerical simulations to be practical on a desktop computer even for relatively large size problems, e.g. several million DOF's and hundreds of cracks. For instance, the parametric studies involving silicon wafer splitting (Chapter 6) are computationally expensive due to the fine-scale discretisation that is needed to accurately capture the micro-crack interactions and coalescence in an SOI wafer specimen that is modelled on the scale of millimetres. The computer implementation is focused primarily on the assembly and updating of the system of equations with respect to the evolving fracture geometry, and on the computation of the fracture energy release rates via the stiffness derivative method, which was described in Section 3.6.

An efficient implementation of XFEM is one which updates the system of equations only where it is necessary by considering the local changes in the enrichment topology as a result of a crack propagation. Although this seems obvious enough, the robust implementation of XFEM for modelling multi-crack growth with intersections tends to be cumbersome because the enrichment needs to be updated in a consistent manner. The complexity of the enrichment tracking and updating of the system of equations further increases since an allowance must be made for elements with multiple enrichment. On the other hand, a *basic* enrichment updating strategy for a propagating crack is to reassemble the entire enrichment from scratch. This avoids having to update the enrichment consistently with the previous enrichment, which tends to be more straightforward insofar as the implementation is concerned. On the downside, the basic enrichment updating approach can lead to a significant computational overhead. Thus, we show via several representative benchmark studies involving multiple crack growth with coalescence the speed-up of updating the enrichment only where it is needed (i.e. where there are changes in the enrichment topology) relative to re-computing the entire enrichment from scratch.

4.2 Aspects of implementation

Although XFEM facilitates mesh independent fracture propagation, the enrichment needs to be updated at each time-step. This is particularly challenging when multiple crack propagations are involved. In the current implementation this is achieved by means of a systematic book-keeping of the element enrichment data, addition and removal of enrichment only where necessary, and a consistent updating of the global system of equations. Consequently, moderate computational times are obtained, even in the current *Matlab* implementation. In the benchmark problems that we solve, the greatest cost by far is in the solution of the linear system of equations rather than in the assembly/updating.

Most XFEM implementations exists in either *C++* or *Fortran* [38, 126, 208], i.e. a compiled language, which naturally provides fast computations. In this respect, *Matlab* or *Python* are inferior as they are interpreted languages, so the simulation speed is generally slower. Concerning the simulations of multiple cracks in XFEM, it can be noted that after each time-step only minor topological changes take place in spite of the size of the system. Provided the enriched part of the stiffness matrix is updated and not completely reassembled, the bottle neck in every time-step is in the solution of the linear system of equations rather than in the post-processing, for which *Matlab* has built-in solvers that are fast and robust.

There exist several different variants of XFEM implementations that mainly differ in the way the local partition of unity enrichment is introduced [3, 31, 89, 91, 150]. Each approach offers a particular balance between accuracy, computational expense and robustness. The following subsections address some of these formulations, the numerical difficulties that arise and how they are mitigated for the optimal performance of the numerical method.

4.2.1 Enrichment in XFEM

The XFEM enrichment functions for the modelling of cracks consist of the Heaviside function and the crack tip branch functions [27, 30, 192]. The Heaviside function (3.55) is used to represent a displacement jump discontinuity across the fracture interface at a

general position along a crack whereas the main purpose of the tip enrichment functions (3.54) is to locate the crack tip and to enhance the standard finite element basis so that the stress singularity and the high gradients close to the tip can be captured more effectively.

There are several common strategies of how the crack tip branch functions may be introduced into the finite element basis. The classic enrichment strategy is to enrich only the nodes whose support is cut by the crack tip. This type of enrichment is known as *topological* enrichment. It achieves the basic goal of locating the crack tip within the element and equipping the element with the necessary basis to reproduce the crack tip singular stress field. Although topological enrichment leads to some improvement in the accuracy of the solution, it proves insufficient to recover the optimal solution convergence rate with mesh refinement (as that of the classic FEM for smooth problems). This is because the standard finite element basis of the (unenriched) elements adjacent to the crack tip can not properly capture the high gradients close to the tip due to the vanishing enrichment domain size as the mesh size approaches zero [24, 158]. To make matters worse, the accuracy tends to deteriorate further when the crack tip happens to be very close to the element edge.

The lack of robustness of topological enrichment motivates the adoption of a different strategy referred to as *geometrical* enrichment [24, 158]. In this case, the nodes within a fixed domain size are enriched with the branch functions. Geometrical enrichment offers better accuracy and convergence of the solution with mesh refinement than topological enrichment; however, the fixed size of the enrichment domain (independent of the mesh) means that with mesh refinement the number of enriched degrees of freedom increases rapidly. Apart from the higher computational cost in the assembly of equations, the condition number of the stiffness matrix increases remarkably due to the nearly linearly dependent branch functions. The high condition number combined with finite precision arithmetic can lead to poor performance of the linear solver being used (e.g. in terms of computational time, accuracy and robustness). Particularly, an iterative solver may be slow to converge if the condition number is very hight. Although the effects of a high condition number are generally less severe on direct linear solvers than on iterative ones, iterative solvers are better suited for large-scale problems [284] due to their more efficient use of computer memory. Of course, if memory is not an issue, a direct solver should be

used for a faster solution time. One way to improve the condition number at the expense of reducing the flexibility of the enriched basis to approximate more general tip fields is to employ the so called enriched degrees-of-freedom *gathering* technique [7, 8, 158, 279].

It is desirable to retain some favourable properties from topological enrichment, such as computational efficiency and low condition number but also exploit some of the benefits of geometrical enrichment, such as better accuracy and robustness of the enrichment method. Thus, the proposed strategy is to enrich a domain size proportional to the local mesh size but to assume an enrichment radius that spans at least a few layers of elements surrounding the crack tip. The additional rings of elements help resolve the high gradients close to the crack tip while keeping the condition number relatively low [112, 172, 303].

4.2.2 Blending elements

The *blending* elements that have only some of their nodes enriched "blend" the fully enriched and un-enriched parts of the approximation to preserve continuity of the displacement field across element boundaries. The fact that the enrichment functions can not be reproduced exactly within the blending elements due to the lack of PU support and that these enriched terms can not be compensated by the standard FE basis, tends to pollute the solution and lead to a sub-optimal solution convergence rate [59, 158, 279].

For the good performance of local partition of unity enrichment a proper construction of blending elements is essential. Numerical difficulties due to blending can be reduced by the addition of hierarchical shape functions in order to compensate for the unwanted terms in the partially enriched elements [279]. However, this approach is better suited for polynomial enrichments than for general (e.g. non-polynomial) enrichments. Therefore, an alternative method is the so-called Corrected XFEM [88] whereby a modified enrichment function is used such that partition of unity and inter-element continuity are satisfied within the enriched domain. The modified enrichment function is obtained by multiplying the enrichment function by a ramp function that is unity in the interior of the enriched domain and which smoothly goes to zero on its boundary. Another method, which is similar in principle to the previous one, is the so-called stabilised GFEM (SGFEM) [111]

whereby the modified enrichment function is computed by subtracting the FE interpolation of the enrichment function from the enrichment function itself. Although on the boundary of the enriched domain the element edge continuity between nodes is compromised, the method offers significantly better conditioning than Corrected XFEM whilst offering better accuracy than standard XFEM. One more method to circumvent blending problems (by avoiding blending elements altogether) is to use a discontinuous Galerkin formulation [103] where inter-element continuity is enforced by using a internal penalty method.

The present variant of XFEM is the so-called Corrected XFEM [88] that assumes the modified crack tip branch functions and a full PU support over the enriched domain [179]. With regard to Heaviside enrichment, no modification of the Heaviside function is required nor is it necessary to handle the Heaviside blending elements in any special way since the Heaviside (3.55) is within the order of the standard finite element approximation.

4.3 Crack representation

Many numerical solutions assume cracks sufficiently far apart such that crack intersections are never given a chance to take place [143–145]. In the present model, cracks are allowed to interact both *weakly* and *strongly*; weak interactions are due to the changes in the local crack tip stresses caused by relative crack propagations whereas strong interactions refer to the possibility of cracks to arbitrarily intersect (similar in principal to the work of [50]). Here, we describe how crack growth and crack merging is managed within the XFEM framework. Particularly, the focus is on how crack intersections are detected, created and how the FE basis is enriched. The numerical limitations of the proposed explicit crack representation scheme are pointed out as the difficulties with crack junction enrichment.

4.3.1 Crack extension length

The enrichment is considered to be contained within the crack tip segment for the following reasons. Firstly, the crack tip branch functions are analytically derived based on the consideration of a straight crack (and not a curved or a kinked crack) [294, 297]. Secondly,

it is simple to incorporate the standard branch functions for a straight crack segment as there is no need for a curvilinear coordinate system in order to map the branch functions along a non-straight crack. Although the mapping procedure is straightforward in case of a smoothly curving crack, it is more complex if the crack has a kink [72]. Nonetheless, several methods have been proposed in the literature [72, 270] that are essentially based on expressing the arguments of the branch functions (3.54) in terms of the values of the level set functions [221, 222] that are used to describe the crack geometry [37, 281, 282].

In the current implementation of XFEM the tip enrichment is contained within the crack tip segment. As a result, crack kinks do not appear inside the branch enriched domain and the assumption of a straight crack, which is made in the original derivations of the crack tip branch functions [294, 297], is fulfilled. With regard to the fracture energy release rates: G_θ (3.81) and H_θ (3.82), the algebraic derivatives of the stiffness matrix with respect to the virtual rotation of the crack tip segment are simpler and numerically more cost effect to compute if the branch enrichment radius is smaller than the length of the crack tip segment; in this case, the domain to experience the virtual geometrical perturbation can be chosen such that the branch enriched elements only undergo virtual rigid translations/rotations, whereas the surrounding unenriched elements undergo virtual distortions (refer to Figure 4.3 for details). This type of a mesh perturbation is chosen so as to avoid having to compute the "distortional" derivatives of the enriched elements as they are more expensive than those of unenriched elements due to the larger element stiffness matrices and the high-order quadrature schemes that are required.

In contrast to the present stiffness derivative approach, the author of [286] proposed the differentiation of the branch enrichment functions rather than of the mesh [228]. Thus, the key advantage of keeping the mesh and the enriched elements fixed is that the derivative of the element's Jacobian with respect to a virtual crack extension vanishes. Consequently, fewer partial derivatives of the stiffness matrix need to be computed. However, the simplicity of the method does not directly extend to computing the stiffness derivatives with respect the virtual rotation of a crack extension. The derivative of the Jacobian of an intergation sub-cell over a split element does not vanish since the rotating crack strains the sub-domains of integration. Also, the derivatives of the stiffness matrix of the

enriched elements are computationally more expensive than the current approach where the derivatives are obtained by a simple rotational transformation of the stiffness matrix. Thus, there seem to be no clear advantages to the method of [286] for computing the derivatives of the stiffness matrix with respect to the virtual rotation of a crack extension.

The main downside of requiring the radius of the branch enriched domain to be within the length of the crack tip segment is that it imposes a constraint on the minimum allowable crack tip extension length. Specifically, the crack increment needs to be bigger than the tip enrichment radius so that crack kinks do not appear within the enriched domain. The constraint on the minimum crack tip extension length can give a wrong solution by the proposed gradient-based energy minimisation approach for fixed-length crack tip extensions that was described in Section 3.3.3. It was shown in Section 3.4 that numerical difficulties could arise in the case of competing unstable crack growth, e.g. Figure 3.7. However, it was subsequently demonstrated that the assumption of fixed-length crack tip extensions would not be detrimental to the critical fracture path solution provided the critical crack tips could be identified correctly. To this end it was proposed to resolve crack tip competition approximately in an off-line solution step that could account for arbitrary crack tip extension lengths. It was shown that this approximate solution would coincide with the exact solution if the crack tip extensions were sufficiently small since the crack growth directions would be relativly uninfluenced (3.42). In the end, the off-line solution would be coarsened in order to fit the current XFEM discretisation based on fixed-length crack tip extensions. This solution strategy proved to be adequate for capturing the critical fracture path (Figure 3.8) even at the instance of unstable competing crack growth.

4.3.2 Managing intersections

In the XFEM implementation of [50], when the distance between one crack tip and another crack surface becomes less than the minimum crack tip extension length, the tip is joint to the middle of the intersected crack's segment. In the present XFEM implementation we allow cracks to intersect arbitrarily. This is accomplished by the following two routines:

- **An intersection criterion** intersection between a growing crack A and a crack B is created once it is detected that A's tip extension crosses B's surface thereby forming an 'X'-type intersection; crack A is pulled back until its tip lies on B's surface.
- **Minimum distance criterion** intersection of crack A onto crack B is forced once the distance between A's tip and B's surface becomes less than a prescribed tolerance (e.g. the size of A's tip enrichment radius); crack A is extended normal to B's surface.

Both techniques are used to improve the robustness of crack intersection detections and to achieve higher resolution intersections. In applying these schemes, a crack intersection is delayed to as late a time as possible and until crack tip branch enrichment makes sense; that is, the tip enrichment is not cut by another crack since this would diminish the usefulness of tip enrichment in the first place.[1] If an intersections happens very close to a crack vertex (node), numerical difficulties due to integration over degenerate sub-cells are avoided by snapping the intersection point onto the crack vertex. In case the intersection takes place very close to a crack tip, the tip enrichment is removed and the tip is frozen.

Once a crack intersection is created, a *junction* enrichment needs to be introduced to the FE basis in order to capture the kinematics of the elements that are cut by the two cracks. The enrichment for a crack junction was originally developed by [27, 62] and used in [50] for modelling multi-crack growth. The enrichment takes the form of a superposition of two Heaviside enrichments (3.55) corresponding to each crack. Note that the general form of the displacement field given by (3.53) is adequate for describing the discontinuous displacement field for any number of intersecting cracks. The key requirement is to correctly *blend* the Heaviside enrichment from the *minor* (intersecting) crack to the *major* (intersected) crack so that non of the Heaviside-enriched shape functions are the same.

4.3.3 Crack junction enrichment

The discontinuous part of the displacement field approximation in the vicinity of two intersecting cracks is described by two sets of Heaviside enriched shape functions. This type of enrichment is collectively called a *junction* enrichment. The proper construction

[1] If topological enrichment (or if DOF's gathering) is used, the tip enrichment domain should not be cut by another crack. On the other hand, the tip enrichment DOF's of geometrical enrichment will allow some local adjustment of the tip enrichment functions so that the solution is more optimal; still the worth is debatable.

of the junction enrichment is essential in order to correctly describe the kinematics of the multiply cut elements and to prevent the linear dependence between the Heaviside enriched shape functions of the minor crack with those of the major crack. The correct way to implement the Heaviside enrichment for the minor crack is to first deflect the minor crack along the major crack – the deflected branch of the minor crack is referred to as the *blending branch* as it overlies the major crack exactly. Next, the Heaviside enrichment for the minor crack is introduced at the nodes whose support is cut by the main and the blending branches of the minor crack. Refer to Figure 4.1 for a schematic diagram.[2] On the other hand, the Heaviside enrichment for the major crack remains unchanged.

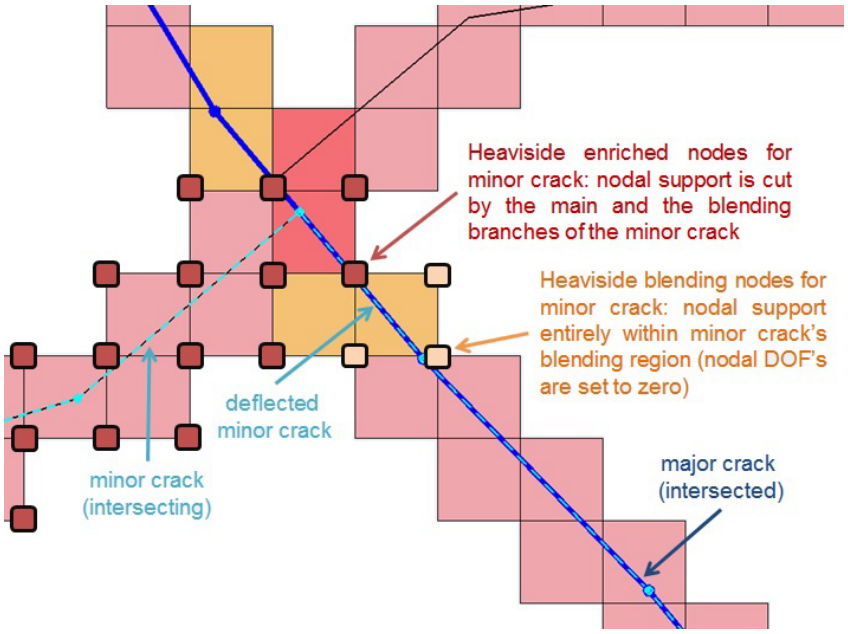

FIGURE 4.1: An example instance of two crack intersections. A junction enrichment is introduced by first deflecting the minor crack along the major crack and then introducing Heaviside enrichment at the nodes whose support is cut by the main and the blending branches of the minor crack.

Note that linear dependence between the Heaviside enriched shape functions of the minor crack with those of the major crack will arise if the enriched shape functions of the minor crack have support only over the blending branch and no support over the main branch of the minor crack. In this case, the enriched shape functions over the blending branch

[2] In 3D the approach to crack junction enrichment is analogous to that in 2D. Specifically, the surface of a minor crack is deflected along the surface of a major crack and the enriched nodes for the minor crack are determined on the basis that they have support over the minor crack both *on* and *outside* its blending region.

of the minor crack will be identical to those of the major crack which then leads to linear dependence. The Heaviside enriched nodes for the minor crack must be selected as those nodes whose support covers both the main and the blending branches of the minor crack.

4.3.4 Enrichment tracking

Enriched elements need to be tracked so that the enrichment can be updated with each crack propagation. In practice, it is advantageous to distinguish between elements even if they are enriched with the same enrichment function as this can facilitate certain element-specific routines, such as: having to introduce the enrichment functions within an element in a particular way so as to mitigate enrichment blending problems [88] (to be discussed later), perform element-type tailored quadrature (e.g. for integrands that are: continuous/discontinuous, low/high order, or singular/non-singular), and for other implementation conveniences. The following enriched element types can be identified:

- Elements enriched with a Heaviside function:
    1. *standard* elements (all nodes of the element are enriched)
    2. *blending* elements (not all element's nodes are enriched)
- Elements enriched with the branch functions:
    1. *crack-tip* element (the element is partially cut by a crack)
    2. standard *crack-split* elements (a crack fully cuts the element)
    3. standard *non-split* elements (a crack does not cut the element)
    4. blending crack-split elements
    5. blending non-split elements

To reiterate, the term *standard* is used to denote that all the nodes of an element are enriched, whereas the term *blending* indicates that not all of the element's nodes are enriched. In general we refer to an element as being *enriched* if any of the element's nodes is enriched. Refer to Figure 4.2 for a comprehensive depiction of the possible enriched element types.

As shown in Figure 4.2, some elements can contain multiple overlapping enrichments. For instance, the Heaviside and the branch enrichments naturally appear along some portion of the crack tip segment. Also, when two crack tips are in a close proximity, it is

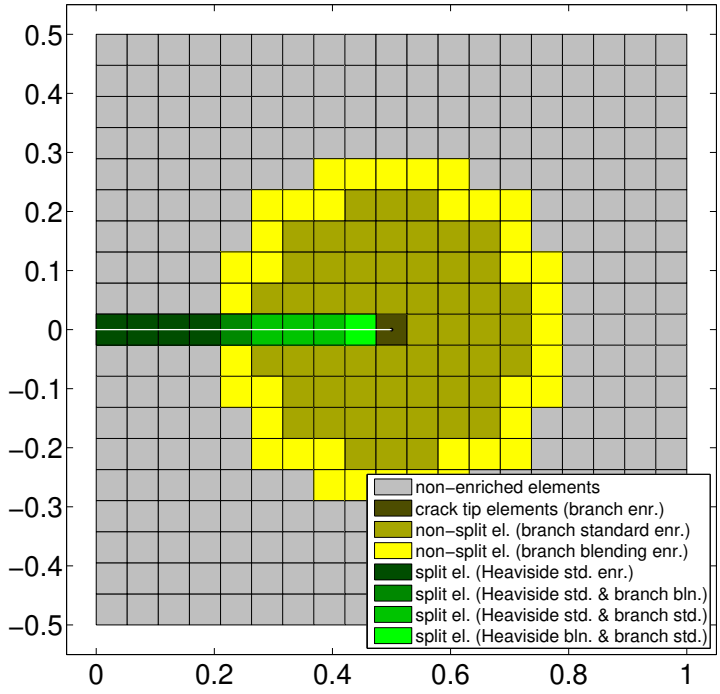

FIGURE 4.2: Classification of elements by enrichment. Note that, in practice, the enrichment domain is 1-2 element layers around the crack tip; hence, some of the enriched element types may not appear in the enriched domain.

possible for an element to be simultaneously enriched with two sets of branch functions. Finally, when two cracks intersect, the intersected element(s) will need to be enriched with two Heaviside functions. In general, we allow for an element to be enriched an arbitrary number of times. Hence, it is necessary to track every enriched element's enrichment functions and generalised enriched nodes (or generalised enriched degrees of freedom).

In *Matlab* we use *cell*-vector to store all elements' enrichment information. In general, each cell-element contains a matrix where the number of columns corresponds to the number of enrichment layers and where each column lists the following enrichment data: (1) the crack the enrichment is for, (2) the enrichment identity (e.g. Heaviside, branch for tip-1, or branch for tip-2), and (3) the preferred quadrature scheme for the particular enrichment. Another *cell*-vector is used for storing the enriched elements' enriched nodes; in this case, each cell-element contains a vector of the enriched nodes for all the layers of enrichment.[3]

[3] A matrix for storing enriched elements' enriched nodes is not practical because elements can have different numbers of enriched nodes due to the arbitrary number of enrichment functions. Of course, an alternative is to pad a vector of enriched nodes with zeros such that a matrix-form of storage of all enriched elements' enriched nodes can be used. However, because most enriched elements contain few enrichment layers and few elements contain multiple enrichment layers, a sparse matrix storage would be preferred.

4.4 Assembly of equations

The XFEM implementation is focused on robustness and efficiency. Some features of the implementation are: multiple enrichment layers over an element, element-type tailored integration routines, and consistent updating of the system of equations with respect to the evolving enrichment topology as a result of crack propagation and coalescence.

One way to speed up the computational time is to avoid recomputations of data that are used regularly. It is considered a fair compromise to store each enriched element's shape functions, shape function derivatives (with respect to the element's natural coordinates) and quadrature weights at Gauss points at the expense of a higher memory demand in order to avoid certain recomputations and, thereby, speed up the solution post-processing and updating times. For example, the post-processing stage of the solution involves computing the crack tip stress intensity factors using the domain form of the interaction integral [308]; thus, having the enriched elements' shape functions at one's disposal allows the integrals to be evaluated readily. Also, the updating stage of the global system of equations sometimes calls for the old elemental equations to be subtracted from the global system of equations; thus, the availability of the enriched elements' shape functions speeds up this task. Finally, notice that as the discretisation of the d-dimensional computational domain is refined, the number of enriched elements scales at a rate of d-1 whereas the total number of elements scales at a rate of d; hence, the memory demand for storing various data of enriched elements scales at a rate d-1 whereas the scaling is d for other big data structures such as: the stiffness matrix, element topology (or connectivity), nodal coordinates and displacements. In other words, the memory demand for the enriched elements' data does not grow prohibitively, even though it can be quite large in practice, e.g. from several to a few tens of percent. Nowadays, however, large computer memories are available even for standard consumer desktop machines (e.g. 32Gb-64Gb) at a relatively low cost in comparison to other computer components. On the other hand, fast CPU's are relatively expensive and a single thread performance is capped at around 4GHz. For this reason, it is computationally affordable to maintain a baggage of (potentially) useful data – even if most of these data end up unused – rather than to resort to recomputations.

What follows is an overview of the implementations of the initial assembly of the system of equations and its updating with respect to the evolving cracks. Moreover, details are provided on the implementation of the the stiffness derivative method (Section 3.6) for the evaluation of the fracture energy release rates (3.81) and their rates (3.82) that are to be used in finding the energetically optimal fracture extension directions at each time step.

4.4.1 Initial assembly

The assembly of the discrete system consists of the following routines: (1) identification of the elements to be enriched, (2) assembly of the enriched elements' topology and enrichment data, (3) determination of enriched elements' quadrature points and weights, (4) evaluation of shape functions, and (5) assembly of the system of equations (as in the classic finite element method). These routines are described in more detail as follows.

Elements that need to be enriched with the crack tip branch functions (3.54) are relatively easy to identify; as the implementation assumes the enrichment domain of a certain radius, elements that fall within this domain are chosen for enrichment. On the other hand, the robust selection of elements for Heaviside enrichment can be more challenging, especially in the presence of crack intersections. Generally, an element is enriched with the Heaviside function if the element's nodal support is cut by a crack and if the node's support does not cover the crack tip. When two cracks intersect, the so-called *minor* (interesting) crack needs to be topologically blended into the *major* (intersected) crack. This is done by first deflecting the minor crack along the major crack to a certain length. The deflected length of the minor crack is called the *blending branch* of the minor crack; it is a fictitious part of the minor crack that is used to smoothly blend the Heaviside enrichment of the minor crack to that of the major crack. Subsequently, the Heaviside enrichment for the minor crack is introduced at the nodes whose support is cut by both the main and the blending branches of the minor crack. The Heaviside enrichment for the major crack remains unchanged.

Once the enriched elements for a specific entity of enrichment have been determined, the enriched elements' topology (i.e. the connectivity matrix of the enriched elements) is obtained by taking the enriched elements' reference connectivity matrix – assuming

the nodes are numbered from 1 to N where N is the number of nodes in the enriched patch – and then offsetting this connectivity matrix by the total number of nodes (i.e. the sum of the standard and the enriched nodes) in the discrete system at the given time. The same routine can be applied to obtain the enriched elements' topology for additional enrichment functions, such as in the case of branch enrichment. The downside of this approach is that the resulting band of the stiffness matrix tends to be large. In the end, each enriched element is equipped with a vector of enriched nodes whose sub-sets match the enrichment functions in the order that they have been introduced. Since an element may generally contain multiple layers of enrichment in any order, each instance of enrichments needs to be tracked. This is managed by the element's enrichment data matrix whose column vectors give: the crack number, the enrichment identity (e.g. Heaviside or branch enrichment for crack tip 1 or 2), and the identity of the enrichment function tailored quadrature scheme. Furthermore, for every discontinuous enrichment the discontinuity intersection with an element needs to be found in order to facilitate integration over sub-domains over which the integrands need to be continuous. However, an element can be intersected multiple times; thus, the crack intersection points with each element need to be tracked before the integration sub-domains can be determined. Once the sub-domains are identified, the integration sub-cells can be obtained based on the Delaunay triangulation.

Since different enriched elements require different orders of quadrature, the governing quadrature for an element containing multiple enrichment functions is selected based on the top-level requirement among the co-existing enrichment functions. For example, an element simultaneously enriched with a Heaviside and the singular branch functions will require the order of quadrature to be tailored to the branch enrichment. Once a suitable integration scheme has been selected for a particular element and the element's quadrature points and weights have been computed, the element's standard shape functions can be evaluated at those points. Next, the enriched shapes are constructed by taking the tensor product of the enrichment function value with the standard shape functions. The enriched shape functions are assembled in the order specified by the enrichment data matrix. Subsequently, the assemblies of the the stiffness matrix and the generalised force vector are possible (3.59)-(3.63), which can be carried out as in the classic finite element method.

4.4.2 Updated assembly

Updating of tip enrichment is relatively simple. All the data structures associated with the old tip enrichment can be annihilated. The new tip enrichment is introduce at the updated crack tip position. On the other hand, the Heaviside enrichment needs to be updated consistently with the old enrichment. In the simplest case, the new Heaviside enrichment along the crack extension is connected to the old Heaviside enrichment along the remainder of the crack by assigning the same enriched nodes at the interface between the old and the new Heaviside enrichments. In rare cases, the crack tip extension may cut an element that is already cut by the same crack. In this event, the additional task in the enrichment updating procedure is to recompute the cut element's enrichment contribution to the global system of equations. This is done by first subtracting the old enriched parts of the elemental equations and then, based on the updated crack geometry, adding the new enriched parts to the global system of equations. If one crack intersects another crack, the intersected element's equations that need to be added to the global system of equations consist not only of the enriched parts due to the new enrichment but also include the interactive terms between the new enrichment and all old enrichments. In general, when a new enrichment needs to be introduced to an element that already contains other enrichments, the new interactive terms between the new enrichment and all other enrichments can be cumbersome to compute if there are many of them. Therefore, our approach is to recompute all the enriched parts of the elemental equations from scratch. Although this is not the most computationally efficient way of updating the elemental equations (since it involves some unnecessary computations), it is by far the simplest to implement in *Matlab*. Furthermore, matrix and vector operations (i.e. vectorisation) are optimised in *Matlab* [13, 170] whereas loop-based scaler operations are relatively slow.

As the system needs to be updated after each time step, the updating procedure involves the annihilation of the former branch enrichments at the crack tips that have advanced. At the element level, this is carried out by deleting each enriched element's: enriched shape functions, enriched nodes, and the enrichment data vector(s) that are linked to the former branch enrichments. On the global level, the degrees of freedom corresponding to

the former branch enrichments are deleted from the stiffness matrix and the force vector. Upon the contraction of the elements' enrichments and the system of equations, gaps in the numbering of the enriched nodes, which are typically tied to the enriched degrees of freedom, are left behind. The practical difficulties of having to reorder the enriched nodes consistently with the enriched DOF's can be avoided by simply pointing the current enriched nodes to consistently ordered enriched DOF's as they are simpler to update.

In the enrichment updating stage, the new enriched elements are identified based on the updated fracture geometry. For each new enrichment, the enriched elements' topology is constructed from a reference topology concerning the patch of elements a particular enrichment is for. For each element in the enriched patch, the vector of enriched nodes for the specific enrichment is added to the element's vector of all enriched nodes and the element's enrichment data matrix is updated to include the new enrichment's data vector, which consists of: the crack number, the enrichment identification and the preferred quadrature scheme for the enriched element. With regard to the Heaviside enrichment, the new enriched elements' topology must be compatibly joined with the existing enriched elements' topology. This can be done by replacing the new enriched nodes with the old enriched nodes at the interface between the two Heaviside-enriched element topologies.

If a new enrichment is introduced to an element and the element already contains other enrichments, the enriched parts of the elemental equations are re-computed from scratch in the current implementation. This is done for the sake of simplicity as it helps to avoid the explicit computations of the new interactive terms between the enriched shape functions that appear in the element stiffness matrix as well as their addition to the global system. Following this course, the old enriched parts of the elemental equations will first need to be subtracted from the global system of equations before the system can be updated to reflect the updated element's enrichment. If the new enrichment calls for a different quadrature scheme, the quadrature points and weights, and the standard shape functions will be re-evaluated. The element's enriched shapes can then be constructed in the order specified by the element's enrichment data matrix. Finally, the enriched parts of the elemental equations are assembled and added to the global system of equations according to the enriched degrees of freedom of the elements whose enrichments have been updated.

4.4.3 Stiffness derivatives

To compute the fracture energy release rates G_θ and H_θ (refer to (3.77) and (3.79) respectively) essentially requires to perform geometrical differentiation of the global stiffness matrix K_g and the force vector f_g with respect to the angular position of the crack tip segment. The variations in K_g and f_g are assumed to come about as the result of the virtual perturbation of the mesh in the vicinity of the crack tip – analogous in principle to the method proposed in [168, 228]. The first and second order derivatives of K_g and f_g are determined by assembling the element-level derivatives of K_el and f_el of those elements affected by the virtual perturbation of the crack tip domain. Figure 4.3 illustrates a typical instance of a finite length crack extension undergoing a clockwise rotation that, in turn, subjects a patch of elements in the crack tip vicinity to rigid rotations/translations and shape distortions. To carry out the geometrical differentiation of the elements due to the rotation of the crack tip segment, it is useful to first separate the elements into those that experience a rigid rotation/translation and into those that experience shape distortion. For these two groups of elements, the derivatives will be computed using different techniques.

For the elements in rigid rotation, the derivatives of K_el (refer to (3.85) and (3.86)) only involve the differentiation of the B-matrix, which can be carried out relatively inexpensively by exploiting the fact that the element is in rigid rotation; hence, the first and second derivatives are obtained as follows: $\delta\mathbf{B}_I = \mathbf{B}_I\delta\mathbf{T}'|_{\theta=0}$, and $\delta^2\mathbf{B}_I = \mathbf{B}_I\delta^2\mathbf{T}'|_{\theta=0}$, where $\mathbf{T}'(\theta) = \left[\begin{smallmatrix}\cos\theta & \sin\theta \\ -\sin\theta & \cos\theta\end{smallmatrix}\right]$ is the global-to-local axis transformation matrix. The derivatives of $\mathbf{T}'(\theta)$ are: $\delta\mathbf{T}' = \left[\begin{smallmatrix}0 & 1 \\ -1 & 0\end{smallmatrix}\right]$ and $\delta^2\mathbf{T}' = \left[\begin{smallmatrix}-1 & 0 \\ 0 & -1\end{smallmatrix}\right]$. An analogous procedure applies to the differentiation of the force vector f_el (refer to (3.89) and (3.90)). In this case, the derivatives of the N-matrix read: $\delta\mathbf{N}_I = \mathbf{N}_I\delta\mathbf{T}'|_{\theta=0}$, and $\delta^2\mathbf{N}_I = \mathbf{N}_I\delta^2\mathbf{T}'|_{\theta=0}$. On the other hand, to compute the geometrical derivatives of the elements subjected to shape distortion, full algebraic differentiation is required. The steps for computing the derivatives of B,N-matrices (and of other relevant terms) were delineated in Section 3.6.2. In contrast to the differentiation of elements in pure rotation, which effectively involve rearrangements of rows and columns of K_el and f_el, algebraic differentiation is considerably more intricate.

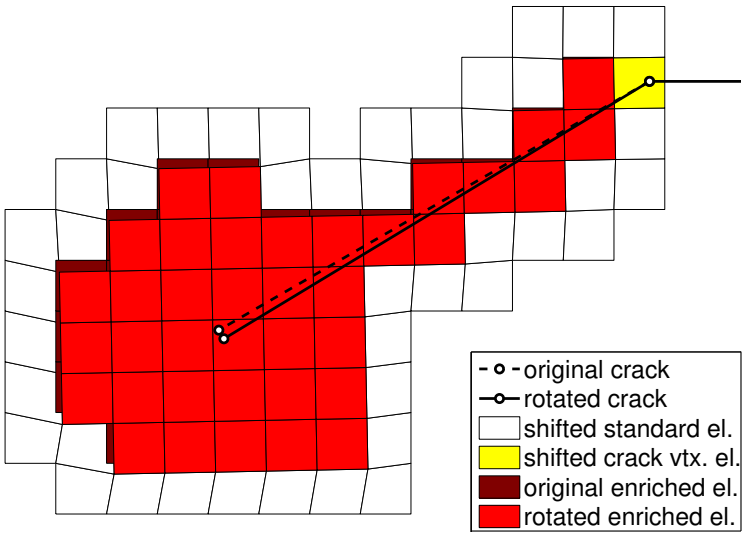

FIGURE 4.3: Virtual perturbation of the mesh in the crack tip vicinity for computing the derivatives of the stiffness matrix and the force vector. The enriched elements (in red) translate coherently with the rotation of the crack tip segment; as such, they experience no change in shape but only a rigid rotation. The ring of unenriched elements (in white), which surrounds the patch of enriched elements, has its outer boundary fixed to the rest of the mesh whereas its inner boundary conformally follows the patch of enriched elements; as such, the surrounding elements experience shape distortion.

Since branch-enriched elements typically contain sever times the number the number of Gauss points than the unenriched elements (to achieve accurate integration), it is computationally expedient to avoid having to do many matrix operations on enriched elements. Besides the high number of Gauss points, the dimension of K_{el} and f_{el} of a branch-enriched element is four times greater than that of an unenriched element; if the element is also enriched with the Heaviside function, then the dimension is five times greater. Consequently, it is practical to assume that the entire patch of branch-enriched elements and the Heaviside-enriched elements (that are entirely cut by the crack tip segment) are subjected to a pure rotation, whereas the surrounding unenriched elements and the Heaviside-enriched crack-kink element are assumed to undergo shape distortion. This separation of enriched and unenriched elements into elements subjected to pure rotation and to shape distortion respectively lends itself to the efficient application of the two geometrical differentiation approaches that have been proposed. The only enriched element that requires algebraic differentiation is the crack vertex element that contains only the Heaviside enrichment. Refer to Figure 4.3 to see how the elements are selected.

Within the XFEM framework, the proposed geometrical differentiation approach seems to be the simplest one to use to compute the derivatives of K_{g} and f_{g} with respect to the virtual rotation of the crack tip branch. Although geometrical differentiation of the enriched elements is technically doable, it is not clear how this would add any benefit or be more practical (given the higher computational effort) than the proposed approach.

The stiffness derivative method provides a general framework for computing the energy release rates with respect to the position of a crack branch. The method in itself is not limited to a particular crack representation, such as a straight crack branch. In fact, it is possible to consider higher order representations of cracks, e.g. by using a spline for the crack branch. It is only required that the parametrisation of the crack branch be functionally related to K_{g} and f_{g} so that differentiation with respect to the parameters makes sense. Within the XFEM framework, this could be accomplished by appropriately enriching the finite element basis to represent an arbitrary crack configuration. This step would likely involve the mapping of the branch functions along a curving crack via the help of a curvilinear coordinate system. The derivatives of K_{g} and f_{g} could then be computed algebraically by considering the derivatives of the enrichment functions [286].

However, there can be difficulties in using the stiffness derivative approach to finding the stationary (minimum) energy of the system per unit fracture advance if the crack is parametrised by many variables (e.g. the incipient crack kink angle, the curvature of the crack branch, etc.) since the energy function may be poly-convex. Consequently, it can prove numerically difficult to find the globally optimal crack branch solution by applying the stationary principal. To this end, a robust solver would be required. In comparison to the multivariate parametrisation of a crack branch, the single variable approach that considers only the angle of the crack extension usually leads to a convex energy function.

By virtue of the versatility of the stiffness derivative method, fracture problems can also be solved in anisotropic and functionally graded materials, where the material properties vary (smoothly) with direction and position, respectively. In this context, spatial differentiation of the constitutive matrix would be required for all elements subjected to the virtual change in position. However, concerning the elements in pure rotation and the case of

an anisotropic material, either the full algebraic differentiation of the element should be used (as with unenriched elements) or the current rotation-based approach, but with a correction. The correction is required due to the whole rotation of an element since the anisotropic material directions are then rotated implicitly. Therefore, to restore the original orientation of the material, the constitutive matrix would need to be counter rotated.

4.4.4 Numerical integration

Each type of an enriched element requires an *ad hoc* quadrature schemes in order to perform adequate integration of the elemental equations [31, 204, 283]. For example, integration over sub-domains is used if the element is cut by a crack. If the element contains a crack tip, an integration scheme that is better suited for the singular integrands is used [158], such as: *polar* [158], *almost-polar* [71] or the *parabolic* [191] integration scheme. Below is a summery of the quadrature schemes used for the different finite element types:

- Linear triangle (**T3**)
  - crack tip polar integration (branch enrichment): $n_r = 16$, $n_\theta = 8$
  - non-split elements (branch enrichment): $n_{\text{gp}} = 19$
  - split elements (branch enrichment, sub-cells): $n_{\text{gp}} = 19$
  - split elements (Heaviside enrichment, sub-cells): $n_{\text{gp}} = 1$
- Bi-linear quadrilateral (**Q4**)
  - crack tip polar integration (branch enrichment): $n_r = 16$, $n_\theta = 8$
  - non-split elements (branch enrichment): $n_{\text{gp}} = 25$
  - split elements (branch enrichment, sub-cells): $n_{\text{gp}} = 19$
  - split elements (Heaviside enrichment, sub-cells): $n_{\text{gp}} = 3$

Concerning the elements with (non-polynomial) branch enrichment, the chosen quadrature rules seemed to give a good balance between the computational time and accuracy. For instance, increasing the number of quadrature points did not produce significant changes in the strain energy for the discretisations used in the numerical benchmarks. Note that, the same quadrature rule is applied to both the branch-enriched *standard* and *blending* elements (see Figure 4.2). For elements with multiple overlapping enrichments, a

single quadrature scheme is used for computing all the enriched parts of the elemental equations. The scheme is selected based on the most demanding enrichment function or the element type. The quadrature schemes are summarised in the order of presidents:

1. crack tip element with branch enrichment
2. split elements with branch enrichment
3. non-split elements with branch enrichment
4. split-elements with Heaviside enrichment

The enrichment data matrix of each enriched element states which type of a quadrature scheme is preferred for a particular enrichment layer. Among multiple such preferences, the critical scheme is selected based on the hierarchy of the element types listed above.

4.5 Numerical benchmarks

The numerical benchmarks have two aims: (1) to verify the implementation of the proposed enrichment updating strategy (so-called *efficient updating*) and (2) to assess its effectiveness in terms of the computational speed-up relative to the basic enrichment updating approach, which is essentially to reassemble the enrichment from scratch (because it is simpler this way). The efficient enrichment updating strategy involves updating the nodal enrichments and the enriched parts of the stiffness matrix only where it is required (as described in Section 4.4.2), whereas in the basic updating approach the enrichment is "updated" by means of recomputing all nodal enrichments and the entire enriched part of the stiffness matrix from scratch (as described in Section 4.4.1). All benchmark problems assume a rectangular 10×1 plate with a roughly uniform distribution of cracks along its length. The domain is discretised using a uniform grid of bilinear quadrilateral elements. The verification is carried out on 4 meshes: 300×30, 600×60, 900×90 and 1200×120, considering 6 crack distributions: 5, 10, 20, 30, 40 and 50, and a crack length of 0.25 units. In all the test cases, the rectangular plate is subjected to a fixed-grip vertical extension.

4.5.1 Verification of updating

The computer implementations of the efficient enrichment updating strategy was verified by checking that the numerical solutions for the fracture paths were the same as those obtained by recomputing all nodal enrichments and reassembling the enriched part of stiffness matrix and force vector from scratch. Figure 4.4 shows the kind of fracture path solutions that were obtained for the 6 crack distributions that had been generated. Figure 4.5 shows the convergence of the fracture profiles with each mesh refinement for the test case of 50 randomly distributed cracks. The maximum distance $d_{\max}$ between the fracture profiles obtained by the enrichment updating and reassembling schemes is computed by (4.1) and the results for the 26 test cases are presented in Table 4.1.

$$d_{\max} = \frac{1}{L_{\text{domain}}} \sqrt{\max_{j\in\{1,2,\ldots,n_{\text{crk}}\}} \max_{i\in\{1,2,\ldots,n_{\text{vtx}}\}} \left((\Delta x_i^j)^2 + (\Delta y_i^j)^2 \right)} \tag{4.1}$$

TABLE 4.1: Maximum distance $d_{\max}$ between the fracture profiles obtained by the enrichment updating and the enrichment recomputing routines.

mesh size	number of cracks					
	5	10	20	30	40	50
300×30	3.99E-15	1.95E-15	2.13E-15	8.00E-15	2.67E-15	3.74E-15
600×60	9.17E-15	1.31E-14	7.26E-15	2.17E-14	2.15E-14	6.63E-15
900×90	2.85E-14	2.02E-14	1.08E-14	6.75E-14	8.97E-14	4.77E-14
1200×120	1.77E-14	2.37E-14	1.33E-14	8.45E-14	2.54E-13	4.84E-14

The solutions by the two enrichment updating strategies differ on the orders from -13 to -15, which is close to the *double*-precision floating point accuracy of 64bit computing. It can be concluded that the enrichment updating routine has been implemented adequately.

4.5.2 Computational speed-up

The speed-up of the proposed efficient updating strategy is assessed. The total computational time of a simulation is composed of 5 parts, namely: *pre-processing*, *initial assembly*, *updated assembly*, *solution of the linear system* and *post-processing*. The first 2 parts need to be done only once whereas the last 3 parts need to be repeated with each time-step. Hence,

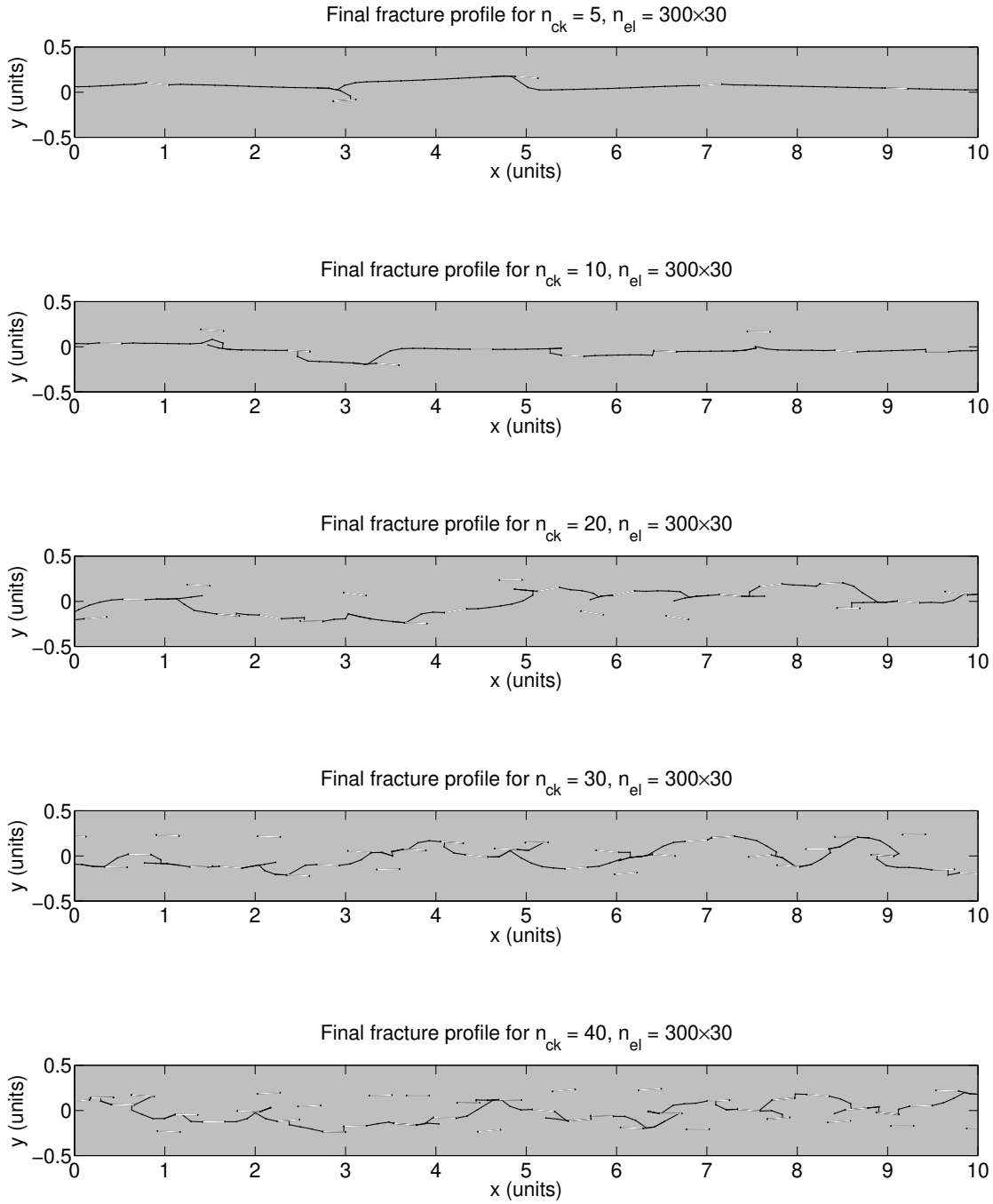

FIGURE 4.4: Fracture profiles for: $n_{\mathrm{crk}} = \{5, 10, 20, 30, 40\}$, $n_{\mathrm{elm}} = 300 \times 30$. The sub-figures show the type of fracture solutions obtained for each crack distribution. The crack extension length is proportional to the mesh size.

for fracture problems involving the growth of many cracks over many times steps, the total computational time will be primarily composed of the solution, post-processing and

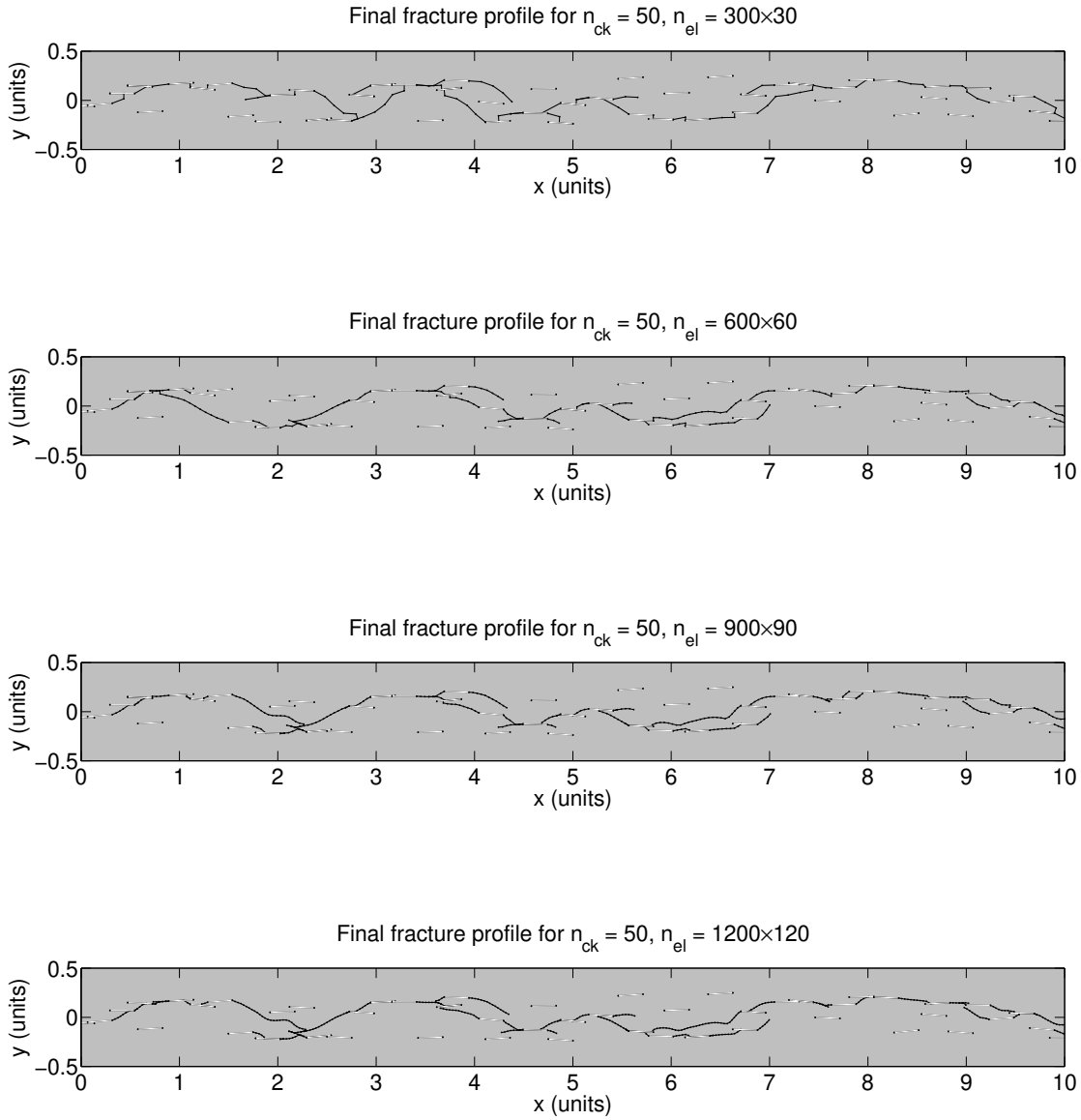

FIGURE 4.5: Illustration of the convergence of the fracture profiles for the case $n_{\mathrm{crk}} = 50$. The crack extension length is proportional to the mesh size.

enrichment updating times. We wish to assess if the relative computational time savings are significant of the proposed enrichment updating strategy relative to the total computational time. Concerning the solution to the linear system of equations, *Matlab*'s built-in direct solver was used since memory was not an issue for the size of the discrete problems that needed to be solved. The particular solver is based on the Cholesky decomposition that is optimised for sparse symmetric positive definite matrices. A pre-conditioner was

not essential because the solution time of a direct solver is little affected by the condition number of the stiffness matrix. On the other hand, a pre-condition would be useful if an iterative linear solver were used instead. Figure 4.6 shows the total computational time spent in updating the discrete system by means of reassembling it relative to the total time of the simulation as a function of the number of cracks. Figure 4.7 gives the corresponding computational time as obtained by the proposed efficient updating strategy. Figure 4.8 shows the speed-up factor of total simulation time as a function of the number of cracks. Figure 4.9 gives the speed-up factor as a function of the number of crack increments.

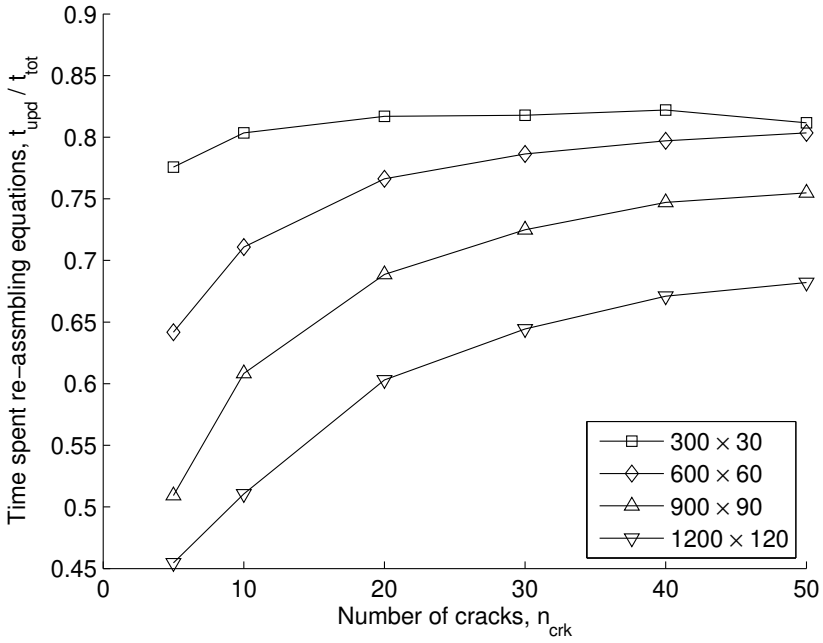

FIGURE 4.6: The relative computational time spent in updating the enrichment by means of reassembly as a function of the number of cracks.

Although the strategy of updating the enrichment from scratch is considerably easier from the point of view of computer implementation, it is found to create a major bottle-neck in the total computational time, especially for problems involving the growth of many cracks over many time steps. The proposed enrichment updating strategy eliminates this bottle-neck such that the largest computational effort is in the solution to the linear system.

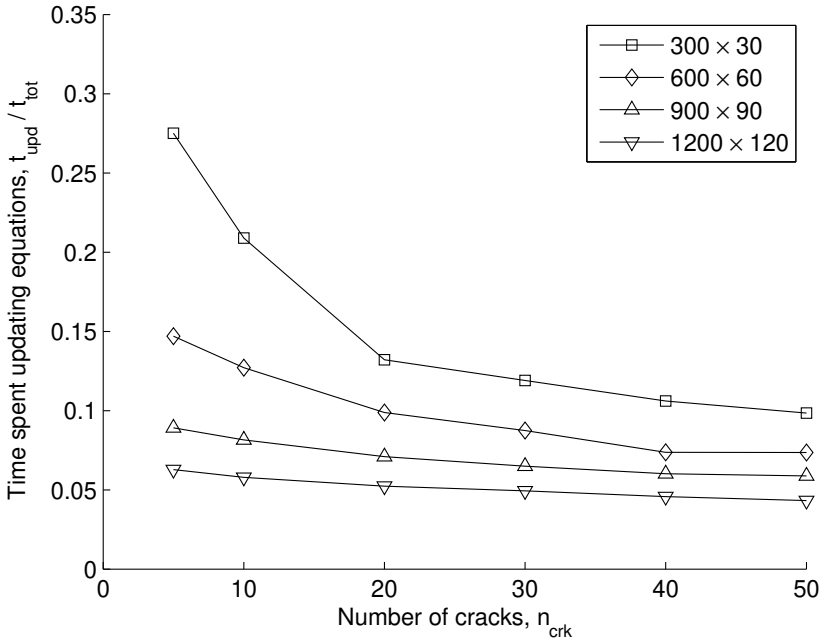

FIGURE 4.7: The relative computational time spent in updating the enrichment by the proposed strategy as a function of the number of cracks.

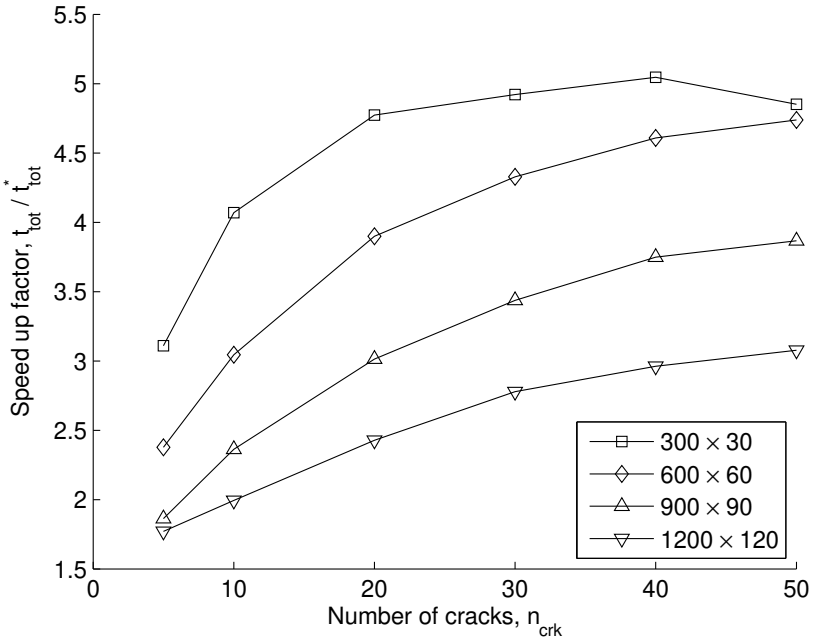

FIGURE 4.8: Speed-up of the efficient enrichment updating strategy. Note that the quantity with superscript "$*$" indicates updating by reassembly.

4.5.3 Remarks on the linear solution

Direct linear solvers are relatively uninfluenced by the condition number of the linear system as the solution is obtained in one large computational step rather than iteratively.

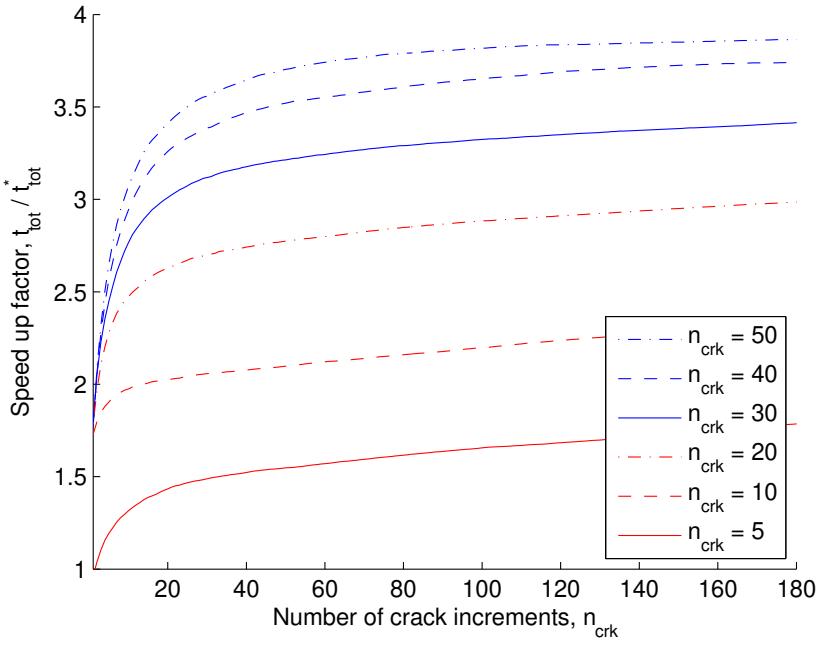

FIGURE 4.9: Speed-up of the efficient enrichment updating strategy. Considering the 1200×120 discretisation. Note that the quantity with superscript "$*$" indicates enrichment updating by means of reassembly of enrichment.

What is more important for a direct solver is the structure of the linear system and that there is sufficient computing memory available. Generally speaking, direct solvers are superior in terms of speed, accuracy and robustness in solving smaller size systems. For large size problems (e.g. silicon wafer splitting, which is the topic of Chapter 6) where memory is likely to be an issue, a direct linear solver may no longer be a viable option. Thus, an iterative solver is preferred because of better memory management. However, the success of the solver in terms of solution time accuracy and robustness depends on how well-conditioned the linear system is. In other words, if the system is ill-conditioned, the direct application of an off-the-shelf iterative solver (e.g. congregate gradient (CG [119]), generalise minimum residual (GMRES) [252] or bi-conjugate gradient stabilised (BiCGStab) [285]) will either lead to slow convergence or to no convergence at all. Unfortunately, XFEM enrichment functions are well-known to lead to a severely ill-conditioned system [24, 91, 158]. For instance, using any of the aforementioned iterative solvers without any preconditioning of the linear system leads to significantly slower solution times than using *Matlab*'s default direct solver. The high condition number arises due to the small support of the enriched degrees of freedom, e.g. if a crack cuts an element very close to a node

or an element edge [24, 38, 62]. Also, the tip enrichment functions are almost linearly dependent with the standard finite element basis such that using geometrical enrichment and *h*-refinement, the condition number tends to increase rapidly [24, 158, 279].

The condition number of the resulting linear system can be improved in two ways. The first way is to improve it on the discretisation level. To this end, the enrichment strategy is tuned to get desirable properties of the stiffness matrix, such as a lower condition number. This includes the so-called stabilised GFEM/XFEM that incorporates the enrichment functions in a special way that make them (almost) orthogonal to the standard FE basis [111]. A simple and efficient preconditioning for the Heaviside enrichment has been proposed by [160], which removes the Heaviside DOF's of those nodes that are barely cut by a crack. Another approach is to apply an eigenvalue decomposition of the enriched element's stiffness matrix and to filter out numerically-zero eigen-modes [173]. Finally, the condition number can be improved by increasing the order of the quadrature used for tip enrichment [24, 158]. Geometrical enrichment with degrees-of-freedom gathering (i.e. assigning the same DOF to all DOF's in an enriched patch) is also effective [158].

The high condition number of the resulting linear system can be mitigated on the solution-level by using a suitable preconditioner. A simple preconditioner based on the local (nodal) Cholesky decomposition has been proposed by [24]. Similarly, a mixed domain decomposition method, such as the local/global model order reduction technique [151, 152] can be used to solve the cracked part of the structure and the rest of the domain separately. Other robust preconditioners based on adaptive domain decomposition approaches have been proposed by [35, 181, 287] that especially lend themselves to parallel computations. Multi-grid preconditioners for iterative linear solvers are used successfully also [35, 217].

Finally, in solving fracture growth problems that involve many time steps, it is computational advantageous to reuse the converged displacement solution from the previous time-step as an initial (trial) solution at the current time-step and, in so doing, speed-up the converge of the iterative solver. This makes sense because with each time-step only minor changes in the discretisation take place such that the solution from the previous time-step is usually a good approximation of the solution at the current time-step.

4.6 Summary

The aim of this section was to show the implementation of XFEM in *Matlab* with particular emphasis on the design of the code in order to enable fast and efficient modelling of fracture problems involving multiple crack growth with intersections. The key features of the computer implementation are: elements with multiple layers of enrichments and the efficient updating of the enriched parts of the stiffness matrix and the force vector during crack propagation. The main limitation of the current implementation is that crack growth is not entirely mesh independent; the crack extension length needs to be at least as big as the tip enrichment radius, which is in turn proportional to the local mesh size. The main reasons for this discretisation choice is that the extra complication of mapping branch enrichment function along a curved or a kinked crack geometry can be avoided.

The main outcomes of this chapter are as follows. It has been shown via multiple benchmarks that the efficient enrichment updating strategy has been implemented correctly since the fracture solutions coincided within machine precision with the those obtained by reassembling the entire enrichment from scratch at each time increment. With regard to the computational time, it has been shown that prior to the implementation of the efficient enrichment updating strategy, the reassembling of enrichment was the main bottle-neck, taking up to 80% of the total computational time, e.g. Figure 4.6. On the other hand, the efficient updating scheme allowed the solution to achieve significant faster times, e.g. Figure 4.7. For the benchmark problems studies the total computational time was at least a few times smaller than that obtained without efficient updating, e.g. Figure 4.9.

Chapter 5

Verification

5.1 Introduction

The rotational energy release rates need to be sufficiently accurate as they are key quantities used to find the minimum energy state of the fracture extension direction. This chapter gives a verification of the proposed algebraic differentiation of the potential energy for the determination of the rotational energy release rates. In addition, the chapter provides a comparison of the fracture path solutions obtained by the energy minimisation approach and the maximum stress criterion. Some insights are provided into two possible formulations of the crack growth criteria within the discrete framework; these are the so-called explicit-in-time and the implicit-in-time formulations. The explicit-in-time form considers the crack tip field and the stress intensity factors at the tip of an infinitesimal branch for the prediction of the incipient crack growth direction. The implicit-in-time formulation considers the application of the governing crack growth principal in the post-incremented crack configuration. It is concluded that the implicit-in-time formulation is more robust within the numerical framework. Finally, multiple case studies are carried out comparing the fracture paths by different criteria. Even though different criteria yield different crack growth directions, the final fracture paths obtained by the stress criterion and the energy minimistation method are found to be very similar on the material length scale such that, for practical purposes, the fracture solutions can be considered the same. This is attribute to the preference of the criteria for the mode-I crack growth. It is found that the stress criterion tends to under-estimate the crack deflection angle whereas the energy-based approach tends to overestimate it. A numerical improvement to the crack growth direction is proposed such that the modified solution leads to a more accurate fracture path for a given discretisation. Moreover, the proposed improvement significantly speeds-up the convergence of the fracture path with respect to the refinement of the finite element mesh.

5.2 Rotational energy release rates

The aim of this section is to show that the implementation concerning the computation of the rotational energy release rates: G_θ and $\partial G_\theta / \partial \theta$, is carried out in the framework of

XFEM correctly. The demonstration is given via two numerical case studies of a square plate with an edge crack for different loading conditions, Figure 5.1. In case-1 the plate is subjected to a vertical tension load, whereas in case-2 the load is internal crack pressure.

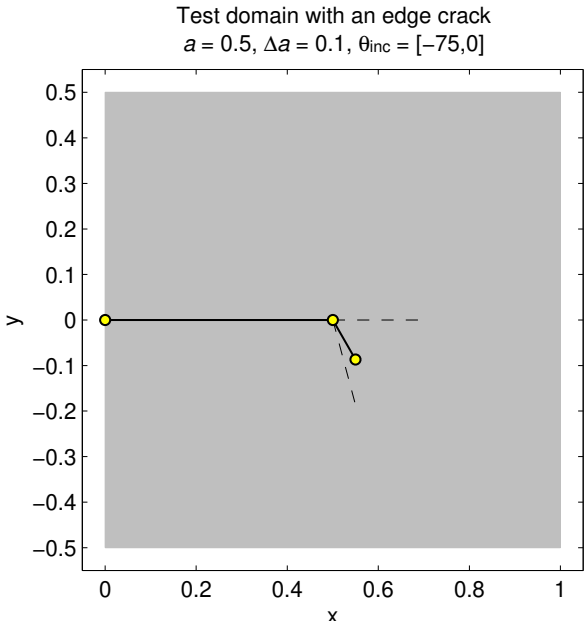

FIGURE 5.1: Test problem for assessing the rotational energy release rates for the crack tip extension Δa at different angles $\theta_{\text{inc}} = \{-75, -74, \ldots, 0\}$.

In each case, the methodology consists of extending the edge crack by Δa over a range of angles $\theta_{\text{inc}} \in [-75, 0]$ (deg.) at one degree increments anti-clock wise. For each instance of $\theta_{\text{inc}} \in \{-75, -74, \ldots, 0\}$, the values of G_θ and $\partial G_\theta / \partial \theta$ are computed in two ways: (1) based on the stiffness derivative approach (herein called as the *analytical* solution), and (2) using numerical central-differencing of the potential energy function (also referred to as the *numerical* solution). The results are recorded for several numerical discretisations of different mesh sizes (in terms of the number of elements) and XFEM enrichment schemes: enrichment of a fixed radius patch (called geometrical enrichment) and enrichment of a fixed number of elements around the crack tip (called topological enrichment). The results for the analytically and numerically determined G_θ and $\partial G_\theta / \partial \theta$ are presented next.

Figure 5.2 shows the rotational energy release rates for different crack tip extension angles as obtained on different mesh sizes and XFEM crack tip enrichment strategies. It is found that the analytically determined G_θ maintains relatively smooth and consistent

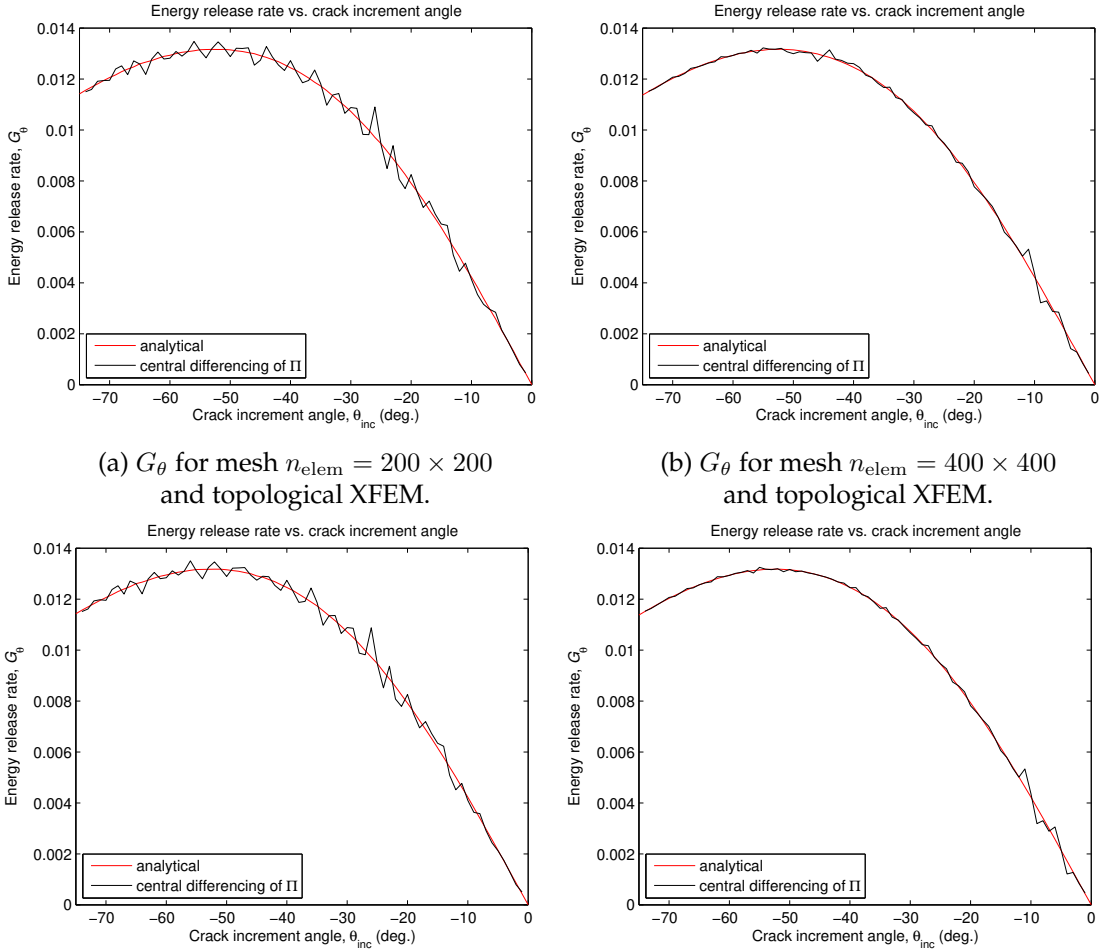

(a) G_θ for mesh $n_{\text{elem}} = 200 \times 200$ and topological XFEM.

(b) G_θ for mesh $n_{\text{elem}} = 400 \times 400$ and topological XFEM.

(c) G_θ for mesh $n_{\text{elem}} = 200 \times 200$ and geometrical XFEM.

(d) G_θ for mesh $n_{\text{elem}} = 400 \times 400$ and geometrical XFEM.

FIGURE 5.2: Comparison of the rotational energy release G_θ as computed analytically and by finite differencing of the potential energy. The test problem is a simply supported square plate with an edge crack that is subjected to vertical tension load. A schematic is given in Figure 5.1.

values as a function of θ_{inc} in comparison to those obtained by finite differencing of the potential energy Π. Both, topological and geometrical variants of XFEM yield almost indistinguishable solutions for G_θ. Figure 5.6 presents the results for the rates of the rotational energy release rates $\mathrm{d}G_\theta/\mathrm{d}\theta$ corresponding to the different discretisations. It is found that with mesh refinement $\mathrm{d}G_\theta/\mathrm{d}\theta$ converges when geometrical enrichment is used and diverges in the case of topological enrichment. Figure 5.4 summarises these findings.

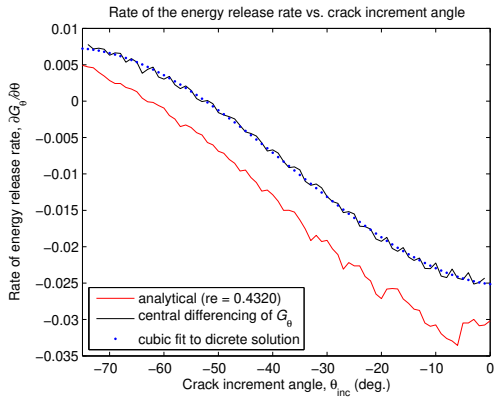

(a) $\mathrm{d}G_\theta/\mathrm{d}\theta$ for mesh $n_{\text{elem}} = 200 \times 200$ and topological XFEM.

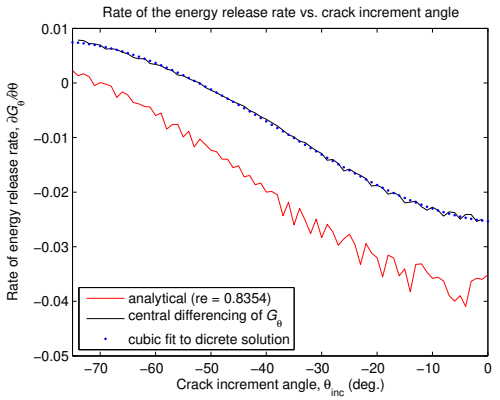

(b) $\mathrm{d}G_\theta/\mathrm{d}\theta$ for mesh $n_{\text{elem}} = 400 \times 400$ and topological XFEM.

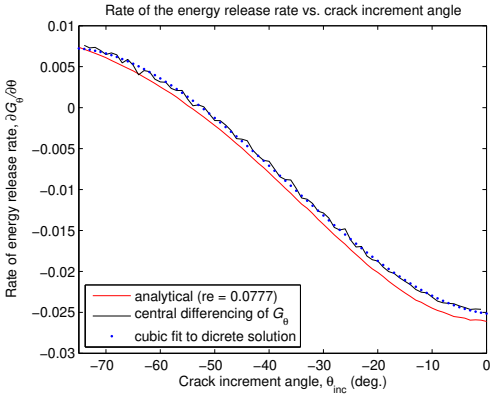

(c) $\mathrm{d}G_\theta/\mathrm{d}\theta$ for mesh $n_{\text{elem}} = 200 \times 200$ and geometrical XFEM.

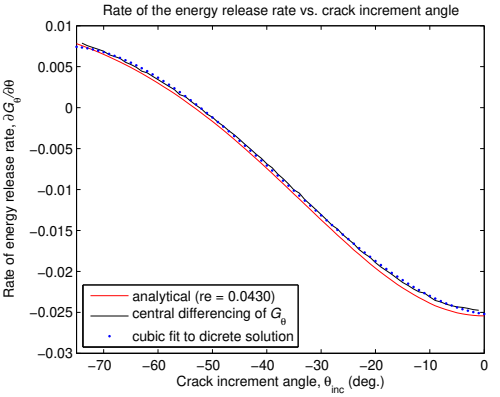

(d) $\mathrm{d}G_\theta/\mathrm{d}\theta$ for mesh $n_{\text{elem}} = 400 \times 400$ and geometrical XFEM.

FIGURE 5.3: Comparison of the rates of rotational energy release $\mathrm{d}G_\theta/\mathrm{d}\theta$ as computed analytically and by finite differencing of the analytical version of G_θ. The test problem is a simply supported square plate with an edge crack that is subjected to vertical tension load. A schematic is given in Figure 5.1.

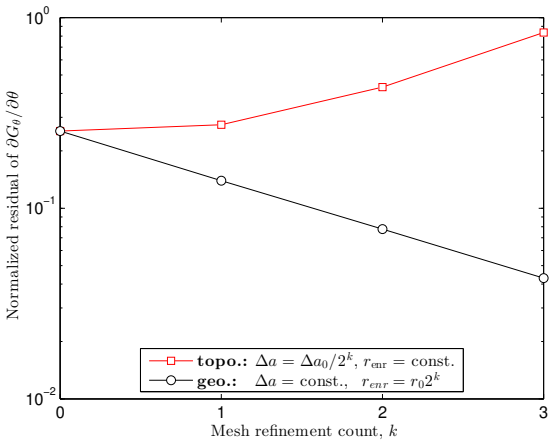

FIGURE 5.4: Discrepancy in $\mathrm{d}G_\theta/\mathrm{d}\theta$ between the analytically computed solution and the best-fit solution to the finite-differencing of the analytical G_θ for geometrical and topological XFEM enrichment schemes.

The case-2 of this numerical study is concerned with the same problem geometry, i.e. an edge crack in a square plate, but assumed different loading conditions. In this case, an internal fracture pressure normal to the fracture surface is prescribed instead of the vertical tension load assumed previously. The results are presented in the same format. Figure 5.5 compares G_θ, Figure 5.6 – $\mathrm{d}G_\theta/\mathrm{d}\theta$, and Figure 5.7 summarises the behaviour of the discrepancy in $\mathrm{d}G_\theta/\mathrm{d}\theta$ between topological and geometrical based XFEM formulations.

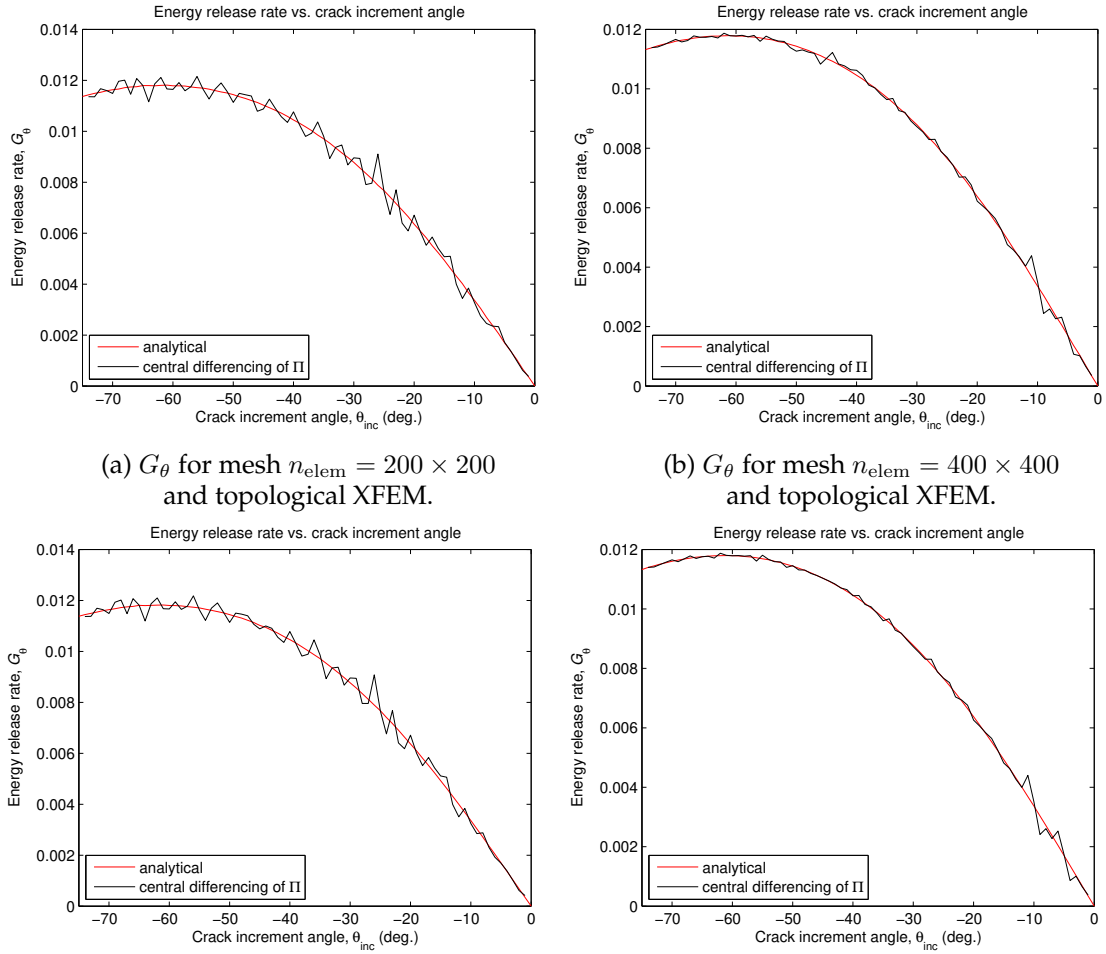

(a) G_θ for mesh $n_{\mathrm{elem}} = 200 \times 200$ and topological XFEM.

(b) G_θ for mesh $n_{\mathrm{elem}} = 400 \times 400$ and topological XFEM.

(c) G_θ for mesh $n_{\mathrm{elem}} = 200 \times 200$ and geometrical XFEM.

(d) G_θ for mesh $n_{\mathrm{elem}} = 400 \times 400$ and geometrical XFEM.

FIGURE 5.5: Comparison of the rotational energy release G_θ as computed analytically and by finite differencing of the potential energy. The test problem is a simply supported square plate with an edge crack that is subjected internal pressure. A schematic is given in Figure 5.1.

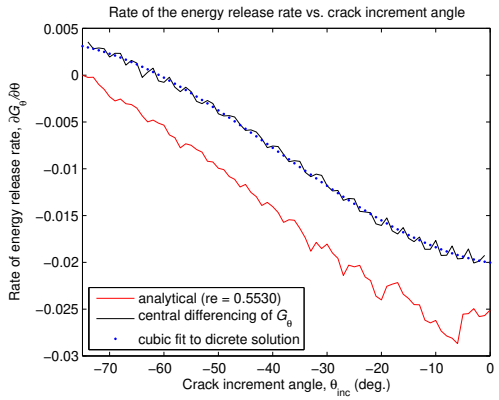

(a) $\mathrm{d}G_\theta/\mathrm{d}\theta$ for mesh $n_{\text{elem}} = 200 \times 200$ and topological XFEM.

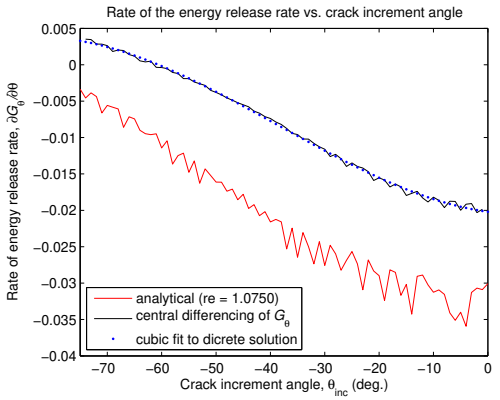

(b) $\mathrm{d}G_\theta/\mathrm{d}\theta$ for mesh $n_{\text{elem}} = 400 \times 400$ and topological XFEM.

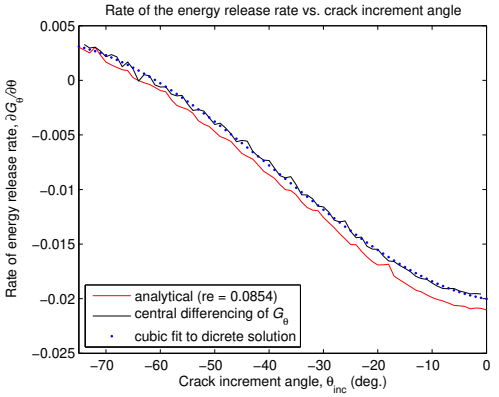

(c) $\mathrm{d}G_\theta/\mathrm{d}\theta$ for mesh $n_{\text{elem}} = 200 \times 200$ and geometrical XFEM.

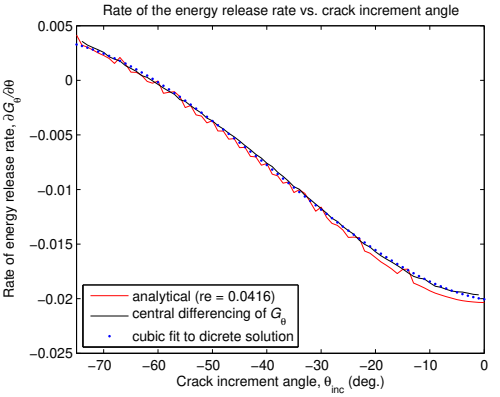

(d) $\mathrm{d}G_\theta/\mathrm{d}\theta$ for mesh $n_{\text{elem}} = 400 \times 400$ and geometrical XFEM.

FIGURE 5.6: Comparison of the rates of rotational energy release $\mathrm{d}G_\theta/\mathrm{d}\theta$ as computed analytically and by finite differencing of the analytical version of G_θ. The test problem is a simply supported square plate with an edge crack that is subjected to internal pressure. A schematic is given in Figure 5.1.

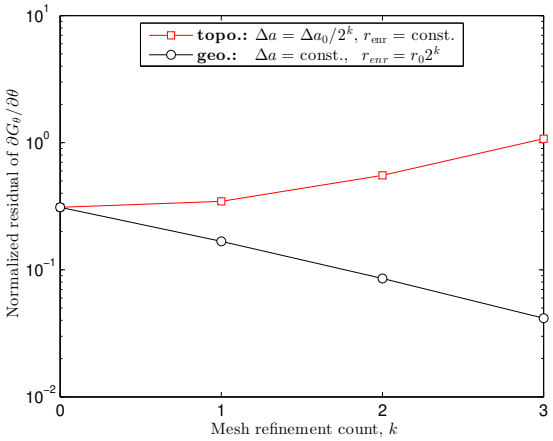

FIGURE 5.7: Discrepancy in $\mathrm{d}G_\theta/\mathrm{d}\theta$ between the analytically computed solution and the best-fit solution to the finite-differencing of the analytical G_θ for geometrical and topological XFEM enrichment schemes.

Thus the analytically computed G_θ has been verified for both external and pressure loading conditions. The numerical results yield accurate solutions for G_θ for different discretisations and XFEM enrichment strategies in comparison to the solutions obtained by finite differencing the potential energy. Regarding $\mathrm{d}G_\theta/\mathrm{d}\theta$, only geometrical enrichment has been shown to lead to consistent and smooth numerical results that matches those obtained by finite differencing of the analytically computed G_θ. The same, however, can not be said with regard to the analytically obtained solution for $\mathrm{d}G_\theta/\mathrm{d}\theta$ based on the topological enrichment strategy. The analytical solution for $\mathrm{d}G_\theta/\mathrm{d}\theta$ diverges with mesh refinement from that obtained by finite differencing of the analytical G_θ. Although the solution for $\mathrm{d}G_\theta/\mathrm{d}\theta$ (as obtained by topological XFEM) is rough, it is not useless. Specifically, it can be used as an approximation of the gradient of G_θ in the Newton iterations for determining the crack tip kink angles, e.g. $\boldsymbol{\theta}_{\mathrm{new}} = \boldsymbol{\theta}_{\mathrm{old}} - \mathbf{H}_\theta^{-1}\mathbf{G}_\theta$.

5.3 Comparison of growth criteria

The purpose of the following numerical test cases is to compare the minimum energy and the maximum hoop-stress crack propagation laws in terms of the directions of incipient crack growth and the energy release rates corresponding to different modes of loading. The same problem geometry is considered as before (Figure 5.1). It is confirmed that the energy-based solution leads to a greater mean energy release rate over a finite length crack extension than the stress-based solution; however, the differences reduce to several percent for smaller crack tip extensions (i.e. finer discretisations) but only up to crack tip kink angles of 70°. For kink angles larger than 70°, as determined by the energy-based criterion, the fracture increment solution significantly exceeds the mean energy release rate of the stress-based solution, which is due to its theoretical upper limit of 70.53°. Upon comparison of the crack tip kink angles for different modes of loading, it is found that the numerical solutions do not converge to the same solution. In general, the discrepancy between the kink angles becomes larger with more significant mode-II loading. The largest discrepancies are in the range of 5-10° for crack tip kink angles of up to 70°, but the differences exceed 20° for kink angles large than 70°. The results of the individual test cases are provided by Figures 5.8, 5.9 and 5.10.

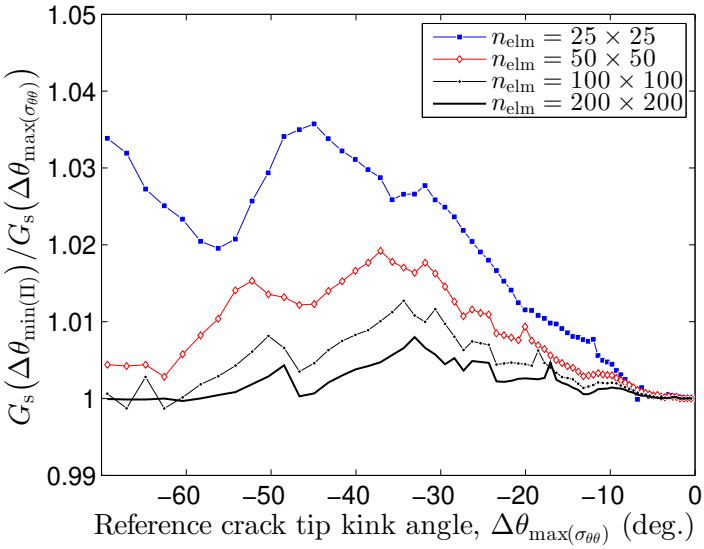

(a) Comparison of mean energy release rates

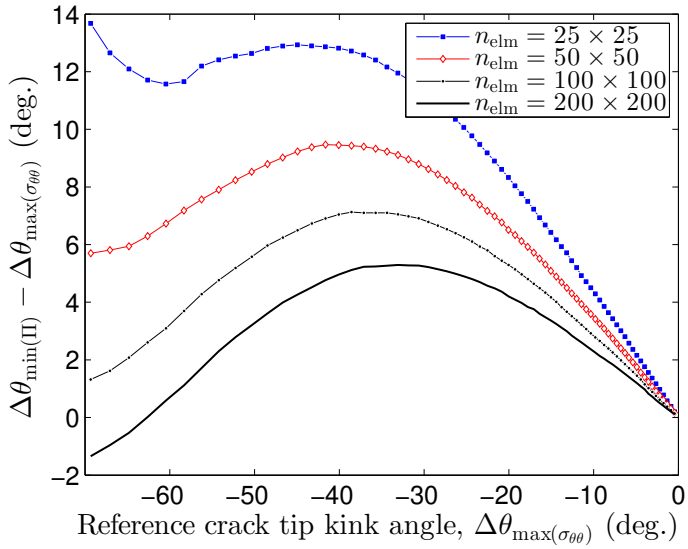

(b) Difference in the crack tip kink angles

FIGURE 5.8: Test case #1. A square plate with an edge crack that is subjected to mixed mode loading by prescribed displacement boundary conditions on the top and bottom edges of the plate such that they induce simultaneous opening (mode-I) and sliding (mode-II) deformations at the tip of the initial crack. Sub-figure 5.8a shows the ratio of the average energy release rates of the solutions obtained using the minimum energy criterion to the solutions determined by the hoop-stress criterion. The average energy release rates are computed by differencing the potential energy between the incremented and the pre-incremented fracture configurations. Sub-figure 5.8b shows the differences in the crack tip kink angles between the two criteria for different mixed-mode loading conditions. The mode-mixity is expressed in terms of the crack tip kink angle that is found by using the stress-based criterion.

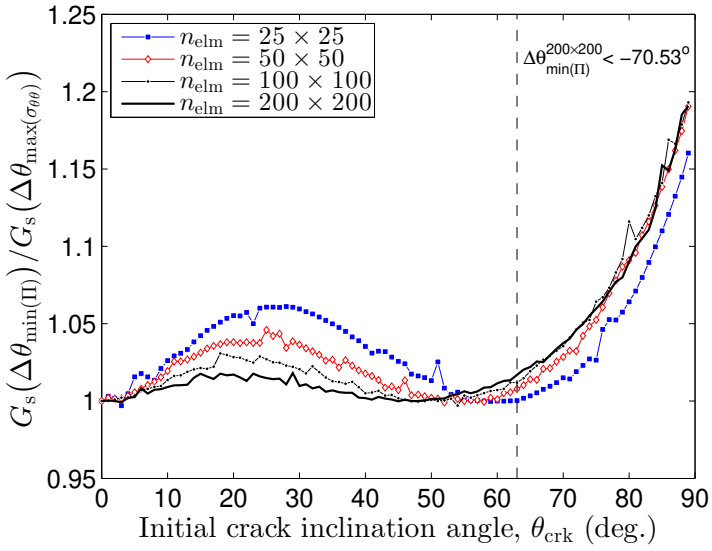

(a) Comparison of mean energy release rates

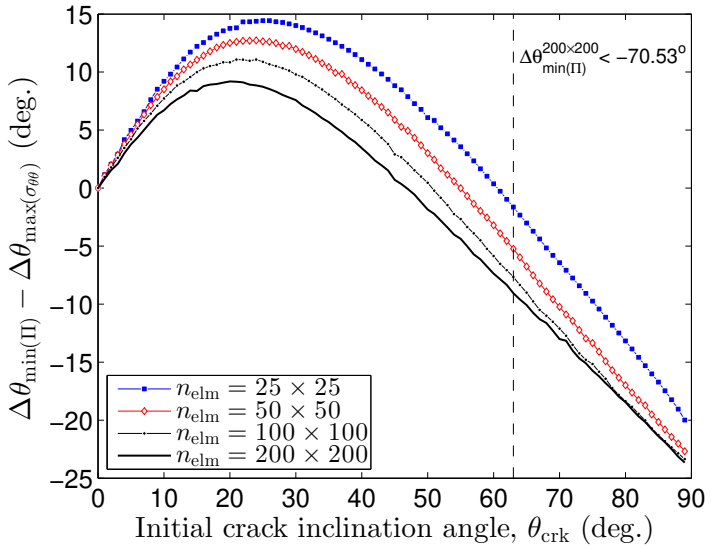

(b) Difference in the crack tip kink angles

FIGURE 5.9: Test case #2. A simply supported square plate with an inclined center crack subjected to a uniform vertical tension. Depending on the crack orientation, the uni-axial tension of the plate induces a mixed-mode loading condition at the tip of the initial crack. The mode mixity can range for pure mode-I (for a horizontal crack) to predominantly mode-II (for a near-vertical crack). The crack orientations considered range from 0 to 89 degrees (at one degree increments). Sub-figure 5.9a shows the ratio of the average energy release rates between the two criteria for a given crack orientation $\theta_{\text{crk}} \in \{0, 2, \ldots, 89\}$. It is found that for large crack inclinations $\theta_{\text{crk}} > 63^{\circ}$ (i.e. significant mode-II loading) the minimum energy based criterion converges to a crack tip kink direction that exceeds the theoretical limit of the stress-based solution $|\Delta\theta_{\max(\sigma_{\theta\theta})}| < 70.53^{\circ}$. Sub-figure 5.9b shows the differences in the crack tip kink angles between the two criteria.

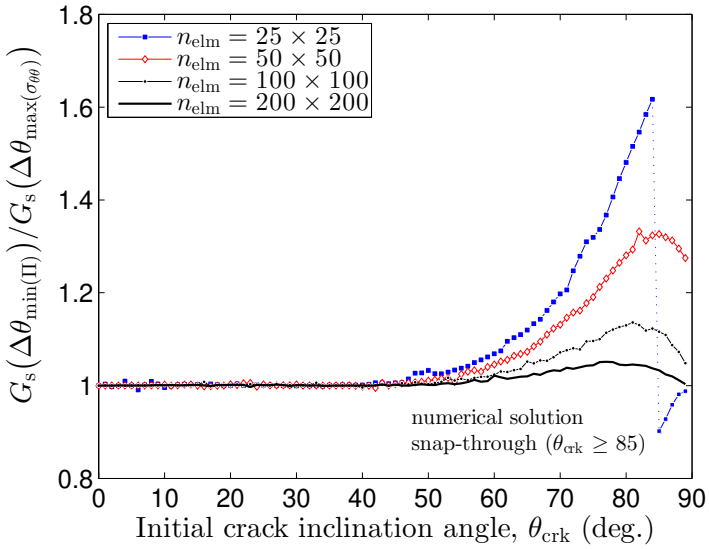

(a) Comparison of mean energy release rates (iterative solution snap-through for $\theta_{\text{crk}} \geq 85$)

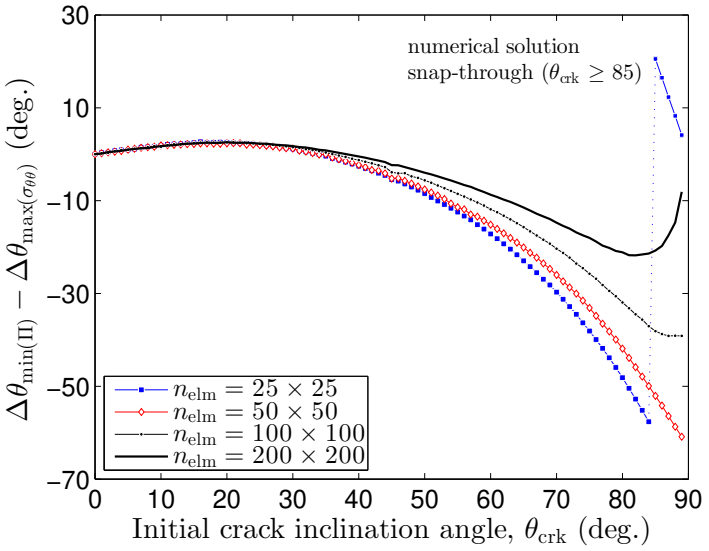

(b) Difference in the crack tip kink angles

FIGURE 5.10: Test case #3. A simply supported square plate with an inclined center crack subjected to a uniform vertical tension load and an internal crack surface pressure. The remote traction is assumed to be equal in magnitude to the internal pressure. Depending on the crack orientation, the uni-axial tension induces a mixed-mode loading condition at the tip of the initial crack. It is found that for the coarsest discretisation the iterative solution method used to find the energy minimising crack tip kink angle happens to converge to a sub-optimal solution when the crack orientation is close to vertical (i.e. $\theta_{\text{crk}} \geq 85$); however, for finer discretisations, the energy minimising solution can be found using the same solution procedure.

5.4 Convergence of fracture paths

As the maximum hoop stress criterion (1.17) is one of the most commonly used criterion in LEFM, it is of practical interest to compare the fracture paths obtained by this criterion with those determined by the global energy minimisation approach (Section 3.3.3). The numerical results for the fracture solutions are shown to be converging with mesh refinement towards what appears to be the same solution (at least when compared on the length-scale of the structure). The is obtained despite the fact that locally at the crack tip the crack kink solutions generally differ under mixed-mode loading conditions (Figure 1.2). The fracture solutions are observed to be converging towards one another as a consequence of the criteria's preference for the mode-I fracture paths (Section 1.8). This result is demonstrated in the following two subsections by the solution of a few benchmark problems considering multiple crack growth subject to remote and internal crack pressure loading conditions.

5.4.1 Square plate with 10 random cracks

The problem of multiple crack growth is considered by using different crack growth direction criteria, namely: the maximum hoop stress criterion and the energy minimisation approach. The test case is a square plate with 10 randomly distributed cracks (the crack distribution is used from [50]). Fracture evolution is computed for two types of boundary conditions. In the first example, the plate is subjected to a bi-axial extension. In the second example, pressure driven crack growth is considered. In both cases, all cracks are allowed to grow at the same rate. The fracture paths for the bi-axially loaded plate is shown in Figure 5.11. The corresponding convergence rate of the fracture paths towards one another, in terms of the L_2-norm of the absolute distance between the crack surfaces, is plotted in Figure 5.13. Similarly, the fracture paths for the pressure-load case are given in Figure 5.12; the convergence rate is plotted in Figure 5.14. It is found that the fracture paths obtained by different criteria convergence towards the same solutions with progressive refinement of the discretisation. In the bi-axially loaded plate, the average rate of convergence (on a log-log scale) is 0.73, whereas in the pressure-load case it is found to be 0.99.

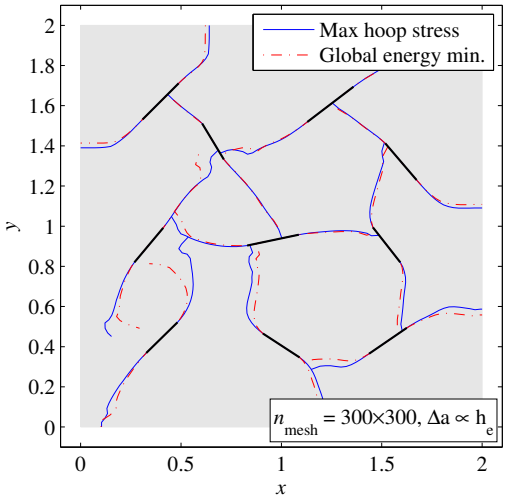

(a) Q4 mesh 300×300.

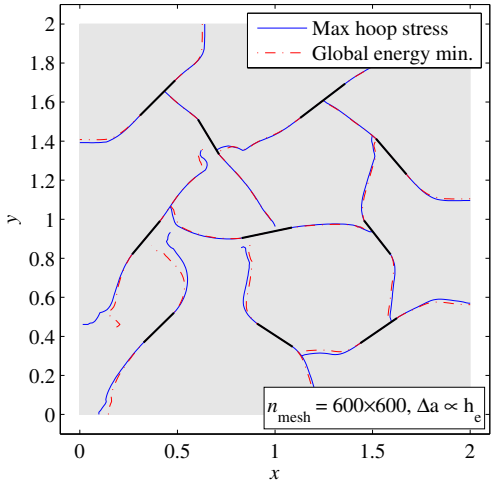

(b) Q4 mesh 600×600.

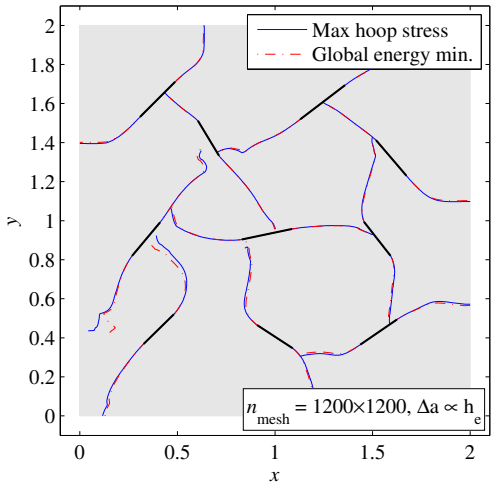

(c) Q4 mesh 1200×1200.

FIGURE 5.11: Comparison of fracture paths as obtained by the hoop-stress and the energy minimisation criteria. The square plate is subjected to a bi-axial extension. All cracks are allowed to grow at the same rate.

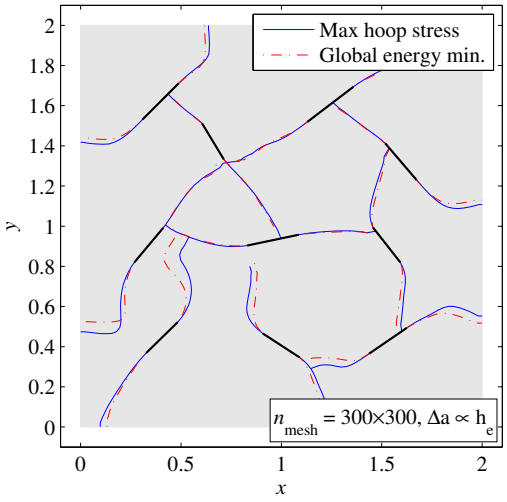

(a) Q4 mesh 300×300.

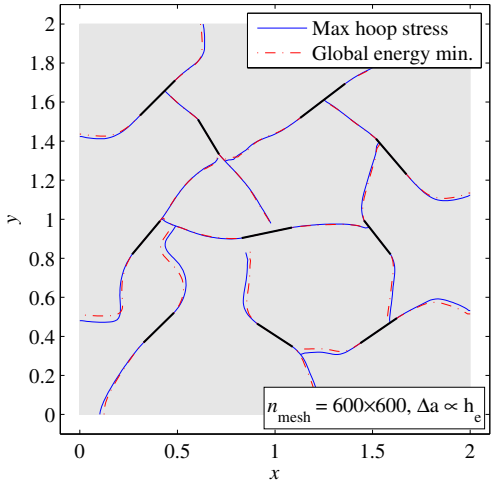

(b) Q4 mesh 600×600.

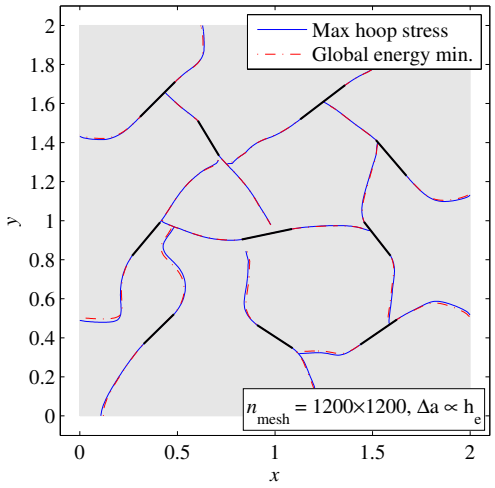

(c) Q4 mesh 1200×1200.

FIGURE 5.12: Comparison of fracture paths as obtained by the hoop-stress and the energy minimisation criteria. The cracks are subjected to a uniform pressure load. All cracks are allowed to grow at the same rate.

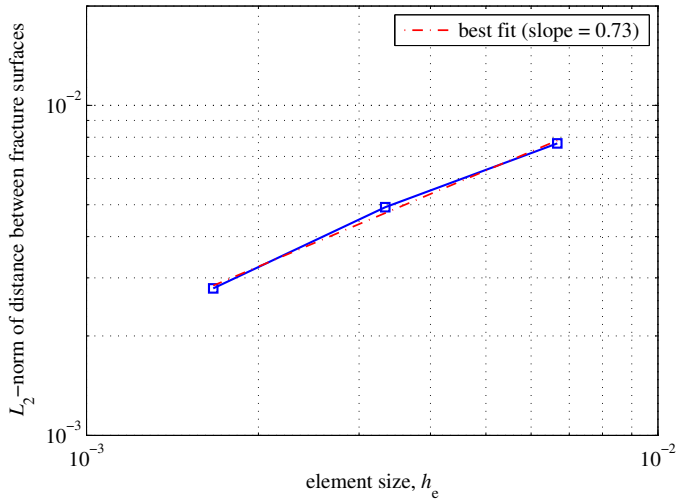

FIGURE 5.13: Convergence to same fracture path by hoop-stress and energy minimisation criteria. The test problem is a square plate with 10 randomly distributed cracks. The plate is subjected to a bi-axial extension. All cracks are allowed to grow at the same rate.

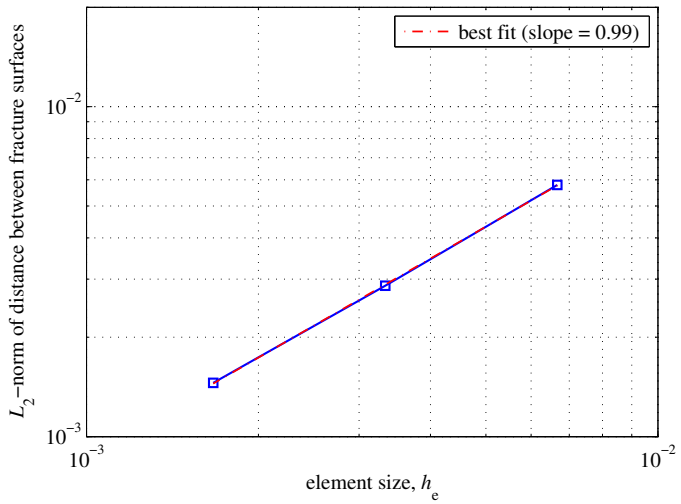

FIGURE 5.14: Convergence to same fracture path by hoop-stress and energy minimisation criteria. The test problem is a square plate with 10 randomly distributed cracks. The plate is subjected to a bi-axial extension. All cracks are allowed to grow at the same rate.

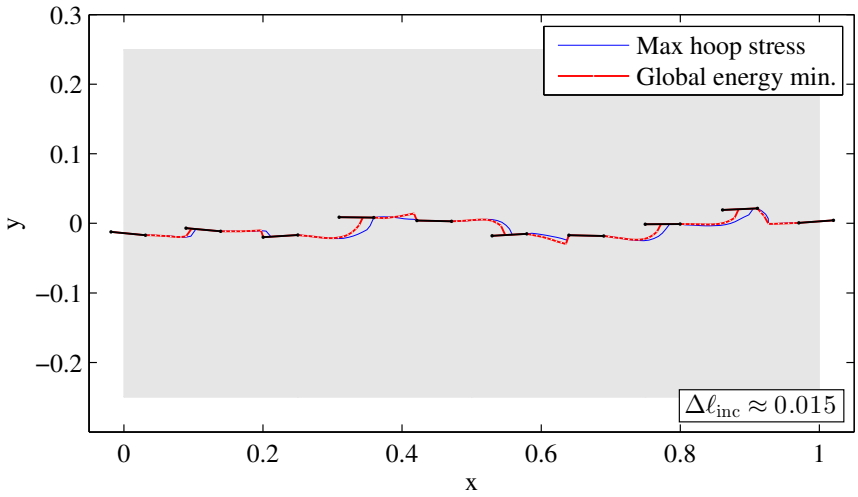

(a) Q4 mesh 100×200.

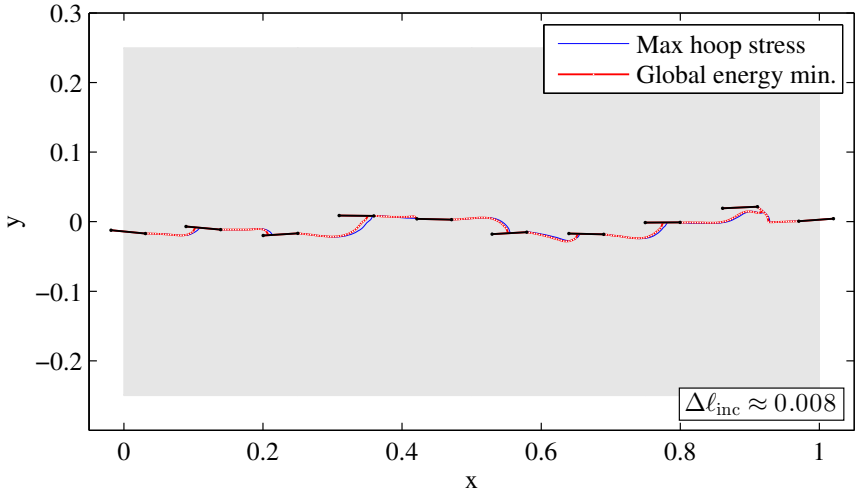

(b) Q4 mesh 200×400.

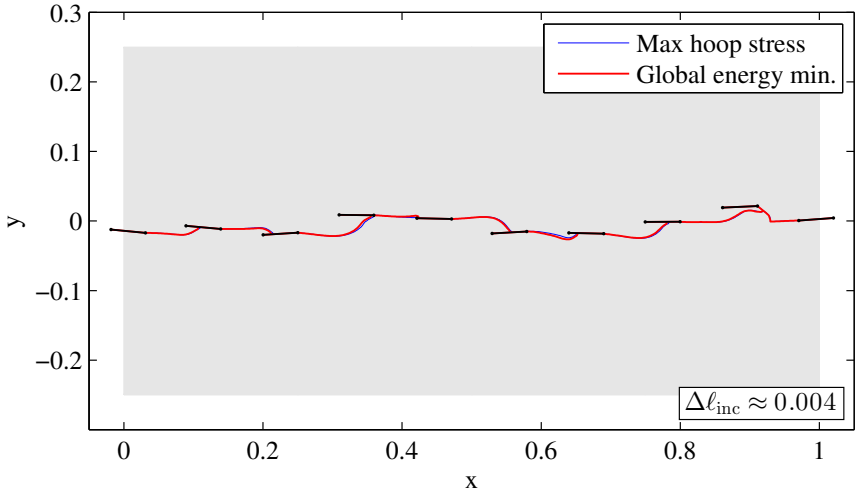

(c) Q4 mesh 400×800.

FIGURE 5.15: Comparison of fracture paths as obtained by the hoop-stress and the energy minimisation criteria for a Q4 discretisations. The plate is subjected to a uniform vertical tension load.

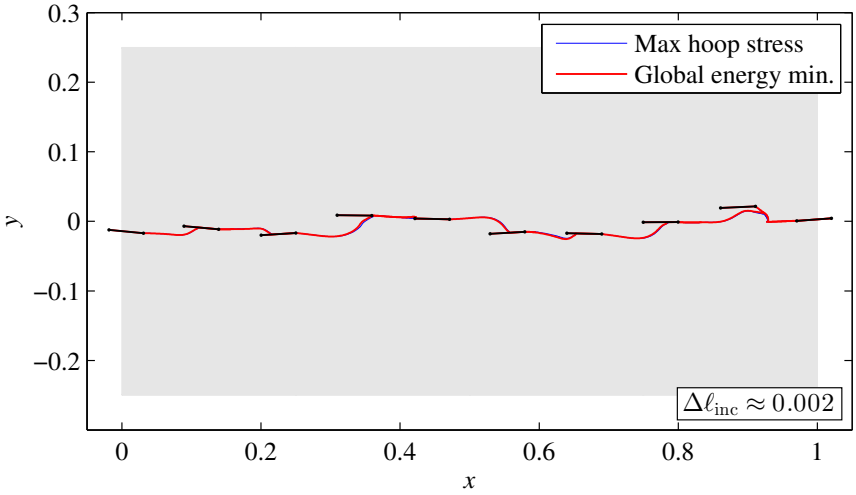

(a) T3 mesh 100×200.

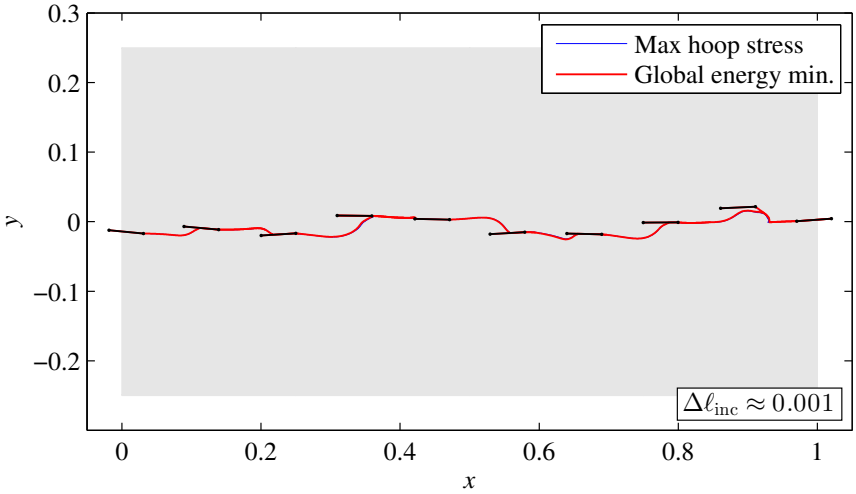

(b) T3 mesh 200×400.

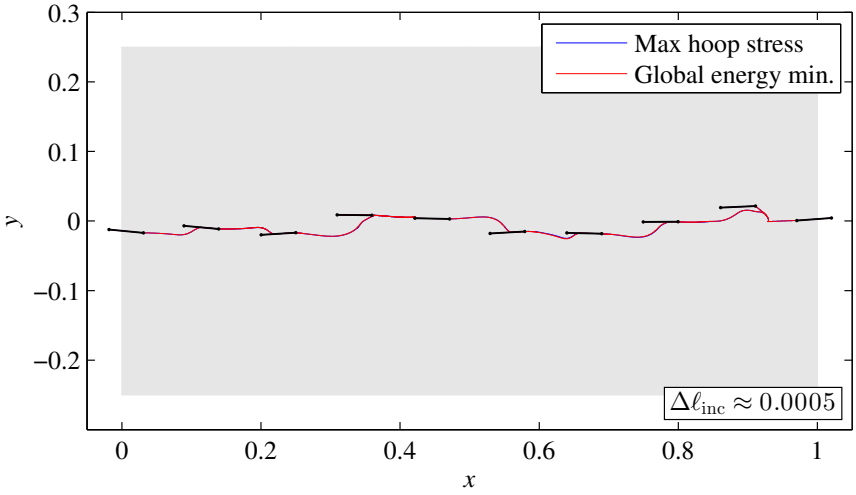

(c) T3 mesh 400×800.

FIGURE 5.16: Comparison of fracture paths as obtained by the hoop-stress and the energy minimisation criteria for T3 discretisations. The plate is subjected to a uniform vertical tension load.

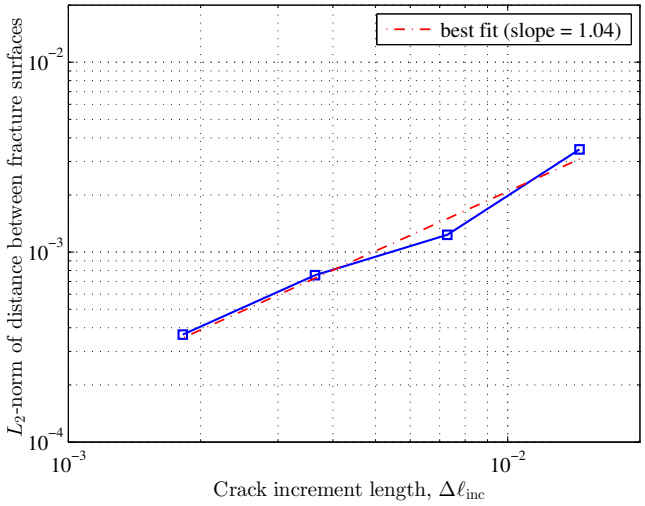

FIGURE 5.17: Convergence to same fracture path by hoop-stress and energy minimisation criteria considering Q4 discretisations. The test problem is a plate in vertical tension with 10 narrowly distributed parallel and initially non-overlapping cracks.

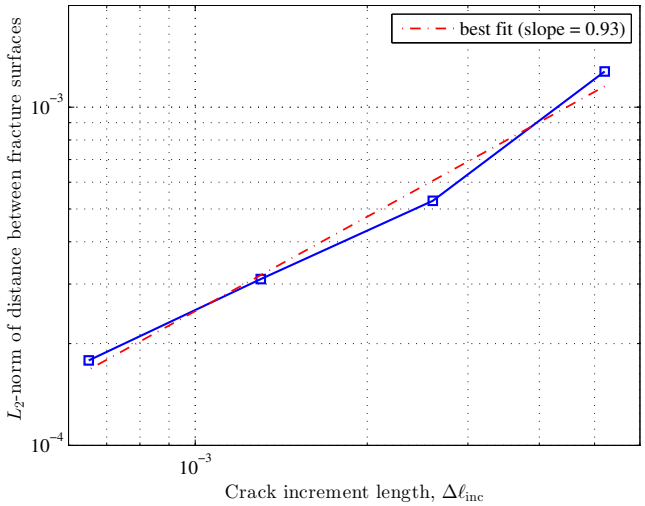

FIGURE 5.18: Convergence to same fracture path by hoop-stress and energy minimisation criteria considering T3 discretisations. The test problem is a plate in vertical tension with 10 narrowly distributed parallel and initially non-overlapping cracks.

5.4.2 Rectangular plate with 10 parallel cracks

In this case study, a rectangular plate with 10 non-overlapping parallel cracks distributed randomly within a narrow band is considered. The plate is simply supported and subjected to a vertical tension load. For the assumed crack distribution, crack growth is found to take place from left to right, causing complete horizontal splitting of the plate. The comparisons of the fracture profiles, as obtained by using different crack growth criteria, are presented for different finite-element types, namely: a 4-node bilinear quadrilateral element (Q4), and a 3-node linear triangular element (T3); the results based on Q4 and T3 meshes of similar numbers of degrees of freedom are given in Figures 5.15 and 5.16, respectively. The convergence rates of the fracture paths towards the same solution are provided by Figures 5.17 and 5.18 for Q4 and T3 discretisations, respectively. The mean convergence rates for Q4 and T3 meshes are found to be 1.04 and 0.93, respectively.

5.5 A numerical improvement to the growth direction

Within a discrete framework, it is observed that the maximum stress criterion consistently underestimates the crack kink angles whereas the global energy minimisation solution tends to overestimate such that with mesh refinement (and the resulting decrease in the fracture extension lengths), the fracture solutions tend to convergence from opposite directions towards each other and towards the solution that lies very close to the middle of the solutions obtained on coarser discretisations by the two criteria. Such convergence behaviours of the time-explicit stress criterion and the time-implicit energy based criterion can be attributed to, respectively, the crack kink angles favoring the mode-I stress field at the tip of an infinitesimal crack branch and at the tip of the finite crack extension.

Motivated by these numerical findings, one is inclined to propose a way to improve the crack growth direction by assuming the arithmetic average of the directions obtained by the stress and the energy-based criteria. Indeed, the accuracy of the numerical solution (especially on coarser meshes) can be improved significantly by this method. In addition, there is a substantial speed-up in the convergence rate of the fracture solution with mesh

refinement. The proposed modification to the crack growth direction is referred to as the *bi-section* method. Satisfactory results are obtained in all test cases that have been attempted. The fracture solutions by the different criteria, namely: the maximum hoop stress, the minimum energy and the bi-section method are presented subsequently.

5.6 Comparison of fracture paths by different criteria

Several 2D test cases are shown that compare the fracture paths obtained by three criteria, namely: maximum hoop stress, minimum energy criterion, and the proposed bi-section method, which averages the directions given by maximum hoop-stress and the minimum energy criteria at each growth instance. The fracture paths, for each test case, are computed for different discretisation densities. It is found in every case that the maximum hoop stress criterion and the minimum energy criterion converge towards the same fracture path. The fracture path obtained using the bi-section approach appears to converge fastest.

The numerical results verify that the proposed bi-section method, i.e. averaging of the crack growth directions obtained by the maximum hoop stress and the energy based criteria, is an effective means of obtaining increased accuracy of the fracture solution and speeding-up the convergence of the fracture path with mesh refinement. It is important to note that for the bi-section method to be consistent with Griffith's law (2.41), the critical crack tips need to be determined by the the energy minimisation approach, as described in Section 3.3.3. However, once the critical tips are identified, the bi-section approach may be used to numerically improve the crack growth direction, especially on coarse meshes.

The bi-section method is most effective for fracture evolutions that are predominantly of mode-I type and that do not involve crack intersections. The reason for the latter is that the position of a crack intersection tends to have a strong influence on the subsequent fracture paths (particularly on courser discretisations). The benefits of the bi-section approach are less apparent if the discretisation is already quite fine because the fracture paths by the stress and the energy-based criteria tend to be in close agreement already, e.g. Figure 5.22.

Double cantilever problem

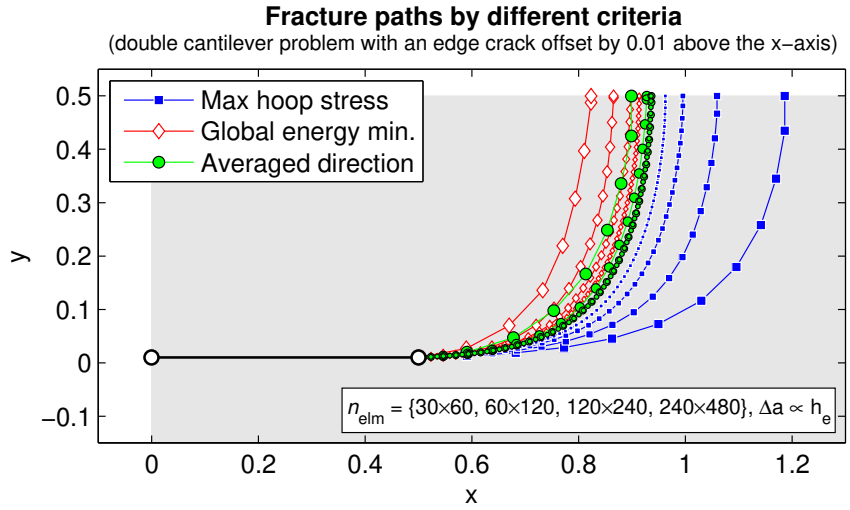

FIGURE 5.19: Fracture paths by different growth criteria for the double cantilever problem with the initial crack positioned 0.01 above the x-axis. The prying action is exerted by prescribed displacements on the left edge.

Two edge crack problem (simple tension loading)

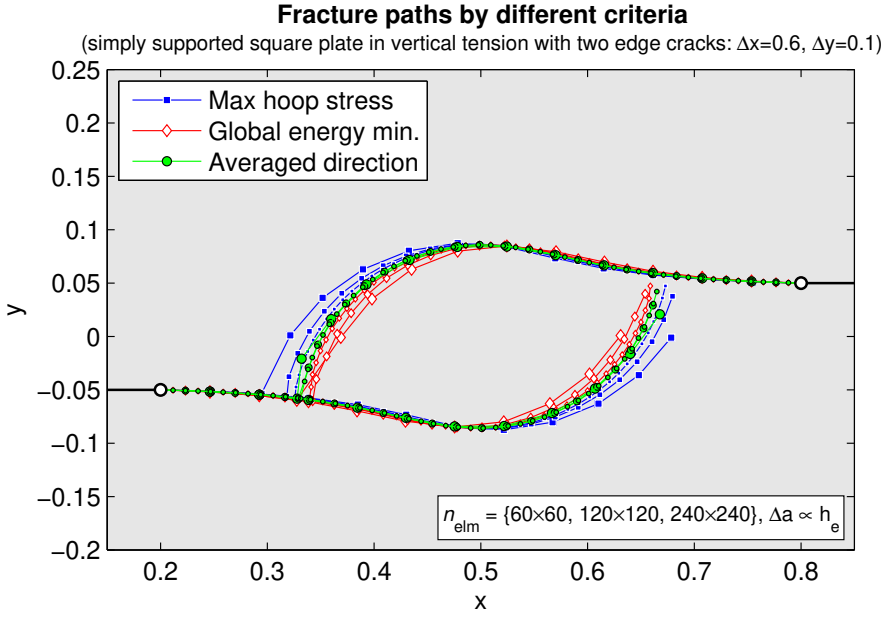

FIGURE 5.20: Fracture paths by different criteria for a simply supported square plate (1×1) in simple vertical tension with two initial edge cracks ($a_1 = a_2 = 0.2$). Crack-tip separation: $\Delta x = 0.6$, $\Delta y = 0.10$.

Three crack problem (pressure loaded centre crack)

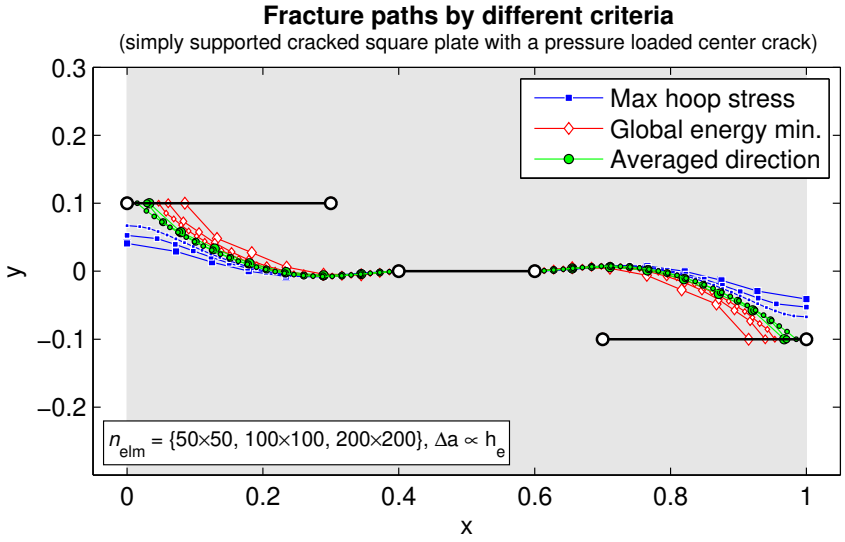

FIGURE 5.21: Fracture paths by different growth criteria for a simply supported square plate with three pre-existing cracks, where the centre crack is subjected to a pressure load acting normal to the crack surface.

Two cracks protruding from holes (vertical tension load)

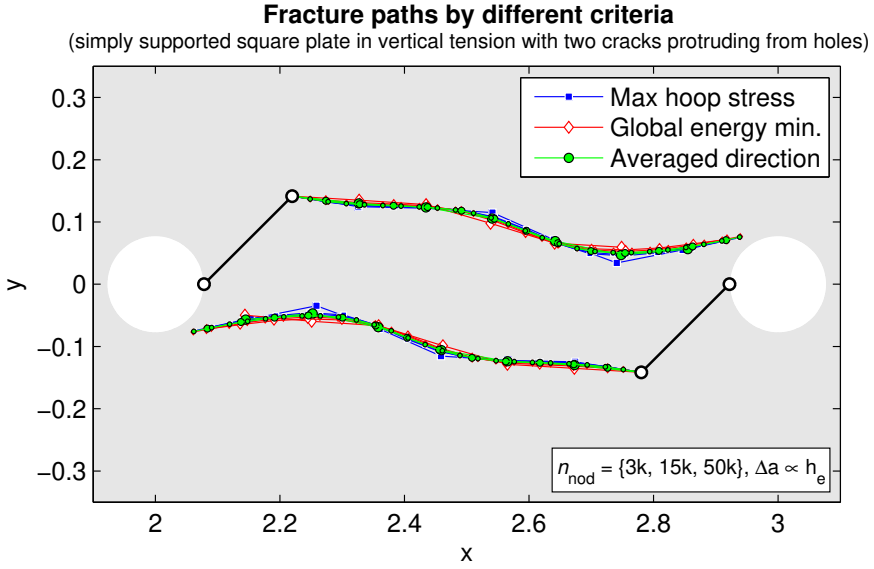

FIGURE 5.22: Fracture paths by different growth criteria for a simply supported square plate with a pair of initial cracks protruding from holes.

Two edge crack problem (crack pressure loading)

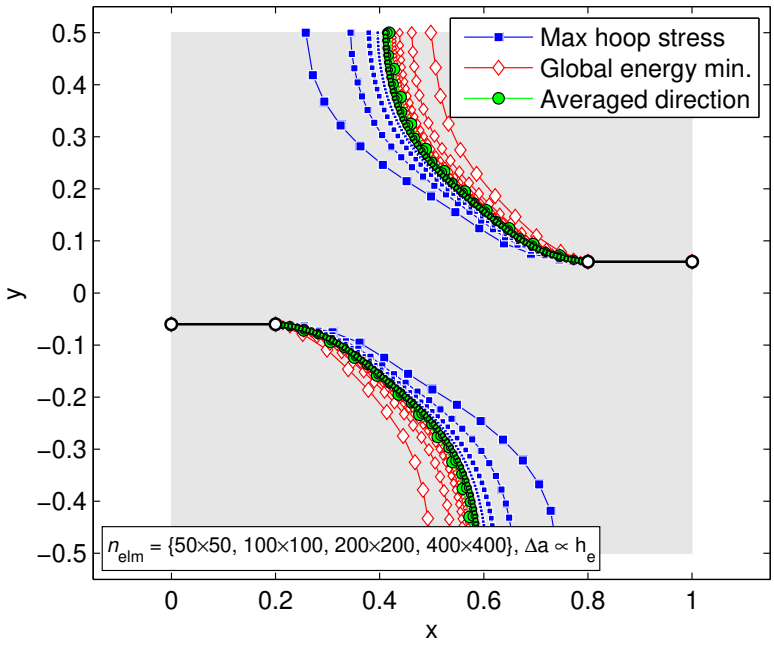

FIGURE 5.23: Fracture paths by different criteria for a simply supported square plate (1×1) with two initial edge cracks ($a_1 = a_2 = 0.2$) that are loaded by pressure. Crack-tip separation: $\Delta x = 0.6$, $\Delta y = 0.12$.

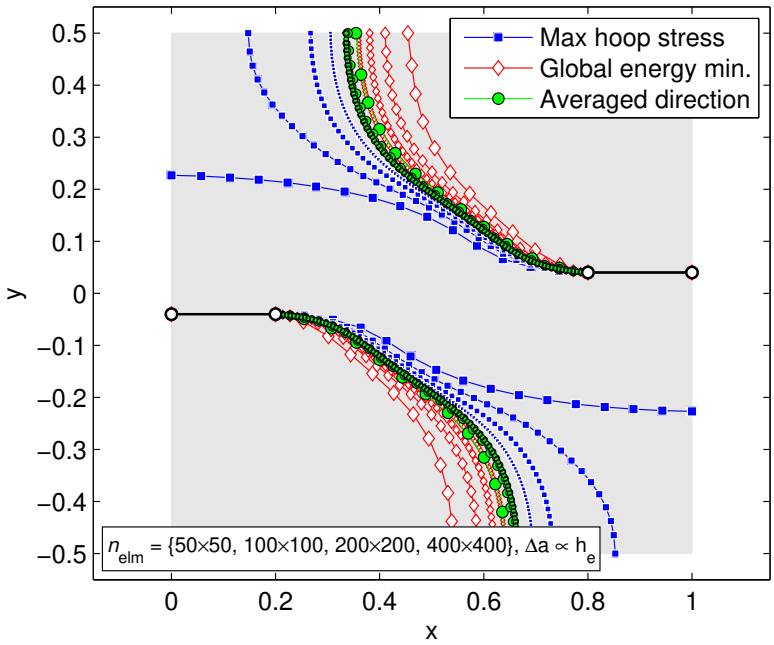

FIGURE 5.24: Fracture paths by different criteria for a simply supported square plate (1×1) with two initial edge cracks ($a_1 = a_2 = 0.2$) that are loaded by pressure. Crack-tip separation: $\Delta x = 0.6$, $\Delta y = 0.08$.

Two-edge crack problem (crack pressure loading) [cont.]

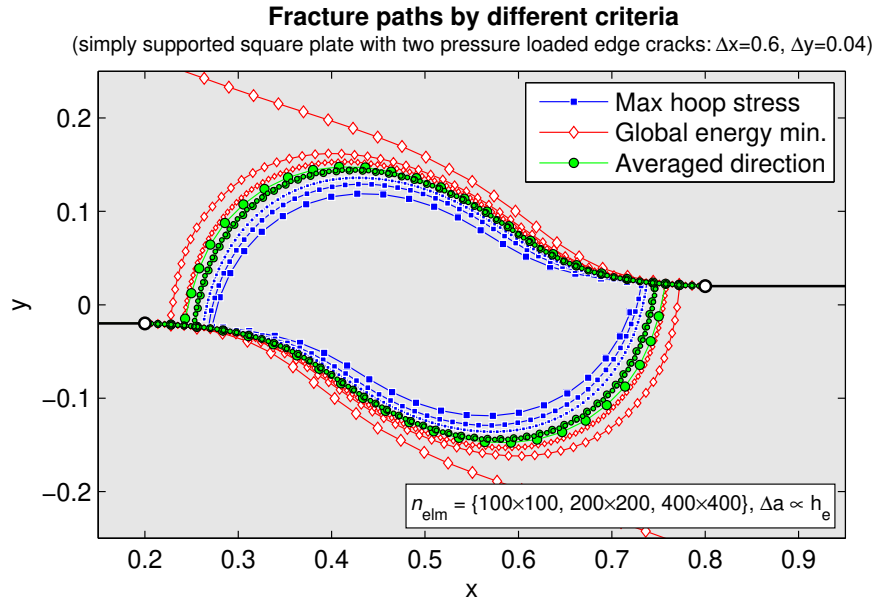

FIGURE 5.25: Fracture paths by different criteria for a simply supported square plate (1×1) with two initial edge cracks ($a_1 = a_2 = 0.2$) that are loaded by pressure. Crack-tip separation: $\Delta x = 0.6$, $\Delta y = 0.04$.

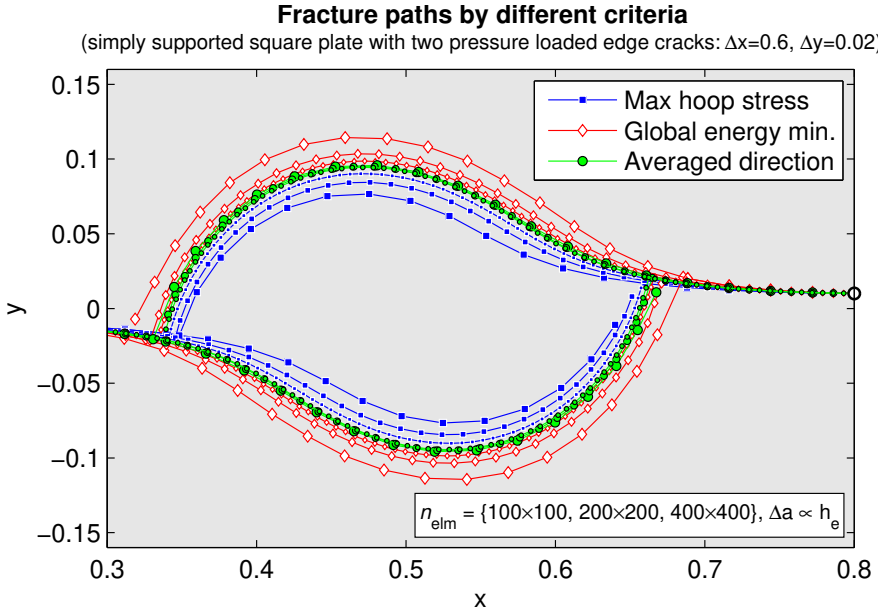

FIGURE 5.26: Fracture paths by different criteria for a simply supported square plate (1×1) with two initial edge cracks ($a_1 = a_2 = 0.2$) that are loaded by pressure. Crack-tip separation: $\Delta x = 0.6$, $\Delta y = 0.02$.

The PMMA beam with a bottom slit (case-1)

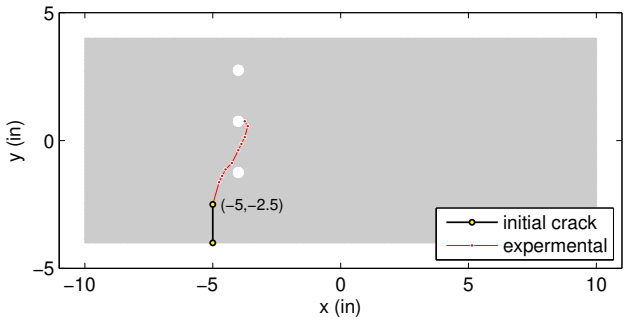

FIGURE 5.27: A simply supported 4×10 (in) PMMA beam with an initial vertical slit of length $a = 1.5$ (in) and a point load mid-way the top-edge.

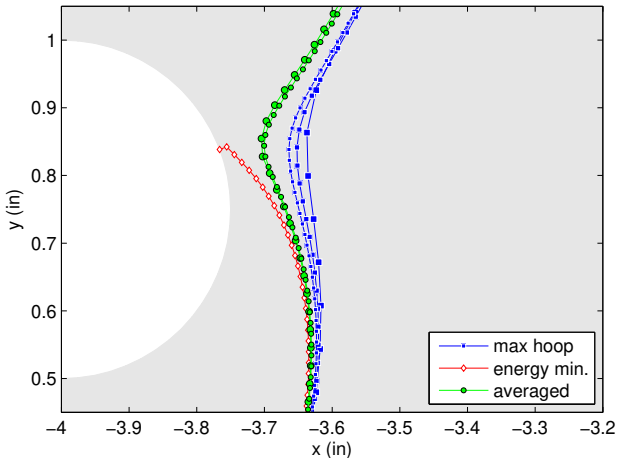

(a) close-up view around middle hole of beam in figure 5.27.

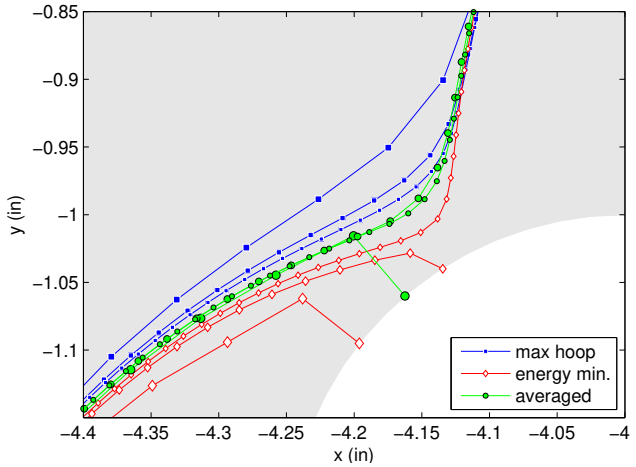

(b) close-up view around bottom hole of beam in figure 5.27.

FIGURE 5.28: Fracture paths by different criteria for the PMMA-beam problem depicted in figure 5.27.

The PMMA beam with a bottom slit (case-2)

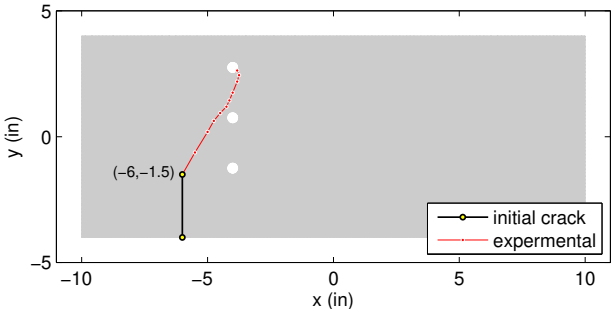

FIGURE 5.29: A simply supported 4×10 (in) PMMA beam with an initial vertical slit of length $a = 2.5$ (in) and a point load mid-way the top-edge.

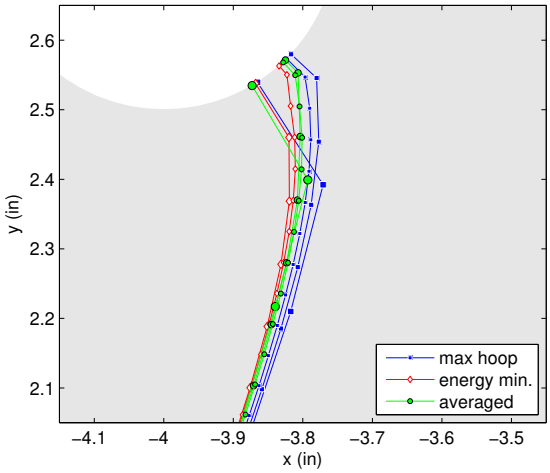

(a) close-up view around top hole of beam in figure 5.29.

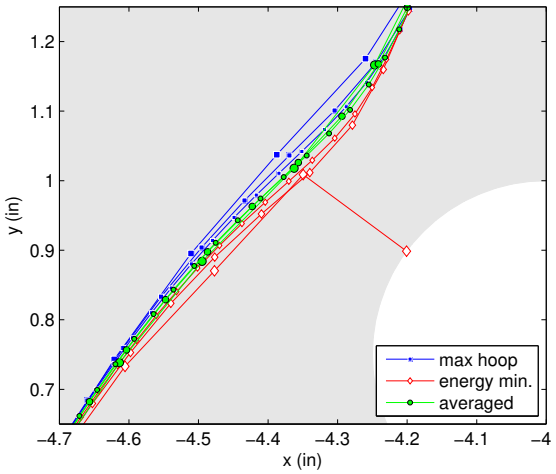

(b) close-up view around middle hole of beam in figure 5.29.

FIGURE 5.30: Fracture paths by different criteria for the PMMA-beam problem depicted in figure 5.29.

A pre-cracked plate with two holes

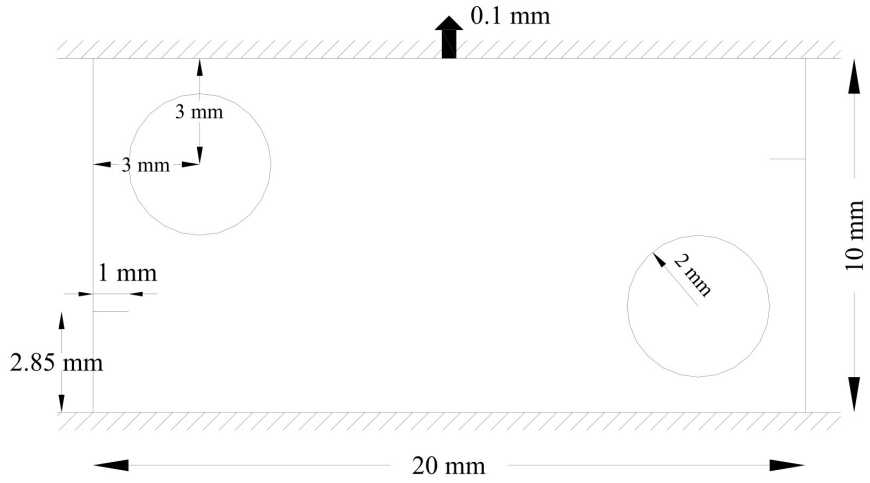

(a) Schematic diagram of the pre-cracked part. (Source: [40])

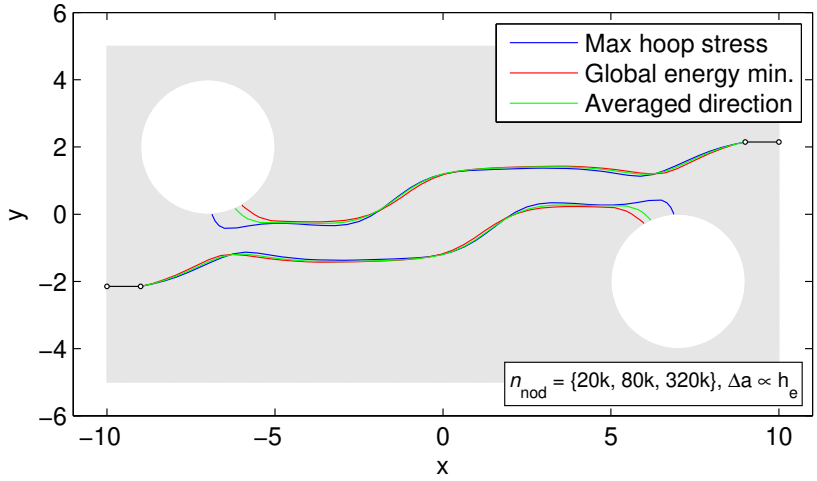

(b) Outline of fracture paths by different criteria.

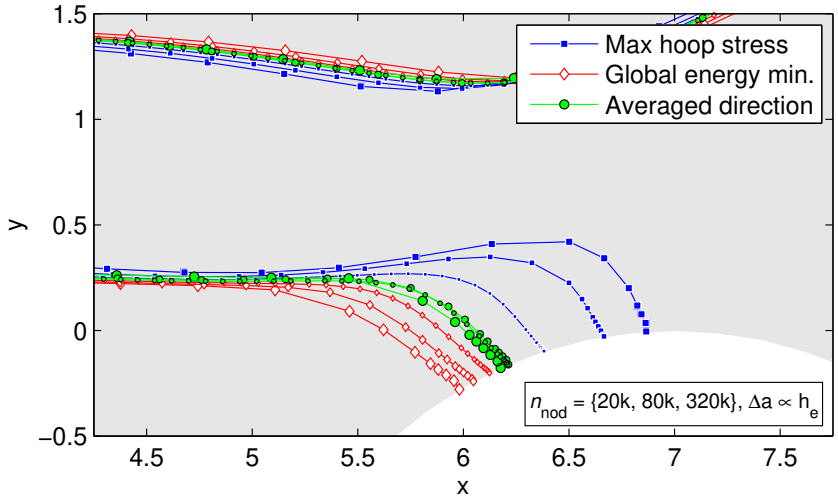

(c) Close-up view of sub-figure (b) around the hole on the right.

FIGURE 5.31: Fracture paths by different criteria for a rectangular plate with two holes and two edge cracks subjected to a vertical extension.

5.7 Summary

This chapter has focused on the verification of the numerical method for determining the crack growth directions based on the principal of minimum energy within the framework of the extended finite element method (XFEM). Firstly, the implementation of the stiffness derivative technique within XFEM for computing the rotational energy release rates of a finite crack extension was verified (Section 5.2). The numerical results showed that, in comparison to the numerical differencing of potential energy, the rotational energy release rate G_θ could computed with very good accuracy using the algebraic differentiation approach (Section 3.6). However, the rate of rotational energy release rate $H_\theta = \partial G_\theta / \partial \theta$, did not give as good an accuracy; nonetheless, it was considered acceptable for the purpose of solving the non-linear problem of energy minimisation (Section 3.3.3) that requires finding the vanishing G_θ with respect to the crack extension direction. The local crack growth solution by the stress and energy-based criteria were then compared in a few benchmark studies (Section 5.3). As expected, the crack growth directions were generally different. The solutions obtained by the energy-based criterion resulted in greater minimisations of potential energy. Although the growth directions by different criteria were found to differ, it was shown that the maximum tension and the minimum energy criteria lead to very similar fracture paths when compared on the material length-scale (Section 5.4). From the several discretisations that were attempted, the fracture solutions appeared to converge towards the same solution such that for practical purposes the converged solutions could be considered as one and the same. Finally, a numerical improvement to the crack growth direction was proposed (Section 5.5) based on the results of multiple test cases (Section 5.6). The criterion assumes an arithmetically averaged crack growth direction of those obtained by the stress and the energy-based criteria. The method proves to be an effective way of obtaining improved accuracy of the fracture path and speeding-up the convergence of the fracture solution with mesh refinement.

Chapter 6

Silicon wafer splitting

6.1 Introduction to Smart-Cut™

Smart-Cut™ [15, 47, 48, 154] is a relatively novel technology that has been developed over the past decade to enable a highly-efficient thin layer transfer from one substrate onto another. The technology is particularly viable in the high-volume commercial production of silicon-on-insulator (SOI) wafers [52], which are used in the modern-day solid-state electrics industries. Some of the most wide-spread applications of SOI's are in the fabrication of integrated circuits and photovoltaics [52]. From an engineering point of view, an SOI wafer is a multi-layer composite material that consists of a thin top-layer of crystalline silicon (Si) followed by an insulating layer (such as silicon-dioxide, SiO_2) which is, in turn, bonded to a handle substrate (such as silicon). The fabrication process of an SOI using Smart-Cut™ is depicted in Figure 6.1; the process steps are summarised as follows:

1. Start with initial silicon wafers: donor part (**A**) and handle part (**B**)
2. Wafer **A** undergoes an oxidation process to create an insulating layer
3. Smart-Cut™ ion implantation in wafer **A** induces an in-depth weakened layer
4. Wafer **A** is hydrophilicly bonded to substrate **B** followed by thermal annealing
5. Smart-Cut™ cleavage at the mean ion penetration depth splits off wafer **A**
6. Product wafer **B** undergoes chemical-mechanical-polishing and is complete
7. Wafer **A** is recycled and the process is repeated from Step-1.

It is intended that after the split (Step-5), the two wafers have sufficiently smooth and uniform fracture surfaces such that any resulting roughness can later be reduced by means of corrective treatments, e.g. chemical/mechanical polishing (CMP), to commercially acceptable levels. However, at times the cleaved surface can result in significant deviations of the fracture path from the mean, creating defects that can no longer be mitigated by CMP. These type of process-related defects can lead to a substantial loss of product. Although considerable theoretical and experimental efforts have addressed these issues and have significantly contributed to the current state of the art technology of Smart-Cut™ [5, 49, 52, 234, 235], the process itself is not completely understood to this day. There are theoretical and practical challenges in the characterisation of different aspects of the

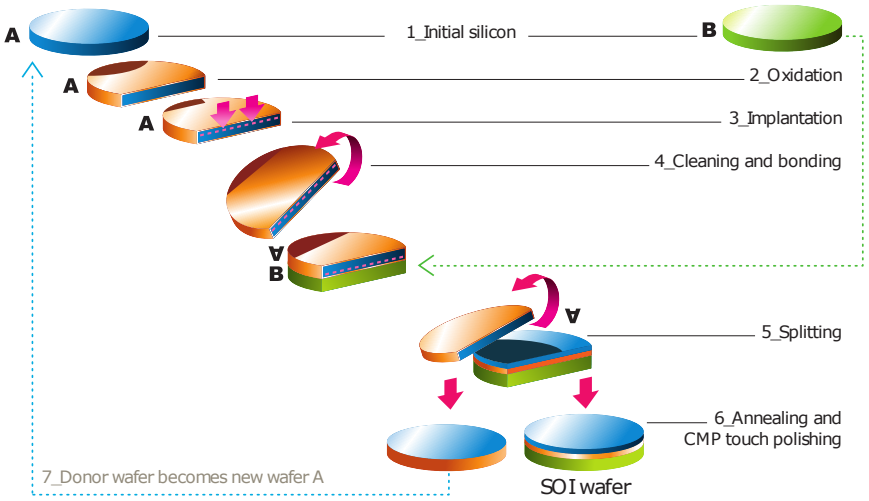

FIGURE 6.1: Basic diagram of the Smart-Cut™ process (Source: [267]).

process such as the competing influence of thermochemical and mechanical interactions in the creation/evolution of voids/cracks [289] and, above all, the influence of different Smart-Cut™ process parameters on the final fracture surface roughness [5, 109, 110].

The aim of this chapter is to quantify the affects of several Smart-Cut™ process parameters on the post-split fracture surface roughness by numerically simulating the wafer splitting process. Due to the physical complexities involved in Smart-Cut™ (to be discusses in the following section), the complete simulation of Smart-Cut™ is difficult, both from a theoretical and a practical side. Nonetheless, useful information can still be derived about the process by considering the problem of splitting from a certain point in time that is better understood in terms of the material behaviour and suitable initial condition about the material state can be provided. The point in time that is of interest is characterised by a well-developed micro-crack distribution. The cracks grow slowly and the material is linear-elastic and brittle. The micro-crack distribution can be given by representative statistical data. This provides the necessary initial conditions for simulating the subsequent evolution of micro-cracks. The goal is to investigate the influence of several process-related control parameters on the evolution of micro-cracks by quantifying the post-split fracture surface properties, such as: the mean depth of splitting, crack deviations from the mean depth of splitting, and the fracture surface roughness. The control parameters consist of:

the initial depth of micro-crack distribution, the micro-crack distribution thickness, the thickness of different SOI layers, and the relative elastic stiffnesses of different SOI layers.

6.2 The physical process

The Smart-Cut™ ion implantation induces the formation of defects in the monocrystalline Si lattice. These defects take the form of vacancies and interstitials. The mechanism that produces such defects can be understood considering the way an ion travels across the Si lattice. As the Si wafer is bombarded by H-ions, some Si atoms are displaced from their lattice positions. The displaced Si atoms can attain sufficient energy to knock out other Si atoms. This results in a cascade of collisions that leads to the creation of a heavily damaged layer in the silicon substrate with a peak damage density occurring somewhat below the top surface. The H-ions tend to settle bellow the depth of peak damage.

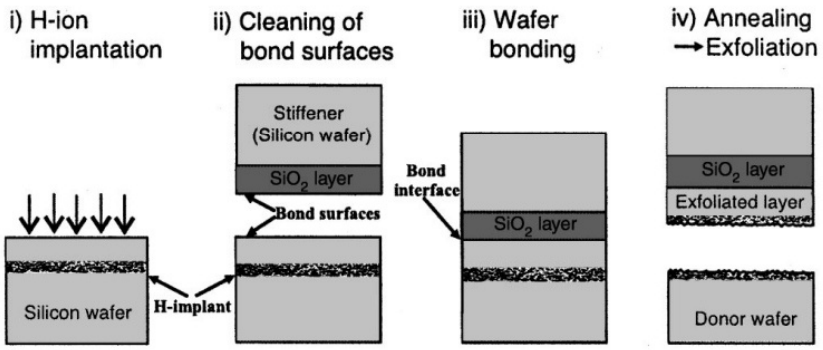

FIGURE 6.2: Schematic of the production of SOI by the ion-cut process: (i) pre-implantation of hydrogen ions into a silicon wafer at a well defined depth, (ii) cleaning of the bond surfaces, (iii) hydrophilic bonding of the implanted wafer to another substrate, a SiO_2 capped silicon wafer, and (iv) annealing of the joined pair. (Source: [121])

The vacancies tend to aggregate into small planar clusters called platelets, most of which are preferentially aligned parallel to the surface of the wafer in the (100) plane due to the out-of-plane tensile stress field that results from ion implantation damage [138, 246]. The implanted hydrogen is known to accumulate at these planar defect sites, passivating any dangling Si bonds and forming what are called hydrogen-decorated platelets. The

platelets, subsequently act as a nuclei for trapping other freely migrating H-ions in the lattice. The presence of hydrogen inside the platelet also reduces the fracture energy of the neighbouring silicon bonds. During annealing, more H-ions diffuse into the platelets where they combine into molecular hydrogen H_2 [289]. The high pressure H_2 gas and the locally reduced fracture toughness of silicon lattice causes the growth of these platelets. A schematic of H-platelet formation and H_2 gas build-up is illustrated in Figure 6.3.

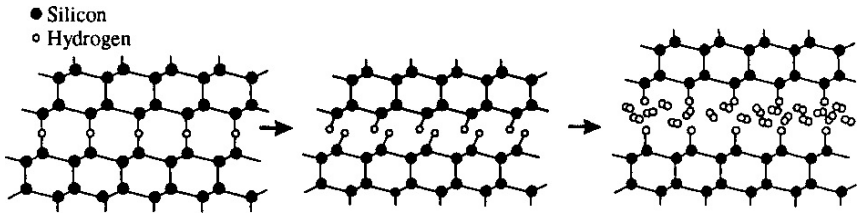

FIGURE 6.3: Schematic of H-platelet formation and development into H_2-gas bubbles (Source: [121])

During the Smart-Cut™ thermal treatment process of the bonded wafers, the evolution of H_2-filled platelets from a few tens of nano-metres to micro-cracks of a few hundreds of micro-metres and onwards is governed by two phenomena: a thermodynamically-driven spontaneous growth of platelets known as Oswald ripening [289], and a mechanically-driven growth of micro-cracks due to the high pressure H_2 gas [107]. The Ostwald ripening phenomenon is dominant in the initial stage of platelet growth whereby larger size platelets preferentially grow in size at the expense of smaller platelets shrinking in size. The mechanical action of the H_2 gas pressure becomes significant at a later stage in the micro-crack evolution process, once the micro-cracks have become sufficiently large.

The evolution of defects can be broken down into several distinct phases along the time-line of the thermal treatment process. Each stage characterises the interplay between different defect growth driving mechanisms [235]. In the beginning, at **0-10%** annealing time, platelet evolution is slow and is predominantly governed by the Ostwald ripening phenomenon [289], which is a thermodynamically driven growth. Platelets are from several tens of nano-metres to a few micro-metres in size. Build-up of H_2-gas within the platelets takes place. In the **10-90%** time frame, the internal crack pressure becomes significant and a competing crack growth mechanism between Ostwald ripening and the

mechanical action of pressure can be observed. At this time, platelets and micro-cracks both grow but some coalescence of micro-cracks takes place. Micro-cracks are up to a few tens of micro-metres in size. At **90-99%** time, the mechanical force of H_2 pressure becomes the dominant factor governing micro-crack growth. A moderate rate of crack growth and significant micro-crack coalescence occurs. A large fraction of cracks is from several tens to several hundreds of micro-metres in diameter. Finally, during the **99-100%** annealing time, rapid growth of micro-cracks takes place whose speed on the order of kilometres per second. The material effectively behaves as a brittle solid. The rapid (dynamic) coalescence of micro-cracks results in the propagation of a macro crack through the whole silicon crystal leading to the complete splitting of wafers and the transfer of the silicon layer.

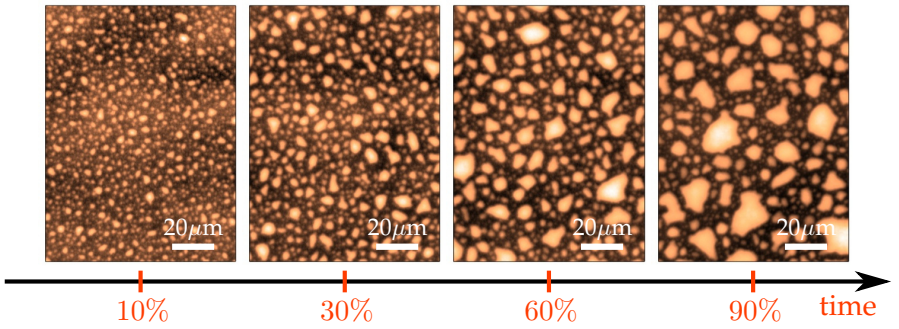

FIGURE 6.4: Evolution of micro-cracks as observed by optical microscopy. (adapted from [234]).

Figure 6.4 illustrates the micro-crack evolution over time. A cross-sectional view of the depth-wise distribution of micro-cracks within a densely damaged silicon layer after a partial anneal of 10% is shown in Figure 6.5.

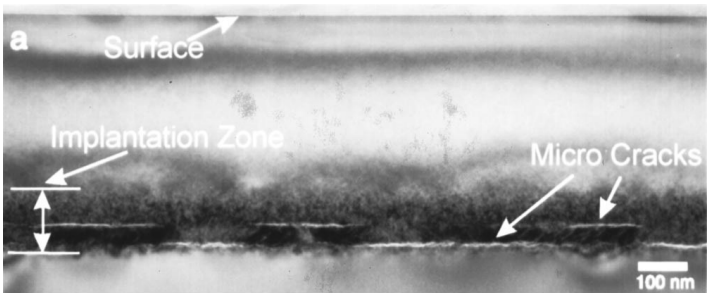

FIGURE 6.5: Cross-sectional view of H-ion irradiated mono-crystalline silicon wafer after a partial anneal. The densely damaged implantation zone (dark field) is visibly permeated at different depths by cracks that are in the sub-micron length scale. (Source: [121])

The focus of the parametric studies will be on the 90-99% time period to complete splitting. This stage is characterised by the relatively slow growth of cracks whose size spans from several tens to hundreds of micro metres (refer to Figure 6.4 for a sample image).

6.3 Modelling considerations

As the initial stage of the fracture process is a host to a variety thermochemical phenomena taking place at the very fine scale (e.g. hydrogen diffusion, weakening and breaking of Si bonds, spontaneous growth/ripening of bigger size cavities at the expense of smaller ones), a model that would represent the multi-physics phenomena of this kind would be computationally difficult to solve unless some suitable multi-scale approach is adopted. However, once the small-scale cavities have grown from several nano-metres into several hundreds of nano-metres, the H_2 pressure begins to exert a significant influence on the fracture evolution such that the mechanical interactions begin to dominate over the thermodynamic forces. Henceforth, the model complexity can be greatly simplified. We are particularly intersected in modelling the Smart-Cut process in the 90-99% of thermal budged to complete splitting of the wafer, which is characterised by the slow and steady micro-crack growth. Before the current model is described in more detail, it is worth reviewing some recent works in modelling of the Smart-Cut process (or certain parts of it).

6.3.1 Previous models

A more recent attempt [199, 200] to characterise platelet development was carried out using a molecular dynamics approach. The study focused on the thermal evolution of horizontal (100) hydrogen-induced platelets within a silicon lattice. The platelets were modelled as 10nm planar defects in 2D in a 25000 Si atom crystalline system with periodic boundary conditions. The model domain equated to a size of 35.0×35.0 nm^2. Another numerical attempt to characterise micro-crack growth and coalescence was carried out by [251]. In this effort, a silicon sample containing a couple of horizontal pre-existing micro-cracks was considered. The weak interactions and coalescence between the cracks were studies

as affected by different boundary conditions and initial crack tip separation distances. The finite element method with cohesive interface elements was applied to model the micro-crack coalescence. A couple of edge cracks were considered. The obtained fracture paths were significantly mesh-biased since crack growth was allowed only along element boundaries. An XFEM discretisation was used subsequently in order to circumvent the solution dependence on the mesh. This lead to physically more reasonable fracture paths. however, because only a couple of cracks were modelled, it was impossible to make useful deductions with regard to the wafer post-split fracture surface roughness as influenced by the initial vertical and horizontal crack spacing. The following subsection describes the present model of SOI wafer splitting with the aim to improve upon the previous results.

6.3.2 Proposed model

The present model assumes a 2D wafer representation (refer to Figure 6.6) and focuses on the material behaviour at the time period 90-99% to complete wafer splitting. The model assumes the entire depth of the wafer structure and multiple initial micro-cracks running along the length of the wafer sample. Quasi-static brittle micro-crack growth is supposed. The following aspects of wafer splitting can be captured by the model: (1) the weak interactions between multiple cracks, (2) multiple crack intersections, and (3) the effects of different material layers on the fracture paths. Finally, by considering the whole depth of the wafer sample, physically meaningful boundary conditions can be imposed.

It is acceptable to consider the micro-crack evolution in the 90-99% time period leading up to catastrophic splitting as essentially a quasi-static process. From a fracture mechanics point of view, quasi-statics (and, hence, necessarily stable) crack growth is promoted by the chemical interactions of hydrogen with silicon that has the effect of reducing the fracture toughness at the crack tip [81, 109, 110]. However, the decrease in the fracture resistance is only local and as soon as sufficient H_2 pressure develops to cause a crack to propagate, fresh silicon is exposed with a higher fracture toughness. This naturally results in stable crack growth, i.e. $\partial G_{\mathrm{s}}/\partial a < \partial G_{\mathrm{c}}/\partial a$, provided that the H_2 pressure is not so high so as to cause catastrophic (unstable) crack growth, i.e. $\partial G_{\mathrm{s}}/\partial a > \partial G_{\mathrm{c}}/\partial a$.

In addition, stable crack growth is promoted by the drop in the H_2 pressure that results from the immediate increase in the crack volume following a crack extension. Due to the relatively slow diffusion of H-ions from the surrounding Si lattice into the crack, there is some delay before sufficient H_2 pressure develops to cause subsequent crack growth.

The material is considered to be isotropic by virtue of the highly amorphous damaged silicon as caused by H-ion implantation damage. At the typical Smart-Cut™ annealing temperatures of 400-500°C, the silicon can be considered as a linear-elastic brittle solid at the microscale (with a negligibly small plastic zone at the crack tips) such that the dominant mechanism of internal (elastic) energy dissipation is through brittle fracture [234, 251]. The fracture surface energy is assumed to be constant in the damaged zone.

It was demonstrated in Section 5.4 that the fracture paths obtained by the energy-minimisation approach (2.55) and the maximum hoop-stress criterion (1.17) converged to very similar fracture solutions. For the sake of computational efficiency, the maximum hoop-stress criterion will be used to determine the onset and the direction of crack growth.

In the current model, it will be supposed that some initial representative micro-crack distribution can be given that suitably characterises the time period corresponding to 90% of thermal budged required for complete splitting of the wafer [234]. At this 90% mark, the cracks have already developed into in the size of a few tens of micro-metres. This micro-crack distribution can be estimated based on empirical laws [234]. Specifically, the depth-wise micro-crack distribution can be approximated by a Gaussian distribution. The length-wise micro-crack spacing can be represented by a uniform random distribution. Finally, the size of the micro-cracks can be given by a uniform random distribution.

6.3.3 Loading conditions

We will investigate the process of micro-crack evolution and wafer splitting for two types of boundary conditions: *pressure* loading by hydrogen gas due to the thermal annealing, and *mechanical* loading by the insertion of a razor blade to manually split the wafers.

Pressure driven splitting

During the thermal annealing of an SOI wafer, the initiation of splitting takes place at a point close to the edge of the wafer. The fracture front propagates through the wafer leading to micro-crack coalescence and complete splitting. It is assumed that crack growth is driven by the H_2 gas pressure. Furthermore, it will be supposed that this pressure remains constant during crack growth and the same in every crack. The 2D model of wafer splitting is idealised in plane-strain. The length and the depth of the SOI wafer sample is considered to be 2mm and 1.5mm respectively. The maximum length of the sample is constrained by the available computational resources. It is assumed that all micro-cracks within the study domain propagate simultaneously. Refer to the diagram in Figure 6.6 for the representation of the 2D model. The problem boundary conditions can be summarised as follows. Zero displacements on the left and right edges of the wafer sample are prescribed, i.e. $u_x|_{x=0} = u_x|_{x=L} = 0$. The top and bottom wafer surfaces are free to translate vertically. Loading is by uniform pressure on all crack surfaces.

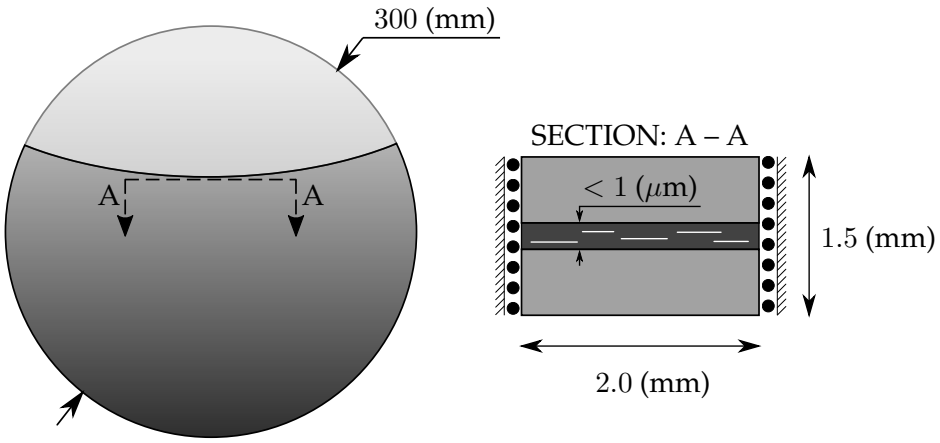

FIGURE 6.6: Diagram of the wafer model. Lite-gray region represents the part of the wafer that has split; dark-gray – the part of the wafer that is still intact. The interface between the two regions marks the fracture front.

Mechanical splitting

Mechanical splitting involves the insertion of a razor blade at approximately the level of the bonding interface between the two wafers (the handle part and the product part). The experimental setup is show by Figure 6.7. In the current simulations, zero H_2 gas pressure is assumed within the pre-existing micro-cracks. The model boundary conditions consist of the prying action of the blade at one end of the wafer sample and a fully built-in other end. The wafer model assumes a sample length of 3 (mm) for computational feasibility reasons. The actual fracture zone studied is 0.5mm in length with an additional clearance of 1.5mm to the right where the blade is inserted, and 1.0mm to the left where the built-in end is located. This serves to reduce the so-called end-effects on the simulation results. The insertion of the blade effectively causes the wafer to open as a double cantilever beam.

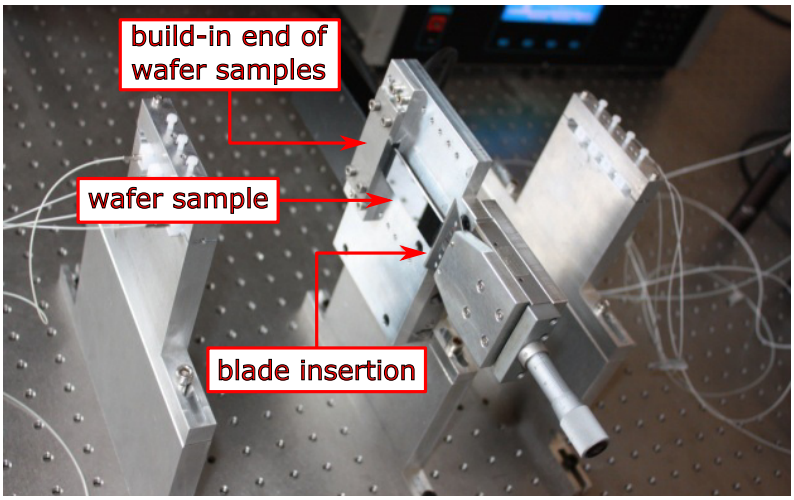

FIGURE 6.7: Experimental setup of mechanical splitting of a wafer sample by means of an insertion of a razor blade at the wafer bonding interface. (Adapted from: [233])

6.3.4 Discretisation aspects

In the discretised domain, the zone of damaged silicon assumes a mesh that is around three orders of magnitude finer than the surrounding mesh of the undamaged silicon, i.e. $h_{\mathrm{e}}^{\mathrm{f}} \approx 0.1$ (μm) and $h_{\mathrm{e}}^{\mathrm{c}} \approx 100$ (μm). The high mesh contrast inevitably results in the

inner silicon layer being somewhat mechanically more compliant than the surrounding silicon. This confinement effect purely due to the numerical discretisation will influence the fracture paths such that the cracks will have a tendency to deviate less in the vertical dimension than if the mesh size were more uniform. To reduce the discretisation bias, the fine mesh is centred about the mean depth of the initial micro-crack distribution and a gradual transition between the coarse and the fine mesh is introduced. Figures 6.8 and 6.9 show the discretisation strategy for the pressure-splitting boundary conditions, whereas Figures 6.10 and 6.11 show the mesh for the mechanical-splitting boundary conditions. Finally, Table 6.1 shows the typical wafer layer thicknesses, which are meshed conformally.

6.3.5 Process parameters

The initial micro-crack sizes are assumed to be of a uniform distribution between 20 and 30 (μm) with 90% of the potential fracture surface already fractured. The depth-wise crack distribution is assumed to obey a normal (Gaussian) distribution that is characterised by the mean crack depth h_{mean} and standard deviation t_{dmg} parameters. Due to limited computational resources, wafer samples of 2×1.5 (mm) for the pressure-splitting boundary conditions and 3×1.5 (mm) for the mechanical splitting boundary conditions were considered. This allowed around 70 micro-cracks to be simulated. The tables below summarise 5 different realisations of randomly generated crack distributions. The Smart-Cut™ process parameters are listed as follows. Mean crack implantation depth, $h_{\text{mean}} = \{0, 300, 400, 500, 600\}$ (nm); buried oxide depth, $t_{\text{box}} = \{0, 100, 200, 300\}$ (nm); crack depth-wise spread $t_{\text{dmg}} = \{0.0, 2.5, 5.0, 7.5, 10.0\}$ (nm); the elastic compliance of the damaged silicon layer relative to the surrounding silicon $\alpha_{\text{dmg}} \equiv \frac{E_{\text{dmg}}}{E_{\text{Si}}} = \{0.85, 0.9, 0.95, 1.00\}$.

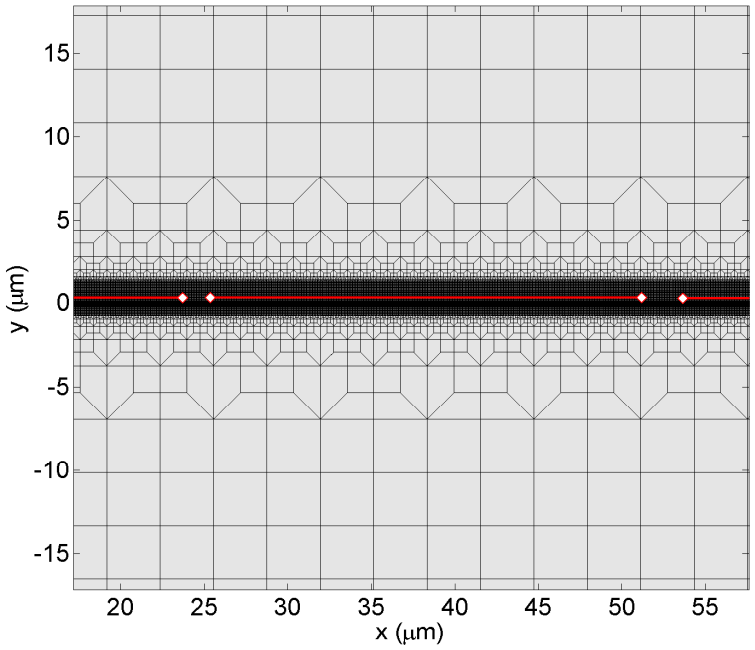

FIGURE 6.8: Discretisation mesh for the case of pressure-splitting boundary conditions. Transitional mesh refinement is provided towards the micro-crack damaged silicon layer. [A far-view of Figure 6.9].

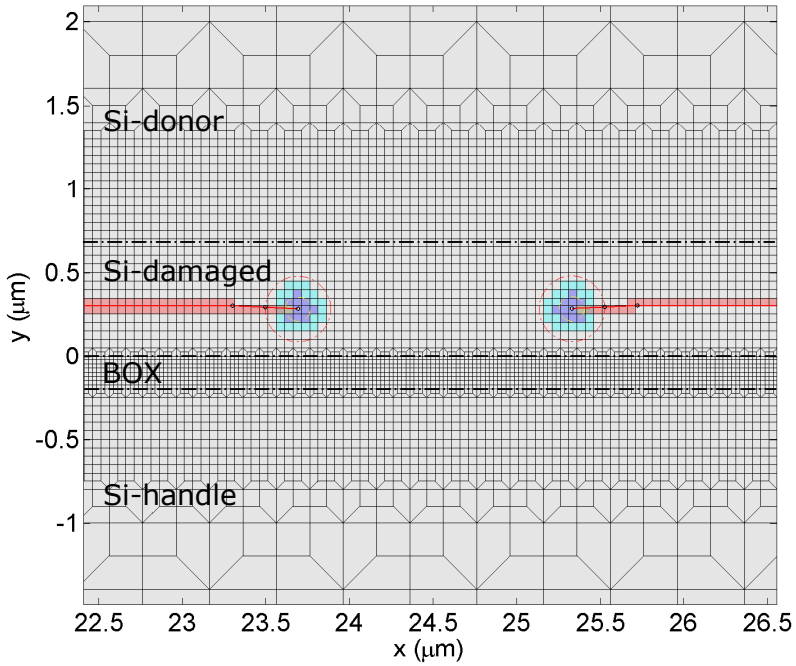

FIGURE 6.9: XFEM discretisation mesh showing different mesh densities for different material layers: Si-donor, Si-damaged, BOX (buried oxide, SiO_2) and Si-handle. Cracks are plotted with enriched elements, which are indicated by different colour shades. [This is a close-up of Figure 6.8].

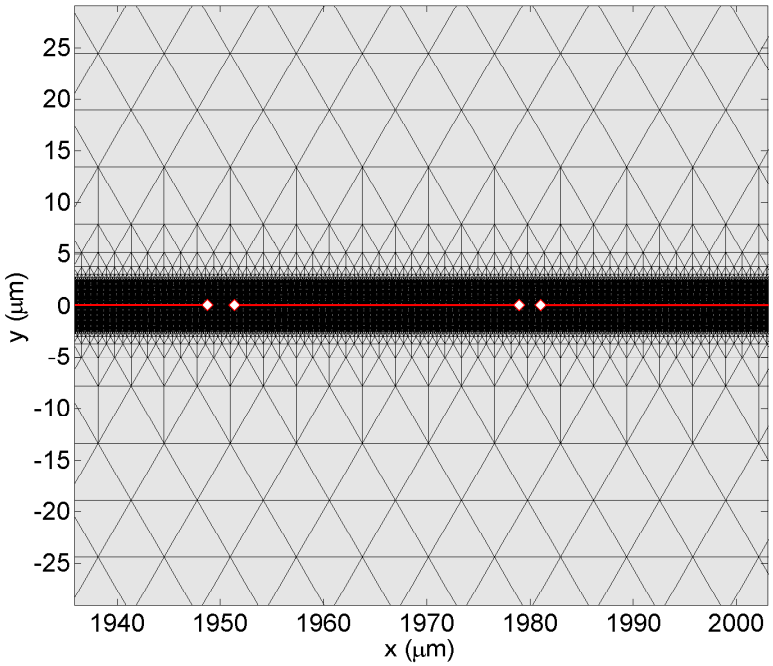

FIGURE 6.10: Discretisation mesh for the case of mechanical-splitting boundary conditions. Transitional mesh refinement is provided towards the micro-crack damaged silicon layer. [A far-view of Figure 6.11].

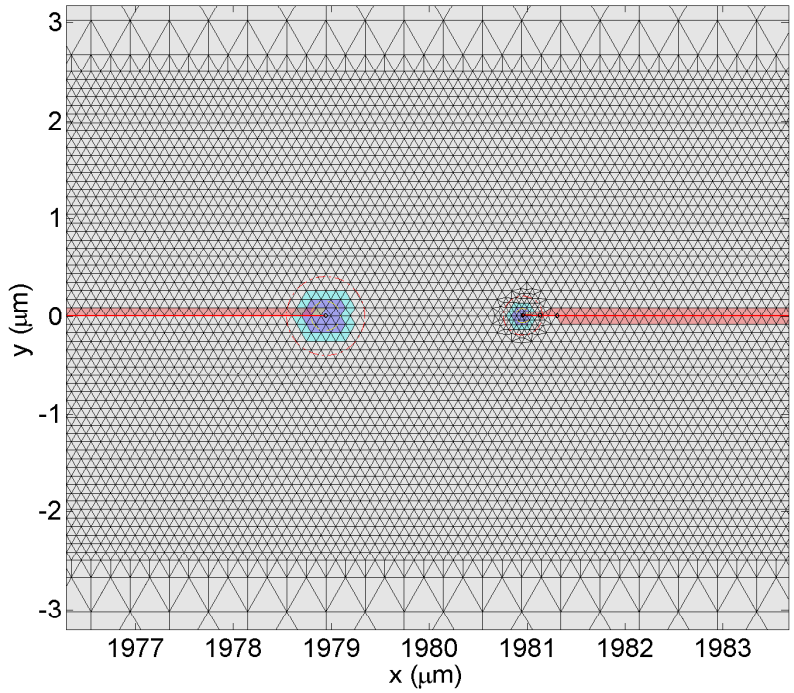

FIGURE 6.11: XFEM discretisation showing different mesh densities. Cracks are plotted with enriched elements, which are indicated by different colour shades. Local crack-tip refinement is used. [A close-up view of Figure 6.10].

TABLE 6.1: Layer thicknesses of bonded wafer structure prior to splitting.

layer depths	**Value**	**Units**
Si-donor	750	μm
Si-damaged	200-300	nm
Si-exfoliated	200-300	nm
SiO_2	100-200	nm
Si-handle	750	μm

TABLE 6.2: Assumed crack distribution parameters.

Parameter	**Value**	**Units**
crack cover percentage	90	%
size distribution (uniformly random)	20-30	μm
crack depth-wise spread (1σ)	10	nm

TABLE 6.3: Crack distributions that were used in the numerical studies.

#	number cracks, N_{tot}	ideal roughness, RMS (nm)
1	72	9.60
2	71	9.61
3	75	9.63
4	73	8.79
5	73	8.75

Ideal roughness of initial crack distribution

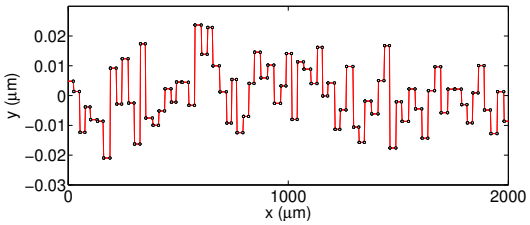

(a) crack distribution #1 ideal roughness (RMS), $R_{q_0} = 9.61$ (nm).

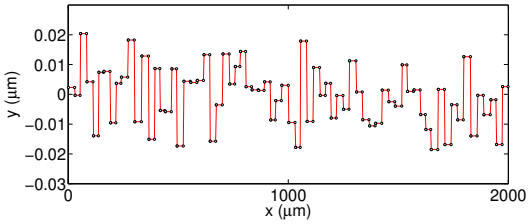

(b) crack distribution #2 ideal roughness (RMS), $R_{q_0} = 9.49$ (nm).

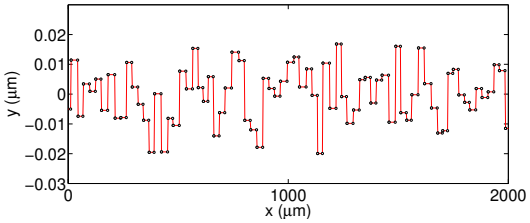

(c) crack distribution #3 ideal roughness (RMS), $R_{q_0} = 8.75$ (nm).

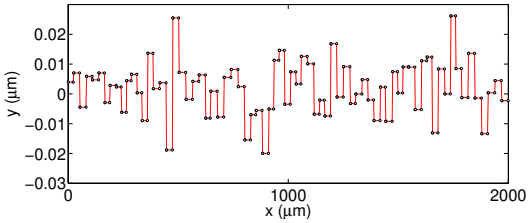

(d) crack distribution #4 ideal roughness (RMS), $R_{q_0} = 8.79$ (nm).

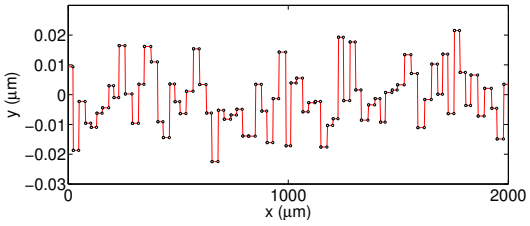

(e) crack distribution #5 ideal roughness (RMS), $R_{q_0} = 9.63$ (nm).

FIGURE 6.12: A set of 5 randomly generated crack distributions. The crack depth-wise spacing is based on a normal distribution with a standard deviation of 10 (nm). The size of cracks is based on a uniform random distribution from $a_{\min} = 20$ (μm) to $a_{\max} = 30$ (μm). The combined fracture length is 90% of the sample length. The crack spacing is uniformly random.

6.4 Simulation results

Thermally induced wafer splitting can be experimentally observed to take place in the depth region close to the maximum density of the highly pressurised micro-cracks since the pressure provides the main driving force for micro-crack growth [5, 233]. Similarly, the mechanically induced wafer splitting can be observed to occur near the depth of the prevailing micro-crack density, since this depth is the weakest location in terms of the fracture toughness of the material [5, 233]. However, in either case, the mean depth of the fracture path and the fracture path deviations about the mean depth can be strongly affected by the process parameters (refer to Section 6.3.5), namely: the relative depths and the mechanical properties of the multi-layer wafer structure, and the geometrical randomness in the micro-crack distribution among other factors, which can lead to large instabilities in the crack propagation path about the mean depth of the micro-crack distribution. The parametric studies are undertaken for the pressure-splitting and mechanical-splitting boundary conditions. The influence of each control parameter is quantified by varying it within its typical range and numerically simulating the process of wafer splitting in order to assess the parameter's influence on the fracture path in terms of the post-split fracture surface roughness. For every parameter instance, 5 representative micro-crack distributions are considered (refer to Tables 6.2 and 6.3) in order to ensure consistency between numerical results and to potentially identify spurious numerical solutions.

6.4.1 Wafer splitting by internal pressure

The numerically computed root-mean-square (RMS) fracture surface roughness R_q of the parametric studies for the pressure splitting boundary conditions are reported by Figures 6.13-6.16. The numerical results appear to agree well with the experimental observations; specifically, the experimentally determined RMS roughness [5] using atomic force microscopy is typically in the range of 5-10 (nm), whereas the numerical results fall between 10 and 16 (nm) for the assumed range of parameter values. Note that the *ideal* RMS of the initial micro-crack distributions are within 9-10 (nm) (refer to Figure 6.12).

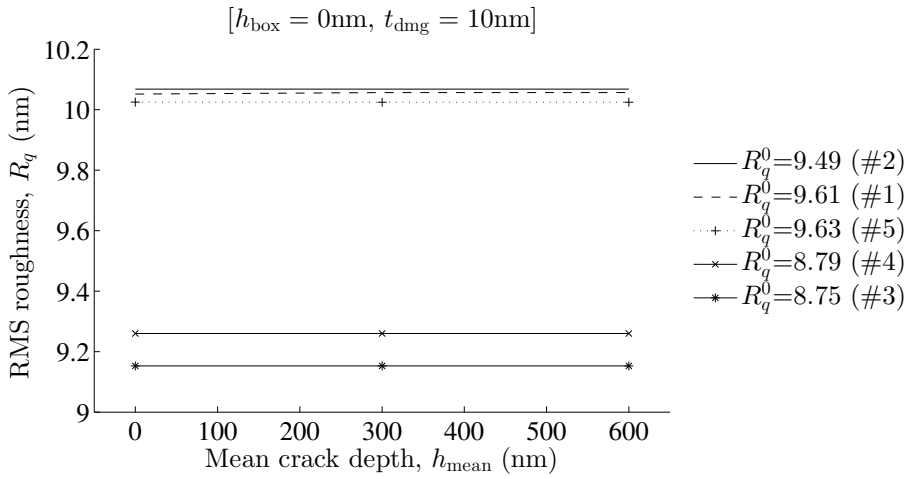

FIGURE 6.13: Post-split fracture roughness (RMS) for different mean-depths of the micro-crack distributions. The buried oxide layer has been omitted.

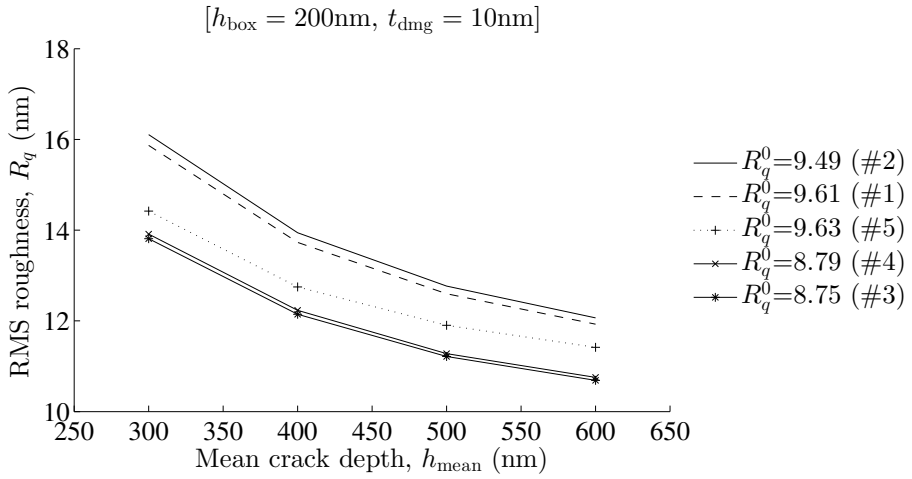

FIGURE 6.14: Post-split fracture roughness (RMS) for different mean-depths of the micro-crack distributions. The buried oxide layer has been included.

6.4.2 Wafer splitting by blade insertion

The numerical results for the post-split fracture surface roughness for the mechanically assisted wafer splitting boundary conditions (assuming zero micro-crack pressure) are presented as follows. Figures 6.17-6.20 report the results for different roughness measures, namely: R_q (RMS), R_t (peak-valley), R_p (peak) and R_v (valley), considering the initial micro-crack distribution thickness t_{dmg} as the free parameter. The case study assumed zero mean micro-crack implantation depth ($h_{\text{mean}} = 0$) and no buried oxide layer ($t_{\text{box}} = 0$). This was the only study for which complete splitting of the wafer sample could be

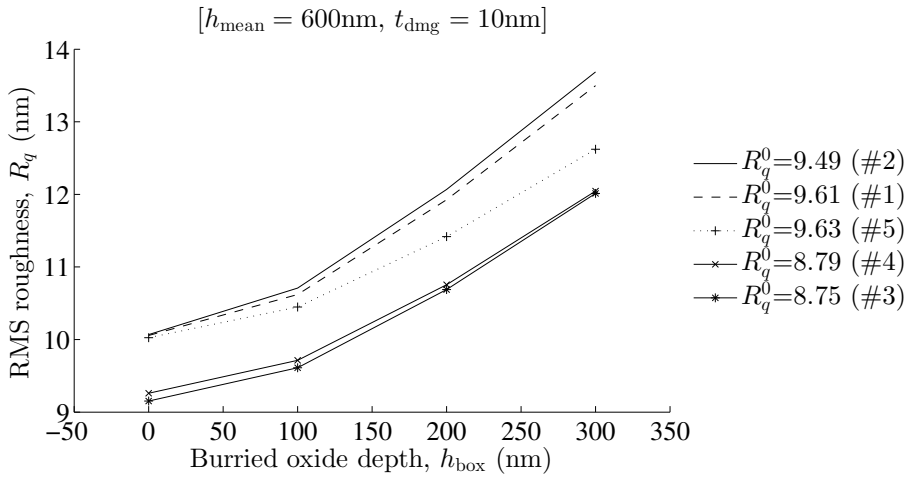

FIGURE 6.15: Post-split fracture roughness (RMS) for different thicknesses of buried oxide layer. Constant mean micro-crack depth is considered.

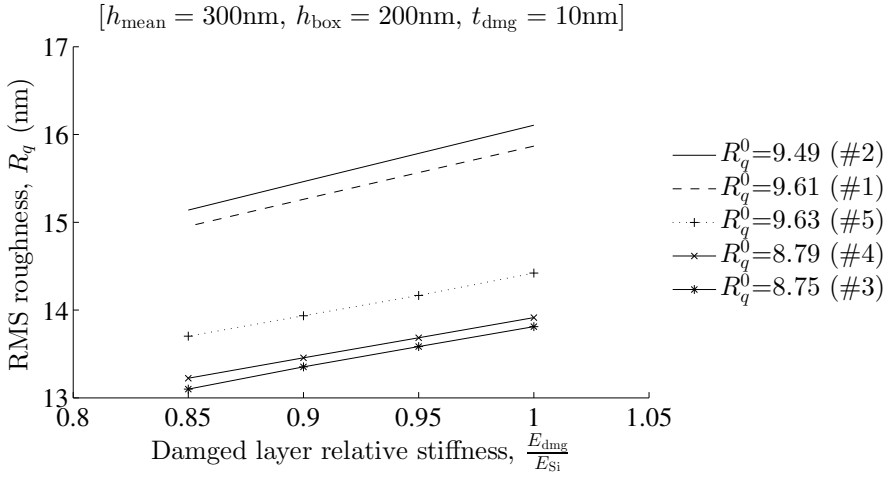

FIGURE 6.16: Post-split fracture roughness (RMS) for different damaged-layer elastic compliances relative the surrounding undamaged silicon. Constant mean micro-crack depth and buried oxide thickness are considered.

obtained. Complete splitting of the wafer sample could not be obtained for all other parametric studies that introduced some form of non-symmetry with respect to the initial mean micro-crack depth. For example, when the buried oxide layer was considered, the fracture paths experienced significant deviations from the initial micro-crack depth towards the oxide layer due to it being elastically more compliant than the surrounding silicon material. Although the micro-cracks naturally provide some stabilisation of the ongoing macro-crack, a micro-crack needs to be sufficiently close to the macro-crack so as to be able to attract it. In other words, a competition exists between the attractive forces of

the micro-cracks and those of the buried oxide layer. Another parametric study for which complete splitting could not be obtained involved the mean initial micro-crack depth parameter h_{mean}. The ongoing macro-crack could not be stabilised by its coalescence with the micro-cracks; hence, the fracture path was found to eventually deflect to the free surface that was closest. The propensity of the fracture path to exhibit such behaviour is common in the splitting of double-cantilever specimens. The mode-I crack growth is inherently unstable in the sense that a small deviation of the crack from the horizontal (mode-I) plane tends to gradually increase with the crack length, e.g. see Figure 5.19.

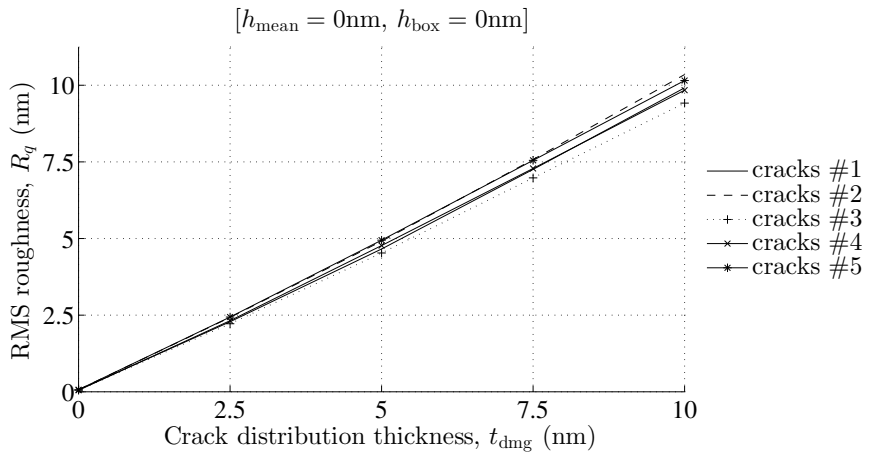

FIGURE 6.17: Post-split fracture roughness (RMS) for different micro-crack distribution thicknesses and blade-splitting BC. The buried oxide layer is omitted. Crack distribution is centred about the mean sample depth.

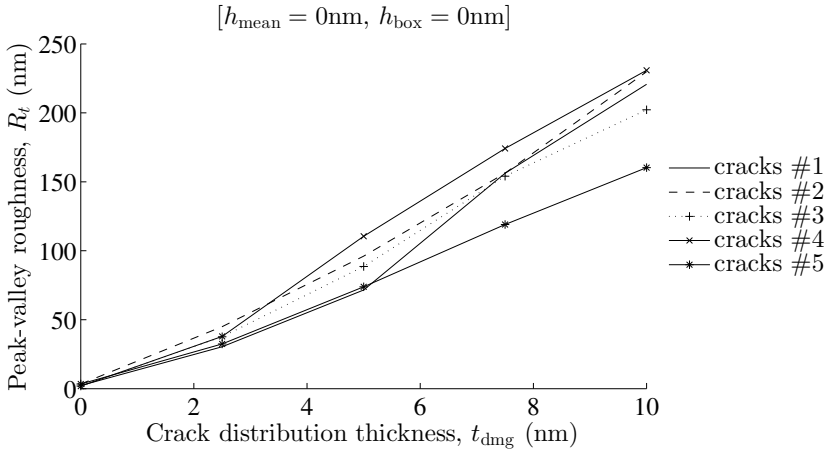

FIGURE 6.18: Post-split fracture roughness (peak-valley) for different micro-crack distribution thicknesses and blade-splitting BC. The buried oxide layer is omitted. Crack distribution is centred at the mean sample depth.

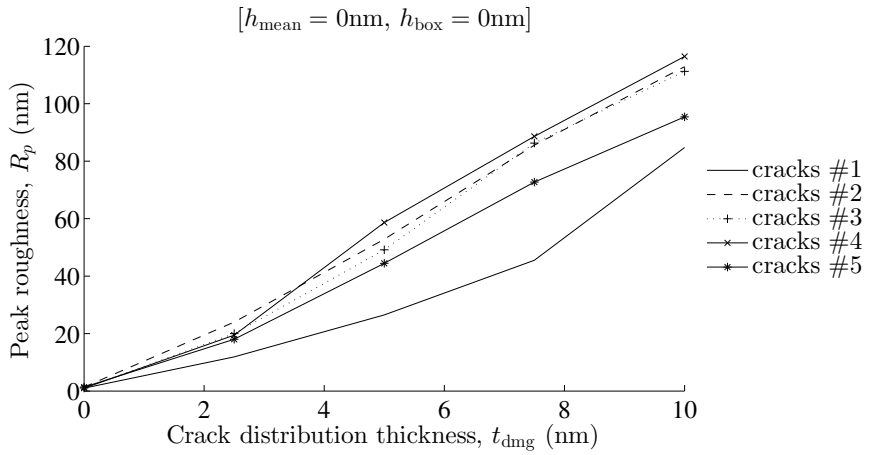

FIGURE 6.19: Post-split fracture roughness (peak) for different micro-crack distribution thicknesses and blade-splitting BC. The buried oxide layer is omitted. Crack distribution is centred at the mean sample depth.

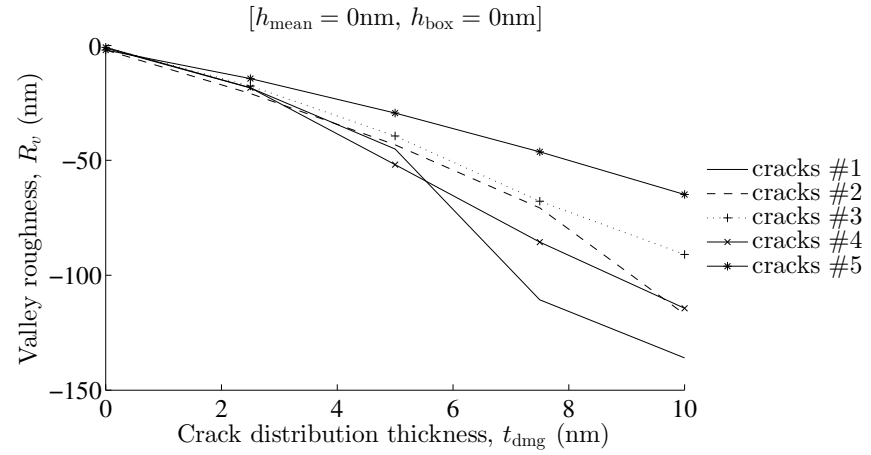

FIGURE 6.20: Post-split fracture roughness (valley) for different micro-crack distribution thicknesses and blade-splitting BC. The buried oxide layer is omitted. Crack distribution is centred about the mean sample depth.

6.5 Summary

For the pressure-splitting boundary conditions, the initial micro-crack depth without the underlying buried oxide layer (BOX) was found to have a negligible influence on the RMS fracture roughness of the post-split surface (Figure 6.13). The loss of symmetry by virtue of the micro-crack distribution appearing slightly above the neutral x-axis of the computational domain did not lead to a noteworthy variation in the cleaved surface roughness. On the other hand, upon inclusion of the BOX, the mean micro-crack

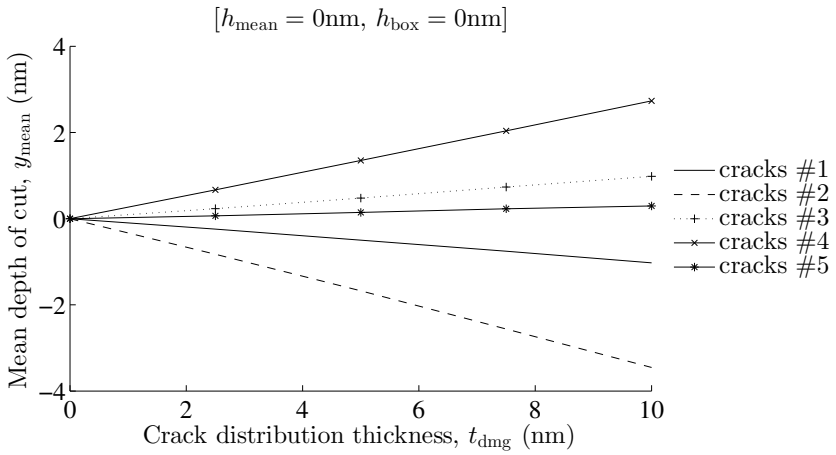

FIGURE 6.21: Depth of ion-cut for different micro-crack distribution thicknesses and blade-splitting BC. The buried oxide layer is omitted. Crack distribution is centred about the mean sample depth.

distribution depth was found to have a strong influence on the fracture path and on the mean depth of splitting (Figure 6.14). In this case, the micro-cracks were attracted by the elastically more compliant BOX. The micro-crack deviations were found to increase with smaller mean depths of the initial micro-crack distributions since the attraction by the BOX was stronger due to its nearer proximity to the micro-cracks. Conversely, when a constant implantation depth was supposed and the BOX depth was varied, the micro-crack deviations increased with deeper BOX (Figure 6.15). Finally, when the damaged zone was considered to have a reduced stiffness (due to the presumed isotropic damage of the Si-lattice by the initial H^+ ion irradiation), the micro-cracks deviated less towards the BOX (Figure 6.16). This result can be attributed to the confinement effect of the more rigid material surrounding the damaged silicon that counteracted the effects of the BOX.

For the mechanically assisted wafer splitting case, complete splitting of the wafer model could be achieved only in the ideally symmetric case where the initial mean micro-crack depth coincided with the neutral x-axis of the computational domain, i.e. $h_{\text{mean}} = 0$, and in the absence of the BOX. The numerical results for the post-split fracture surface roughness as a function of the initial micro-crack distribution thickness t_{dmg} revealed that the micro-crack deviations about the mean micro-crack depth were symmetric with similar deflections above and below h_{mean}, e.g. compare Figure 6.19 with Figure 6.20. The micro-crack deviations increased with larger t_{dmg}, e.g. see Figure 6.17 and Figure 6.18.

Chapter 7

Summary of thesis

7.1 Summary

In Chapter 2, the problem of quasi-static crack growth in a linear-elastic isotropic solid was defined. The static equilibrium equations were posed in a weak-form (2.18). The weak solution for the displacement field minimised the potential energy of the solid (2.23) for a given fracture configuration. The fracture evolution was assumed to obey the principals of linear linear-elastic fracture mechanics. In this case, Griffith's fracture growth criterion was assumed to govern crack growth. Under the assumed quasi-static conditions, the evolution of the cracks and the material needed to be such that the energy dissipation was always maximum (2.43). The principle of global maximality meant that the problem of fracture evolution could be formulated as a total energy (2.49) minimisation (2.50). More specifically, the evolutions of the fractures and the displacement field corresponded to the time-continuous minimisation of this total energy function (2.55). At the instance of competing crack growth, which is characterised by the existence of multiple fracture growth solutions of equivalent energy dissipation rate, the critical solution is one that maximises the rate of the energy dissipation rate (i.e. the curvature of the total energy function) (2.62). This lead to a quadratic constrained optimisation problem for the solution to the competing crack growth problem. Several solution methods were proposed based on the behaviour of the energy function, specifically whether the energy was positive definite, negative definite or indefinite. For the general case, it was suggested to use a gradient based solution approach with multiple trial solutions for increased robustness since other solution methods were only suitable for convex energy functions. Finally, the problem of the crack growth direction was addressed. According to Griffith, a crack extends in the direction where the fracture driving force minus the material's surface energy (i.e. the net dissipation) is maximised (2.93). This condition was reformulated as the fracture extension direction that minimised the total energy function (2.94) or, alternatively, as the direction for which the energy dissipation rate with respect to the angular rotation of the extension vanished (2.96). This condition was referred to as the principle of vanishing rotational energy release rate. The advantage of the reformulation was that it lent itself to a straightforward application to discrete fracture increments.

In Chapter 3, the discrete fracture growth problem was considered. Depending on the curvature of the total energy function, different solution methods were proposed, namely: crack length control, load control, and energy gradient based solution methods. For the general, it was proposed to use the gradient based solution approach for its superior robustness since other methods were extremum-based and, as such, relied on a convex total energy function. In other words, extremum-based solution strategies could fail if the total energy function were non-convex. Concerning competing crack growth, the numerical discretisation based on fixed-length crack tip extensions posed a difficulty in reliably identifying the critical competing crack tips. This was due to the reduced solution search space consisting only of fixed-length crack tip extensions which was found to lead to the miss-identification of the critical crack tips. Since determining the critical tips exactly was key to the success of resolving the competing crack growth problem, it was proposed to approximate the total energy function by a quadratic function using Tailor's expansion and to minimise this approximation with respect to arbitrary crack tip extensions. The approximate solution would then be best-fitted to the discrete framework of fixed-length crack tip extension. This strategy proved to be effective. In Chapter 4, the focus was on an efficient XFEM implementation within the *Matlab* environment. The main challenge was the implementation of an efficient updating routines for the system of equations and keeping track of topological entities describing multiple cracks and their intersections. The proposed implementation enabled multiple overlapping enrichments, enrichment addition and subtraction on the fly and an efficient integration of the domain quantities by tailoring quadrature routines to the individual enrichment functions. The efficient implementation of XFEM proved to be useful in solving larger size fracture problems since the mechanical system could be updated only where it was required. It was found that by far the largest amount of computational time was spent in the solution of the linear system rather than in the assembly of equation and post-processing of the solution. Solution post-processing routines benefited as well since the proposed data structures enabled fast access to relevant quantities instead of having to resort to recomputations on the fly.

The XFEM implementation and the fracture solution by the energy minimisation approach were verified in Chapter 5. It was demonstrated that the minimum energy fracture path

was in a very close agreement to the solution obtained by the maximum stress criterion such that for practical purposes the solution could well be considered the same. This was due to both criteria favouring crack growth directions of diminishing mode-II stress field at the crack tip. The criteria deviated in the crack growth directions under significant mode-II loading conditions; however, by virtue of crack kinking towards the mode-I stress field, the fracture paths were found to inevitably align to the path of local symmetry, i.e. zero mode-II stress field. From multiple numerical test cases, it was found that the stress criterion consistently underestimated the crack kink angle whereas the energy criterion tended to overestimate it as the mesh was refined. Being motivated by these findings, a modified crack growth direction criterion was proposed that assumed the arithmetic average of the crack growth directions obtained by the stress and energy based criteria separately. The average-direction criterion (also referred to as the bi-section criterion) was found to be of practical advantage since fracture solutions saw substantial improvements in accuracy (especially on coarse discretisations) as well as an increased convergence rate with mesh refinement. Some limitations of the proposed criterion were noted. Particularly, the effectiveness of the bi-section criterion reduced for problems consisting of multiple cracks that involved crack intersections. Also, the performance of the criterion diminished for significant mode-II loading conditions. On the other hand, the solution by the bi-section criterion was never outside the zone bounded by the fracture paths determined by the stress and the energy based criteria. Thus, the modified criterion could be effectively used to solve problems of practical interest. To be consistent with Griffith's law, the bi-section criterion may be used only once the critical crack tip extensions have been identified using the energy based approach. The main purpose of the bi-section criterion is to numerically improve the crack growth direction since it does not poses any physical significance.

In Chapter 6, the Smart-Cut™ problem of silicon wafer splitting was addressed. Due to the multi-physics phenomena involved in the wafer splitting process, the simulation of the complete process was not possible. Instead, the focus was centred on one stage of the splitting process that, nonetheless, had a significant effect on the post-split fracture surface properties. This stage is characterised by the time period of 90-99% thermal budged to complete splitting of the wafer. During this time, the micro-cracks are assumed to have

developed in size to several tens of micro-metres in diameter. The fracture growth rate is assumed to be relatively slow and the material behaviour to be essentially brittle such that the main mechanism of internal (elastic) energy dissipation is through fracture surface energy. Under these assumptions, a quasi-static linear-elastic material model was used to simulate brittle fracture process. The aim was to quantify the post-split fracture surface roughness and assess the influence of different process parameters relating to the initial distribution of micro-cracks. For the numerical solution to be computationally viable – owing to the physical size of the problem and the fine-scale resolution of the discretisation that is needed to capture important features of the fracture path – the maximum stress criterion was used. This was considered to be a satisfactory alternative to the energy based approach since the fracture paths by both criteria had been demonstrated in Chapter 5 to converge to virtually the same solutions. The effects of two types of boundary conditions were studied. The first type corresponded to the so-called mechanical splitting case whereby a razor blade was inserted at one end and the second one – the pressure driven splitting case. In the mechanical splitting case, the wafer specimen was modelled as a double cantilever beam with a built-in end at one side and prescribed opening displacements (due to the insertion of a blade) at the other end. For the pressure driven splitting case, a rectangular domain with fixed left and right ends was supposed such that the micro-crack cavity pressure provided the sole driving force for the splitting the wafer sample by causing half of the wafer to pop-off. The pressure and blade splitting boundary conditions were assumed in a set of parametric studies aimed to assess the influence of different Smart-Cut™ process parameters on the post-split fracture roughness. The parametric studies produced results for the post-slit fracture roughness that were reasonable and fell in the experimental range. This finding also served to validate the assumptions of brittle material behaviour, quasi-statics, and linear-elastic fracture mechanics to be the governing factors during the micro-crack evolution stage.

7.2 Contributions

One of the main aims of this work was to apply energy minimisation principles (based on Griffith's crack growth law) in order to robustly model complex multi-crack fracture phenomena within the framework of the extended finite element method. Another aim was to apply the numerical model to simulate the process of Smart-Cut™ silicon wafer splitting in order to assess the influence of different process parameters on the post-split fracture surface roughness. The main outcomes of this work are summarised below:

- A robust approach to determining multiple crack growth solution using the linear-elastic fracture mechanics approach and the principle of minimum total energy within the framework of XFEM for general loading conditions.
- Determination of crack growth direction posed as a principle of vanishing rotational energy release rate of a discrete crack extension. Energy release rates computed algebraically within the XFEM framework, based on the stiffness derivative approach.
- Proposed methods for solving competing crack growth (and when it needs to be solved), both as a rate problem and within a discrete framework. It was shown that solutions were possible even for fixed-length crack tip extensions.
- For the accurate determination of the critical crack tips, it was proposed to solve an "off-line" problem: minimise a quadratic approximation of the total energy function independently of the underlying XFEM discretisation. Subsequently, this "ideal" solution is coarsened to fit the numerical discretisation of XFEM.
- An improved crack growth direction criterion was proposed that offered better accuracy and faster convergence of the fracture solution, especially on coarse discretisations. The criterion was verified against multiple test cases.
- An efficient computer implementation of XFEM within the *Matlab* environment was proposed that lead to significantly improved computational times. Consequently, the largest computational expense was in the solution of the linear system of equations and not in assembly, updating or post-processing of the system.
- Application of the methods to the simulation of silicon wafer cutting. A parametric study was undertaken to quantify the influence of Smart-Cut™ process parameters on the post-split fracture roughness. A reasonable agreement was obtained between the numerical and experimental results.
- Finally, a robust general purpose XFEM code for 2D numerical modelling for multi-crack fracture has been developed in *Matlab* that can be used for future research.

7.3 Recommendations

It is possible to extend the present material model based on linear-elastic fracture mechanics, which is limited by the assumptions of quasi-statics, isotropy, and homogeneity of material, to account for other factors that may play an important part in Smart-Cut™ wafer splitting process. A few simple improvements to the model are put forth.

For the modelling of the silicon wafer splitting process, it is of immediate interest to assess the effects of dynamic crack growth and material anisotropy, among other interests. It is known that the dynamic aspect is important in the final stage of wafer splitting when coalescence of large cracks takes place. The roughness that results from dynamic crack coalescence can be substantial; indeed, the dynamic effect is known to be the cause of some particular defects in the post-split fracture surface, e.g. surface pits. The current crack growth model assumes quasi-statics. In practice, unstable crack growth problems can not be modelled adequately under such assumptions because unstable fracture is inherently catastrophic. Thus, it is important to take into account the inertial effect. In order to include the dynamic aspect of crack growth into the current model, the main requirements are: the computation of the mass matrix and the computations of its derivatives (to determine the rates of energy transfer between internal, kinetic, and fracture surface energies). Within the current implementation this can be achieved straightforwardly by virtue of the well organised data structures: generic equation assemblies and updating, book-keeping of element data (shape function, integration), computation of derivatives, etc. In other words, the changes to the model/code are not challenging from the implementation standpoint because similar computations are already carried out, which serve as templates. Apart from the interest to model dynamic crack propagation, it is also relevant to consider the anisotropic effect of silicon in terms of the elastic properties of the constitutive stress-strain law and the material toughness with respect to different principle planes of silicon. The current model assumes a simplified material, one that is isotropic, homogeneous and of a uniform fracture toughness (both spatially and directionally). Firstly, if anisotropy is to be introduced into the current material model via an appropriate constitutive stress-strain law,

the computations of the rotational energy release rates G_θ using the generalised stiffness-derivative approach will need to take this into account. Specifically, the computations of the stiffness matrix derivatives of the elements in pure (rigid) rotation require that the axis of anisotropy be rotated back to its original orientation. In the numerical implementation, this can be achieved by subtracting the stiffness matrix partial derivative with respect to the variation of the constitutive matrix $\mathbf{C}$. The term to be subtracted from each finite element in pure rotation, reads: $\delta_{\mathbf{C}} K_{\mathrm{e}} = \int_{\Omega_{\mathrm{e}}} \mathbf{B}^{\mathrm{T}} \delta_\theta \mathbf{C} \mathbf{B} \, \mathrm{d}V$, where

$$\delta_\theta \mathbf{C} = \delta_\theta(\mathbf{T}_\sigma^{-1})|_{\theta=0} \, \mathbf{C} \, \mathbf{T}_\varepsilon|_{\theta=0} + \mathbf{T}_\sigma^{-1}|_{\theta=0} \mathbf{C} \, \delta_\theta(\mathbf{T}_\varepsilon)|_{\theta=0} \tag{7.1}$$

and where $\mathbf{T}_\sigma$ and $\mathbf{T}_\varepsilon$ are, respectively, the global-to-local stress and strain transformation matrices, θ is the anti-clockwise rotation angle of the crack tip increment, and $\mathbf{C}$ is the anisotropic constitutive stress-strain matrix. Alternatively, the derivatives of the element stiffness matrix can be computed by performing geometrical differentiation of the rigid elements, which is analogous in principle to the differentiation of the elements undergoing shape distortion (Figure 4.3), though this procedure is likely to be computationally more expensive. Concerning the anisotropic effect due to the direction-dependent fracture toughness, the energy minimisation approach can take this into account by introducing the fracture toughness (or, the critical energy release rate) as a function of crack growth angle. This will likely require a regularisation technique to be used in order to describe the critical energy release rate sufficiently smoothly with respect to the fracture growth angle. In this case, the criterion for the fracture extension direction is posed as the vanishing rotational dissipation, i.e. $\mathcal{D}_\theta = 0$ where $\mathcal{D}_\theta \equiv -\partial\Pi/\partial\theta|_{\Delta\ell} - \mathrm{d}G_{\mathrm{c}}/\mathrm{d}\theta \cdot \Delta\ell$.

There are also many other important modelling considerations with regard to the Smart-Cut™ wafer splitting process. A few future work directions are pointed out as follows: (1) to investigate the effect of imperfect wafer bonding and the resulting lack of stiffness and local stress field variations on the fracture paths, (2) to model the diffusion of hydrogen into micro-cracks so as to determine the actual gas pressure within cavities, (3) to consider the effect of the micro-crack/defect distribution in the irradiation damaged silicon layer on the evolution of the macro-cracks by using a suitable multi-scale approach.

Appendix A

Algorithms

A.1 Competing crack growth solution: a strictly stable fracture front

Algorithm 1 Compute $\dot{a} = \arg\max_{v \in \mathcal{A}} \left(\frac{1}{2} v^{\mathrm{T}} H_s v\right)$,
subject to the constraints: $\|\dot{a}\|_1 - 1 = 0$ and $\dot{a}_i \geq 0$, and
where $H_s^* = \left(I - \frac{\mathbf{e}^{\mathrm{T}}\mathbf{e}}{\mathbf{e}\mathbf{e}^{\mathrm{T}}}\right) H_s \left(I - \frac{\mathbf{e}^{\mathrm{T}}\mathbf{e}}{\mathbf{e}\mathbf{e}^{\mathrm{T}}}\right)$ is negative semidefinite.

Require: $\sum \dot{a}_i = 1$ and $\dot{a}_i \geq 0$ for $i \in \mathcal{I}_{\mathrm{crit}}$ {feasible initial guess}
  $n \leftarrow |\mathcal{I}_{\mathrm{crit}}|$ {get size of set of critical crack tips}
  $d \leftarrow \mathrm{zeros}(n, 1)$ {initialize fracture advance direction}
  $e \leftarrow \mathrm{ones}(n, 1)$ {gradient of the equality-constraint equation}
  $p \leftarrow \mathrm{true}(n, 1)$ {logical form of the working set}
  while 1 **do**
    $\dot{a}_0 \leftarrow \dot{a}$ {store current solution as reference}
    while 1 **do**
      $d[p] \leftarrow \frac{H_s[p,p]^{-1} e[p]}{e[p]^{\mathrm{T}} H_s[p,p]^{-1} e[p]} - \dot{a}[p]$ {trial advance satisfying $\sum_{i=1}^{n} d[i] = 0$}
      $q \leftarrow \mathrm{and}(d < 0, \dot{a} < \mathrm{tol})$ {get infeasible points}
      if $\mathrm{any}(q = \mathbf{true})$ **then**
        $d[q] \leftarrow 0$ {discard all infeasible points}
        $p[q] \leftarrow 0$ {update working set}
      else
        break {working set is feasible}
      end if
    end while
    $q \leftarrow \mathrm{and}(d < 0, \dot{a} > 0)$ {get imminent constraints}
    $w \leftarrow \min\left(\left\{\frac{\dot{a}[q]}{-d[q]}, 1\right\}\right)$ {projection weight factor}
    $\dot{a} \leftarrow \dot{a} + wd$ {update previous solution}
    if $\mathrm{or}(1 - w < \mathrm{tol}, \|\dot{a} - \dot{a}_0\| < \mathrm{tol})$ **then**
      break {solution converged}
    end if
  end while
  return $\dot{a}$

A.2 Competing crack growth solution: a partially (un)stable fracture front

Algorithm 2 Compute $\dot{a} = \arg\max_{v \in \mathcal{A}} \left(\frac{1}{2} v^{\mathrm{T}} H_s v\right)$,
subject to the constraints: $\|\dot{a}\|_1 - 1 = 0$ and $\dot{a}_i \geq 0$, and
where $H_s^* = \left(I - \frac{\mathbf{e}^{\mathrm{T}}\mathbf{e}}{\mathbf{e}\,\mathbf{e}^{\mathrm{T}}}\right) H_s \left(I - \frac{\mathbf{e}^{\mathrm{T}}\mathbf{e}}{\mathbf{e}\,\mathbf{e}^{\mathrm{T}}}\right)$ is positive semidefinite.

Require: $\sum \dot{a}_i = 1$ and $\dot{a}_i \geq 0$ for $i \in \mathcal{I}_{\mathrm{crit}}$ {feasible initial guess}
  $n \leftarrow |\mathcal{I}_{\mathrm{crit}}|$ {get size of set of critical crack tips}
  $e \leftarrow \mathrm{ones}(n, 1)$ {gradient of the equality-constraint}
  $\dot{a}_{\mathrm{all}} \leftarrow \mathrm{zeros}(n, n)$ {for storing all converged solutions}
  $\Psi_{\mathrm{all}} \leftarrow \mathrm{zeros}(n, 1)$ {for storing objective function values}
  for $i = 1$ **to** n **do**
    $\dot{a} \leftarrow \mathrm{zeros}(n, 1)$
    $\dot{a}[i] \leftarrow 1$ {trial}
    while 1 **do**
      $\dot{a}_0 \leftarrow \dot{a}$ {store current solution as reference}
      $g \leftarrow H_s a$ {gradient of the objective function}
      $d \leftarrow \mathrm{zeros}(n, 1)$ {initialize fracture advance vector}
      $p \leftarrow \mathrm{true}(n, 1)$ {logical form of the working set}
      while 1 **do**
        $d[p] \leftarrow g[p] - \mathrm{mean}(g[p])$ {steepest gradient advance satisfying $\sum_{i=1}^{n} d[i] = 0$}
        $q \leftarrow \mathrm{and}(d < 0, \dot{a} < \mathrm{tol})$ {get infeasible points}
        if $\mathrm{any}(q = \mathbf{true})$ **then**
          $d[q] \leftarrow 0$ {discard all infeasible points}
          $p[q] \leftarrow 0$ {update working set}
        else
          break {working set is feasible}
        end if
      end while
      $q \leftarrow \mathrm{and}(d < 0, \dot{a} > 0)$ {get imminent constraints}
      $w \leftarrow \min\left(\left\{\frac{\dot{a}[q]}{-d[q]}\right\}\right)$ {projection weight factor}
      if $d^{\mathrm{T}} H_s d < 0$ **then**
        {objective function is concave along d as projected from a}
        $w \leftarrow \min\left(w, \frac{d^{\mathrm{T}} H_s a}{d^{\mathrm{T}} H_s d}\right)$ {use the optimum weight factor if possible}
      end if
      $\dot{a} \leftarrow \dot{a} + wd$ {update previous solution}
      if $\|\dot{a} - \dot{a}_0\| < \mathrm{tol}$ **then**
        break {solution converged}
      end if
    end while
    $\dot{a}_{\mathrm{all}}[:, i] \leftarrow \dot{a}$
    $\Psi_{\mathrm{all}}[i] \leftarrow \frac{1}{2} \dot{a}^{\mathrm{T}} H_s \dot{a}$
  end for
  $i_{\max} \leftarrow \mathrm{find}(\Psi = \max(\Psi_{\mathrm{all}}))$
  return $\dot{a} \leftarrow \dot{a}_{\mathrm{all}}[:, i_{\max}]$

Bibliography

[1] E ASTM. "813-81, Standard Test Method for JIc, a Measure of Fracture Toughness". In: *West Conshohocken, PA: American Society for Testing and Materials* (1981).

[2] S. Abbas, A. Alizada, and T. P. Fries. "The XFEM for high-gradient solutions in convection-dominated problems". In: *International Journal for Numerical Methods in Engineering* 82.8 (2009), pp. 1044–1072. ISSN: 00295981. DOI: 10.1002/nme.2815.

[3] Y. Abdelaziz and A. Hamouine. "A survey of the extended finite element". In: *Computers & Structures* 86.11-12 (2008), pp. 1141–1151. ISSN: 00457949. DOI: 10.1016/j.compstruc.2007.11.001.

[4] F. F. Abraham, D. Brodbeck, W. E. Rudge, and X. Xu. "A molecular dynamics investigation of rapid fracture mechanics". In: *Journal of the Mechanics and Physics of Solids* 45.9 (1997), pp. 1595–1619. ISSN: 00225096. DOI: 10.1016/S0022-5096(96)00103-2.

[5] P. E. Acosta Alba. "Influence of Smart CutâĎć technological steps on thickness uniformity of SOI wafers: Multi-Scale approach." PhD Thesis. Université Toulouse III, Paul Sabatier, 2014.

[6] S. H. Advani and J. K. Lee. "Finite Element Model Simulations Associated With Hydraulic Fracturing". In: *Society of Petroleum Engineers Journal* 22.02 (1982), pp. 209–218. ISSN: 01977520. DOI: http://dx.doi.org/10.2118/8941-PA.

[7] K. Agathos, E. Chatzi, and S. P. A. Bordas. "Stable 3D extended finite elements with higher order enrichment for accurate non planar fracture". In: *Computer Methods in Applied Mechanics and Engineering* 306.October 2015 (2016), pp. 19–46. ISSN: 00457825. DOI: 10.1016/j.cma.2016.03.023.

[8] K. Agathos, E. Chatzi, S. P. A. Bordas, and D. Talaslidis. "A well-conditioned and optimally convergent XFEM for 3D linear elastic fracture". In: *International Journal for Numerical Methods in Engineering* 105.9 (2016), pp. 643–677. ISSN: 00295981. DOI: 10.1002/nme.4982.

[9] G. Alfano and M. A. Crisfield. "Finite element interface models for the delamination analysis of laminated composites: mechanical and computational issues". In: *International Journal for Numerical Methods in Engineering* 50.7 (2001), pp. 1701–1736. ISSN: 0029-5981. DOI: 10.1002/nme.93.

[10] M. Ambati, T. Gerasimov, and L. De Lorenzis. "A review on phase-field models of brittle fracture and a new fast hybrid formulation". In: *Computational Mechanics* 55.2 (2015), pp. 383–405. ISSN: 0178-7675. DOI: 10.1007/s00466-014-1109-y.

[11] M. Amestoy and J. B. Leblond. "Crack paths in plane situationsâĂŤII. Detailed form of the expansion of the stress intensity factors". In: *International Journal of Solids and Structures* 29.4 (1992), pp. 465–501. ISSN: 00207683. DOI: 10.1016/0020-7683(92)90210-K.

[12] T. L. Anderson. *Fracture Mechanics: Fundamentals and Applications*. Third Edit. Boca Raton: CRC Press, 2005. ISBN: 978-1-4200-5821-5.

[13] I. Anjam and J. Valdman. "Fast MATLAB assembly of FEM matrices in 2D and 3D: Edge elements". In: *Applied Mathematics and Computation* 267.13 (2015), pp. 252–263. ISSN: 00963003. DOI: 10.1016/j.amc.2015.03.105. arXiv: arXiv:1409.4618v1.

[14] M. P. Areias and T. Belytschko. "Analysis of three-dimensional crack initiation and propagation using the extended finite element method". In: *International Journal for Numerical Methods in Engineering* 63.5 (2005), pp. 760–788. ISSN: 0029-5981. DOI: 10.1002/nme.1305.

[15] B. Aspar et al. "Basic mechanisms involved in the Smart-Cut® process". In: *Microelectronic Engineering* 36.1-4 (1997), pp. 233–240. ISSN: 01679317. DOI: 10.1016/S0167-9317(97)00055-5.

[16] H. Awaji and S. Sato. "Combined Mode Fracture Toughness Measurement by the Disk Test". In: *Journal of Engineering Materials and Technology* 100.2 (1978), p. 175. ISSN: 00944289. DOI: 10.1115/1.3443468.

[17] I. Babuška and B. Q. Guo. "The h, p and h-p version of the finite element method; basis theory and applications". In: *Advances in Engineering Software* 15.3-4 (1992), pp. 159–174. ISSN: 09659978. DOI: 10.1016/0965-9978(92)90097-Y.

[18] G. Baker. "Thermodynamics in solid mechanics: a commentary". In: *Philosophical Transactions of the Royal Society A: Mathematical, Physical and Engineering Sciences* 363.1836 (2005), pp. 2465–2477. ISSN: 1364-503X. DOI: 10.1098/rsta.2005.1669.

[19] G. I. Barenblatt. "The Mathematical Theory of Equilibrium Cracks in Brittle Fracture". In: *Advances in Applied Mechanics*. 7. 1962, pp. 55–129. ISBN: 0065-2156. DOI: 10.1016/S0065-2156(08)70121-2.

[20] G. Barenblatt. "The formation of equilibrium cracks during brittle fracture. General ideas and hypotheses. Axially-symmetric cracks". In: *Journal of Applied Mathematics and Mechanics* 23.3 (1959), pp. 622–636. ISSN: 00218928. DOI: 10.1016/0021-8928(59)90157-1.

[21] R. S. Barsoum. "On the use of isoparametric finite elements in linear fracture mechanics". In: *International Journal for Numerical Methods in Engineering* 10.1 (1976), pp. 25–37. ISSN: 0029-5981. DOI: 10.1002/nme.1620100103.

[22] R. S. Barsoum. "Triangular quarter-point elements as elastic and perfectly-plastic crack tip elements". In: *International Journal for Numerical Methods in Engineering*

11.1 (1977), pp. 85–98. ISSN: 0029-5981. DOI: 10.1002/nme.1620110109. arXiv: arXiv:1011.1669v3.

[23] Z. P. BazÌŇant and G. Pijaudier-Cabot. "Nonlocal Continuum Damage, Localization Instability and Convergence". In: *Journal of Applied Mechanics* 55.2 (1988), p. 287. ISSN: 00218936. DOI: 10.1115/1.3173674.

[24] E. Béchet, H. Minnebo, N. Moës, and B. Burgardt. "Improved implementation and robustness study of the X-FEM for stress analysis around cracks". In: *International Journal for Numerical Methods in Engineering* 64.8 (2005), pp. 1033–1056. ISSN: 0029-5981. DOI: 10.1002/nme.1386.

[25] J. Begley and J. Landes. *The J integral as a fracture criterion*. Tech. rep. West Conshohocken: American Society for Testing and Materials, 1972, pp. 1–23. DOI: 10.1520/STP514-EB.

[26] T. Belytschko, Y. Y. Lu, and L. Gu. "Element-free Galerkin methods". In: *International Journal for Numerical Methods in Engineering* 37.2 (1994), pp. 229–256. ISSN: 0029-5981. DOI: 10.1002/nme.1620370205.

[27] T. Belytschko, N. Moës, S. Usui, and C. Parimi. "Arbitrary discontinuities in finite elements". In: *International Journal for Numerical Methods in Engineering* 50.4 (2001), pp. 993–1013. ISSN: 0029-5981. DOI: 10.1002/1097-0207(20010210)50:4<993::AID-NME164>3.0.CO;2-M.

[28] T. Belytschko, Y. Y. Lu, L. Gu, and M. Tabbara. "Element-free galerkin methods for static and dynamic fracture". In: *International Journal of Solids and Structures* 32.17-18 (1995), pp. 2547–2570. ISSN: 00207683. DOI: 10.1016/0020-7683(94)00282-2.

[29] T. Belytschko et al. "Meshless methods: An overview and recent developments". In: *Computer Methods in Applied Mechanics and Engineering* 139.1 (1996), pp. 3–47. ISSN: 00457825. DOI: 10.1016/S0045-7825(96)01078-X.

[30] T. Belytschko and T. Black. "Elastic crack growth in finite elements with minimal remeshing". In: *International Journal for Numerical Methods in Engineering* 45.5 (1999), pp. 601–620. ISSN: 0029-5981. DOI: 10.1002/(SICI)1097-0207(19990620)45:5<601::AID-NME598>3.0.CO;2-S.

[31] T. Belytschko, R. Gracie, and G. Ventura. "A review of extended/generalized finite element methods for material modeling". In: *Modelling and Simulation in Materials Science and Engineering* 17.4 (2009), p. 043001. ISSN: 0965-0393. DOI: 10.1088/0965-0393/17/4/043001.

[32] T. Belytschko and M. Tabbara. "Dynamic fracture using element-free Galerkin methods". In: *International Journal for Numerical Methods in Engineering* 39.6 (1996), pp. 923–938. ISSN: 0029-5981. DOI: 10.1002/(SICI)1097-0207(19960330)39:6<923::AID-NME887>3.0.CO;2-W.

[33] T. Belytschko, W. K. Liu, B. Moran, and K. I. Elkhodary. *Nonlinear Finite Elements for Continua and Structures*. Vol. 104. 1. John Wiley & Sons, Ltd, 2014, pp. 1–8. ISBN: 0122030532. DOI: 10.1016/S0065-230X(09)04001-9.

[34] E. Benvenuti, A. Tralli, and G. Ventura. "A regularized XFEM model for the transition from continuous to discontinuous displacements". In: *International Journal for Numerical Methods in Engineering* 74.6 (2008), pp. 911–944. ISSN: 00295981. DOI: 10.1002/nme.2196.

[35] L. Berger-Vergiat et al. "Inexact Schwarz-algebraic multigrid preconditioners for crack problems modeled by extended finite element methods". In: *International Journal for Numerical Methods in Engineering* 90.3 (2012), pp. 311–328. ISSN: 00295981. DOI: 10.1002/nme.3318. arXiv: 1010.1724.

[36] P. E. Bernard, N. Moës, and N. Chevaugeon. "Damage growth modeling using the Thick Level Set (TLS) approach: Efficient discretization for quasi-static loadings". In: *Computer Methods in Applied Mechanics and Engineering* 233-236 (2012), pp. 11–27. ISSN: 00457825. DOI: 10.1016/j.cma.2012.02.020.

[37] S. P. A. Bordas and B. Moran. "Enriched finite elements and level sets for damage tolerance assessment of complex structures". In: *Engineering Fracture Mechanics* 73.9 (2006), pp. 1176–1201. ISSN: 00137944. DOI: 10.1016/j.engfracmech.2006.01.006.

[38] S. P. A. Bordas et al. "An extended finite element library". In: *International Journal for Numerical Methods in Engineering* 71.6 (2007), pp. 703–732. ISSN: 00295981. DOI: 10.1002/nme.1966.

[39] M. J. Borden et al. "A phase-field description of dynamic brittle fracture". In: *Computer Methods in Applied Mechanics and Engineering* 217-220.2012 (2012), pp. 77–95. ISSN: 00457825. DOI: 10.1016/j.cma.2012.01.008.

[40] P. Bouchard, F. Bay, and Y. Chastel. "Numerical modelling of crack propagation: automatic remeshing and comparison of different criteria". In: *Computer Methods in Applied Mechanics and Engineering* 192.35-36 (2003), pp. 3887–3908. ISSN: 00457825. DOI: 10.1016/S0045-7825(03)00391-8.

[41] P. Bouchard, F. Bay, Y. Chastel, and I. Tovena. "Crack propagation modelling using an advanced remeshing technique". In: *Computer Methods in Applied Mechanics and Engineering* 189.3 (2000), pp. 723–742. ISSN: 00457825. DOI: 10.1016/S0045-7825(99)00324-2.

[42] B. Bourdin, G. A. Francfort, and J. J. Marigo. "Numerical experiments in revisited brittle fracture". In: *Journal of the Mechanics and Physics of Solids* 48.4 (2000), pp. 797–826. ISSN: 00225096. DOI: 10.1016/S0022-5096(99)00028-9.

[43] B. Bourdin, G. A. Francfort, and J. J. Marigo. "The Variational Approach to Fracture". In: *Journal of Elasticity* 91.1-3 (2008), pp. 5–148. ISSN: 0374-3535. DOI: 10.1007/s10659-007-9107-3.

[44] W. F. Brace and E. G. Bombolakis. "A note on brittle crack growth in compression". In: *Journal of Geophysical Research* 68.12 (1963), pp. 3709–3713. ISSN: 01480227. DOI: 10.1029/JZ068i012p03709.

[45] C. A. Brebbia, J. C. F. Telles, and L. Wrobel. *Boundary element techniques: theory and applications in engineering*. Springer Science & Business Media, 2012.

[46] S. C. Brenner and L. R. Scott. *The Mathematical Theory of Finite Element Methods*. Ed. by L. R. Scott. 3rd ed. Vol. 15. Texts in Applied Mathematics. New York, NY: Springer New York, 2008. ISBN: 978-0-387-75933-3. DOI: 10.1007/978-0-387-75934-0.

[47] M. Bruel. "Silicon on insulator material technology". In: *Electronics letters* 31.14 (1995), pp. 1201–1202.

[48] M. Bruel. "Application of hydrogen ion beams to Silicon On Insulator material technology". In: *Nuclear Instruments and Methods in Physics Research Section B: Beam Interactions with Materials and Atoms* 108.3 (1996), pp. 313–319. ISSN: 0168583X. DOI: 10.1016/0168-583X(95)01056-4.

[49] M. Bruel. "The History, Physics, and Applications of the Smart-Cut® Process". In: *MRS Bulletin* 23.12 (1998), pp. 35–39. ISSN: 0883-7694. DOI: 10.1557/S088376940002981X.

[50] E. Budyn, G. Zi, N. Moës, and T. Belytschko. "A method for multiple crack growth in brittle materials without remeshing". In: *International Journal for Numerical Methods in Engineering* 61.10 (2004), pp. 1741–1770. ISSN: 0029-5981. DOI: 10.1002/nme.1130.

[51] M. Buliga. "Energy Minimization Brittle Crack Propagation". In: *Journal of Elasticity* 52.3 (1998), pp. 201–238. ISSN: 03743535. DOI: 10.1023/A:1007545213010.

[52] G. Celler and M. Wolf. *What is Smart Cut?* Tech. rep. July 2003. 2004, p. 8.

[53] A. Chambolle, G. A. Francfort, and J. J. Marigo. "When and how do cracks propagate?" In: *Journal of the Mechanics and Physics of Solids* 57.9 (2009), pp. 1614–1622. ISSN: 00225096. DOI: 10.1016/j.jmps.2009.05.009.

[54] R. J. Charles. "Static Fatigue of Glass. II". In: *Journal of Applied Physics* 29.11 (1958), p. 1554. ISSN: 00218979. DOI: 10.1063/1.1722992.

[55] R. J. Charles. "Static fatigue of glass. I". In: *Journal of Applied Physics* 29.11 (1958), pp. 1554–1560. ISSN: 00218979. DOI: 10.1063/1.1722992.

[56] G. Cherepanov. "Cracks in solids". In: *International Journal of Solids and Structures* 4.8 (1968), pp. 811–831. ISSN: 00207683. DOI: 10.1016/0020-7683(68)90059-0.

[57] J. Chessa and T. Belytschko. "Arbitrary discontinuities in space-time finite elements by level sets and X-FEM". In: *International Journal for Numerical Methods in Engineering* 61.15 (2004), pp. 2595–2614. ISSN: 0029-5981. DOI: 10.1002/nme.1155.

[58] J. Chessa, P. Smolinski, and T. Belytschko. "The extended finite element method (XFEM) for solidification problems". In: *International Journal for Numerical Methods in Engineering* 53.8 (2002), pp. 1959–1977. ISSN: 0029-5981. DOI: 10.1002/nme.386.

[59] J. Chessa, H. Wang, and T. Belytschko. "On the construction of blending elements for local partition of unity enriched finite elements". In: *International Journal for Numerical Methods in Engineering* 57.7 (2003), pp. 1015–1038. ISSN: 0029-5981. DOI: 10.1002/nme.777.

[60] D. L. Chopp and N. Sukumar. "Fatigue crack propagation of multiple coplanar cracks with the coupled extended finite element/fast marching method". In: *International Journal of Engineering Science* 41.8 (2003), pp. 845–869. ISSN: 00207225. DOI: 10.1016/S0020-7225(02)00322-1.

[61] A. P. Cisilino and M. H. Aliabadi. "Three-dimensional boundary element analysis of fatigue crack growth in linear and non-linear fracture problems". In: *Engineering Fracture Mechanics* 63.6 (1999), pp. 713–733. ISSN: 00137944. DOI: 10.1016/S0013-7944(99)00047-8.

[62] C. Daux et al. "Arbitrary branched and intersecting cracks with the extended finite element method". In: *International Journal for Numerical Methods in Engineering* 48.12 (2000), pp. 1741–1760. ISSN: 0029-5981. DOI: 10.1002/1097-0207(20000830)48:12<1741::AID-NME956>3.0.CO;2-L.

[63] B. R. Davis, P. A. Wawrzynek, and A. R. Ingraffea. "3-D simulation of arbitrary crack growth using an energy-based formulation - Part I: Planar growth". In: *Engineering Fracture Mechanics* 115 (2014), pp. 204–220. ISSN: 00137944. DOI: http://dx.doi.org/10.1016/j.engfracmech.2013.11.005.

[64] B. R. Davis, P. A. Wawrzynek, and A. R. Ingraffea. "Simulation of Arbitrary Mixed-Mode Crack Growth Using an Energy-Based Approach". In: ed. by J. Carroll and S. Daly. Cham: Springer International Publishing, 2015. Chap. Simulation, pp. 1–9. ISBN: 978-3-319-06977-7. DOI: 10.1007/978-3-319-06977-7_1.

[65] R. DeBorst. "Fracture in quasi-brittle materials: a review of continuum damage-based approaches". In: *Engineering Fracture Mechanics* 69.2002 (2002), pp. 95–112. ISSN: 00137944. DOI: 10.1016/S0013-7944(01)00082-0.

[66] G. Del Piero, G. Lancioni, and R. March. "A variational model for fracture mechanics: Numerical experiments". In: *Journal of the Mechanics and Physics of Solids* 55.12 (2007), pp. 2513–2537. ISSN: 00225096. DOI: 10.1016/j.jmps.2007.04.011.

[67] C. A. Duarte and J. T. Oden. "An h-p adaptive method using clouds". In: *Computer Methods in Applied Mechanics and Engineering* 139.1-4 (1996), pp. 237–262. ISSN: 00457825. DOI: 10.1016/S0045-7825(96)01085-7.

[68] C. A. Duarte and J. T. Oden. "h-p Clouds âĂŤ An h-p meshless method". In: *Numerical Methods for Partial Differential Equations* 12.6 (1996), pp. 673–705. ISSN: 0749-159X. DOI: 10.1002/(SICI)1098-2426(199611)12:6<673::AID-NUM3>3.0.CO;2-P.

[69] C. Duarte, I. Babuška, and J. Oden. "Generalized finite element methods for three-dimensional structural mechanics problems". In: *Computers & Structures* 77.2 (2000), pp. 215–232. ISSN: 00457949. DOI: 10.1016/S0045-7949(99)00211-4.

[70] R. Duddu, S. Bordas, D. Chopp, and B. Moran. "A combined extended finite element and level set method for biofilm growth". In: *International Journal for Numerical Methods in Engineering* 74.5 (2008), pp. 848–870. ISSN: 00295981. DOI: 10.1002/nme.2200. arXiv: 1010.1724.

[71] M. G. Duffy. "Quadrature Over a Pyramid or Cube of Integrands with a Singularity at a Vertex". In: *SIAM Journal on Numerical Analysis* 19.6 (1982), pp. 1260–1262. ISSN: 0036-1429. DOI: 10.1137/0719090.

[72] M. Duflot. "A study of the representation of cracks with level sets". In: *International Journal for Numerical Methods in Engineering* 70.11 (2007), pp. 1261–1302. ISSN: 00295981. DOI: 10.1002/nme.1915.

[73] D. Dugdale. "Yielding of steel sheets containing slits". In: *Journal of the Mechanics and Physics of Solids* 8.2 (1960), pp. 100–104. ISSN: 00225096. DOI: 10.1016/0022-5096(60)90013-2.

[74] P. Dumstorff and G. Meschke. "Crack propagation criteria in the framework of X-FEM-based structural analyses". In: *International Journal for Numerical and Analytical Methods in Geomechanics* 31.2 (2007), pp. 239–259. ISSN: 03639061. DOI: 10.1002/nag.560.

[75] F. Erdogan and G. C. Sih. "On the Crack Extension in Plates Under Plane Loading and Transverse Shear". In: *Journal of Basic Engineering* 85.4 (1963), p. 519. ISSN: 00219223. DOI: 10.1115/1.3656897.

[76] F. Ericson, S. Johansson, and J.-Å. Schweitz. "Hardness and fracture toughness of semiconducting materials studied by indentation and erosion techniques". In: *Materials Science and Engineering: A* 105-106.PART 1 (1988), pp. 131–141. ISSN: 09215093. DOI: 10.1016/0025-5416(88)90489-2.

[77] J. Eshelby. "The Continuum Theory of Lattice Defects". In: 1956, pp. 79–144. DOI: 10.1016/S0081-1947(08)60132-0.

[78] H. D. Espinosa and P. D. Zavattieri. "A grain level model for the study of failure initiation and evolution in polycrystalline brittle materials. Part I: Theory and numerical implementation". In: *Mechanics of Materials* 35.3-6 (2003), pp. 333–364. ISSN: 01676636. DOI: 10.1016/S0167-6636(02)00285-5.

[79] H. D. Espinosa and P. D. Zavattieri. "A grain level model for the study of failure initiation and evolution in polycrystalline brittle materials. Part II: Numerical examples". In: *Mechanics of Materials* 35.3-6 (2003), pp. 365–394. ISSN: 01676636. DOI: 10.1016/S0167-6636(02)00287-9.

[80] F. Fantoni. "Fracture growth in brittle and embrittled materials: variational formulations and crack tracking algorithms". Mathematical Methods and Models for Engineering. Universita Degli Studi Di Brescia, 2016.

[81] X. Q. Feng and Y. Huang. "Mechanics of Smart-Cut® technology". In: *International Journal of Solids and Structures* 41.16-17 (2004), pp. 4299–4320. ISSN: 00207683. DOI: 10.1016/j.ijsolstr.2004.02.054.

[82] X. Q. Feng, M. Xu, X. Wang, and B. Gu. "Fracture mechanics analysis of three-dimensional ion cut technology". In: *Journal of Mechanics of Materials and Structures* 2.9 (2007), pp. 1831–1852. ISSN: 1559-3959. DOI: 10.2140/jomms.2007.2.1831.

[83] M. Fleming and Y. A. Chu. "Enriched element-free Galerkin methods for crack tip fields". In: *International Journal for Numerical Methods in Engineering* 40.January 1996 (1997), pp. 1483–1504.

[84] G. Francfort and J.-J. Marigo. "Revisiting brittle fracture as an energy minimization problem". In: *Journal of the Mechanics and Physics of Solids* 46.8 (1998), pp. 1319–1342. ISSN: 00225096. DOI: 10.1016/S0022-5096(98)00034-9.

[85] G. A. Francfort and A. Garroni. "A Variational View of Partial Brittle Damage Evolution". In: *Archive for Rational Mechanics and Analysis* 182.1 (2006), pp. 125–152. ISSN: 0003-9527. DOI: 10.1007/s00205-006-0426-5.

[86] M. Frémond and B. Nedjar. "Damage, gradient of damage and principle of virtual power". In: *International Journal of Solids and Structures* 33.8 (1996), pp. 1083–1103. ISSN: 00207683. DOI: 10.1016/0020-7683(95)00074-7.

[87] L. B. Freund. "A lower bound on implant density to induce wafer splitting in forming compliant substrate structures". In: *Applied Physics Letters* 70.26 (1997), p. 3519. ISSN: 00036951. DOI: 10.1063/1.119219.

[88] T. P. Fries. "A corrected XFEM approximation without problems in blending elements". In: *International Journal for Numerical Methods in Engineering* 75.5 (2008), pp. 503–532. ISSN: 00295981. DOI: 10.1002/nme.2259. arXiv: 1010.1724.

[89] T. P. Fries. "Overview and comparison of different variants of the XFEM". In: *PAMM* 14.1 (2014), pp. 27–30. ISSN: 16177061. DOI: 10.1002/pamm.201410008.

[90] T. P. Fries and M. Baydoun. "Crack propagation with the extended finite element method and a hybrid explicitâĂŞimplicit crack description". In: *International Journal for Numerical Methods in Engineering* 89.November 2011 (2012), pp. 1527–1558. DOI: 10.1002/nme.3299.

[91] T. P. Fries and T. Belytschko. "The extended/generalized finite element method: An overview of the method and its applications". In: *International Journal for Numerical Methods in Engineering* (2010), n/a–n/a. ISSN: 00295981. DOI: 10.1002/nme.2914.

[92] O. Garcia, E. a. Fancello, C. S. D. Barcellos, and C. A. Duarte. "hp-Clouds in Mindlin ' s thick plate model". In: May 1999 (2000), pp. 1381–1400.

[93] J. Garzon, P. O'Hara, C. A. Duarte, and W. G. Buttlar. "Improvements of explicit crack surface representation and update within the generalized finite element method with application to three-dimensional crack coalescence". In: *International Journal for Numerical Methods in Engineering* 97.4 (2014), pp. 231–273. ISSN: 00295981. DOI: 10.1002/nme.4573.

[94] C. Geuzaine and J. F. Remacle. "Gmsh: A 3-D finite element mesh generator with built-in pre- and post-processing facilities". In: *International Journal for Numerical*

Methods in Engineering 79.11 (2009), pp. 1309–1331. ISSN: 00295981. DOI: 10.1002/nme.2579. arXiv: 1010.1724.

[95] A. Giacomini. "Ambrosio-Tortorelli approximation of quasi-static evolution of brittle fractures". In: *Calculus of Variations* 22.2 (2005), pp. 129–172. ISSN: 0944-2669. DOI: 10.1007/s00526-004-0269-6. arXiv: 0303040 [math].

[96] R. A. Gingold and J. J. Monaghan. "Smoothed particle hydrodynamics: theory and application to non-spherical stars". In: *Monthly Notices of the Royal Astronomical Society* 181.3 (1977). Ed. by Intergovernmental Panel on Climate Change, pp. 375–389. ISSN: 0035-8711. DOI: 10.1093/mnras/181.3.375. arXiv: arXiv:1011.1669v3.

[97] R. V. Gol'dstein and R. L. Salganik. "Brittle fracture of solids with arbitrary cracks". In: *International Journal of Fracture* 10.4 (1974), pp. 507–523. ISSN: 03769429. DOI: 10.1007/BF00155254.

[98] V. F. González-Albuixech et al. "Domain integral formulation for 3-D curved and non-planar cracks with the extended finite element method". In: *Computer Methods in Applied Mechanics and Engineering* 264 (2013), pp. 129–144. ISSN: 00457825. DOI: 10.1016/j.cma.2013.05.016.

[99] R. Goodman, R. Taylor, and T. Brekke. "A model for the mechanics of jointed rock". In: *Journal of Soil Mechanics & Foundations Div* 94.3 (1968), pp. 637–659, ISSN: 0044-7994.

[100] E. Gordeliy and A. Peirce. "Coupling schemes for modeling hydraulic fracture propagation using the XFEM". In: *Computer Methods in Applied Mechanics and Engineering* 253.2013 (2013), pp. 305–322. ISSN: 00457825. DOI: 10.1016/j.cma.2012.08.017.

[101] E. Gordeliy and A. Peirce. "Enrichment strategies and convergence properties of the XFEM for hydraulic fracture problems". In: *Computer Methods in Applied Mechanics and Engineering* 283 (2015), pp. 474–502. ISSN: 00457825. DOI: 10.1016/j.cma.2014.09.004.

[102] E. Gordeliy and A. Peirce. "Implicit level set schemes for modeling hydraulic fractures using the XFEM". In: *Computer Methods in Applied Mechanics and Engineering* 266 (2013), pp. 125–143. ISSN: 00457825. DOI: 10.1016/j.cma.2013.07.016.

[103] R. Gracie, H. Wang, and T. Belytschko. "Blending in the extended finite element method by discontinuous Galerkin and assumed strain methods". In: *International Journal for Numerical Methods in Engineering* 74.11 (2008), pp. 1645–1669. ISSN: 00295981. DOI: 10.1002/nme.2217. arXiv: 1010.1724.

[104] A. Gravouil, N. Moës, and T. Belytschko. "Non-planar 3D crack growth by the extended finite element and level sets-Part II: Level set update". In: *International Journal for Numerical Methods in Engineering* 53.11 (2002), pp. 2569–2586. ISSN: 00295981. DOI: 10.1002/nme.430.

[105] A. A. Griffith. "The Phenomena of Rupture and Flow in Solids". In: *Philosophical Transactions of the Royal Society of London* A221 (1920), pp. 163–198.

[106] A. A. Griffith. "The Phenomena of Rupture and Flow in Solids". In: *Philosophical Transactions of the Royal Society of London. Series A, Containing Papers of a Mathematical or Physical Character* 221 (1921), pp. 163–198.

[107] J. Grisolia et al. *TEM measurement of hydrogen pressure within a platelet*. 2001. DOI: 10.1557/PROC-681-I3.2.

[108] B. Gu et al. "Fracture mechanics analysis of the effects of temperature and material mismatch on the Smart-Cut® technology". In: *Engineering Fracture Mechanics* 75.17 (2008), pp. 4996–5006. ISSN: 00137944. DOI: 10.1016/j.engfracmech.2008.06.026.

[109] B. Gu et al. "Fracture mechanics analysis on Smart-Cut® technology. Part 1: Effects of stiffening wafer and defect interaction". In: *Acta Mechanica Sinica* 25.1 (2009), pp. 73–81. ISSN: 0567-7718. DOI: 10.1007/s10409-008-0192-8.

[110] B. Gu et al. "Fracture mechanics analysis on Smart-Cut® technology. Part 2: Effect of bonding flaws". In: *Acta Mechanica Sinica* 25.2 (2009), pp. 197–203. ISSN: 0567-7718. DOI: 10.1007/s10409-008-0193-7.

[111] V. Gupta, C. A. Duarte, I. Babuška, and U. Banerjee. "Stable GFEM (SGFEM): Improved conditioning and accuracy of GFEM/XFEM for three-dimensional fracture mechanics". In: *Computer Methods in Applied Mechanics and Engineering* 289 (2015), pp. 355–386. ISSN: 00457825. DOI: 10.1016/j.cma.2015.01.014.

[112] V. Gupta and C. A. Duarte. "On the enrichment zone size for optimal convergence rate of the Generalized/Extended Finite Element Method". In: *Computers & Mathematics with Applications* (2016). ISSN: 08981221. DOI: 10.1016/j.camwa.2016.04.043.

[113] E. Gürses. "Aspects of Energy Minimization in Solid Mechanics : Evolution of Inelastic Microstructures and Crack Propagation". PhD thesis. 2007. ISBN: 3937859071.

[114] Y. D. Ha and F. Bobaru. "Studies of dynamic crack propagation and crack branching with peridynamics". In: *International Journal of Fracture* 162.1-2 (2010), pp. 229–244. ISSN: 0376-9429. DOI: 10.1007/s10704-010-9442-4.

[115] G. Hahn and A. Rosenfield. "Local yielding and extension of a crack under plane stress". In: *Acta Metallurgica* 13.3 (1965), pp. 293–306. ISSN: 00016160. DOI: 10.1016/0001-6160(65)90206-3.

[116] K. Hayashi and S. Nemat-Nasser. "Energy-Release Rate and Crack Kinking Under Combined Loading". In: *Journal of Applied Mechanics* 48.3 (1981), p. 520. ISSN: 00218936. DOI: 10.1115/1.3157666.

[117] T. K. Hellen. "Virtual crack extension methods for non-linear materials". In: *International Journal for Numerical Methods in Engineering* 28.4 (1989), pp. 929–942. ISSN: 0029-5981. DOI: 10.1002/nme.1620280414.

[118] R. D. Henshell and K. G. Shaw. "Crack tip finite elements are unnecessary". In: *International Journal for Numerical Methods in Engineering* 9.3 (1975), pp. 495–507. ISSN: 0029-5981. DOI: 10.1002/nme.1620090302.

[119] M. R. Hestenes and E. Stiefel. "Methods of Conjugate Gradients for Solving Linear Systems 1". In: 49.6 (1952).

[120] A. Hillerborg, M. Modéer, and P. E. Petersson. "Analysis of crack formation and crack growth in concrete by means of fracture mechanics and finite elements". In: *Cement and Concrete Research* 6.6 (1976), pp. 773–781. ISSN: 00088846. DOI: 10.1016/0008-8846(76)90007-7.

[121] T. Hochbauer, A. Misra, M. Nastasi, and J. W. Mayer. "Investigation of the cut location in hydrogen implantation induced silicon surface layer exfoliation". In: *Journal of Applied Physics* 89.11 I (2001), pp. 5980–5990. ISSN: 00218979. DOI: 10.1063/1.1353561.

[122] J. A. Hodgdon and J. P. Sethna. "Derivation of a general three-dimensional crack-propagation law: A generalization of the principle of local symmetry". In: 47.9 (1993). DOI: http://dx.doi.org/10.1103/PhysRevB.47.4831.

[123] B. L. Holian and R. Ravelo. "Fracture simulations using large-scale molecular dynamics". In: *Physical Review B* 51.17 (1995), pp. 11275–11288. ISSN: 0163-1829. DOI: 10.1103/PhysRevB.51.11275.

[124] M. Holl, S. Loehnert, and P. Wriggers. "An adaptive multiscale method for crack propagation and crack coalescence". In: *International Journal for Numerical Methods in Engineering* 93.1 (2013), pp. 23–51. ISSN: 00295981. DOI: 10.1002/nme.4373. arXiv: 1010.1724.

[125] D. Holland and M. Marder. "Ideal Brittle Fracture of Silicon Studied with Molecular Dynamics". In: *Physical Review Letters* 80.4 (1998), pp. 746–749. ISSN: 0031-9007. DOI: 10.1103/PhysRevLett.80.746.

[126] R. Huang, N. Sukumar, and J. H. Prévost. "Modeling quasi-static crack growth with the extended finite element method Part II: Numerical applications". In: *International Journal of Solids and Structures* 40.26 (2003), pp. 7539–7552. ISSN: 00207683. DOI: 10.1016/j.ijsolstr.2003.08.001.

[127] C. Y. Hui and A. Ruina. "Why K? High order singularities and small scale yielding". In: *International Journal of Fracture* 72.2 (1995), pp. 97–120. ISSN: 0376-9429. DOI: 10.1007/BF00042823.

[128] M. A. Hussain, S. L. Pu, and J. Underwood. "Strain Energy Release Rate for a Crack Under Combined Mode I and Mode II". In: *Fracture analysis* 560 (1974), pp. 2–28. DOI: 10.1520/STP33130S.

[129] C. G. Hwang and A. R. Ingraffea. "Virtual crack extension method for calculating the second order derivatives of energy release rates for multiply cracked systems". In: *Engineering Fracture Mechanics* 74.9 (2007), pp. 1468–1487. ISSN: 00137944. DOI: 10.1016/j.engfracmech.2006.08.009.

[130] C. G. Hwang, P. A. Wawrzynek, A. K. Tayebi, and A. R. Ingraffea. "On the virtual crack extension method for calculation of the rates of energy release rate". In: *Engineering Fracture ...* 59.4 (1998), pp. 521–542.

[131] C. E. Inglis. "Stresses in a plate due to the presence of cracks and sharp corners". In: *Spie Milestone series MS* 137 (1913), pp. 3–17.

[132] G. R. Irwin. "Analysis of Stresses and Strains Near the End of a Crack Traversing a Plate". In: *SPIE MILESTONE SERIES MS* 137 (1997), pp. 167–170.

[133] G. R. Irwin. "Crack-Extension Force for a Part-Through Crack in a Plate". In: *Journal of Applied Mechanics* 29.4 (1962), p. 651. ISSN: 00218936. DOI: 10.1115/1.3640649.

[134] G. R. Irwin. "Relation of stresses near a crack to the crack extension force". In: *9th Cong. App. Mech., Brussels*. Brussels, 1957.

[135] G. R. Irwin, J. M. Krafft, P. C. Paris, and A. A. Wells. *Basic Aspects of Crack Growth and Fracture*. Tech. rep. Naval Research Lab., Washington, D. C., 1967.

[136] G. R. Irwin. "Fracture dynamics". In: *Fracturing of metals* 147 (1948), p. 166.

[137] G. R. Irwin and J. A. Kies. "Fracturing and fracture dynamics". In: *Welding Journal* 31.2 (1952), pp. 95–100.

[138] H. Iwata, M. Takagi, Y. Tokuda, and T. Imura. "Analysis of platelet distribution in H ion-implanted silicon". In: *Journal of Crystal Growth* 210.1-3 (2000), pp. 94–97. ISSN: 00220248. DOI: 10.1016/S0022-0248(99)00654-5.

[139] J. Jaśkowiec. "Three-dimensional analysis of a cohesive crack coupled with heat flux through the crack". In: *Advances in Engineering Software* 89 (2015), pp. 98–107. ISSN: 09659978. DOI: 10.1016/j.advengsoft.2014.12.012.

[140] J. Jaśkowiec and F. P. Meer. "A consistent iterative scheme for 2D and 3D cohesive crack analysis in XFEM". In: *Computers & Structures* 136 (2014), pp. 98–107. ISSN: 00457949. DOI: 10.1016/j.compstruc.2014.01.029.

[141] H. Ji, D. Chopp, and J. E. Dolbow. "A hybrid extended finite element/level set method for modeling phase transformations". In: *International Journal for Numerical Methods in Engineering* 54.8 (2002), pp. 1209–1233. ISSN: 0029-5981. DOI: 10.1002/nme.468.

[142] L. M. Kachanov. "Time of the rupture process under creep conditions". In: *Izv Akad Nauk S S R Otd Tech Nauk* 8 (1958), pp. 26–31. DOI: citeulike-article-id:5466815.

[143] M. Kachanov, E. L. E. Montagut, and J. P. Laures. "Mechanics of crack-microcrack interactions". In: *Mechanics of Materials* 10.1-2 (1990), pp. 59–71. ISSN: 01676636. DOI: 10.1016/0167-6636(90)90017-A.

[144] M. Kachanov. "A simple technique of stress analysis in elastic solids with many cracks". In: *International Journal of Fracture* 28.1 (1985), R11–R19.

[145] M. Kachanov. "Elastic solids with many cracks: A simple method of analysis". In: *International Journal of Solids and Structures* 23.1 (1987), pp. 23–43. ISSN: 00207683. DOI: 10.1016/0020-7683(87)90030-8.

[146] Ł. Kaczmarczyk, M. M. Nezhad, and C. Pearce. "Three-dimensional brittle fracture: Configurational-force-driven crack propagation". In: *International Journal for Numerical Methods in Engineering* 97.7 (2014), pp. 531–550. ISSN: 00295981. DOI: 10.1002/nme.4603. arXiv: 1304.6136.

[147] B. L. Karihaloo. "On crack kinking and curving". In: *Mechanics of Materials* (1982).

[148] B. L. Karihaloo and L. M. Keer. "Approximate description of crack kinking and curving". In: *Journal of Applied Mechanics* September 1981 (1981), pp. 515–519.

[149] B. L. Karihaloo, L. M. Keer, and S. Nemat-Nasser. "Crack kinking under nonsymmetric loading". In: *Engineering Fracture Mechanics* 13.4 (1980), pp. 879–888. ISSN: 0013-7944. DOI: http://dx.doi.org/10.1016/0013-7944(80)90018-1.

[150] B. L. Karihaloo and Q. Xiao. "Modelling of stationary and growing cracks in FE framework without remeshing: a state-of-the-art review". In: *Computers & Structures* 81.3 (2003), pp. 119–129. ISSN: 00457949. DOI: 10.1016/S0045-7949(02)00431-5.

[151] P. Kerfriden, J. C. Passieux, and S. P. A. Bordas. "Local/global model order reduction strategy for the simulation of quasi-brittle fracture". In: *International Journal for Numerical Methods in Engineering* 89.2 (2012), pp. 154–179. ISSN: 00295981. DOI: 10.1002/nme.3234. arXiv: arXiv:1108.3167v2.

[152] P. Kerfriden, O. Allix, and P. Gosselet. "A three-scale domain decomposition method for the 3D analysis of debonding in laminates". In: *Computational Mechanics* 44.3 (2009), pp. 343–362. ISSN: 0178-7675. DOI: 10.1007/s00466-009-0378-3. arXiv: arXiv:1109.6111v1.

[153] J. Kim and C. A. Duarte. "A new generalized finite element method for two-scale simulations of propagating cohesive fractures in 3-D". In: *International Journal for Numerical Methods in Engineering* 104.13 (2015), pp. 1139–1172. ISSN: 00295981. DOI: 10.1002/nme.4954.

[154] V. V. Kozlovskii, V. A. Kozlov, and V. N. Lomasov. "Modification of semiconductors with proton beams. A review". In: *Semiconductors* 34.2 (2000), pp. 123–140. ISSN: 1063-7826. DOI: 10.1134/1.1187921.

[155] R. Krueger. "Virtual crack closure technique: History, approach, and applications". In: *Applied Mechanics Reviews* 57.2 (2004), p. 109. ISSN: 00036900. DOI: 10.1115/1.1595677.

[156] P. Krysl and T. Belytschko. "The Element Free Galerkin method for dynamic propagation of arbitrary 3-D cracks". In: *International Journal for Numerical Methods in Engineering* 44.6 (1999), pp. 767–800. ISSN: 0029-5981. DOI: 10.1002/(SICI)1097-0207(19990228)44:6<767::AID-NME524>3.0.CO;2-G.

[157] T. Kundu. *Fundamentals of Fracture Mechanics*. Boston: CRC Pres Taylor & Francis Group, 2004. ISBN: 1-4020-7745-9.

[158] P. Laborde, J. Pommier, Y. Renard, and M. Salaün. "High-order extended finite element method for cracked domains". In: *International Journal for Numerical Methods in Engineering* 64.3 (2005), pp. 354–381. ISSN: 0029-5981. DOI: 10.1002/nme.1370.

[159] M. Lan, H. Waisman, and I. Harari. "A High-order extended finite element method for extraction of mixed-mode strain energy release rates in arbitrary crack settings based on Irwin's integral". In: *International Journal for Numerical Methods in Engineering* 96.12 (2013), pp. 787–812. ISSN: 00295981. DOI: 10.1002/nme.4584.

[160] C. Lang, D. Makhija, A. Doostan, and K. Maute. "A simple and efficient preconditioning scheme for heaviside enriched XFEM". In: *Computational Mechanics* 54.5 (2014), pp. 1357–1374. ISSN: 0178-7675. DOI: 10.1007/s00466-014-1063-8. arXiv: 1312.6092.

[161] J. B. Leblond. "Crack paths in three-dimensional elastic solids. i: two-term expansion of the stress intensity factorsâĂŤapplication to crack path stability in hydraulic fracturing". In: *International Journal of Solids and Structures* 36.1 (1999), pp. 79–103. ISSN: 00207683. DOI: 10.1016/S0020-7683(97)00276-X.

[162] T. Lee, M. Leok, and N. H. McClamroch. "Comparison of a phase-field model and of a thick level set model for brittle and quasi-brittle fracture". In: *Proceedings of the 2011 American Control Conference* February (2011), pp. 1885–1891. ISSN: 0743-1619. DOI: 10.1002/nme. arXiv: 1010.1724.

[163] D. Leguillon. "A criterion for crack nucleation at a notch in homogeneous materials". In: *Comptes Rendus de l'Académie des Sciences - Series IIB - Mechanics* 329.2 (2001), pp. 97–102. ISSN: 16207742. DOI: 10.1016/S1620-7742(01)01302-2.

[164] D. Leguillon. "Strength or toughness? A criterion for crack onset at a notch". In: *European Journal of Mechanics - A/Solids* 21.1 (2002), pp. 61–72. ISSN: 09977538. DOI: 10.1016/S0997-7538(01)01184-6.

[165] S. C. Li and Y. M. Cheng. "Enriched meshless manifold method for two-dimensional crack modeling". In: *Theoretical and applied fracture mechanics* 44.3 (2005), pp. 234–248.

[166] S. Li, Z. Xu, G. Ma, and W. Yang. "An adaptive mesh refinement method for a medium with discrete fracture network: The enriched Persson's method". In: *Finite Elements in Analysis and Design* 86 (2014), pp. 41–50. ISSN: 0168874X. DOI: 10.1016/j.finel.2014.03.008.

[167] L. D. Libersky and A. G. Petschek. "Smooth particle hydrodynamics with strength of materials". In: *Advances in the Free-Lagrange Method Including Contributions on Adaptive Gridding and the Smooth Particle Hydrodynamics Method*. Berlin, Heidelberg: Springer Berlin Heidelberg, 1991, pp. 248–257. DOI: 10.1007/3-540-54960-9_58.

[168] S. C. Lin and J. F. Abel. "Variational approach for a new direct-integration form of the virtual crack extension method". In: *International Journal of Fracture* 235.3 (1988), pp. 217–235. DOI: 10.1007/BF00034286.

[169] C. Linder and F. Armero. "Finite elements with embedded strong discontinuities for the modeling of failure in solids". In: *International Journal for Numerical Methods in Engineering* 72.12 (2007), pp. 1391–1433. ISSN: 00295981. DOI: 10.1002/nme.2042. arXiv: 1010.1724.

[170] S. Linge and H. P. Langtangen. *Programming for Computations - MATLAB/Octave*. Vol. 14. Texts in Computational Science and Engineering. Cham: Springer International Publishing, 2016. ISBN: 978-3-319-32451-7. DOI: 10.1007/978-3-319-32452-4.

[171] W. Liu et al. "An Accurate and Efficient Augmented Finite Element Method for Arbitrary Crack Interactions". In: *Journal of Applied Mechanics* 80.4 (2013), p. 041033. ISSN: 0021-8936. DOI: 10.1115/1.4007970.

[172] X. Y. Liu, Q. Z. Xiao, and B. L. Karihaloo. "XFEM for direct evaluation of mixed mode SIFs in homogeneous and bi-materials". In: *International Journal for Numerical Methods in Engineering* 59.8 (2004), pp. 1103–1118. ISSN: 0029-5981. DOI: 10.1002/nme.906.

[173] S. Loehnert. "A stabilization technique for the regularization of nearly singular extended finite elements". In: *Computational Mechanics* 54.2 (2014), pp. 523–533. ISSN: 0178-7675. DOI: 10.1007/s00466-014-1003-7.

[174] E. Lorentz and S. Andrieux. "A variational formulation for nonlocal damage models". In: *International Journal of Plasticity* 15.2 (1999), pp. 119–138. ISSN: 07496419. DOI: 10.1016/S0749-6419(98)00057-6.

[175] E. Lorentz and S. Andrieux. "Analysis of non-local models through energetic formulations". In: *International Journal of Solids and Structures* 40.12 (2003), pp. 2905–2936. ISSN: 00207683. DOI: 10.1016/S0020-7683(03)00110-0.

[176] J. J. Marigo. "Initiation of Cracks in Griffith's Theory: An Argument of Continuity in Favor of Global Minimization". In: *Journal of Nonlinear Science* 20.6 (2010), pp. 831–868. ISSN: 0938-8974. DOI: 10.1007/s00332-010-9074-x.

[177] G. D. Maso, G. A. Francfort, and R. Toader. "Quasistatic Crack Growth in Nonlinear Elasticity". In: *Archive for Rational Mechanics and Analysis* 176.2 (2005), pp. 165–225. ISSN: 0003-9527. DOI: 10.1007/s00205-004-0351-4. arXiv: arXiv:1604.08338v1.

[178] Y. G. Matvienko. "Maximum average tangential stress criterion for prediction of the crack path". In: *International Journal of Fracture* 176.1 (2012), pp. 113–118. ISSN: 03769429. DOI: 10.1007/s10704-012-9715-1.

[179] J. Melenk and I. Babuška. "The partition of unity finite element method: Basic theory and applications". In: *Computer Methods in Applied Mechanics and Engineering*

139.1-4 (1996), pp. 289–314. ISSN: 00457825. DOI: 10.1016/S0045-7825(96)01087-0.

[180] J. M. Melenk. "On generalized finite element methods". PhD thesis. The University of Maryland, 1995.

[181] A. Menk and S. P. A. Bordas. "A robust preconditioning technique for the extended finite element method". In: *International Journal for Numerical Methods in Engineering* 85.13 (2011), pp. 1609–1632. ISSN: 00295981. DOI: 10.1002/nme.3032.

[182] T. Menouillard, J.-H. Song, Q. Duan, and T. Belytschko. "Time dependent crack tip enrichment for dynamic crack propagation". In: *International Journal of Fracture* 162.1-2 (2010), pp. 33–49. ISSN: 0376-9429. DOI: 10.1007/s10704-009-9405-9.

[183] R. Merle and J. Dolbow. "Solving thermal and phase change problems with the eXtended finite element method". In: *Computational Mechanics* 28.5 (2002), pp. 339–350. ISSN: 0178-7675. DOI: 10.1007/s00466-002-0298-y.

[184] G. Meschke and P. Dumstorff. "Energy-based modeling of cohesive and cohesionless cracks via X-FEM". In: *Comput Method Appl M* 196.21-24 (2007), pp. 2338–2357. DOI: 10.1016/j.cma.2006.11.016.

[185] A. Mesgarnejad, B. Bourdin, and M. M. Khonsari. "Validation simulations for the variational approach to fracture". In: *Computer Methods in Applied Mechanics and Engineering* 290 (2015), pp. 420–437. ISSN: 00457825. DOI: 10.1016/j.cma.2014.10.052.

[186] Y. Mi, M. A. Crisfield, G. A. O. Davies, and H. B. Hellweg. "Progressive Delamination Using Interface Elements". In: *Journal of Composite Materials* 32.14 (1998), pp. 1246–1272. ISSN: 0021-9983. DOI: 10.1177/002199839803201401.

[187] C. Miehe, F. Welschinger, and M. Hofacker. *Thermodynamically consistent phase-field models of fracture: Variational principles and multi-field FE implementations*. 2010. DOI: 10.1002/nme.2861. arXiv: 1010.1724.

[188] C. Miehe, M. Hofacker, and F. Welschinger. "A phase field model for rate-independent crack propagation: Robust algorithmic implementation based on operator splits". In: *Computer Methods in Applied Mechanics and Engineering* 199.45-48 (2010), pp. 2765–2778. ISSN: 00457825. DOI: 10.1016/j.cma.2010.04.011.

[189] C. Miehe and S. Mauthe. "Phase field modeling of fracture in multi-physics problems. Part III. Crack driving forces in hydro-poro-elasticity and hydraulic fracturing of fluid-saturated porous media". In: *Computer Methods in Applied Mechanics and Engineering* 304.2015 (2016), pp. 619–655. ISSN: 00457825. DOI: 10.1016/j.cma.2015.09.021.

[190] I. C. Mihai. "Micromechanical constitutive models for cementitious composite materials". PhD thesis. Cardiff University, 2012.

[191] H. Minnebo. "Three-dimensional integration strategies of singular functions introduced by the XFEM in the LEFM". In: *International Journal for Numerical Methods in Engineering* 92.13 (2012), pp. 1117–1138. ISSN: 00295981. DOI: 10.1002/nme.4378.

[192] N. Moës, J. Dolbow, and T. Belytschko. "A finite element method for crack growth without remeshing". In: *Int. J. Numer. Meth. Engng* 150.February (1999), pp. 131–150. ISSN: 00295981. DOI: 10.1002/(SICI)1097-0207(19990910)46:1<131::AID-NME726>3.0.CO;2-J.

[193] N. Moës and T. Belytschko. "Extended finite element method for cohesive crack growth". In: *Engineering Fracture Mechanics* 69.7 (2002), pp. 813–833. ISSN: 00137944. DOI: 10.1016/S0013-7944(01)00128-X.

[194] N. Moës, C. Stolz, P.-E. Bernard, and N. Chevaugeon. "A level set based model for damage growth: The thick level set approach". In: *International Journal for Numerical Methods in Engineering* 86.3 (2011), pp. 358–380. ISSN: 00295981. DOI: 10.1002/nme.3069.

[195] S. G. Mogilevskaya. "Numerical modeling of 2-D smooth crack growth". In: *International Journal of Fracture* 87.4 (1997), pp. 389–405. ISSN: 03769429. DOI: 10.1023/A:1007465204062.

[196] S. G. Mogilevskaya. "The universal algorithm based on complex hypersingular integral equation to solve plane elasticity problems". In: *Computational Mechanics* 18.2 (1996), pp. 127–138. ISSN: 0178-7675. DOI: 10.1007/BF00350531.

[197] S. Mohammadi. *Extended Finite Element Method for Fracture Analysis of Structures*. 2008, p. 280. ISBN: 1405170603.

[198] B. Moran and C. F. Shih. "Crack tip and associated domain integrals from momentum and energy balance". In: *Engineering Fracture Mechanics* 27.6 (1987), pp. 615–642. ISSN: 00137944. DOI: 10.1016/0013-7944(87)90155-X.

[199] G. Moras, G. Csanyi, M. Payne, and A. De Vita. "A novel molecular dynamics approach to large semiconductor systems". In: *Physica B: Condensed Matter* 376-377 (2006), pp. 936–939. ISSN: 09214526. DOI: 10.1016/j.physb.2005.12.233.

[200] G. Moras, L. Colombi Ciacchi, G. Csanyi, and A. De Vita. "Modelling (100) hydrogen-induced platelets in silicon with a multi-scale molecular dynamics approach". In: *Physica B: Condensed Matter* 401-402.2007 (2007), pp. 16–20. ISSN: 09214526. DOI: 10.1016/j.physb.2007.08.104.

[201] D. Motamedi and S. Mohammadi. "Dynamic crack propagation analysis of orthotropic media by the extended finite element method". In: *International Journal of Fracture* 161.1 (2010), pp. 21–39. ISSN: 0376-9429. DOI: 10.1007/s10704-009-9423-7.

[202] S. Murakami. *Continuum Damage Mechanics*. Vol. 185. Solid Mechanics and Its Applications. Dordrecht: Springer Netherlands, 2012. ISBN: 978-94-007-2665-9. DOI: 10.1007/978-94-007-2666-6.

[203] N. Muthu, B. Falzon, S. Maiti, and S. Khoddam. "Modified crack closure integral technique for extraction of SIFs in meshfree methods". In: *Finite Elements in Analysis and Design* 78.2014 (2014), pp. 25–39. ISSN: 0168874X. DOI: 10.1016/j.finel.2013.09.005.

[204] S. Natarajan. "Enriched finite element methods: advances & applications". PhD thesis. Cardiff University, 2011.

[205] S. Nemat-Nasser and H. Horii. "Compression-induced nonplanar crack extension with application to splitting, exfoliation, and rockburst". In: *Journal of Geophysical Research* 87.B8 (1982), p. 6805. ISSN: 0148-0227. DOI: 10.1029/JB087iB08p06805.

[206] Q. S. Nguyen and S. Andrieux. "The non-local generalized standard approach: a consistent gradient theory". In: *Comptes Rendus Mécanique* 333.2 (2005), pp. 139–145. ISSN: 16310721. DOI: 10.1016/j.crme.2004.09.010.

[207] V. P. Nguyen. "Multiscale failure modelling of quasi-brittle materials". PhD Thesis. TU Delft, Delft University of Technology, 2011. ISBN: 9789461910110.

[208] V. P. Nguyen. "An object-oriented approach to the extended finite element method with applications to fracture mechanics". MSc Thesis. Hochiminh City University of Technology, 2005.

[209] V. P. Nguyen, T. Rabczuk, S. P. A. Bordas, and M. Duflot. "Meshless methods: A review and computer implementation aspects". In: *Mathematics and Computers in Simulation* 79.3 (2008), pp. 763–813. ISSN: 03784754. DOI: 10.1016/j.matcom.2008.01.003.

[210] J. Nocedal and S. J. Wright. *Numerical Optimization*. Ed. by P. Glynn and S. M. Robinson. Vol. 11. 1. Springer, 1999, p. 198. ISBN: ISBN 0-387-98793-2.

[211] V. Novozhilov. "On a necessary and sufficient criterion for brittle strength". In: *Journal of Applied Mathematics and Mechanics* 33.2 (1969), pp. 201–210. ISSN: 00218928. DOI: 10.1016/0021-8928(69)90025-2.

[212] J. T. Oden, C. A. M. Duarte, and O. C. Zienkiewicz. "A new cloud-based hp finite element method". In: *Computer Methods in Applied Mechanics and Engineering* 153.1-2 (1998), pp. 117–126. ISSN: 00457825. DOI: 10.1016/S0045-7825(97)00039-X.

[213] J. Oliver. "Continuum modelling of strong discontinuities in solid mechanics using damage models". In: *Computational Mechanics* 17.1-2 (1995), pp. 49–61. ISSN: 0178-7675. DOI: 10.1007/BF00356478.

[214] J. Oliver. "Modelling Strong Discontinuities in Solid Mechanics via Strain Softening Constitutive Equations. Part 1: Fundamentals". In: *International Journal for Numerical Methods in Engineering* 39.21 (1996), pp. 3575–3600. ISSN: 0029-5981. DOI: 10.1002/(SICI)1097-0207(19961115)39:21<3575::AID-NME65>3.0.CO;2-E.

[215] J. Oliver. "Modelling Strong Discontinuities in Solid Mechanics via Strain Softening Constitutive Equations. Part 2: Numerical Simulation". In: *International Journal for Numerical Methods in Engineering* 39.21 (1996), pp. 3601–3623. ISSN: 0029-5981. DOI:

10.1002/(SICI)1097-0207(19961115)39:21<3601::AID-NME64>3.0.CO;2-4.

[216] J. Oliver, A. Huespe, and P. Sánchez. "A comparative study on finite elements for capturing strong discontinuities: E-FEM vs X-FEM". In: *Computer Methods in Applied Mechanics and Engineering* 195.37-40 (2006), pp. 4732–4752. ISSN: 00457825. DOI: 10.1016/j.cma.2005.09.020.

[217] C. W. Oosterlee and T Washio. "On the use of multigrid as a preconditioner". In: *Proceedings of Ninth International Conference on Domain Decomposition Methods*. 1996, pp. 441–448.

[218] D. Organ, M. Fleming, T. Terry, and T. Belytschko. "Continuous meshless approximations for nonconvex bodies by diffraction and transparency". In: *Computational Mechanics* 18.3 (1996), pp. 225–235. ISSN: 0178-7675. DOI: 10.1007/BF00369940.

[219] E. Orowan. "Energy criteria of fracture". In: *Welding Journal* 34 (1955), pp. 157–160.

[220] E. Orowan. "Fracture and strength of solids". In: *Reports on Progress in Physics* 12.1 (1949), p. 309. ISSN: 00344885. DOI: 10.1088/0034-4885/12/1/309.

[221] S. Osher, R. Fedkiw, and K. Piechor. *Level set methods and dynamic implicit surfaces*. Vol. 57. 3. 2004, B15. ISBN: 0387954821. DOI: 10.1115/1.1760520.

[222] S. Osher and R. P. Fedkiw. "Level Set Methods: An Overview and Some Recent Results". In: *Journal of Computational Physics* 169.2 (2001), pp. 463–502. ISSN: 00219991. DOI: 10.1006/jcph.2000.6636.

[223] K. Palaniswamy and W. G. Knauss. "Propagation of a crack under general, in-plane tension". In: *International Journal of Fracture Mechanics* 8.1 (1972), pp. 114–117. ISSN: 0020-7268. DOI: 10.1007/BF00185207.

[224] A. Paluszny, X. H. Tang, and R. W. Zimmerman. "Fracture and impulse based finite-discrete element modeling of fragmentation". In: *Computational Mechanics* 52.5 (2013), pp. 1071–1084. ISSN: 0178-7675. DOI: 10.1007/s00466-013-0864-5.

[225] A. Paluszny and S. K. Matthäi. "Numerical modeling of discrete multi-crack growth applied to pattern formation in geological brittle media". In: *International Journal of Solids and Structures* 46.18-19 (2009), pp. 3383–3397. ISSN: 00207683. DOI: 10.1016/j.ijsolstr.2009.05.007.

[226] A. Paluszny and R. W. Zimmerman. "Numerical fracture growth modeling using smooth surface geometric deformation". In: *Engineering Fracture Mechanics* 108 (2013), pp. 19–36. ISSN: 00137944. DOI: 10.1016/j.engfracmech.2013.04.012.

[227] A. Paluszny and R. W. Zimmerman. "Numerical simulation of multiple 3D fracture propagation using arbitrary meshes". In: *Computer Methods in Applied Mechanics and Engineering* 200.9-12 (2011), pp. 953–966. ISSN: 00457825. DOI: 10.1016/j.cma.2010.11.013.

[228] D. M. Parks. "A stiffness derivative finite element technique for determination of crack tip stress intensity factors". In: *International Journal of Fracture* 10.4 (1974), pp. 487–502. ISSN: 0376-9429. DOI: 10.1007/BF00155252.

[229] H. Pathak, A. Singh, and I. V. Singh. "Fatigue crack growth simulations of 3-D problems using XFEM". In: *International Journal of Mechanical Sciences* 76 (2013), pp. 112–131. ISSN: 00207403. DOI: 10.1016/j.ijmecsci.2013.09.001.

[230] B. Patzak and M. Jirasek. "Process zone resolution by extended finite elements". In: *Engineering Fracture Mechanics* 70 (2003), pp. 957–977. ISSN: 00137944. DOI: 10.1016/S0013-7944(02)00160-1.

[231] R. H. J. Peerlings, R. DeBorst, W. A. M. Brekelmans, and M. G. D. Geers. "Gradient-enhanced damage modelling of concrete fracture". In: *Mechanics of Cohesive-frictional Materials* 3.4 (1998), pp. 323–342. ISSN: 1082-5010. DOI: 10.1002/(SICI)1099-1484(1998100)3:4<323::AID-CFM51>3.0.CO;2-Z.

[232] R. H. J. Peerlings et al. "Some observations on localisation in non-local and gradient damage models". In: *European Journal of Mechanics a-Solids* 15.6 (1996), pp. 937–953.

[233] J. D. Penot. "Fragilisation et dynamique de la rupture du silicium implanté". Thèse de doctorat. Université de Grenoble, 2010.

[234] J. D. Penot et al. "Development of microcracks in hydrogen-implanted silicon substrates". In: *Journal of Applied Physics* 114.12 (2013), p. 123513. ISSN: 00218979. DOI: 10.1063/1.4821239.

[235] S. Personnic. "Etude des mécanismes de rupture du silicium induits par l'implantation ionique d'hydrogène dans le cadre de la technologie Smart CutâĎć". PhD Thesis. Ecole Nationale Supérieur des Mines, Saint-Etienne, 2007.

[236] G. Pijaudier-Cabot and Z. P. Bažant. "Nonlocal Damage Theory". In: *Journal of Engineering Mechanics* 113.10 (1987), pp. 1512–1533. ISSN: 0733-9399. DOI: 10.1061/(ASCE)0733-9399(1987)113:10(1512). arXiv: /dx.doi.org/10.1061/(ASCE)0733-9399(1987)113:10(1512) [http:].

[237] G. Pijaudier-Cabot and N. Burlion. "Damage and localisation in elastic materials with voids". In: *Mechanics of Cohesive-frictional Materials* 1.2 (1996), pp. 129–144. ISSN: 1082-5010. DOI: 10.1002/(SICI)1099-1484(199604)1:2<129::AID-CFM7>3.0.CO;2-2.

[238] A. Portela, M. H. Aliabadi, and D. P. Rooke. "The dual boundary element method: Effective implementation for crack problems". In: *International Journal for Numerical Methods in Engineering* 33.6 (1992), pp. 1269–1287. ISSN: 0029-5981. DOI: 10.1002/nme.1620330611.

[239] R. M. Pradeilles-Duval and C. Stolz. "Mechanical transformations and discontinuities along a moving surface". In: *Journal of the Mechanics and Physics of Solids* 43.1 (1995), pp. 91–121. ISSN: 00225096. DOI: 10.1016/0022-5096(94)00061-9.

[240] T. Rabczuk and T. Belytschko. "Cracking particles: a simplified meshfree method for arbitrary evolving cracks". In: *International Journal for Numerical Methods in Engineering* 61.13 (2004), pp. 2316–2343. ISSN: 0029-5981. DOI: 10.1002/nme.1151.

[241] T. Rabczuk, S. P. A. Bordas, and G. Zi. "A three-dimensional meshfree method for continuous multiple-crack initiation, propagation and junction in statics and dynamics". In: *Computational Mechanics* 40.3 (2007), pp. 473–495. ISSN: 0178-7675. DOI: 10.1007/s00466-006-0122-1.

[242] Y. N. Rabotnov. "Creep rupture". In: *Applied Mechanics*. Berlin, Heidelberg: Springer Berlin Heidelberg, 1969, pp. 342–349. DOI: 10.1007/978-3-642-85640-2_26.

[243] Y. N. Rabotnov. "On the equation of state of creep". In: *ARCHIVE: Proceedings of the Institution of Mechanical Engineers, Conference Proceedings 1964-1970 (vols 178-184), Various titles labelled Volumes A to S* 178.31 (1963), pp. 117–122. ISSN: 0367-8849. DOI: 10.1243/PIME_CONF_1963_178_030_02.

[244] P. Randles and L. Libersky. "Smoothed Particle Hydrodynamics: Some recent improvements and applications". In: *Computer Methods in Applied Mechanics and Engineering* 139.1-4 (1996), pp. 375–408. ISSN: 00457825. DOI: 10.1016/S0045-7825(96)01090-0.

[245] B. N. Rao and S. Rahman. "An efficient meshless method for fracture analysis of cracks". In: *Computational Mechanics* 26.4 (2000), pp. 398–408. ISSN: 0178-7675. DOI: 10.1007/s004660000189.

[246] S. Reboh et al. "Orientation of H platelets under local stress in Si". In: *Applied Physics Letters* 93.2 (2008), p. 022106. ISSN: 00036951. DOI: 10.1063/1.2958212.

[247] L. Ren, Z. Zhu, Q. Yang, and T. Ai. "Investigation on the Applicability of Several Fracture Criteria to the Mixed Mode Brittle Fractures". In: *Advances in Mechanical Engineering* 2013 (2013), pp. 1–11. ISSN: 1687-8132. DOI: 10.1155/2013/545108.

[248] J. R. Rice. "A path independent integral and the approximate analysis of strain concentration by notches and cracks". In: 35 (1968), pp. 379–386.

[249] J. R. Rice. "Mathematical analysis in the mechanics of fracture". In: *Fracture: an advanced treatise* 2 (1968), pp. 191–311.

[250] J. R. Rice. *Thermodynamics of the quasi-static growth of Griffith cracks*. 1978. DOI: 10.1016/0022-5096(78)90014-5.

[251] G. Roland. "Fragilisation et rupture du silicium implanté dans le procédé Smart CutâĎć: modélisation et simulation par éléments finis". Thèse de doctorat. INSA de Lyon, 2010.

[252] Y. Saad and M. H. Schultz. "GMRES: A Generalized Minimal Residual Algorithm for Solving Nonsymmetric Linear Systems". In: *SIAM Journal on Scientific and Statistical Computing* 7.3 (1986), pp. 856–869. ISSN: 0196-5204. DOI: 10.1137/0907058.

[253] A. Salvadori. "Crack kinking in brittle materials". In: *Journal of the Mechanics and Physics of Solids* 58.11 (2010), pp. 1835–1846. ISSN: 00225096. DOI: 10.1016/j.jmps.2010.08.002.

[254] A. Salvadori. "A plasticity framework for (linear elastic) fracture mechanics". In: *Journal of the Mechanics and Physics of Solids* 56.5 (2008), pp. 2092–2116. ISSN: 00225096. DOI: 10.1016/j.jmps.2007.10.011.

[255] H. Sauerland and T. P. Fries. "The stable XFEM for two-phase flows". In: *Computers & Fluids* 87 (2013), pp. 41–49. ISSN: 00457930. DOI: 10.1016/j.compfluid.2012.10.017.

[256] J. C. J. Schellekens and R. DeBorst. "On the numerical integration of interface elements". In: ... *Journal for Numerical Methods* ... (1993).

[257] A. Seweryn. "A non-local stress and strain energy release rate mixed mode fracture initiation and propagation criteria". In: *Engineering fracture mechanics* (1998), pp. 737–760.

[258] A. Seweryn. "Brittle fracture criterion for structures with sharp notches". In: *Engineering Fracture Mechanics* 47.5 (1994), pp. 673–681. ISSN: 00137944. DOI: 10.1016/0013-7944(94)90158-9.

[259] A. Seweryn and A. Łukaszewicz. "Verification of brittle fracture criteria for elements with V-shaped notches". In: *Engineering Fracture Mechanics* 69.13 (2002), pp. 1487–1510. ISSN: 00137944. DOI: 10.1016/S0013-7944(01)00138-2.

[260] G. C. Sih. *Mechanics of fracture initiation and propagation*. 1991. ISBN: 9789401056601. DOI: 10.1007/978-94-011-3734-8.

[261] G. C. Sih. "Strain-energy-density factor applied to mixed mode crack problems". In: *International Journal of fracture* 10.3 (1974), pp. 305–321.

[262] S. A. Silling and E. Askari. "A meshfree method based on the peridynamic model of solid mechanics". In: *Computers & Structures* 83.17-18 (2005), pp. 1526–1535. ISSN: 00457949. DOI: 10.1016/j.compstruc.2004.11.026.

[263] S. A. Silling and R. B. Lehoucq. "Convergence of Peridynamics to Classical Elasticity Theory". In: *Journal of Elasticity* 93.1 (2008), pp. 13–37. ISSN: 0374-3535. DOI: 10.1007/s10659-008-9163-3.

[264] I. Singer-Loginova and H. M. Singer. "The phase field technique for modeling multiphase materials". In: *Reports on Progress in Physics* 71.10 (2008), p. 106501. ISSN: 0034-4885. DOI: 10.1088/0034-4885/71/10/106501.

[265] J. Sladek, V. Sladek, and S. Atluri. "Path-independent integral in fracture mechanics of quasicrystals". In: *Engineering Fracture Mechanics* 140 (2015), pp. 61–71. ISSN: 00137944. DOI: 10.1016/j.engfracmech.2015.03.039.

[266] I. N. Sneddon. "The Distribution of Stress in the Neighbourhood of a Crack in an Elastic Solid". In: *Proceedings of the Royal Society A: Mathematical, Physical and*

Engineering Sciences 187.1009 (1946), pp. 229–260. ISSN: 1364-5021. DOI: 10.1098/rspa.1946.0077.

[267] Soitec. *Smart Cut*.

[268] J. H. Song, H Wang, and T Belytschko. "A comparative study on finite element methods for dynamic fracture". In: *Computational Mechanics, Springer-Verlag* 42.2 (2008), pp. 239–250. ISSN: 0178-7675. DOI: 10.1007/s00466-007-0210-x.

[269] M. Stolarska and D. L. Chopp. "Modeling thermal fatigue cracking in integrated circuits by level sets and the extended finite element method". In: *International Journal of Engineering Science* 41.20 (2003), pp. 2381–2410. ISSN: 00207225. DOI: 10.1016/S0020-7225(03)00217-9.

[270] M. Stolarska, D. L. Chopp, N. Moes, and T. Belytschko. "Modelling crack growth by level sets in the extended finite element method". In: January 2000 (2001), pp. 943–960.

[271] C. Stolz and N. Moës. "A new model of damage: a moving thick layer approach". In: *International Journal of Fracture* 174.1 (2012), pp. 49–60. ISSN: 0376-9429. DOI: 10.1007/s10704-012-9693-3.

[272] T. Strouboulis, I. Babuška, and K. Copps. "The design and analysis of the generalized finite element method". In: *Computer methods in applied ...* 181 (2000).

[273] H. Stumpf and K. C. Le. "Variational principles of nonlinear fracture mechanics". In: *Acta Mechanica* 83.1-2 (1990), pp. 25–37. ISSN: 0001-5970. DOI: 10.1007/BF01174730.

[274] N. Sukumar, D. L. Chopp, and B. Moran. "Extended finite element method and fast marching method for three-dimensional fatigue crack propagation". In: *Engineering Fracture Mechanics* 70.1 (2003), pp. 29–48. ISSN: 00137944. DOI: 10.1016/S0013-7944(02)00032-2.

[275] N. Sukumar, D. L. Chopp, N. Moës, and T. Belytschko. "Modeling holes and inclusions by level sets in the extended finite-element method". In: *Computer Methods in Applied Mechanics and Engineering* 190.46-47 (2001), pp. 6183–6200. ISSN: 00457825. DOI: 10.1016/S0045-7825(01)00215-8.

[276] D. Sulsky, Z. Chen, and H. Schreyer. "A particle method for history-dependent materials". In: *Computer Methods in Applied Mechanics and Engineering* 118.1-2 (1994), pp. 179–196. ISSN: 00457825. DOI: 10.1016/0045-7825(94)90112-0.

[277] D. Sulsky and H. L. Schreyer. "Axisymmetric form of the material point method with applications to upsetting and Taylor impact problems". In: *Computer Methods in Applied Mechanics and Engineering* 139.1-4 (1996), pp. 409–429. ISSN: 00457825. DOI: 10.1016/S0045-7825(96)01091-2.

[278] D. Sulsky, S.-J. Zhou, and H. L. Schreyer. "Application of a particle-in-cell method to solid mechanics". In: *Computer Physics Communications* 87.1-2 (1995), pp. 236–252. ISSN: 00104655. DOI: 10.1016/0010-4655(94)00170-7.

[279] J. E. Tarancón, A. Vercher, E. Giner, and F. J. Fuenmayor. "Enhanced blending elements for XFEM applied to linear elastic fracture mechanics". In: *International Journal for Numerical Methods in Engineering* 77.1 (2009), pp. 126–148. ISSN: 00295981. DOI: 10.1002/nme.2402. arXiv: 1010.1724.

[280] A. Turon, C. G. Dávila, P. P. Camanho, and J. Costa. "An engineering solution for mesh size effects in the simulation of delamination using cohesive zone models". In: *Engineering Fracture Mechanics* 74.10 (2007), pp. 1665–1682. ISSN: 00137944. DOI: 10.1016/j.engfracmech.2006.08.025.

[281] G. Ventura, E. Budyn, and T. Belytschko. "Vector level sets for description of propagating cracks in finite elements". In: *International Journal for Numerical Methods in Engineering* 58.10 (2003), pp. 1571–1592. ISSN: 0029-5981. DOI: 10.1002/nme.829.

[282] G. Ventura, J. X. Xu, and T. Belytschko. "A vector level set method and new discontinuity approximations for crack growth by EFG". In: *International Journal for Numerical Methods in Engineering* 54.6 (2002), pp. 923–944. ISSN: 0029-5981. DOI: 10.1002/nme.471.

[283] G. Ventura, R. Gracie, and T. Belytschko. "Fast integration and weight function blending in the extended finite element method". In: *International Journal for Numerical Methods in Engineering* 77.1 (2009), pp. 1–29. ISSN: 00295981. DOI: 10.1002/nme.2387.

[284] G. Vigueras et al. "An XFEM/CZM implementation for massively parallel simulations of composites fracture". In: *Composite Structures* 125 (2015), pp. 542–557. ISSN: 02638223. DOI: 10.1016/j.compstruct.2015.01.053.

[285] H. A. Vorst. "Bi-CGSTAB: A Fast and Smoothly Converging Variant of Bi-CG for the Solution of Nonsymmetric Linear Systems". In: *SIAM Journal on Scientific and Statistical Computing* 13.2 (1992), pp. 631–644. ISSN: 0196-5204. DOI: 10.1137/0913035.

[286] H. Waisman. "An analytical stiffness derivative extended finite element technique for extraction of crack tip Strain Energy Release Rates". In: *Engineering Fracture Mechanics* 77.16 (2010), pp. 3204–3215. ISSN: 00137944. DOI: 10.1016/j.engfracmech.2010.08.015.

[287] H. Waisman and L. Berger-Vergiat. "An adaptive domain decomposition preconditioner for crack propagation problems modeled by XFEM". In: *International Journal for Multiscale Computational Engineering* 11.6 (2013).

[288] Y. Wang and H. Waisman. "From diffuse damage to sharp cohesive cracks: A coupled XFEM framework for failure analysis of quasi-brittle materials". In: *Computer Methods in Applied Mechanics and Engineering* 299 (2016), pp. 57–89. ISSN: 00457825. DOI: 10.1016/j.cma.2015.10.019.

[289] J. Weber et al. "Properties of hydrogen induced voids in silicon". In: *Journal of Physics: Condensed Matter* 17.22 (2005), S2303–S2314. ISSN: 0953-8984. DOI: 10.1088/0953-8984/17/22/019.

[290] M. K. Weldon et al. "Mechanism of silicon exfoliation induced by hydrogen/helium co-implantation". In: *Applied Physics Letters* 73.25 (1998), p. 3721. ISSN: 00036951. DOI: 10.1063/1.122875.

[291] A. Wells. "Crack opening displacements from elastic-plastic analyses of externally notched tension bars". In: *Engineering Fracture Mechanics* 1.3 (1969), pp. 399–410. ISSN: 00137944. DOI: 10.1016/0013-7944(69)90001-0.

[292] G. N. Wells and L. J. Sluys. "A new method for modelling cohesive cracks using finite elements". In: *International Journal for Numerical Methods in Engineering* 50.12 (2001), pp. 2667–2682. ISSN: 0029-5981. DOI: 10.1002/nme.143.

[293] L. Wen and R. Tian. "Improved XFEM: Accurate and robust dynamic crack growth simulation". In: *Computer Methods in Applied Mechanics and Engineering* 308 (2016), pp. 256–285. ISSN: 00457825. DOI: 10.1016/j.cma.2016.05.013.

[294] H. M. Westergaard. "Bearing pressures and cracks". In: *Journal of Applied Mechanics* 18 (1939), A49–A53. DOI: /publication/216756690.

[295] S. M. Wiederhorn and L. H. Bolz. "Stress Corrosion and Static Fatigue of Glass". In: *Journal of the American Ceramic Society* 53.10 (1970), pp. 543–548. ISSN: 1551-2916. DOI: doi:10.1111/j.1151-2916.1970.tb15962.x.

[296] J. G. Williams. "On the calculation of energy release rates for cracked laminates". In: *International Journal of Fracture* 36.2 (1988), pp. 101–119. ISSN: 0376-9429. DOI: 10.1007/BF00017790.

[297] M. Williams. "On the Stress Distribution at the Base of a Stationary Crack". In: *ASME Journal of applied mechanics* 24.109 (1957), p. 114.

[298] C. H. Wu. "Fracture under combined loads by maximum energy release rate criterion". In: *Journal of Applied Mechanics* 45.553 (1978), pp. 553–558.

[299] C. H. Wu. "Maximum-energy-release-rate criterion applied to a tension-compression specimen with crack". In: *Journal of Elasticity* 8.3 (1978), pp. 235–257. ISSN: 0374-3535. DOI: 10.1007/BF00130464.

[300] C. H. Wu. "Elasticity problems of a slender Z-crack". In: *Journal of Elasticity* 8.2 (1978), pp. 183–205. ISSN: 0374-3535. DOI: 10.1007/BF00052482.

[301] J. Y. Wu, F. B. Li, and S. L. Xu. "Extended embedded finite elements with continuous displacement jumps for the modeling of localized failure in solids". In: *Computer Methods in Applied Mechanics and Engineering* 285 (2015), pp. 346–378. ISSN: 00457825. DOI: 10.1016/j.cma.2014.11.013.

[302] Q. Z. Xiao and B. L. Karihaloo. "Direct evaluation of accurate coefficients of the linear elastic crack tip asymptotic field". In: *Fatigue and Fracture of Engineering Materials and Structures* 26.8 (2003), pp. 719–729. ISSN: 8756758X. DOI: 10.1046/j.1460-2695.2003.00648.x.

[303] Q. Z. Xiao and B. L. Karihaloo. "Improving the accuracy of XFEM crack tip fields using higher order quadrature and statically admissible stress recovery". In: *International Journal for Numerical Methods in Engineering* 66.9 (2006), pp. 1378–1410. ISSN: 0029-5981. DOI: 10.1002/nme.1601.

[304] S. Xiao and T. Belytschko. "A bridging domain method for coupling continua with molecular dynamics". In: *Computer Methods in Applied Mechanics and Engineering* 193.17-20 (2004), pp. 1645–1669. ISSN: 00457825. DOI: 10.1016/j.cma.2003.12.053.

[305] X. P. Xu and A. Needleman. "Numerical simulations of fast crack growth in brittle solids". In: *Journal of the Mechanics and Physics of Solids* 42.9 (1994), pp. 1397–1434. ISSN: 00225096. DOI: 10.1016/0022-5096(94)90003-5.

[306] V. Yamakov, E. Saether, D. R. Phillips, and E. H. Glaessgen. "Molecular-dynamics simulation-based cohesive zone representation of intergranular fracture processes in aluminum". In: *Journal of the Mechanics and Physics of Solids* 54.9 (2006), pp. 1899–1928. ISSN: 00225096. DOI: 10.1016/j.jmps.2006.03.004.

[307] F. Yang. "Hydrogen-induced silicon wafer splitting". In: *Journal of Applied Physics* 94.3 (2003), p. 1454. ISSN: 00218979. DOI: 10.1063/1.1586959.

[308] J. F. Yau, S. S. Wang, and H. T. Corten. "A Mixed-Mode Crack Analysis of Isotropic Solids Using Conservation Laws of Elasticity". In: *Journal of Applied Mechanics* 47.2 (1980), p. 335. ISSN: 00218936. DOI: 10.1115/1.3153665.

[309] A. Yazid, N. Abdelkader, and H. Abdelmadjid. "A state-of-the-art review of the X-FEM for computational fracture mechanics". In: *Applied Mathematical Modelling* 33.12 (2009), pp. 4269–4282. ISSN: 0307904X. DOI: 10.1016/j.apm.2009.02.010.

[310] Z. Yosibash, A. Bussiba, and I. Gilad. "Failure criteria for brittle elastic materials". In: *International Journal of Fracture* 1957 (2004), pp. 307–333. ISSN: 03769429. DOI: 10.1007/978-1-4614-1508-4.

[311] G. Zi and T. Belytschko. "New crack-tip elements for XFEM and applications to cohesive cracks". In: *International Journal for Numerical Methods in Engineering* 57.15 (2003), pp. 2221–2240. ISSN: 0029-5981. DOI: 10.1002/nme.849.

[312] O. C. Zienkiewicz and R. L. Taylor. *The Finite Element Method: Solid Mechanics*. 5th ed. Vol. 2. Oxford: Butterworth-Heinemann, 2000. ISBN: 0750650559.

[313] O. C. Zienkiewicz and R. L. Taylor. *The Finite Element Method: The Basis*. 5th ed. Vol. 1. Butterworth-Heinemann, 2000, p. 708. ISBN: 0 7506 5049 4.